المجلّة الدَّولية للعُلوم والتِّقنِية

مجلة علمية محكمة تصدر عن

مركز العلوم والتقنية للبحوث والدراسات

العدد السادس و العشرون
يوليو 2021

WWW.STC-RS.COM

كلمة العدد

الحمد لله حمداً كثيراً على نعمته التي أنعم الله بها علينا و ألهمنا و وفقنا لإنجاز هذا العمل. و إنه لمن دواعي سرورنا أن نشهد بتوفيق من الله صدور العدد **السادس و العشرون** من **المجلة الدولية للعلوم والتقنية** و الذي نأمل ان يكون مصدرا من مصادر العلوم الهندسية والتطبيقية و التقنية التي ينهل منها البحّاث المهتمين في هذه المجالات ولتوفير و إعطاء المعلومة والنتيجة الصحيحة لطلاب العلم و المعرفة.

و لقد حرصنا في هذا العدد أن تكون جميع الورقات العلمية المنشورة في المستوى المطلوب و أن تقدم المفيد لخدمة البحث العلمي. من هذا المنطلق فإن هيئة تحرير المجلة تجدد حرصها الدائم على استمرارية صدور المجلة برصانة و منهجية في البحث العلمي وذلك بإتباع الأساليب العلمية المحكّمة في تقييم البحوث العلمية المقدمة من الأساتذة و البحّاث بإشراف أساتذة متخصصين في جميع فروع العلوم و التقنية آخذين في الاعتبار الطرق المتبعة في المجلات العلمية العريقة في هذا المجال.

وبهذه المناسبة يسر هيئة التحرير بالمجلة أن تثمن عالياً جهود جميع البحّاث و الأساتذة المهتمين الذين اختاروا صفحات هذه المجلة لنشر أبحاثهم و أوراقهم العلمية، كما أنها تتقدم بجزيل الشكر و العرفان لكل من ساهم في تحرير و مراجعة البحوث المقدمة للمجلة وتقديم هذا الصرح العلمي للوجود.

هيئة التحرير

هيئة التحرير

رئيس هيئة التحرير

د. أحمد الصغير جاب الله

أستاذ مشارك

في مجال الهندسة الميكانيكية وعلوم المواد

من جامعة بودابست التقنية – دولة المجر

أ. عبد الحميد الطاهر زنبيل

استاذ مساعد – تخطيط موارد بشرية .

المعهد التخطيط للدراسات العليا

أ.م. محمد المنير حدود

استاذ مساعد في مجال هندسة علوم

المواد جامعة بلغراد – صربيا

أ.م. محمد علي القانقا

استاذ مساعد في مجال الهندسة الالكترونية

وتقنية المعلومات من جامعة شفيلد هالم ـ

بريطانيا- 2008

جدول المحتويات

الحصول على مسبوكات ذات بنية معززة من خلال تسليح نماذج القالب وامتزاجه أثناء الصب بالطور السائل

شالفسكا إينا أناتولفنا [1] ، جمال إبراهيم مصباح[2]

1– المعهد التكنولوجي للفيزياء وسبائك المعادن بالأكاديمية الوطنية للعلوم أوكرانيا – كييف.

2– قسم الهندسة الميكانيكية ، كلية العلوم والتقنية – بني وليد.

jamal.1982.musbah@gmail.com

التعريفات

1. مكونات النظام : نقصد بمكونات النظام في هذه الدراسة سبيكة المصفوفة ، نموذج القالب ، الجسيمات المزروعة داخل النموذج ، قالب السباكة .

2. نماذج الرغوة المفقودة المحسنة: عبارة عن حبيبات البولي استيلين المشكلة تحت الضغط والتي عملنا لدراسة طرق تحسينها كما في الدراسة [7] .

3. CT3 : سبيكة من الحديد الصلب تحتوي على نسبة كربون 0.14–0.22 % طبقا للمواصفات السوفيتية .

4. MC (سبائك المصفوفة) :عبارة عن سبيكة الأساس (حديد زهر، الومنيوم ..الخ) مصفوفة بداخلها مواد التعزيز أو التقوية (حديد صلب ، زركون ..الخ) .

5. ЛАК : سبائك ذات بنية بلورية معززة .

6. АФ : طور التعزيز وهو عبارة عن جسيمات مزروعة ومصفوفة داخل السبيكة الغرض منها تقوية بنية سبيكة المصفوفة .

7. قضبان : نقصد بالقضبان في هذا البحث المعنى اللغوي لا الاصطلاحي ،والذي يعني اشكال اسطوانية صغيرة ذات اقطار لا تتجاوز 5 ملم وأطوال لا تزيد عن 0.7 ملم.

International Science and Technology Journal
المجلة الدولية للعلوم والتقنية

العدد 26
Volume 26

ISTJ
المجلة الدولية للعلوم والتقنية
International Science and Technology Journal

8. Ст20 : سبيكة من حديد الصلب تحتوي على كربون بنسبة 0.17 – 0.24% طبقا للمواصفات السوفيتية .

9. غشاء : عبارة عن قضبان او شبكات من الصلب المستخدمة في تقوية السبيكة عند التصاهر مع الزهر تكون ما يسمى غشاء او حاجز .

10. Пг1; Пд0,5 : نسبة البرلايت في الطور وفقا للمقاييس السوفيتية .

11. Ст5 : سبيكة من الحديد الصلب تحتوي على كربون بنسبة 0.28 – 0.37% طبقا للمواصفات السوفيتية .

12. ЧПГ : حديد الزهر الرمادي.

13. ВЧШГ : حديد الدكتايل عالي الصلادة ذو الجرافيت الكروي .

Abstract:

This paper is a translation of a study we conducted in the foundry laboratories of the Technological Institute of Physics and Alloys of Metals of the National Academy of Sciences Ukraine - Kiev. In this study, we discussed the possibility of improving the mechanical, physical and chemical properties of metal alloys on the basis of iron and carbon by cultivating steel particles whose diameters do not exceed 5 mm Within the polystyrene models to obtain reinforced alloys, where the process requires a broad understanding of the technological foundations of metal casting, such as studying the microstructure of matrix alloys, reinforcement phases and diffusion regions, in addition to the methods of casting, cooling, freezing time, impregnation rate and other foundations, where the study relied on providing clear criteria for reinforcement operations. Where the study was conducted on samples of gray cast iron and ductile iron with spheroidal graphite as matrix alloys, reinforced with steel bars as reinforcement phases, and a large and good diffusion of carbon was found from cast iron to steel iron, and this diffusion of carbon was harmful to the difference in concentration in the chemical composition of each iron cast iron and steel, where the amount of diffusion depends on the contact

International Science and
Technology Journal
المجلة الدولية للعلوم والتقنية

العدد 26
Volume 26

المجلة الدولية للعلوم والتقنية
ISTJ

surface temperature and duration of To solidify the alloy, to get rid
of unstable chemical bonds and corrosion, the impregnation time is
increased without violating the cooling speed and freezing rate.
Based on the microscopic studies that were conducted on the
samples, it was found that there are no clear boundaries for the
diffusion zones of heterogeneous minerals, and a difference in
crystal structure was found between the base metal, the diffusion
region and the reinforcement metal, and this discrepancy in the
crystal structure leads to an improvement in some mechanical
properties.

الملخص

هذه الورقة عبارة عن ترجمة لدراسة قد أجريناها في معامل السباكة في المعهد
التكنولوجي للفيزياء وسبائك المعادن بالأكاديمية الوطنية للعلوم أوكرانيا – كييف ،وقد
تناولنا في هذه الدراسة امكانية تحسين الخصائص الميكانيكية والفيزيائية والكيميائية
لسبائك المعادن على اساس الحديد والكربون وذلك بزراعة جسيمات من الصلب لا
تتجاوز اقطارها 5مم داخل نماذج البولي استيلين للحصول على سبائك معززة ، حيث
تتطلب العملية فهما واسعا للأسس التكنولوجية لسباكة المعادن ، كدراسة البنية المجهرية
لسبائك المصفوفة (MC) واطوار التعزيز (AΦ) ومناطق الانتشار اضافة الى طرق
الصب والتبريد ومدة التجميد ومعدل التشريب وغيرها من الاسس ، حيث اعتمدت
الدراسة على تقديم معايير واضحة لعمليات التعزيز حيث اجريت الدراسة على عينات
من حديد الزهر الرمادي (ЧПГ) وحديد الدكتايل ذو الجرافيت الكروي (ВЧШГ)
كسبائك مصفوفة (MC) ، معززة بقضبان من الصلب (CT3،Cт20) كأطوار
للتعزيز (AΦ) ، وقد وجد انتشار كبير وجيد للكربون من حديد الزهر الى حديد
الصلب ، وهذا الانتشار للكربون أذى الى اختلاف التركيز في التركيب الكيميائي لكل
من حديد الزهر وحديد الصلب ، حيث تعتمد كمية الانتشار على درجة حرارة سطح
التلامس ومدة التجمد للسبيكة ، وللتخلص من الروابط الكيميائية الغير المستقرة والتآكل
يتم زيادة مدة التشريب دون الاخلال بسرعة التبريد ومعدل التجميد .

International Science and
Technology Journal
المجلة الدولية للعلوم والتقنية

العدد 26
Volume 26

ISTJ
المجلة الدولية للعلوم والتقنية
International Science and Technology Journal

وبناء على الدراسات المجهرية التي تم اجراؤها على العينات تبين عدم وجود حدود واضحة لمناطق الانتشار للمعادن الغير متجانسة ، كما وجد اختلافا في التركيب البلوري بين معدن الاساس ومنطقة الانتشار ومعدن التعزيز ، وهذا التباين في البنية البلورية يؤدي الى تحسين في بعض الخصائص الميكانيكية.

الكلمات المفتاحية: مصبوبات مركبة ، بنية مصبوبة معززة، الطور المعزز ، صب بنماذج الرغوة المفقودة ، بنية دقيقة .

المقدمة

يتم النظر في خيارات الحصول على مواد الصب المركبة ذات الخصائص الوظيفية وذلك بتحليل طرق تعزيز سبائك المصفوفة بواسطة مرحلة طور التعزيز ، وقد ثبت أن الطريقة الأكثر فعالية لتكوين مواد ذات خصائص وظيفية جيدة للسبائك الحديدية و الغير حديدية هي تعزيز هذه السبائك من خلال امتزاج الطور السائل بمكونات النظام، وذلك باستخدام طريقة الصب بنماذج الرغوة المفقودة المحسنة، حيث يقلل استخدام هذه الطريقة من سعة العمل وتعقيد العمليات من خلال موقع طور التعزيز في تجويف النموذج ، لأنه من الممكن تثبيته في مرحلة صنع النماذج ،ومن خلال البحث وجد أن الاطوار المعززة لها تأثير واضح على الشكل البلوري وخصائص التصميم لسبائك الحديد والكربون ، واستنادًا إلى الدراسات المعدنية التي تم إجراؤها، وجد انه أثناء الحصول على المصبوبات معززة التصميم (حيث تم استخدام الحديد الزهر الرمادي عالي القوة كسبيكة مصفوفة) ، تنتقل فيها (عند الانتشار) منطقة غير واضحة الحدود لأسطح الفصل بين المعادن المتباينة، و في هذه الحالة ، فان البنية المجهرية للطبقة الانتقالية في بنية السبيكة المصفوفة تختلف عن بنية طور التعزيز، فعلى سبيل المثال ، يتسبب التدفق المكثف لعمليات التبادل الحراري في تفاعل الحديد الزهر مع حاجز(غشاء) من الفولاذ CT3 في ذوبان كبير للحاجز ، وبالتالي تتشكل منطقة انتقالية عريضة جدا (0.15−0.18 مم) وهناك تشبع شديد للصلب بكربون حديد الزهر وذلك بسبب تراكم الكربون في الطور السائل أثناء التفكك البلوري ، عند تعزيز المسبوكات من الحديد الزهر الرمادي وحديد الدكتايل (جرافيت كروية) بقضبان بقطر 2 و 5 ملم من

International Science and
Technology Journal
المجلة الدولية للعلوم والتقنية

العدد 26
Volume 26

المجلة الدولية للعلوم والتقنية
International Science and Technology Journal
ISTJ

الفولاذ 20 ، تم العثور على كربنة عميقة إلى حد ما وانتشار كبير للكربون من حديد الزهر إلى الفولاذ ، والذي يعتمد على درجة الحرارة عند سطح التلامس للمراحل السائلة والصلبة وسرعة التبريد و التجمد للمسبوكة، وتتراوح القيمة الإجمالية لمنطقة الانتشار (المنطقة الانتقالية) من 0.4 – 0.6 ملم.

لقد وجد أن تكوين البنية المجهرية وحجم منطقة الانتشار يتأثران بالتركيب الكيميائي لسبائك المصبوبة وطور التعزيز ، ودرجة حرارة المسبوكة في الحالة السائلة ومعدل التبريد عند الصب ، والذي يرتبط أيضًا بكمية طور التعزيز المقدم.

منهجية البحث

تنشأ الحاجة إلى المصبوبات ذات الخصائص الوظيفية العالية اعتمادا على ظروف التشغيل للآلات والآليات ، سواء كانت مقاومة عالية للتآكل لطبقة العمل ، مزيج من قلب ناعم مع طبقة خارجية صلبة ، زيادة الصلابة ، مقاومة الانكماش ، الهيدروستاتيك ، مقاومة التآكل ، الموصلية الحرارية...الخ [1].

في العقود الأخيرة ، أصبحت المواد المصبوبة المركبة منتشرة على نطاق واسع ، والتي يتم إنتاجها بطرق مختلفة في الطور السائل وذلك بربط المصفوفات المعدنية بمواد تقوية عالية القوة في شكل جزيئات دقيقة وجسيمات ، بالإضافة الى أشكال كقضبان وأسلاك وألياف وألواح وصفائح وشبكات ، حيث يتم عرض المخططات التكنولوجية الرئيسية لإنتاج المسبوكات المركبة في الدراسة [1].

بعد النضر في القوانين العامة لعمليات السباكة ، وتدفق المصهور في القالب ، والحصول على سبائك ذات تراكيب مختلفة (معززة)، أوصى الباحثون في هذه الدراسة بالعمل على تطوير الخصائص باستخدام سبائك المصفوفة واطوار التعزيز المختلفة . وعلى هذا القول ، وباعتبار تعقيدات التصميم ، فان انسب طريقة لتوزيع اطوار التعزيز وصفها داخل معدن الاساس باستخدام عمليات الصب بواسطة نماذج من البولي استيلين (نماذج الرغوة المفقودة) .

International Science and
Technology Journal
المجلة الدولية للعلوم والتقنية

العدد 26
Volume 26

المجلة الدولية للعلوم والتقنية
International Science and Technology Journal
ISTJ

لقد لاقت عمليات تقوية الصلب و الزهر وتقوية أسطحهما اهتمام العديد من الدارسين ، والتي أشارت إلى تحسن الخصائص الميكانيكية للمسبوكات وطبقاتها السطحية نتيجة للتعزيز .

إن تقوية سبائك الألومنيوم المصبوب بواسطة جزيئات وألياف مشتتة أدى إلى زيادة صلابة وصلادة المواد، كما في الدراسة [2] .

قام المؤلفون بالبحث في تركيب مصفوفة الألومنيوم المعزز بالزركون ، والصب في قوالب تحت الضغط مع التحريك لتحسين خاصية مقاومة التآكل.

هناك أيضًا نتائج دراسات التعزيز الدقيق لسبائك الألومنيوم مع كربيد السليكون والتيتانيوم لتعزيز مقاومة التآكل وبعض الخصائص الميكانيكية [3].

حيث أجريت هذه الدراسة في كلية كونغو للهندسة بإقليم نادو تاميل بالهند ، و كانت عملية الصب على مرحلتين لضمان الخلط الجيد .

إن من ضمن الخيارات المعروفة لتعزيز الحديد الزهر عند محتوى (اليوتيكتيك) ، بإضافة الخزف لتحسين مقاومته للتآكل وقابليته للتشكيل ، لقد وجد أنه من أجل ضمان توزيع موحد للجسيمات في الصب ، من الضروري إدراج السيراميك في تجويف القالب و هذا يؤدي إلى زيادة التعقيد في تصنيع المسبوكات [4] .

إن أفضل طرق السباكة ملاءمة لتصنيع المسبوكات المسلحة (قطع التعزيز) هي تقنية الصب بنماذج الرغوة المفقودة ، هناك العديد من التقنيات المحلية لتعزيز مواد الصب منها على سبيل المثال مصفوفات معدنية على أساس الكربيد الحراري المقاوم للتآكل وذلك بإدراجهم في قوالب من نماذج البوليسترين [5].

يمكن استخدام الطريقة المقترحة لإنشاء مناطق معززة محليًا في تصنيع المسبوكات. هناك نتائج دراسة تأثير طور التعزيز الدقيق على إزالة درجة حرارة السبيكة الزائدة ومعدل التبريد [6] .

لكن الورقة لا تأخذ في الاعتبار العمليات الفيزيائية و الكيميائية التي تحدث عند حدود مادة التسليح وسبائك المصفوفة ، عند الحصول على المسبوكة المقواة باستخدام الجسيمات الدقيقة الموضوعة في تجويف القالب أو في نماذج البوليسترين الرغوي ،

تظهر أنظمة جديدة متعددة المكونات لنظرية عمليات المسبك : "المعدن – النموذج – الجسيمات المزروعة – القالب " و "المعدن – طور التعزيز – القالب " [7].

إن الطريقة الأكثر فاعلية لتشكيل المواد ذات الخصائص الوظيفية الخاصة للسبائك الغير حديدية والسبائك الحديدية هي تعزيز هذه السبائك من خلال مزجهم في الطور السائل لمكونات النظام.

لذلك و في المقام الأول ، من الضروري النظر في المخططات الأساسية للحصول على مثل هذه الفئة من المواد ، بالإضافة إلى تحديد الشروط الاساسية والمعايير التكنولوجية عند الحصول على سبائك البنى البلورية المعززة (ЛАК).

يجب أن تكون بنية المواد غير متجانسة وأن تتكون من حبيبات صلبة ، موزعة بالتساوي في مصفوفة بلاستيكية تحوي بعض المرونة ، ويجب الحفاظ على رابطة لاصقة بين المكونات، وبهذه المتطلبات فقط يمكننا تعزيز سبائك المواد .

يتم تنفيذ العملية التكنولوجية لتصنيع المسبوكات المسلحة بطريقة الصب بواسطة نماذج الرغوة المفقودة وفقًا للمخططات التالية:

– تحضير المكونات (معايرة وتنظيف وتكسية السطح ، مع توفير هيكل التعزيز بالشكل والتكوين اللازمين) ؛

– إنتاج نماذج رغوة البوليسترين وإدماج عناصر التعزيز ؛

– تجميع القالب ؛

– صب السبيكة ، التشريب ؛

– ترسيخ تصلب الطور السائل؛

– ازالة المسبوكة من القالب .

– المعالجة الحرارية أو الميكانيكية للمنتجات المعززة.

تتميز عملية الحصول على ЛАК بالبساطة وسهولة التنفيذ في ظروف الإنتاج القياسية والتحضير الرخيص للمواد والمعدات التكنولوجية وإمكانية التشغيل الآلي وانخفاض رأس مال الإنتاج، وتشمل العيوب استحالة الحصول على مصبوبات معززة ذات شكل معقد ، ووجود بعض العيوب في وجود المسامات الغازية وتشكيل بنية غير كاملة عند الحصول على ЛАК ، مع مستوى عالٍ من المتطلبات التشغيلية.

International Science and
Technology Journal
المجلة الدولية للعلوم والتقنية

العدد 26
Volume 26

المجلة الدولية للعلوم والتقنية
International Science and Technology Journal
ISTJ

يتطلب تحقيق نتائج مثالية لجمع مكونات الأنظمة المعززة فهمًا واضحًا للأساس التكنولوجي لمثل هذا التجميع ، أولاً وقبل كل شيء من حيث تشكيل الهياكل الغير المتجانسة ، وظهور روابط بسيطة بين مختلف عناصر النظام ، ونتيجة لذلك ، ظهور عمليات التفاعل الفيزيائي والكيميائي على حدود الاتصال بينهم ،و يمكن تحقيق ذلك عن طريق زيادة قابلية التشريب بين العناصر ، ومنع تكوين الترابط الكيميائية الغير مستقر و الطبقات ذات السماكة المفرطة ، ومنع التآكل الكيميائي ، ومنع هشاشة (AФ) أثناء تلامس سطح المصهور مع سبيكة المصفوفة.

على هذا النحو فقط يمكن تحقيق نتائج تكنولوجية أفضل لتخطيط الانتاج ، كما يجب تقديم المعايير الواضحة لعمليات التجميع (بما في ذلك العمليات التحضيرية) ، وعلى ذلك يمكن الحصول على ЛAK بمواصفات تشغيلية عالية تواكب المتطلبات المقدمة في هذا الوقت لمثل هذه المواد .

عند دراسة خصائص مواد التعزيز ، من المهم تقديم الكميات المجهرية التي توفر الخصائص الفيزو– كيميائية للمكونات ونسبة التبادل والتركيز ونوع التعزيز .

من أجل تأكيد البيانات حول تأثير (AФ) على تشكيل الهياكل وموصفات الهياكل المعززة ، تم إنشاء تغييرات هيكلية في المواد المدعمة المصبوبة على أساس سبائك الحديد والكربون (الزهر الرمادي وحديد الدكتايل) ، حيث تم في مرحلة التعزيز(AФ) استخدام قضبان معدنية بأقطار2ملم و 5 مم و بسمك 0.7 ملم من فولاذ20 (Ст20) وصفائح من فولاذ3 (Ст3) .

تم إجراء دراسة مجهرية على عينات من المسبوكات من سبائك الحديد والكربون التي تم الحصول عليها بواسطة نماذج التغوير(نماذج البولي استيلين) مع إدخال تقنية (AФ)، حيث أجريت الدراسات بواسطة مجهر ضوئي МИМ8-М ، و تم تقييم البنية المجهرية وفقًا لـ GOST 3443-87 و GOST 5639-82 (طبقا للمواصفات القياسية الروسية) ، ومن أجل مسح واعداد العينات تم استخدام محلول 2% من HNO_3 (حمض النتريك) في كحول الإيثانول.

عند العمل على سبائك من الزهر مع صفائح من الصلب يجب استيفاء شرط أن تكون درجة حرارة المواد الصلبة والسائلة (L+S) لحديد الزهر أقل من درجة حرارة الصلب

International Science and
Technology Journal
المجلة الدولية للعلوم والتقنية

العدد 26
Volume 26

ISTJ
المجلة الدولية للعلوم والتقنية
International Science and Technology Journal

حيث يؤثر تكثيف عمليات التبادل الحراري على الكتلة : أي أن تجاوز كتلة حديد الزهر كتلة صفائح الصلب ، وبذلك فإن حرارة حديد الزهر كافية لإذابة وحل صفائح الصلب، تساهم ميزة زيادة كتلة الحديد الزهر على الفولاذ في زيادة كثافة عمليات التبادل الحراري في المنطقة الانتقالية وزيادة في قيم معاملات الانتشار الفعالة للعناصر الكيميائية ، من المعروف أنه كلما زادت درجة الترابط لعناصر السبك ،كلما انخفضت معاملات الانتشار الفعالة بسبب انخفاض حركة ذرات عناصر السبائك في المنطقة الانتقالية .

عند الفحص البصري لعينة مجهرية مع غشاء 0.3 ملم ، أظهر انحراف وتشوهات بسبب تأثير التدفقات الديناميكية للغاز في القالب وفي مكان إمداد المعدن ، وقد وجد أن الجزء العلوي للغشاء والذي يكون قريب من مركز المسبوكة يتذاءب في عدة اماكن، أما في النصف السفلي للغشاء محافظا تمامًا على التبلور المتسارع للمعدن. تم عرض نتائج جيدة باستخدام صفيحة فولاذية (Ст3) بسمك 0.7 ملم، وتؤكد عدة أقسام على طول مقطع السبيكة الحفاظ الكامل على الغشاء (الشكل 1).

يتم تحديد جودة مركب الانتشار وخصائص قوة الطبقة الانتقالية من خلال ظروف درجة الحرارة والعمليات الفيزو كيميائية على الحدود البينية، حيث يتسبب التدفق المكثف لعمليات التبادل الحراري في تفاعل حديد الزهر مع أقسام الصلب (Ст3) في ذوبان كبير لتلك الاقسام.

يشار إلى ذلك من خلال الشكل (1) حيث يوضح إتساعاً كافياً للمنطقة الانتقالية في حدود (0.15–0.18) ملم، وذلك في سياق التفاعل، نتج من ذلك تشبع كثيف لصفائح الصلب بالكربون الموجود في حديد الزهر ، مكونا بذلك على طول الحدود المترابطة بنية مجهرية من صفائح البيرلايت (Пг1; Пд0,5) المميزة للفولاذ (Ст5) ، وتتكون البنية المجهرية لحديد الزهر على أساس البرلايت مع الكربيد (السمنتيت) والغرافيت. بالنسبة لظروف الحصول على مصبوبات متعددة الطبقات ، فإن السمة المميزة هي التكوين الفوري لطبقة من الأكسيد على سطح السبيكة السائلة ، مما يغير بشكل كبير العمليات على الحدود البينية للأطوار ، ويعيق تفاعل الانتشار بين السبيكتين. في عملية إرتباط معدنين ، تخترق ذرات الأكسجين للمعدن السائل من خلال طبقة أكسيد رقيقة بالمعدن الصلب الى العمق ، مع الطبقة السفلية التالية المحتوية على الكربون

International Science and
Technology Journal
المجلة الدولية للعلوم والتقنية

العدد 26
Volume 26

المجلة الدولية للعلوم والتقنية
International Science and Technology Journal
ISTJ

في الطبقة السطحية للمعدن الصلب، و تعتمد سرعة هذه العملية على الظروف الديناميكية الحرارية : درجة الحرارة والضغط ومحتوى الطور الغازي .

في حدود الاسطح بين أطوار المعدن السائل وصفائح الصلب تحدث العديد من تفاعلات الأكسدة والاختزال .

إن التفاعل الكيميائي بين الزهر السائل وبين صفائح الصلب يختلف باختلاف السرعة العالية والتغلغل الكافي للذرات داخل صفيحة فولاذية وذلك بالنظر للاختلاف الكبير في التركيب الكيميائي وكتلة حديد الزهر مقارنة مع الغشاء .
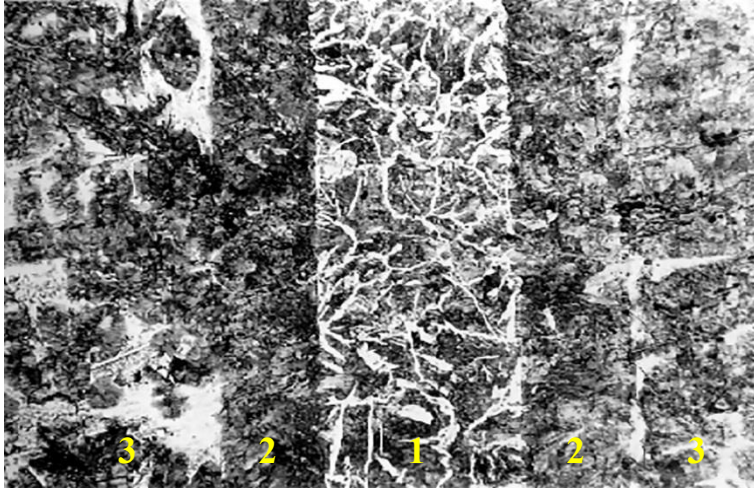
الشكل(1)– البنية المجهرية لسبيكة من حديد الزهر مع غشاء أو صفيحة من الصلب بسمك 0.7 ملم: 1–غشاء ؛ 2 – طبقة انتقالية ؛ 3 – حديد الزهر

بتنشيط وتكثيف الحرارة العالية لعمليات الأكسدة والاختزال يساهم ويطيل ابقاء الزهر في الحالة السائلة عند نقطة توريد المعدن.

إن كربنة الطبقة السطحية لغشاء الصلب يُحدث تراكم محليا عند طور الكربون السائل الذي بدوره يدمر القالب ، معتمد على التدفق الهيدروديناميك والطاقة الحرارية في المصهور عند عملية ملء القالب بالمعدن.

International Science and Technology Journal
المجلة الدولية للعلوم والتقنية

العدد 26
Volume 26

ISTJ
المجلة الدولية للعلوم والتقنية
International Science and Technology Journal

عند إجراء الدراسات المجهرية على عينات لسبائك معززة من حديد الزهر الرمادي (ЧПГ) و حديد الدكتايل عالي القوة ذو الجرافيت الكروي (ВЧШГ) مع (АФ) على شكل قضبان بقطر 2 و 5 ملم من فولاذ20 ، وجد انتشار كبير وجيد للكربون من حديد الزهر في طور الصلب المعزز(АФ) وبعمق جيد (كربنة) ، إن تشبع (АФ) بالكربون يؤدي بشكل أساسي إلى اختلافً تركيز العناصر في التركيب الكيميائي لحديد الزهر (سبيكة المصفوفة MC) والفولاذ 20 لـ(АФ) ، وتعتمد كمية الانتشار على درجة الحرارة عند سطح التلامس في الطور السائل والصلب ومدة التجمد للسبيكة، حيث يبلغ الحجم الإجمالي لمنطقة الانتشار (المنطقة الانتقالية) 0.4 – 0.6 ملم (الشكل 2).

تكون منطقة الانتشار على جانب حديد الزهر عبارة عن طبقة بسماكة تتراوح بين 0.1 – 0.16 ملم مع بنية برلايتية (П100) ، بينما تكون منطقة الانتشار على جانب (АФ) بسمك يتراوح بين 0.3 – 0.4 ملم وتتكون من ثلاث طبقات متساوية في الحجم تقريبا (الشكل 2 – أ ، ب).

لا يوجد حدود واضحة بين منطقتي الانتشار ،والتي تشير الى قلة أو غياب تلك الحدود تحت الصخر لـ (АФ) ،ولكن يوجد بشكل واضح خط التلامس بين المعدن الأصلي و(АФ) ،والذي يمكن توضيحه باختلاف اتجاه الحبيبات والبنية البلورية الغير متساوية للبرلايت من جهة حديد الزهر وطور التعزيز(АФ) ، (الشكل 2 – أ ، ب).

كل المكونات البلورية في مناطق الانتشار لجميع العينات لا تتغير وتشير إلى أن تشبع الكربون في منطقة الانتشار عند (АФ) لـ20Ст ، يحدث في نقاط اليوتكتويد(eutectoid) وبعد اليوتكتويد (hypereutectoid) ، ومن خصائص بنية الهييبروتوكتويد للصلب هي سلاسة الذوبان في بنية اليوتوكتويد ، وبالتالي الى البنية الاساسية لـ (АФ) .

في عينة السبيكة للشكل(2– ب) (ВЧШГ مع АФ لـ20Ст) لوحظ وجود حدود الجرافيت الصلبة بسماكة تصل إلى 0.02 مم على كامل سطح السبيكة، بينما عمليًا لا توجد في منطقة الانتشار لـ (АФ) ، وفي حديد الزهر يكون شريط من الفريت يصل سمكه إلى 0.05 ملم، وفي هذه الحالة ، على ما يبدو ، لا يوجد رابط معدني بين

سبيكة المصفوفة و(AΦ)،و تحدث إفرازات الجرافيت على سطح التلامس MC-AΦ على شكل مرتب ومتسلسل.
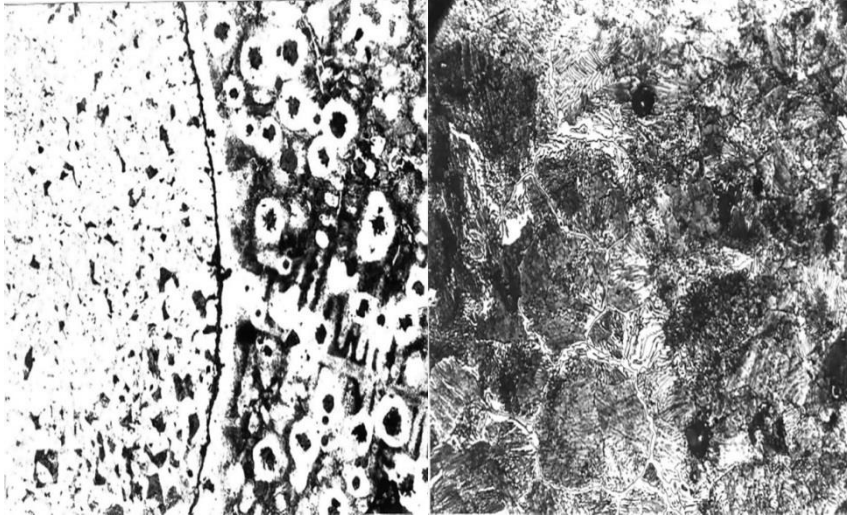
(ب)   (أ)

الشكل (2) – البنية المجهرية لسطح التلامس لعينة من الزهر الرمادي (2 أ) وحديد الدكتايل (2 ب)، مع صلب20 لطور التعزيز بقطر (أ– Ø5mm , ب– Ø 2mm) ، 400 ×

الاستنتاجات

بناءً على دراسات المجهرية التي تم إجراؤها ، تم استنتاج الاتي :

1. عند الحصول على بنية سبائكية معززة على أساس سبائك المصفوفة (MC) ، حيث ثم استخدام ЧПГ, ВЧШГ وكانت مناطق الانتقال (منطقة الانتشار) بدون حدود واضحة لأسطح الانقسام بين المعادن الغير متجانسة.

2. تختلف البنية المجهرية للطبقة الانتقالية عن بنية سبيكة المصفوفة وعن بنية AΦ.

3. يتأثر تكوين البنية المجهرية وحجم المنطقة الانتقالية بالتركيب الكيميائي لسبائك المصفوفة و AΦ ، ودرجة حرارة السائل MC ، وسرعة تبريد السبيكة ، والذي يرتبط أيضًا بكمية AΦ المقدمة.

International Science and Technology Journal
المجلة الدولية للعلوم والتقنية

العدد 26
Volume 26

المجلة الدولية للعلوم والتقنية
International Science and Technology Journal
ISTJ

المراجع

[1] Lysenko, T. V., Jasjukov, V. V., Prokopovich, I. V. (2019). Koncepcii upravlenija formoobrazovaniem otlivok: monografija [Casting Formation Management Concepts: Monograph]. Odessa: Ekologija [in Russian].

[2] Sakthivelu, S., Meignanamoorthy, M., Ravichandran, M., Sethusundaram, P. P. (2019). Tribological Behavior of AA7050-ZrSiO4 Composites Synthesized by Stir Casting Technique. Mechanics and Mechanical Engineering. 23, 198–201. DOI: 10.2478/mme-2019-0026 [in English].

[3] Sambathkumar, M., Navaneethakrishnan, P., Ponappa, K., Sasikumar, K.S.K. (2017). Mechanical and Corrosion Behavior of Al7075 (Hybrid) Metal Matrix Composites by Two Step Stir Casting Process. Latin American Journal of Solids and Structures. 14 (2), 243-255. DOI: http://dx.doi.org/10.1590/1679-78253132 [in English].

[4] Dulska, A., Studnicki, A. & Szajnar, J. (2017). Reinforcing cast iron with composite insert. Archives of Metallurgy and Materials. 62 (1), 355-357. DOI: 10.1515/amm-2017-0055 [in English].

[5] Anikeev, A.N., Chumanov, I.V. (2018). Microstructure and Hardness of a Dispersion-Reinforced Casting. Russian Metallurgy (Metally), 2018, 1161-1164. DOI: 10.1134/S0036029518120030 [in English].

[6] Shalevskaja, I.A. (2019). Issledovanie teploobmennyh processov v litejnoj forme s armirujushhej fazoj [Investigation of heat transfer processes in a mold with a reinforcing phase]. Lit'e i metallurgija – Casting and metallurgy. 3, 54-59. DOI: https://doi.org/10.21122/1683-6065-2019-3-54-59 [in Russian].

[7] Shinsky, I., Shalevska, I., Musbah, J. (2015). Efficiency of influence of a metal macroreinforcing phase on process of solidification of large-sized castings. TEKA. Commission of Motorization and Energetics in Agriculture. 15 (2), 51-58 [in English].

بناء وتصميم تطبيق التبرع بالدم لمدينة زليتن بليبيا

Mr. Mahmoud H. S. Hasan   **Mr. Hatem Abdullah Hasan Alziriqany**

tea_mhs@asmarya.edu.ly   Hatemabdullah1999@gmail.com
Al-asmarya Islamic University College of Information Technology
Department: Information Systems
Zliten – Libya

Mr. Abd Alhakim Muftah Salem Ibrahim   **Mr. Abdulaziz Abdulhadi Abdullah Esghire**

Hkim9677@gmail.com   Azizz11228899@gmail.com
Al-asmarya Islamic University College of Information Technology
Department: Computer Science
Zliten – Libya

الملخص

توفر الدم في الوقت المناسب يحمي حياة المرضى، وفي معظم الحالات عند الحاجة إلى الدم لا يمكن توفيره في الوقت المحدد و ذلك لعدم توفر قاعدة بيانات للوصول إلى المتبرعين في الوقت المناسب خاصة عندما تكون حالة المريض خطيرة وبحاجة ماسة إلى الدم، بالإضافة إلى الحاجة إلى بلازما الدم من المتعافين من بعض الأوبئة كمرض فيروس الكورونا (Covid 19) ولتسهيل البحث عن الراغبين في التبرع بالدم، حيث قمنا في هذه الورقة بعمل تطبيق اندرويد لتسهيل التواصل بين محتاجي ومتبرعي الدم حيث قمنا ببناء هذا التطبيق باستخدام برنامج (Android Studio) وباستخدام لغة البرمجة جافا (Java) وبالاعتماد على قاعدة بيانات Google Firebase. حيث يتم ربط كلٍّ من المحتاج و المتبرع للدم من خلال عدة وسائل اتصال مثل المكالمات الهاتفية المباشرة أو عبر برامج التواصل عبر الانترنت مثل برنامج (Whatsapp). كما يوفر التطبيق إمكانية إضافة طلب لفصيلة دم معينة بحيث يتم توفيرها في أسرع وقت ممكن، بالإضافة إلى ربط مرضى فيروس كورونا والذين يتعافون من الفيروس للاستفادة من بلازما الدم لديهم. يهدف هذا التطبيق إلى تسهيل وتقليل الوقت في البحث

International Science and
Technology Journal
المجلة الدولية للعلوم والتقنية

العدد 26
Volume 26

المجلة الدولية للعلوم والتقنية
International Science and Technology Journal
ISTJ

عن فصيلة الدم المطلوبة وتسهيل التواصل بين المتبرع والمستفيد. بالإضافة إلى إنشاء سياسة أمنية لمستخدمي التطبيق لضمان مصادقة مستخدمي التطبيق على أرقام هواتفهم المحمولة.

الكلمات المفتاحية : برنامج اندرويد ، التبرع بالدم ، تطبيقات الهاتف المحمول.

Abstract

The timely availability of blood protects the lives of patients, and in most cases when blood is needed, it cannot be provided on time because there is no database to reach the donors in time، especially when the patient's condition is in danger, in addition to Corona Virus (Covid 19) patients who are looking for blood plasma from recovered people. Where in this paper we made an Android application to facilitate communication between the needy of blood and blood donors, as we built this application using (Android Studio) using the Java programming language (java) and based on Google Firebase. Where the needy and the blood donor are connected through many communication technologies such as direct phone calls or online communication programs such as WhatsApp. The application also provides the ability to add a request for blood type so that it is provided as quickly as possible،
In addition to linking patients with the Coronavirus and those recovering with the virus to benefit from their blood plasma. This application aims to facilitate and reduce the time in the search for the required blood type and facilitate communication between the donor and the beneficiary. In addition to creating a security policy for the users of the application to ensure that the users of the application authenticate their mobile phone numbers.

1. المقدمة

مصرف الدم أو بنك الدم (Blood bank) هو مخزن حفظ الدم ومكوناته ، والتي يتم جمعها من المتبرعين ، إذ يتم جمع وتخزين الدم ومكوناته والحفاظ عليها لاستخدامها لاحقًا في العمليات التي تتطلب نقل الدم. ويشير مصطلح "بنك الدم" إلى قسم في

International Science and
Technology Journal
المجلة الدولية للعلوم والتقنية

العدد 26
Volume 26

المجلة الدولية للعلوم والتقنية
International Science and Technology Journal
ISTJ

المستشفيات حيث يتم تخزين الدم ومنتجاته بعد أن يتم إجراء الاختبارات اللازمة للحد من المخاطر المتعلقة بنقل الدم (1).

وفي عصرنا الحالي أصبحت التكنولوجيا أمراً لا يمكن الاستغناء عنه في حياتنا اليومية، ولقد اثبتت التقنيات الحديثة كتطبيقات التبرع بالدم فعاليتها في انجاز هذه العملية (2). حيث سنتناول في هذه الورقة امكانية تيسير هذه التقنيات. من خلال تطبيق يعمل على الربط بين المحتاج للدم والمتبرع بالدم عن طريق الاتصال بالهاتف مباشرة أو عن طريق برامج الاتصال عبر الإنترنت. حيث يوفر هذا التطبيق إمكانية طلب فصيلة دم لم يتم الحصول عليها في قائمة المتبرعين من قبل المحتاجين للدم بالإضافة الى الباحثين على صفائح الدم من المتعافين من مرض فيروس الكورونا (Covid 19). ومن المعروف انه في عام 2020 ، اجتاح فيروس كورونا (COVID-19) العالم بأسره واصبح يهدد الناس في جميع انحاء العالم (3). ويتميز التطبيق بأمنية البيانات حيث لا يمكن للمستخدم التعديل على بياناته إلا بعد مطابقة رقم الهاتف ، وكذلك سهولة الاستخدام.

2. مشكلة البحث

- ضياع الكثير من الوقت والجهد في البحث عن فصيلة دم أو البحث عن محتاجين للدم.
- صعوبة إيجاد فصيلة الدم المطلوبة.
- عدم الدراية بالأشخاص المحتاجين للدم.
- صعوبة العثور على الأشخاص المتعافين من بعض الاوبئة مثل مرض فيروس الكورونا (Covid 19) وذلك للاستفادة من بلازما الدم الخاصة بهم لعلاج مرضى هذا المرض.

3. الدراسات السابقة

في هذه الورقة (4) تم تطوير تطبيق بنك الدم في نينوى وهو تطبيق أندرويد للربط بين مانحي الدم وطالبي الدم الذين يعيشون في محافظة نينوى بالعراق. يمكن لطالب الدم البحث من قائمة جميع المتبرعين الذين لديهم نفس فصيلة الدم والاتصال بهم مباشرة دون تدخل أي طرف ثالث. ينشئ تطبيق (NINEVEH BLOOD) الملف الشخصي

International Science and Technology Journal
المجلة الدولية للعلوم والتقنية

العدد 26
Volume 26

المجلة الدولية للعلوم والتقنية
International Science and Technology Journal
ISTJ

للمانح / الطالب من خلال قاعدة بيانات (GOOGLE FIREBASE REALTIME).

تطبيق بنك الدم ليبيا (5) اهو عبارة عن تطبيق اندرويد موجود على موقع GooglePlay تستطيع من خلاله البحث عن آلاف المتبرعين بالدم من مختلف المدن في ليبيا ومختلف فصائل الدم و يمكنك إضافة نفسك كمتبرع لمساعدة الآخرين وإرسال واستقبال طلبات التبرع وذلك للتسهيل على الاشخاص المحتاجين للدم من الوصول للمتبرعين بكل سهولة ويسر ولكن يفتقر لوسائل الامان التي تضمن التحقق من هوية المتبرعين للدم بالإضافة الى عدم السيطرة او التحقق من عدد خانات ارقام الهواتف المدخلة للمستخدمين حيث يمكن لأي مستخدم من التلاعب وتغيير في بيانات المتبرعين.

4. المساهمة الرئيسية

في هذه الورقة قمنا بعمل تطبيق اندرويد لتسهيل التواصل بين محتاجي ومتبرعي الدم حيث قمنا ببناء هذا التطبيق باستخدام برنامج (Android Studio) وباستخدام لغة البرمجة جافا (Java) وبالاعتماد على قاعدة بيانات Google Firebase.

حيث يتيح التطبيق رؤية قائمة بجميع متبرعي الدم بمجرد فتح التطبيق وكذلك الاطلاع على قائمة طلبات الدم لفصيلة محددة وقائمة المتعافين من فيروس الكورونا (Covid 19) وتم تسهيل عملية البحث وذلك بإمكانية البحث حسب فصيلة الدم. وفي حالة كان مستخدم جديد يريد التسجيل في التطبيق فلابد من ان يختار احد الصفات التالية (متبرع او طلب فصيلة او متعافي كورونا) وان يملك رقم هاتف خاص به حيث تم اضافة ميزة للتحقق من هوية المستخدم التي تساهم في تحسين الخدمة بين المتبرعين و المحتاجين حيث قمنا بإضافة هذه الميزة وذلك بإرسال رسالة نصية تحتوي على رقم يتكون من ستة خانات يتم توليده بشكل عشوائي لمستخدم التطبيق وذلك للتأكد من ملكية رقم الهاتف للشخص بالإضافة الى التحقق من صحة البيانات المدخلة لنموذج الاشتراك المتبرعين و المحتاجين مثل التحقق من عدد خانات الهاتف ولا يسمح لإدخال الحروف في خانة الهاتف على سبيل المثال بالإضافة عدم السماح بالتعديل على بيانات حسابات

International Science and
Technology Journal
المجلة الدولية للعلوم والتقنية

العدد 26
Volume 26

المجلة الدولية للعلوم والتقنية
International Science and Technology Journal
ISTJ

المستخدمين الا لمن يملك الحساب فقط له صلاحية التعديل على بيانات الخاصة به وذلك بعد التأكد من صحة ملكية الحساب.

1.4 الحوسبة السحابية

تقوم الحوسبة السحابية بتوفير بعض الموارد للأنظمة الحاسوبية كتخزين البيانات من خلال خدمة عند الطلب عبر الشبكة (6). يتم استخدام خدمة Google Firebase كخدمة تعمل كخلفية أي تعمل كخادم وهي خدمة (Backend-as-a-Service BaaS) التي أنشأتها Google في 2014 وتعمل على (Google Cloud Platform) (6). حيث تكون قاعدة البيانات المستندة إلى NoSQL والتي تعمل بمفهوم مختلف عن إدارة قواعد البيانات العلائقية (relational database) حيث لا يوجد علاقات مباشرة بين الجداول ويتم تخزين البيانات ككائن JSON "موصوف ذاتيًا" (7).

يتم استخدام قاعدة البيانات الوقت الفعلي (Real Time DataBase) التي توفرها Firebase حيث من مزايا هذه القاعدة مشاركة البيانات لجميع المستخدمين بشكل سريع وفعال وذلك باستخدام بروتوكول WebSocket في نقل البيانات حيث تُستخدم هذه القاعدة (الوقت الفعلي) الذي يوفره Firebase لتخزين قائمة المتبرعين المتاحين ، وطلبات المحتاجين بالإضافة الى قائمة بالمتعافين من فيروس الكورونا (Covid 19). وذلك بتوفير قناة اتصال ثنائية الاتجاه بين العميل والخادم و تكون عملية المزامنة في WebSocket أسرع من استدعاء HTTP ولا تتطلب إنشاء جلسة اتصال جديدة في كل مرة أثناء الاتصال بين العميل و الخادم. على العكس من HTTP الذي يتطلب إنشاء طلب HTTP في كل مرة يتم فيها تحديث البيانات (8).

5. تحليل وتصميم النظام

في هذا الجزء سنستخدم بعضا من الأدوات التي تساعدنا على فهم واستيعاب هيكلية التطبيق وكيفية سير العمليات داخل النظام.
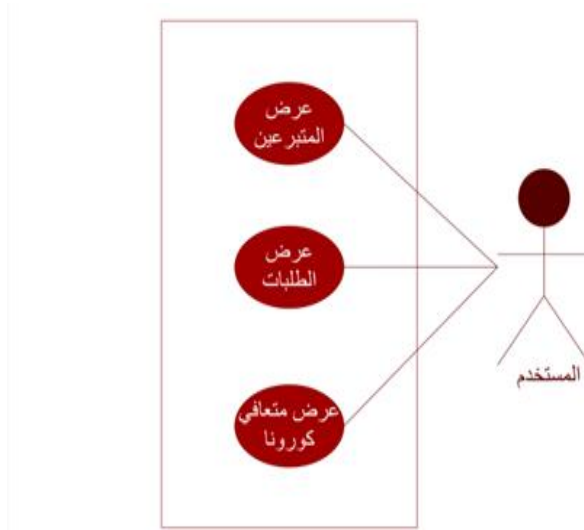
1.5 مخطط حالات الاستخدام

مخطط حالة الاستخدام هو أبسط عرض لتفاعلات المستخدم مع النظام حيث تُمثل حالات الاستخدام على شكل دوائر أو أشكال بيضاوية، وهو يعرض العلاقات بين المستخدم وحالات الاستخدام المختلفة التي يشارك فيها. يمكن لمخطط الاستخدام أيضا أن يعرض أنواع المستخدمين وحالات الاستخدام المختلفة.

وفيما يلي مخططات حالات الاستخدام التي تم استخدامها في النظام :
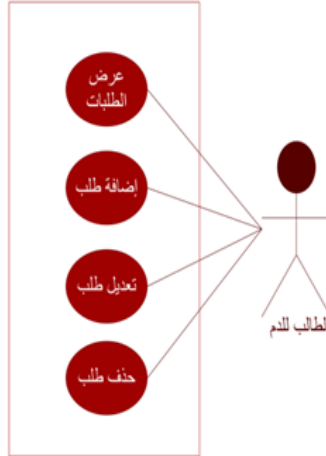
• مخطط حالات الاستخدام للمستخدم:

في الشكل (1) يوضح حالات استخدام مستخدم التطبيق حيث يتيح له التطبيق عرض بيانات المتبرعين و عرض بيانات الطلبات لفصائل الدم المختلفة بالإضافة الى عرض بيانات المتعافين من فيروس كورونا (19 Covid).

شكل (1) مخطط حالات الاستخدام للمستخدم
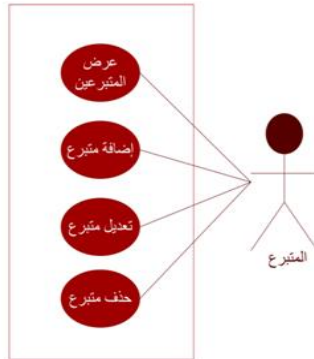
• مخطط حالات الاستخدام للمتبرع:

في الشكل (2) يوضح حالات استخدام المتبرع حيث يتيح له التطبيق عرض بيانات المتبرعين و اضافة نفسه كمتبرع والتعديل على بياناته بالإضافة الى حذف بياناته.

شكل (2) مخطط حالات الاستخدام للمتبرع

• مخطط حالات الاستخدام لطالب للدم :

في الشكل (3) يوضح حالات استخدام الطالب لدم حيث يتيح له التطبيق عرض بيانات المتبرعين و اضافة طلب لفصيلة محددة و تعديل على طلبه و حذف الطلب الذي قام
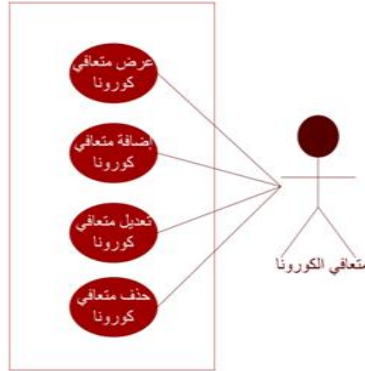

بإضافته.

شكل (3) مخطط حالات الاستخدام لطالب الدم

• مخطط حالات الاستخدام لمتعافي الكورونا:

في الشكل (4) يوضح حالات استخدام لمتعافي فيروس كورونا حيث يتيح له التطبيق عرض بيانات جميع المتعافين من فيروس كورونا (Covid 19) كما يمكن اضافة متعافي كورونا و التعديل على بيانات المعافى بالإضافة الى حذف متعافي كورونا.

شكل (4) مخطط حالات الاستخدام لمتعافي فيروس الكورون

2.5 تصميم جداول قاعدة البيانات

فيما يلي نوضح الجداول التي تم انشائها في قاعدة البيانات وهي كما موضح الجدول (1) جدول يوضح الحقول المستخدمة لبيانات المتبرعين و الجدول (2) جدول يوضح الحقول المستخدمة لبيانات الطلبات و الجدول (3) جدول يوضح الحقول المستخدمة لبيانات المتعافين من فيروس كورونا (Covid 19).

جدول (1) جدول المتبرعين

القيد	عدد الخانات	نوع البيانات	وصف الحقل	إسم الحقل
PK	10	Integer	رقم الهاتف	Phone
	3	String	فصيلة الدم	Btype
	20	Date	آخر تبرع	Ltime
	1	Integer	وسيلة الاتصال	Ctype
	20	String	وقت الاتصال	Ctime
	30	Date & Time	تاريخ ووقت التسجيل	Today

جدول (2) جدول الطلبات

القيد	عدد الخانات	نوع البيانات	وصف الحقل	إسم الحقل
PK	10	Integer	رقم الهاتف	Ophone
	3	String	فصيلة الدم	Obtype

International Science and
Technology Journal
المجلة الدولية للعلوم والتقنية

العدد 26
Volume 26

المجلة الدولية للعلوم والتقنية
International Science and Technology Journal
ISTJ

	20	String	نوع التبرع	Odtype
	1	Integer	وسيلة الاتصال	Octype
	30	String	المنطقة	Oaddress
	60	String	ملاحظات	Onote
	30	Date & Time	تاريخ ووقت التسجيل	Otoday

جدول (3) جدول المتعافين من الكورونا

القيد	عدد الخانات	نوع البيانات	وصف الحقل	إسم الحقل
PK	10	Integer	رقم الهاتف	Cphone
	3	String	فصيلة الدم	Cbtype
	20	Date	تاريخ الشفاء	Chtime
	1	Integer	وسيلة الاتصال	Cctype
	20	String	وقت الاتصال	Cctime
	30	Date & Time	تاريخ ووقت التسجيل	Ctoday

6. تنفيذ ونتائج التطبيق

سوف يتم فيما يلي استعراض معظم وظائف واجهات التطبيق المقترح التي يقوم بها التطبيق حيث تمت عملية التنفيذ باستخدام بيئة التطوير (Android Studio) بالاعتماد على مجموعة ادوات (SDK Software Development Kit) وهي تعني مجموعة تطوير البرامج وهي عبارة عن مجموعة أدوات تمكّن المطورين من إنشاء تطبيقات لنظام التشغيل Android. يتضمن المكتبات المطلوبة لإنشاء تطبيقات Android ، ومصحح أخطاء ، ومحاكي ، وواجهات برمجة التطبيقات و توفر مجموعة من الوظائف للتواصل مع قاعدة بيانات FireBase التي توفرها شركة Google (4).

عند فتح التطبيق سوف تظهر شاشة الترحيب لعدة ثواني كما موضح في الشكل (5) ثم تُفتح شاشة المتبرعين كما موضح بالشكل (6) التي يمكن من خلالها البحث على فصيلة دم محددة كما يمكن التواصل مباشرة مع المتبرع اما بالاتصال الهاتفي او ارسال رسالة نصية او عن طريق استخدام تطبيق Whatsapp بالطبع على حسب وسائل

الاتصال التي اختارها المتبرع عند التسجيل بالتطبيق كما يمكن الضغط على زر اضافة الذي يحتوي على الخيارات (الإضافة والتعديل والحذف) للمتبرع كما موضح بالشكل (7) ولا يمكن تنفيذ أي خيار من الخيارات السابقة الا بتأكيد على ملكية رقم الهاتف المدخل من قبل المستخدم. كما يمكن التطبيق مستخدميه من البحث عن فصيلة دم محددة كما موضح بالشكل (8).

شكل (6) شاشة المتبرعين

شكل (5) شاشة تشغيل البرنامج

شكل (8) توضيح إمكانية البحث باستخدام فصيلة الدم

شكل (7) توضيح زر الخيارات

شكل (9) شاشة حول التطبيق   شكل (10) شاشة توضح شروط التبرع

شكل (11) شاشة توضح فوائد التبرع

وما تم تنفيذه للمستخدم من نوع متبرع تم تطبيقه على المستخدم من نوع طلب فصيلة بالإضافة الى مستخدم من نوع متعافي كورونا وفيما يلي الشاشات الارشادية الخاصة بمستخدمي التطبيق حيث ان الشكل (9) يوضح شاشة حول التطبيق و الشكل (10) يوضح شاشة شروط التبرع بالإضافة الى الشكل (11) يوضح شاشة فوائد التبرع.

International Science and
Technology Journal
المجلة الدولية للعلوم والتقنية

العدد 26
Volume 26

المجلة الدولية للعلوم والتقنية
International Science and Technology Journal
ISTJ

7. الخلاصة

من خلال ما توصلنا إليه في هذه الورقة وبعد تمت عملية تجربة النظام توصلنا الى ان هذا التطبيق يتسم بسهولة الاستخدام و سرعة الوصول إلى البيانات و بساطة الواجهات و المرونة في التعامل مع البيانات كما يمكن توسعة نطاق عمله ليخدم جميع المواطنين بليبيا بالإضافة الى انه يعتبر اكثر امنا من التطبيقات الموجودة حاليا وتعمل داخل بلادنا بالإضافة الى إمكانية الوصول إلى البيانات التي تم تحميلها مسبقا في حال انقطاع الاتصال بالإنترنت كما يتيح لمستخدمي التطبيق اكثر من وسيلة تواصل مثل الاتصال المباشر او رسائل النصية او استخدام تطبيق Whatsapp للمراسلة.

8. المراجع

[1] M. N. Sahid Ramadhan, A. Amyus, A. N. Fajar, S. Sfenrianto, A. F. Kanz, and M. S. Mufaqih, "Blood Bank Information System Based on Cloud Computing In Indonesia," J. Phys. Conf. Ser., vol. 1179, p. 012028, Jul. 2019, doi: 10.1088/1742-6596/1179/1/012028

[2] A. Casabuena et al., "BloodBank PH: A Framework for an Android-based Application for the Facilitation of Blood Services in the Philippines.," TENCON 2018 - 2018 IEEE Reg. 10 Conf. Jeju, Korea (South)., pp. 1637–1641, 2018, doi: 10.1109/TENCON.2018.8650395.

[3] K. Pagano, M. B., Hess, J. R., Tsang, H. C., Staley, E., Gernsheimer, T., Sen, N., ... & Alcorn, "Prepare to adapt: blood supply and transfusion support during the first 2 weeks of the 2019 novel coronavirus (COVID-19) pandemic affecting Washington State," Transfusion, vol. 60, no. 5, pp. 908–911, 2020..

[4] Ahmed A. Mostfa, Aya A. Alabass and Abdel-Nasser Sharkawy "Nineveh Blood: Android Based Blood Donation Application for Nineveh Governorate in Iraq ", AL-Rafidain

Journal of Computer Sciences and Mathematics, Pages 85-96, 2020.

[5] محمود القائد, "بنك الدم ليبيا", 2021. [Mobile app]. Available: https://play.google.com/store/apps/details?id=libyabloodbank.mahmoud.com.blood&hl=ar&gl=US.

[6] M. Armbrust et al., "A view of cloud computing," Commun. ACM, vol. 53, no. 4, pp. 50–58, Apr. 2010.

[7] L. Moroney, "Firebase Cloud Messaging," in The Definitive Guide to Firebase, Berkeley, CA: Apress, 2017, pp. 163–188.

[8] I. Fette and A. Melnikov, "The WebSocket Protocol," Dec. 2011. doi: 10.17487/rfc6455.

[9] J. Paul Cardle, "Android App Development in Android Studio" , Manchester Academic Publishers , England , 2017.

تأثير الركام الناعم على مقاومة الضغط للخرسانة العادية وخرسانة ذاتية الدمك

زينب عمر القضقاض
المعهد العالي للعلوم والتقنية/طرابلس
eng.civilz@yahoo.com

شريفة محمد الحمروني
المعهد العالي للعلوم والتقنية/طرابلس
Ahmed.elhamroni@gmail.com

ايمان امحمد الحمروني
المعهد العالي للعلوم والتقنية/طرابلس
imanelhamruni@gmail.com

الملخص

الركام الخشن هو أحد المكونات الأساسية للخرسانة ويحتل أكبر حجم في الخليط حيث يشغل حوالي (70-75) % من الخلطة الخرسانية [1]. ويؤثر بشكل كبير على تصميم مزيج الخرسانة وخصائصها مثل القوة، والحجم الأقصى والشكل وامتصاص الماء الذي يؤثر في الطلب على الماء، وكمية الأسمنت والركام الناعم في خليط الخرسانة.

وتهدف هذه الدراسة إلى معرفة تأثير رمل زليتن وسيدي السائح وجرينيليا على مقاومة الضغط للخرسانة العادية والخرسانة ذاتية الدمك.

الكلمات الدليلية: الخرسانة، خلطة خرسانية، مقاومة الضغط، المحتوى المائي، الأسمنت البورتلاندي

ABSTRACT

Coarse aggregate is one of the basic components of concrete and occupies the largest volume in the mixture (70-75) % [1]. Therefore, it significantly influences the concrete mixture design and properties such as strength, maximum size, shape and water absorption which affect the water demand and the amount of fine cement and fine aggregate in the concrete mixture.

This study aims to investigate the effect of utilization of Zliten, Sidi-Alsayeh and Greenilia sand on the compressive strength of normal and self-compacting concrete.

International Science and Technology Journal
المجلة الدولية للعلوم والتقنية

العدد 26
Volume 26

المجلة الدولية للعلوم والتقنية
International Science and Technology Journal
ISTJ

Key boards: Concrete, mixture concrete, compressive strength, water content, Portland cement

1. المقدمة

الخرسانة هي بنيان وتتركب من عدة مواد والجزء الأكبر في هذا البنيان هو الركام الذي يتماسك مع بعضه في صورة شبيهة بالكتلة الحجرية ويتضح من ذلك أن الركام هو المكون الأساسي لجسم الخرسانة. والركام يعتبر مادة رخيصة نسبيا بالإضافة إلى أنه يعمل على تقليل التغير الحجمي للخرسانة الناتج من عمليتي الشد والتصلد. الخرسانة في حالة المتصلدة تبدو كمادة صخرية ذات مقاومة عالية للضغط أما في حالتها الطازجة فلها خاصية اللدونة التي تسمح بتشكلها في أي قالب معماري مطلوب [1].

تعد الخرسانة ذاتية الدمك واحدة من أهم التطورات في تكنولوجيا الخرسانة والبناء في الوقت الحالي وذلك لقدرة الخرسانة الذاتية الدمك على التدفق الحر في القوالب وعلى رص نفسها بنفسها وعلى طرد الهواء المحصور دون استخدام الهزازات [2,3,4] وأن قدرة الخرسانة ذاتية الدمك على التحمل هو نتيجة الكثافة العالية والحد من الفراغات بشكل ممتاز وكذلك الحد من ظاهرة النضح بالإضافة إلى زيادة قوة التلاصق بين الخرسانة وحديد التسليح، حيث أثبتت الاختبارات أن الخرسانة ذاتية الدمك تعطي تلاصق أعلى بنسبة (50-70%) بالمقارنة مع الخرسانة التقليدية التي يتم دمكها بالكامل بالإضافة إلى المقاومة العالية.

كما تعتبر الخرسانة ذاتية الدمك غير مكلفة اقتصاديا ولكنها ذات كثافة عالية ومن جانب أخر فإنها تختزل كافة عمليات الدمك المتبعة في حالة الخرسانة التقليدية وتقلل تأثير الضوضاء في موقع العمل، كما أن هذه الخرسانة تساعد المصممين على إمكانية أنجاز الأشكال المعقدة المكتظة بحديد التسليح والتي يصعب دمكها بالهزازات في حالة الخرسانة العادية، للحصول على خرسانة بجودة عالية يجب التمعن في اختيار المواد المكونة لها وحيث أن الركام يشغل حيزا كبيرا في الخلطة الخرسانية. وهذه الدراسة استهدفت مقارنة تأثير استخدام الرمل المستعمل في السوق المحلية متمثلة في رمل

International Science and
Technology Journal
المجلة الدولية للعلوم والتقنية

العدد 26
Volume 26

المجلة الدولية للعلوم والتقنية
International Science and Technology Journal
ISTJ

زليتن ورمل سيدي السائح وجرينيليا على مقاومة الضغط للخلطة الخرسانية العادية وذاتية الدمك.

الدراسات السابقة

1- في دراسة سابقة استهدفت مقارنة بين تأثير استخدام رمل الشاطئ (منطقة زليتن) ورمل الكثبان الرماية (منطقة سيدي السائح) على خواص الخرسانة والتي بينت أن رمل الشاطئ أعطى مقاومة ضغط للخرسانة أعلى منها في رمل الكثبان، وأرجع الباحث ذلك إلى التوزيع الجزيئي الأفضل لحبيبات رمل الشاطئ وكذلك شكل الحبيبات وحجمها [5].

2-وفي دراسة أخرى استهدفت اختيار مدى تأثير رمل زليتن ورمل بورويه مصراته دون خلطه بأي أنواع أخرى من الرمل في الخرسانة الذاتية الدمك، كانت النتائج متفاوتة ولكن عند معالجة الركام الناعم بإضافة الركام المجروش (الجرينيليا) ظهر تحسن في الانسياب في كلتا الخلطتين إلا أن الخلطة المنفذة برمل (بورويه) كان انسيابها الأفضل [6].

من الدراسات السابقة تبين انه لم يتم تقييم تأثير كلا من استخدام الجرينيليا في الخرسانة العادية ورمل سيدي السائح في الخرسانة الذاتية الدمك وهما نوعيين مستخدمان في السوق المحلي.

المواد المستخدمة والتجارب المعملية

أولا المواد المستخدمة

الأسمنت

تم استخدام الأسمنت البورتلاندي العادي طبقا للمواصفات البريطانية للخرسانة العادية والخرسانة ذاتية الدمك.

الماء

يجب أن يكون الماء المستخدم في الخلطة الخرسانية خالي من الزيوت والشحوم والأحماض والأملاح والقلويات والمواد العضوية، وقد تم استخدام مياه صالحة للشرب وبذلك فهي صالحة للاستخدام في الخلطات الخرسانية.

International Science and
Technology Journal
المجلة الدولية للعلوم والتقنية

العدد 26
Volume 26

المجلة الدولية للعلوم والتقنية
International Science and Technology Journal
ISTJ

1- يوصي باستخدام مياه الشرب لصنع الخلطة الخرسانة ويجب أن يكون الرقم الهيدروجيني للماء المستخدم في الخلطة الخرسانية في حدود من 6 إلى 8.

2- يجب أن يكون الماء نظيفا وخاليا من الزيوت والأحماض والقلويات والأملاح والمواد العضوية وما إلى ذلك.

3- وجود هذه الشوائب يؤدي إلى تأكل الفولاذ أو تدهور الخرسانة من خلال تفاعلات كيميائية مختلفة.

الركام الناعم

تم استخدام ثلاث أنواع من الركام الناعم وهي: الركام الناعم الطبيعي المستجلب من محاجر منطقة زليتن والركام الناعم الطبيعي المستجلب من محاجر منطقة سيدي السايح والركام المجروش (جرينيليا) المستجلب من محاجر القديح بمنطق اسبيعة.

الركام الخشن

الركام الخشن مادة صلبة وهي تشكل مع الماء والأسمنت والرمل المكونات الأساسية من اجل خلطة خرسانية ذات جودة عالية يجب ان يكون الركام نظيف وقوي، وغير مغطى بإي نوع من أنواع الطين، تكون جزيئات الركام خالية من الكيماويات، وفي هذه الدراسة تم استخدام عينتين من الركام الخشن رقم (1,1.5) من محاجر قريبة من مدينة طرابلس.

التجارب المعملية

تجرى الاختبارات الخاصة لكل من الركام الخشن والرمل (سيدي السائح، زليتن، جرينيليا) بهدف معرفة خواصهم.

1- التجارب التي أجريت على الركام الخشن(1و1.5) وهي اختبار معامل الصدم والتهشيم ونسبة الامتصاص ووزن وحدة الحجوم واختبار الوزن النوعي والنتائج موضحة في الجدول رقم (2)، (3).

2- التجارب التي أجريت على الركام الناعم (سيدي السائح، زليتن، جرينيليا) هي اختبار معامل النعومة والوزن النوعي واختبار وزن وحدة الحجوم والنتائج موضحة في الجدول رقم (1).

International Science and
Technology Journal
المجلة الدولية للعلوم والتقنية

العدد 26
Volume 26

المجلة الدولية للعلوم والتقنية
International Science and Technology Journal
ISTJ

3- تصميم ثلاث خلطات خرسانية مختلفة باختلاف نوع الرمل مع ثبات نسبة الماء للأسمنت التي استنتجت من تصميم الخلطات الخرسانية بالطريقة البريطانية وفقا للمواصفات البريطانية (BS:882,1985) وكانت في خلطات الخرسانة العادية (W/C=0.68) وفي الخرسانة ذاتية الدمك (W/C=0.45) كما موضح في الجداول رقم (4,5) الذي يوضح مقاومة الضغط لمكعبات خرسانية أبعادها (150*150*150) ملم بعد 28 يوم.

الركام الناعم

ثم استخدام الركام الناعم الطبيعي من محاجر منطقة زليتن وسيدي السائح ورمل جرينيليا والجدول رقم (1) يوضح الخواص الفيزيائية للركام الناعم.

جدول رقم (1) الخواص الفيزيائية للركام الناعم

المواصفة الليبية (م.ق.ل) 2002:49	النتائج	الاختبارات
2.7-2.6	2.69	الوزن النوعي لرمل سيدي السائح
2.7-2.6	2.63	الوزن النوعي لرمل زليتن
2.7-2.6	2.63	الوزن النوعي لرمل جرينيليا
1800-1400	1650.5	وزن وحدة الحجوم لرمل سيدي السائح
1800-1400	1569.5	وزن وحدة الحجوم لرمل جرينيليا
1800-1400	1542	وزن وحدة الحجوم لرمل زليتن
1.4-1.8	1.715	معامل النعومة لرمل سيدي السائح
1.4-1.8	1.49	معامل النعومة لرمل زليتن
1.4-1.8	2.427	معامل النعومة لرمل جرينيليا

الركام الخشن

تم استخدام الركام الخشن رقم (1,1.5) والجدولين (2,3) يوضحان نتائج الاختبارات الفيزيائية والميكانيكية للركام الخشن (1,1.5)

International Science and
Technology Journal
المجلة الدولية للعلوم والتقنية

العدد 26
Volume 26

المجلة الدولية للعلوم والتقنية
ISTJ

جدول رقم (2) نتائج الاختبارات الفيزيائية والميكانيكية للركام الخشن رقم 1.0

الاختبارات	النتائج	المواصفة الليبية (م.ق.ل) 2002:49
الوزن النوعي	2.69	2.6-2.7
وزن وحدة الحجوم	1416.6	1400-1800
نسبة الامتصاص	1.7%	لا تزيد عن 3%
معامل التهشيم	6.87%	لا تزيد عن 45%
معامل الصدم	13.28%	لا تزيد عن45%

جدول رقم (3) نتائج الاختبارات الفيزيائية والميكانيكية للركام الخشن رقم 1.5

الاختبارات	النتائج	المواصفة الليبية (م.ق.ل) 2002:49	المواصفة الليبية (م.ق.ل) 2002:49
الوزن النوعي	2.69	2.6-2.7	2.6-2.7
وزن وحدة الحجوم	1366.6	1400-1800	1400- 1800 كجم/م3
نسبة الامتصاص	1.01%	لا تزيد عن 3%	
معامل التهشيم	5.17%	لا تزيد عن 45%	
معامل الصدم	17.52%	لا تزيد عن45%	

جدول رقم (4) يوضح نسب وأوزان الخلطات الخرسانية المختلفة للمتر المكعب للخرسانة العادية

MIX	W/C Ratio	C Kg/m	W Kg/m	FA Kg/m	CA (1) Kg/m	CA (1.5) Kg/m
M1 رمل سيدي السائح	0.68	1220	600	830	1620	1321
M2 رمل زليتن	0.68	330	425	598	850	364
M3 رمل جرينيليا	0.68	1310	710	810	1715	1420

CA (1) = الوزن النوعي للركام الخشن رقم (1)

CA (1.5) = الوزن النوعي للركام الخشن رقم (1.5)

FA = وزن الرمل   C = وزن الاسمنت   W= وزن المياه

International Science and
Technology Journal
المجلة الدولية للعلوم والتقنية

العدد 26
Volume 26

ISTJ

جدول رقم (5) يوضح نسب وأوزان الخلطات الخرسانية المختلفة للمتر المكعب للخرسانة
ذاتية الدمك

MIX	W/C ratio	C Kg/m	W Kg/m	FA Kg/m	CA (1) Kg/m	CA (1.5) Kg/m
M1 رمل زليتن	0.45	433	178	780	1034	1034
M2 رمل سيدي السائح	0.45	480	206	633	934	934
M3 رمل جرينيليا	0.45	422	190	880	882	882

العلاقة بين مقاومة الضغط وعدد الأيام للخلطات الثلاثة لعينة رمل جرينيليا (خرسانة عادية)
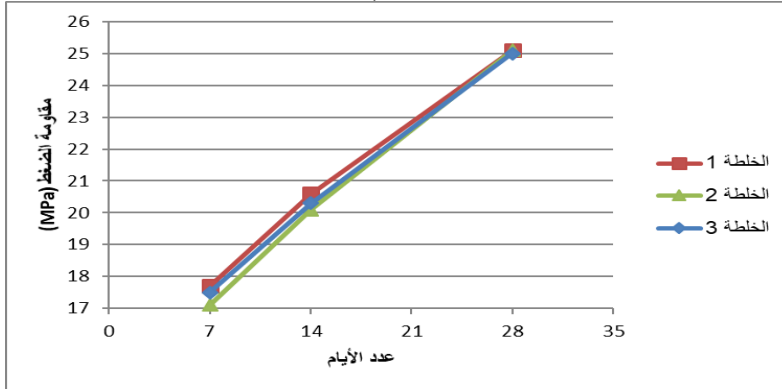
الشكل رقم (1) يوضح العلاقة بين مقاومة الضغط وعدد الأيام لخرسانة عادية باستخدام رمل
جرينيليا

International Science and
Technology Journal
المجلة الدولية للعلوم والتقنية

العدد 26
Volume 26

المجلة الدولية للعلوم والتقنية
International Science and Technology Journal
ISTJ

العلاقة بين مقاومة الضغط وعدد الأيام للخلطات الثلاثة لعينة رمل زليتن (خرسانة عادية)
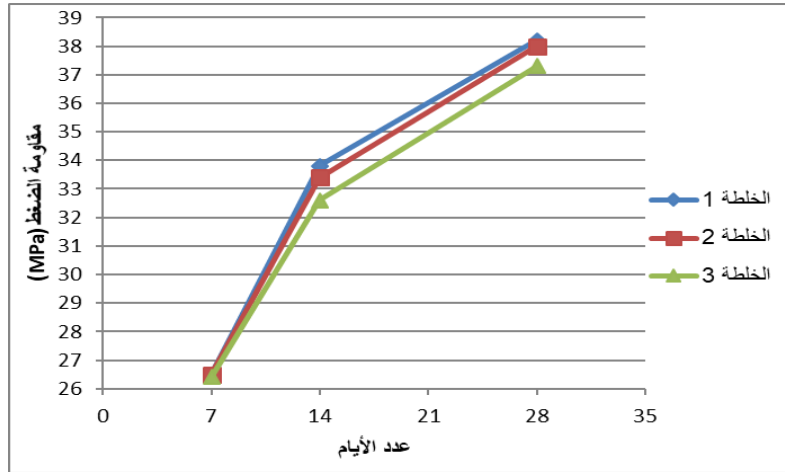
الشكل رقم (2) يوضح العلاقة بين مقاومة الضغط وعدد الأيام لخرسانة عادية باستخدام رمل زليتن

العلاقة بين مقاومة الضغط وعدد الأيام للخلطات الثلاثة لعينة رمل سيدي السائح (خرسانة عادية)

International Science and
Technology Journal
المجلة الدولية للعلوم والتقنية

العدد 26
Volume 26

ISTJ
المجلة الدولية للعلوم والتقنية
International Science and Technology Journal
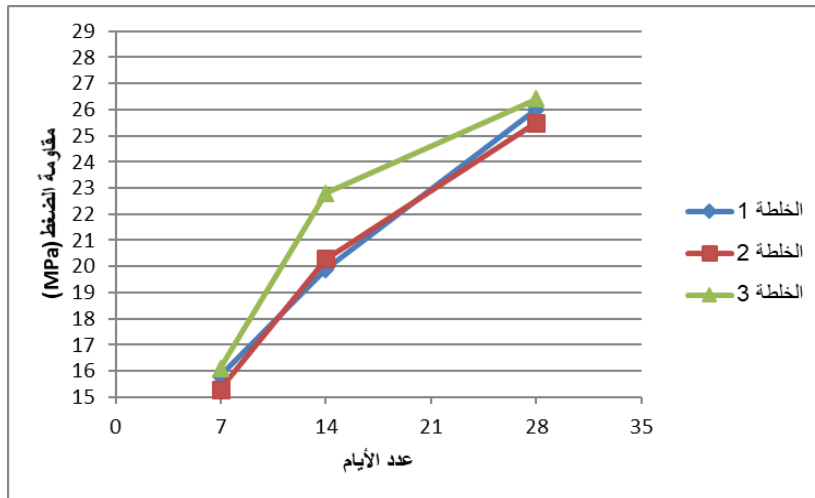
الشكل رقم (3) يوضح العلاقة بين مقاومة الضغط وعدد الأيام لخرسانة عادية باستخدام رمل سيدي السائح

العلاقة بين مقاومة الضغط وعدد الأيام للخلطة الخرسانية رقم (1) لخرسانة ذاتية الدمك
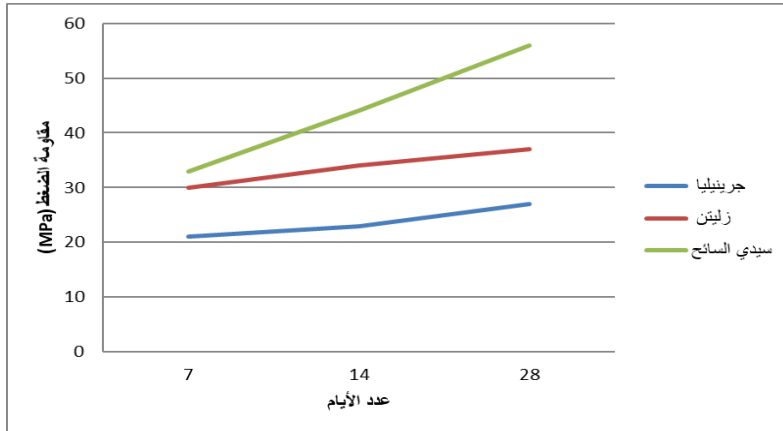
الشكل رقم (4) يوضح العلاقة بين مقاومة الضغط وعدد الأيام لخرسانة ذاتية الدمك للخلطة رقم (1)

العلاقة بين مقاومة الضغط وعدد الأيام للخلطة الخرسانية رقم (2) لخرسانة ذاتية الدمك
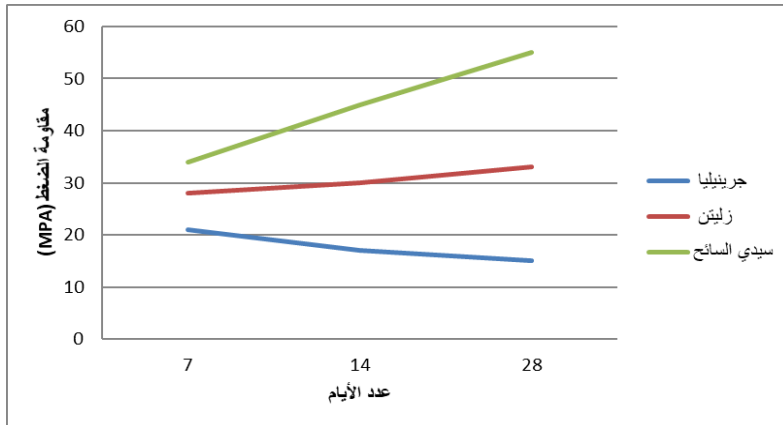
الشكل رقم (5) يوضح العلاقة بين مقاومة الضغط وعدد الأيام لخرسانة ذاتية الدمك للخلطة رقم (2)

International Science and
Technology Journal
المجلة الدولية للعلوم والتقنية

العدد 26
Volume 26

المجلة الدولية للعلوم والتقنية
International Science and Technology Journal
ISTJ

العلاقـة بين مقاومـة الضـغط وعدد الأيـام للخلطـة الخرسانية رقم (3) لخرسـانة ذاتيـة الدمك
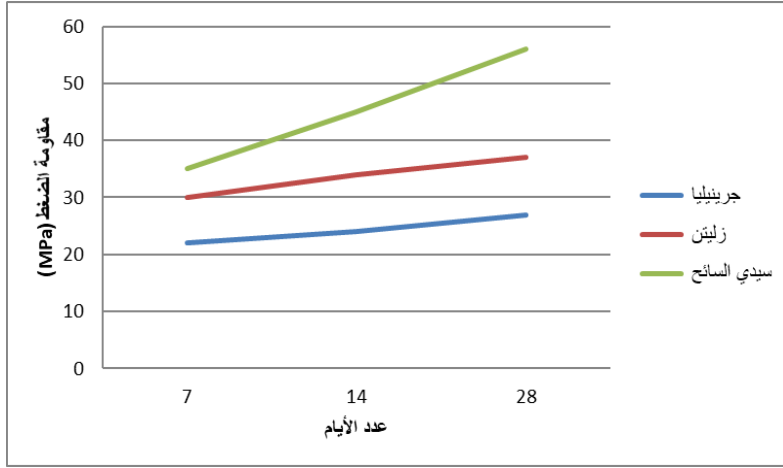
الشكل رقم (6) يوضح العلاقة بين مقاومة الضغط وعدد الأيام لخرسانة ذاتية الدمك
للخلطة رقم (3)

مناقشة النتائج

1– من الأشكال (1,2,3) أن الخرسانة العادية كانت مقاومة الضغط لرمل زليتن
أعطت أعلى النتائج بعد 28 يوم وكانت (38.5ميجاباسكال).

2– بينما في الخرسانة ذاتية الدمك الأشكال (4,5,6) أعطت رمل سيدي السائح أعلى
النتائج في مقاومة الضغط بعد 28 يوم وكانت (50ميجاباسكال).

3– نتائج الخواص الميكانيكية والفيزيائية للركام الخشن رقم (1,1.5) كانت ضمن
المواصفات كما موضحة في الجدول رقم (3,2).

4– نتائج الخواص الميكانيكية والفيزيائية للركام الناعم كانت ضمن المواصفات كما
موضحة في الجدول رقم (1).

الاستنتاجات

وفقا للاختبارات والنتائج التي أجريت على الخرسانة ذاتية الدمك يستخلص الآتي: –

International Science and
Technology Journal
المجلة الدولية للعلوم والتقنية

العدد 26
Volume 26

المجلة الدولية للعلوم والتقنية
International Science and Technology Journal
ISTJ

1-مقاومة الضغط عالية في خليط رمل زليتن مع خليط الركام في الخرسانة العادية أي مقاومة ضغطها أعلى من خليط الخرسانة التي بها رمل سيدي السائح وجرينيليا.

2- مقاومة الضغط عالية في خليط رمل سيدي السائح مع خليط الركام في الخرسانة ذاتية الدمك أي مقاومة ضغطها أعلى من خليط الخرسانة التي بها رمل زليتن وجرينيليا.

3- معامل النعومة ليس له تأثير في مقاومة الضغط فنلاحظ في رمل زليتن كان معامل النعومة (1.49) وكانت مقاومة الضغط أعلى من الخلطة الخرسانية التي بها رمل جرينيليا التي معامل نعومتها (2.427) في الخرسانة العادية.

4- مقاومة الضغط للخلطة الخرسانية لرمل سيدي السائح الذي معامل نعومته (1.715) أعلى من مقاومة الضغط للخلطة الخرسانية برمل جرينيليا الذي معامل نعومته (2.427).

المراجع

[1] محمود امام (2002)، خواص الخرسانة والجودة والاختبارات، مصر: جامعة المنصورة.

[2] Alireza k, John L et al. Effect of molecular architecture of polycarboxylate ethers on plasticizing performance in alkali-activated slag paste (J). J Mater Sci, 2014(49):2461-2772

[3] Alone M, Palacios M, et al. compatibility between polycarboxylate-based admixtures and blended-cement pastes (J). Cement and concrete composites,2013, (35):151-162

[4] Yamada K, Takahashi T,HaneharaS,et al. Effects of the chemical structure on the properties of poly carboxylate-type Super plasticizer(J). Cement and concrete Research,2000,30)2):197-207.

[5] S.Alsadey, A.Omran, Effect of the Type of Sand on the Properties of Concrete, Journal of Engineering and Applied Sciences Vol.16, March (2021), pp. 111-113.

[6] فاطمة المزوغي (2019)، المشاكل المصاحبة لإنتاج الخرسانة ذاتية الدمك، المؤتمر الثاني للعلوم الهندسية والتقنية: صبراته.

مقارنة بين أهم أدوات محاكاة أداء المبني
Comparison Between Important Building Performance Simulation tools

د. نضال فتحي إبراهيم   د. إيمان عطية يوسف   د. أمال سعيد الفيتوري
أغفير   ساسي   احسيرات

كلية الفنون والعمارة _ جامعة عمر المختار

ahsairat@gmail.com   emansasi77@gmail.com   Ankara5566@yahoo.com

الملخص:

محاكاة أداء المبنى Building Performance Simulation هي عملية تطوير نموذج مبسط لمبنى ذو نظام معقد واستخدام النموذج لتحليل المؤثرات البيئية من إضاءة ودرجة حرارة ورطوبة قبل تنفيذه على أجهزة كمبيوتر ببرامج معينة تسمي أدوات محاكاة Simulation Tools يتم استخدامها من قبل المعماريين والمهندسين بهدف مساعدتهم في التقييم أثناء عملية التصميم وقبل التنفيذ. أهمية المحاكاة ترجع إلي إنها توفر لمصممي المباني المعلومات التي يحتاجونها للتنبؤ بالمؤثرات البيئية المحيطة بالمبنى مثل حركة الهواء وعمليات نقل الحرارة داخل وحول المباني و الظروف الحدودية مثل تأثير المناخ وقياس كفاءة الطاقة Energy Efficiency مصادر الطاقة الداخلية وأنظمة التدفئة والتهوية وتكييف الهواء وتستخدم المحاكاة أيضًا عندما يكون النظام الحقيقي للمبنى شديد التعقيد مثل المباني الحديثة ذات المساحات الكبيرة. هدف هذه الدراسة عرض أهم أدوات المحاكاة Simulation Tools شائعة الاستخدام في العالم المتطور في الوقت الحاضر وعرضها وتسليط الضوء على أهميتها . منهجية الدراسة تعتمد على تحليل الدراسات السابقة في العقد الماضي كما تقدم مقارنة لخمس أدوات محاكاة Simulation Tools شائعة الاستخدام في التقييم داخل عملية التصميم وذلك من خلال تحديد الجوانب الإيجابية والسلبية للأدوات بهدف اختيار أفضل أداة للاستخدام المتقدم. الأدوات التي تم فحصها تشمل DesignBuilder و ECOTECT و HEED و IES VE و BSim. تستند المقارنة

إلى معايير تشمل الخبرة المطلوبة و المستخدمون و التعلم و السرعة و الدقة، الهدف الرئيسي و البرامج المستخدمة و إيجابية للاستخدام و سلبية للاستخدام. ستكون نتيجة هذه الدراسة مهمة للمعماريين والمهندسين بهدف مساعدتهم في تصميمهم أثناء عملية التصميم في المستقبل ومجارة العالم المتطور في هذا المجال .

الكلمات المفتاحية : محاكاة أداة المبنى Building Performance Simulation _ Energy Efficiency _أدوات المحاكاة Simulation Tools_أسماء أدوات المحاكاة Design Builder و ECOTECT و HEED و IES VE و BSim

Abstract:
Simulation is a method for the implementation of a model over time, [1] Performance simulation is "the process of developing a simplified model of a complex system and using the model to analyze and predict the behavior of the original system." [2] It is using by architects and engineers in the aim to help them in their design during the design process. Simulation is used in many contexts, for example, it gives building designers information they need for detailed prediction of air flow and heat transfer processes in and around building spaces –boundary conditions such as effect of climate, internal energy sources. Simulation is also used when the real system is very a complex.

So, this paper will describe some simulation tools which are important for advanced studies nowadays. The paper will compare five tools which they need for design process. By Defines the positive and negative of the tools in the aim to choose the best tool for advanced using as result of this paper, so the examined tools include Design Builder, ECOTECT, HEED, IES VE and BSim. The comparison is based on five criteria including; Expertise Required, Users, learn, speed, Accuracy, Main aim, Programs to use, Positive to use, and Negative to use. The result for this study will be important for architects and engineers in the aim to help them in their design during the design process in future.

Key word: Simulation Tools -Building Performance simulation- Design Process- Design Builder, ECOTECT, HEED, IES VE and BSim.

منهجية الدراسة :

اعتمدت منهجية الدراسة على استعراض الدراسات السابقة لموضوع الدراسة ومقارنة نتائجها للوصول إلي استنتاج خاص بالدراسة يهدف للتعرف على أفضل أدوات المحاكاة لتشجيع المتخصصين على استخدامها في عملية التصميم نتيجة فائدتها الكبيرة و لنشر المعرفة في هذا المجال.

الهدف من الدراسة :

▪ عرض أهم أدوات المحاكاة Simulation Tools للتعرف على ايجابياتها وسلبياتها والتعريف على كيفية التعامل معها .

▪ مقارنة أدوات المحاكاة Simulation Tools للتعرف على أهم الأدوات من ناحية سهولة الاستخدام وأكثرها معالجة للبيئة.

▪ مواكبة العصر في استخدام أدوات المحاكاة Simulation Tools المتطورة والتعرف على طرق معالجة المبنى بيئيا قبل إنشاءه لتفادي أي مشاكل بيئية الأمر الذي يساعد في خلق بيئة مبنية ناجحة ومريحة حراريا .

أهمية الدراسة :

▪ تستعرض الدراسة تعريفات مهمة لأهم أدوات المحاكاة Simulation Tools المعروفة عالميا والمستخدمة في توضيح علاقة المبنى بالبيئة المحيطة .

▪ التعرف على إمكانيات هذه الأدوات من حيث إمكانية التحكم البيئي من خلال برامج هندسية مساعدة في تقييم الإضاءة والتهوية ودرجات الحرارة قبل تنفيذ المبنى حتى يساعد في خلق فضاء داخلي مريح بيئيا للمستخدمين.

▪ تفيد نتائج هذه الدراسة المتخصصين في مجال الهندسة المعمارية وتعرفهم على أفضل أدوات المحاكاة المعروفة عالميا لفعاليتها العالية في تقييم أداء المبني قبل التنفيذ .

International Science and
Technology Journal
المجلة الدولية للعلوم والتقنية

العدد 26
Volume 26

ISTJ

■ تشجيع المتخصصين على استخدام هذه البرامج نتيجة سهولة استخدامها مع عظم فائدتها في توفير فضاء مريح للعيش من ناحية الحرارة والإضاءة والتهوية .

1. المقدمة :

عرفت أدوات المحاكاة بأنها "طريقة لتنفيذ نموذج هندسي قبل التنفيذ ووضعه تحت الاختبار بيئيا لتفادي أي مشاكل على ارض الواقع لاحقا " [1] ، وترجع أهمية برامج محاكاة أداء الطاقة المستخدمة على نطاق واسع في الوقت الحاضر لكونها أدوات فعالة لدراسة أداء الطاقة والراحة الحرارية خلال دورة حياة المبنى. علاوة على ذلك، فإنها توفر لمصممي المباني المعلومات التي يحتاجونها للتنبؤ المفصل بتدفق الهواء وعمليات نقل الحرارة داخل وحول مساحات المباني والظروف الحدودية مثل تأثير المناخ ومصادر الطاقة الداخلية وأنظمة التدفئة والتهوية وتكييف الهواء. لذلك تصف هذه الدراسة خمس أدوات للطاقة بهدف المقارنة بينها بشكل عام، وطريقة استخدام البرامج، وتشمل هذه المقارنة وقت الاستخدام و عدد المستخدمين، والهدف من الاستخدام كما سوف نستعرض لاحقا.

2. الدراسات السابقة :

استعراض مقدمة تعريفية للبرامج المحاكاة المختارة في هذه الدراسة :

■ استعراض مهم للأدوات المحاكاة Simulation Tools مثل Design Builder–ECOTECT– HEED– IES VE –BSim كما موضح بالشكل (1) :

■ استعراض للدراسات السابقة عن تعريف البرنامج وهدف البرنامج وماهية المدخلات والمخرجات بشكل عام للتعرف على إمكانيات كل برنامج من مميزات وعيوب.
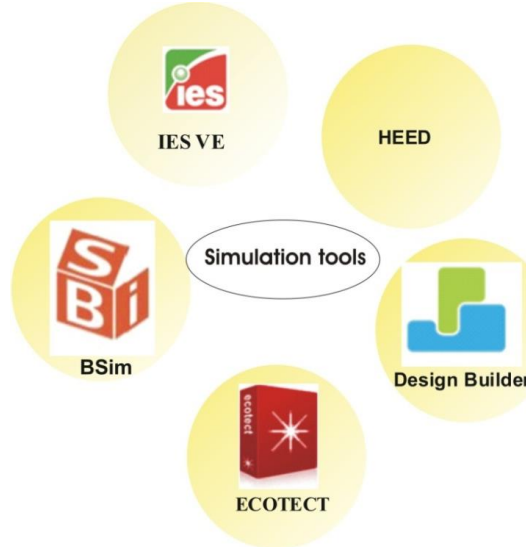
شكل (1) أدوات المحاكاة المطروحة للدراسة (المصدر البحاث) .

▪ **طرق استعمال برامج المحاكاة بشكل عام** : في الغالب تستخدم المحاكاة خلال مرحلة التصميم و قبل مرحلة التنفيذ:

1. تحميل البرنامج المحدد على الجهاز المعد للمحاكاة حيث أن جميع البرامج متوفرة على شبكة الانترنت ومحضرة للتحميل.
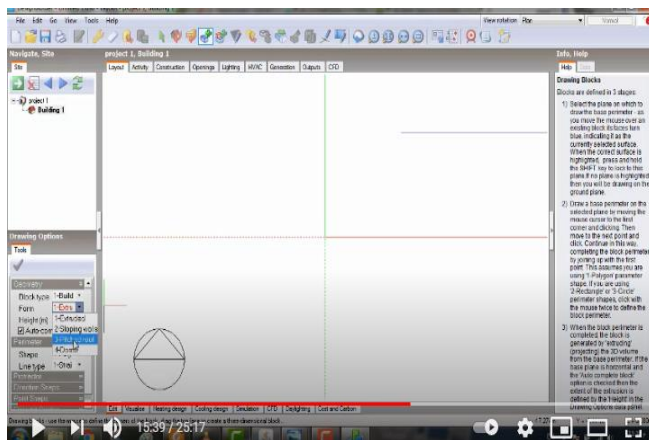

شكل (2) شاشة البرنامج قبل تنزيل المدخلات .

2. تحديد موقع المبنى حتى نسمح للبرنامج بالتعرف على المناخ العام الخاص بالموقع وعليه يقوم البرنامج مباشرة بتنزيل كافة البيانات المناخية للموقع مثلا سرعة الرياح ودرجات الحرارة والرطوبة والتوجيه للشمسي على مدار السنة في الموقع المحدد.
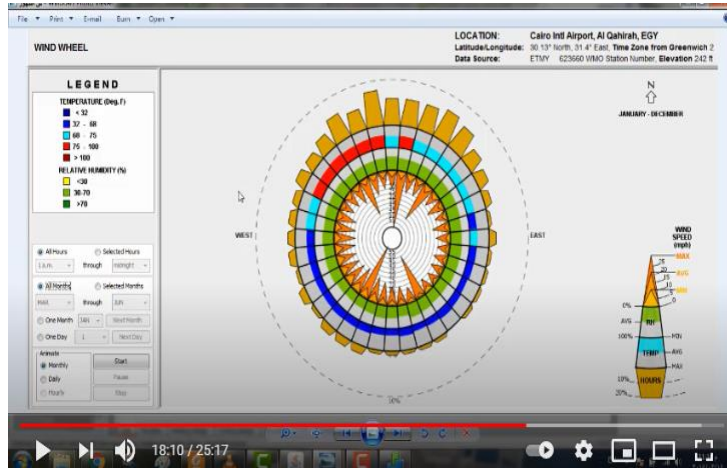
شكل (3) التعرف على بيانات المناخ للموقع المراد تقييم أداء المبنى به مثال (تقييم سرعة الرياح).

3. رسم المبنى هندسيا على البرنامج المختار حسب متطلبات البرنامج من رسم المبنى باتجاهين 2D او 3D

4. تحديد حجم وشكل الفتحات والتفاصيل الداخلية لكل طابق على حده أو لكل فضاء على حدة كمدخلات للبرنامج Input.
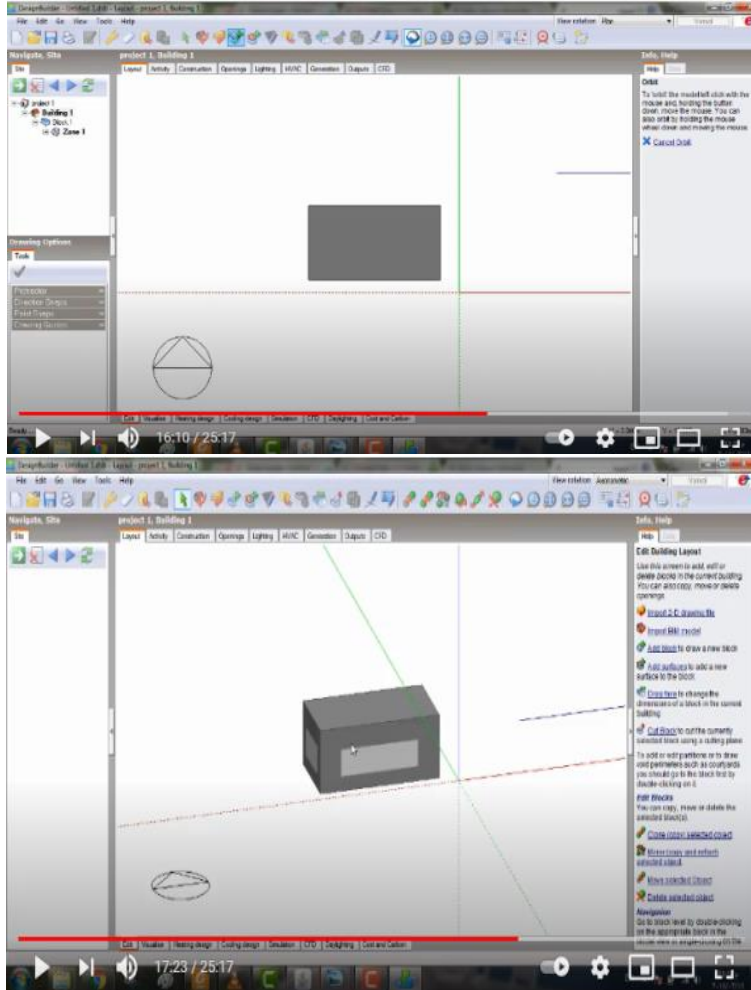
شكل (4) رسم المبنى هندسيا على البرنامج بالبعد الثالث لتوضيح مواقع الفتحات .

5.‏ إعطاء أمر للبرنامج لتطبيق المحاكاة ومن ثم تظهر المخرجات وهي Output على شكل رسم هندسي ثلاثي الأبعاد يوضح عليه حركة الشمس والظلال أو حركة الرياح وجداول ورسومات بيانية بدرجات الحرارة ووردة الرياح .
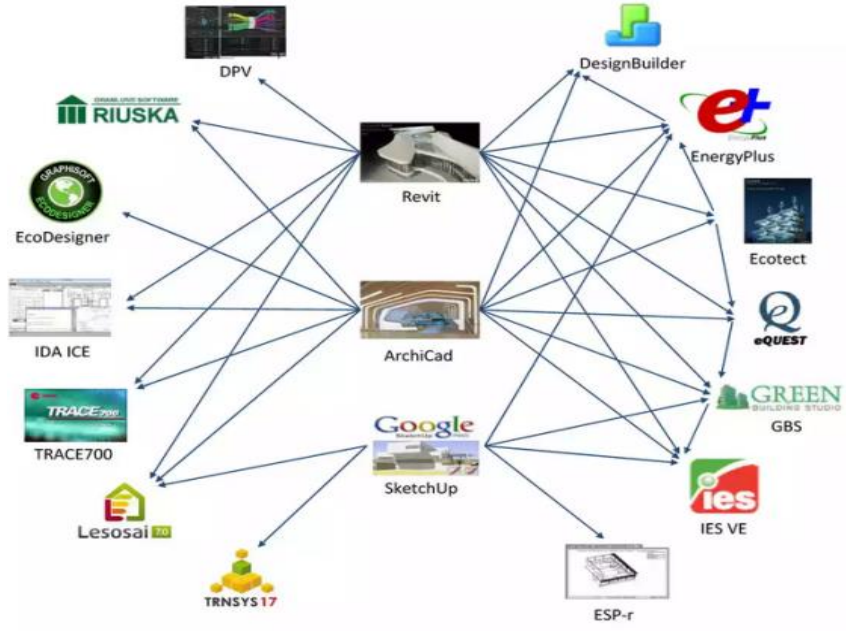
International Science and Technology Journal
Technology Journal
المجلة الدولية للعلوم والتقنية

العدد 26
Volume 26

المجلة الدولية للعلوم والتقنية
International Science and Technology Journal
ISTJ
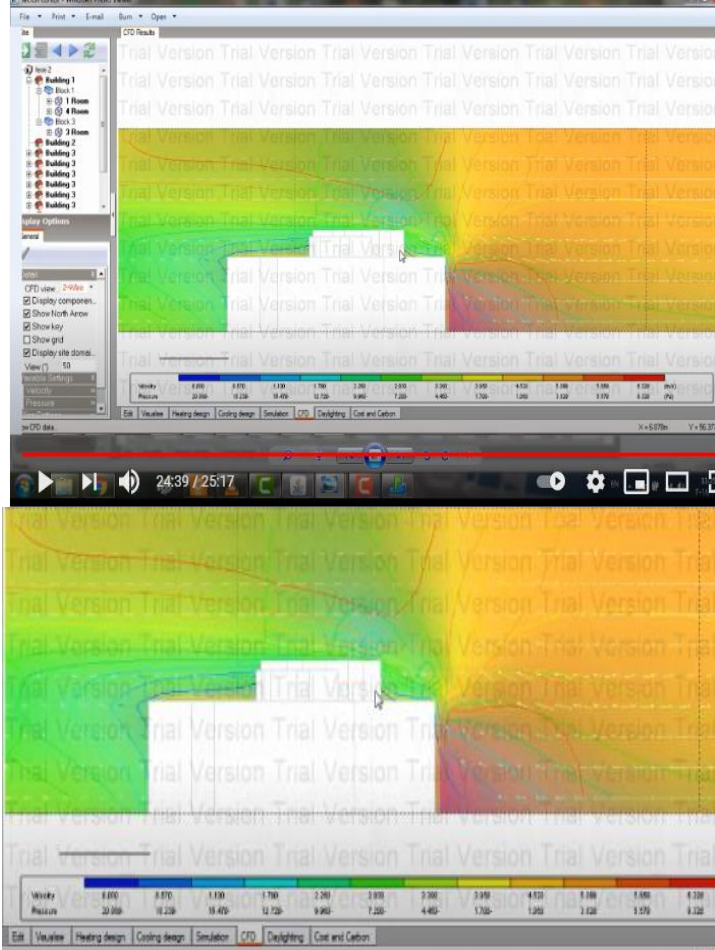
شكل (5) Output المخرجات الخاصة بتوضيح شكل الرياح وتأثيرها المباشر على المبنى.

6. ترجع أهمية هذه النتائج في التعرف على عيوب التصميم قبل التنفيذ لتلافي
أي أخطاء تؤدي إلى مشاكل بيئية غير مريحة لمستخدمين المبنى مستقبلا .
نموذج توضيحي لمدخلات برامج المحاكاة بشكل عام (input):

International Science and
Technology Journal
المجلة الدولية للعلوم والتقنية

العدد 26
Volume 26

المجلة الدولية للعلوم والتقنية
International Science and Technology Journal
ISTJ
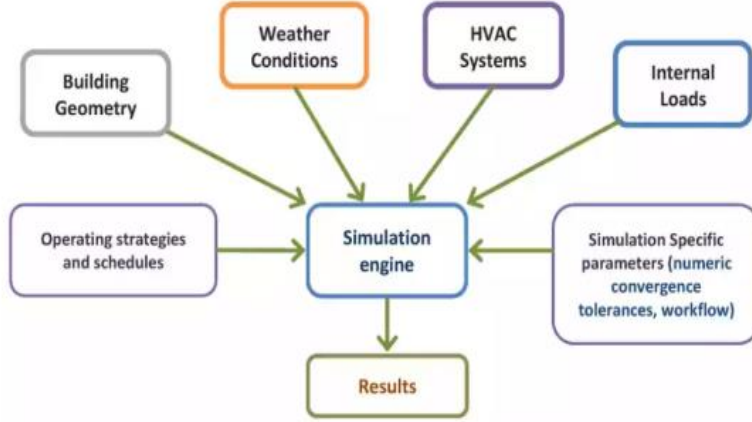
شكل (6) نموذج توضيحي لمدخلات Input برامج المحاكاة بشكل عام .

شكل (7) مثال لنوع البرامج الهندسية التي تساعد في تطبيق أدوات المحاكاة .

International Science and
Technology Journal
المجلة الدولية للعلوم والتقنية

العدد 26
Volume 26

المجلة الدولية للعلوم والتقنية
ISTJ
International Science and Technology Journal

اسم البرنامج : ECOTECT Tool

الرمز :

تعريف : ECOTECT هو برنامج فريد يستخدم من قبل المهندسين المعماريين كأداة تحليل (Performance analysis tools) في بدايات التصميم و وأيضا خلال مراحل التصميم. يستخدم البرنامج في البعد الثالث للمبنى مع عدد من أوامر التحليل . [3]ويظهر البرنامج بواجهة تصميم ثلاثية الإبعاد مع مجموعه من الأوامر لتحليل الأداء البيئي للمباني ثلاثية الإبعاد 3D building models من حيث الإضاءة والصوت والحرارة. [2]

الهدف الأساسي للبرنامج :

1. يستخدم في تحليل نماذج المباني ثلاثية الأبعاد من حيث: الإضاءة [1] و الراحة والأداء الصوتي والحراري والإضاءة والتضليل وتأثير المناخ والطاقة [4]

2. البرنامج يساعد المتخصصين في التعامل بمرونة مع إمكانيات التصميم واختبار المبنى هيكليا للتوصل إلى حل مثالي للتصميم قبل التنفيذ .

3. يستخدم في تحليل العناصر التي تؤثر على استدامة التصميم والهيكل المبنى للوصول إلى أفضل التصاميم التي تحقق المعايير البيئية . [2]

المدخلات Input: رسم ثلاثي الإبعاد للمبني 3D models يوضح هيكل المبنى الداخلي والخارج مع كافة تفاصيل المبنى من نوافذ وأبواب في البعد الثالث 3D [5]، لمعرفة أداء الحرارة، الإنارة، الصوت و تدفق الهواء داخل المبنى انظر الشكل (8):

نموذج توضيحي لمدخلات برامج المحاكاة بشكل عام (input):

International Science and
Technology Journal
المجلة الدولية للعلوم والتقنية

العدد 26
Volume 26

المجلة الدولية للعلوم والتقنية
International Science and Technology Journal
ISTJ

جدول 1 : توضح استعمال البرنامج والبرامج الهندسية المساعدة الداخلة في التقييم

البرامج الهندسية المساعدة	هدف المحاكاة	البرنامج Tool
Imports CAD-BIM models from most CAD software	التصميم البيئي ، النموذج ثلاثي الأبعاد (تصميم ثلاثي الأبعاد) ، التصميم والتحليل الحراري ، أحمال التسخين والتبريد ، التحقق من الصحة ؛ التحكم في الطاقة الشمسية ، التعتيم ، السائد ، تدفق الرياح والهواء ، الإضاءة الطبيعية والاصطناعية ، تقييم دورة الحياة ، تكلفة دورة الحياة ، الجدولة ، التحليل الصوتي الهندسي والإحصائي .	ECOTECT
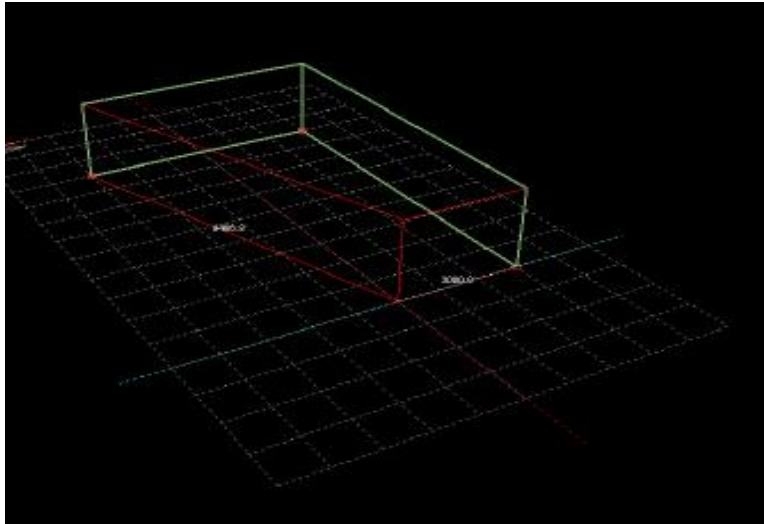
شكل (8) نموذج توضيحي مدخلات البرنامج input المبنى في بعده الثالث .

المخرجات Output : تحويل المعلومات لتحليل الوظائف الخاصة ECOTECT إلي رسومات بيانية 3D وجداول بيانية وبسهوله [5]، انظر الشكل (3):

Daylight Autonomy [300lux]
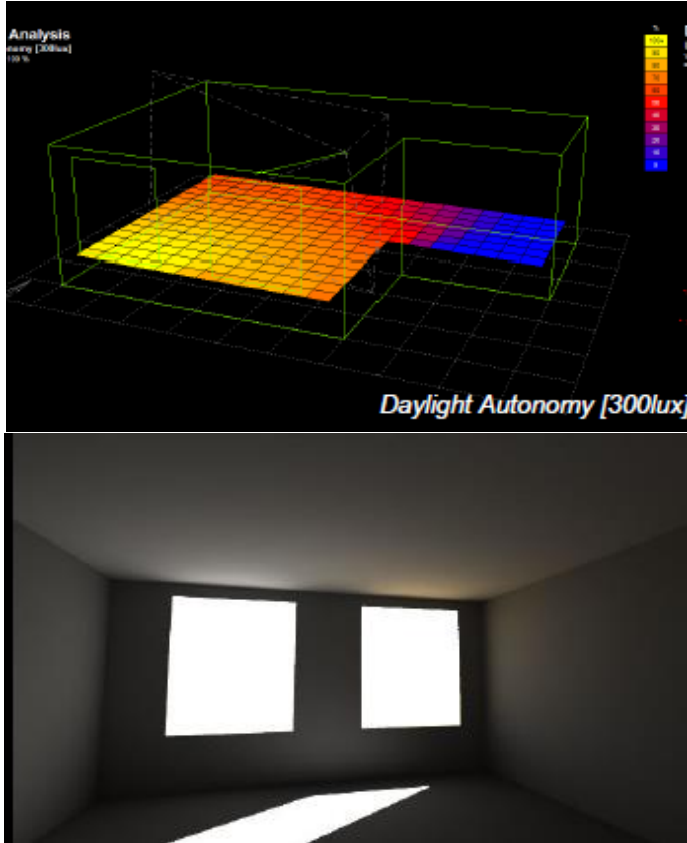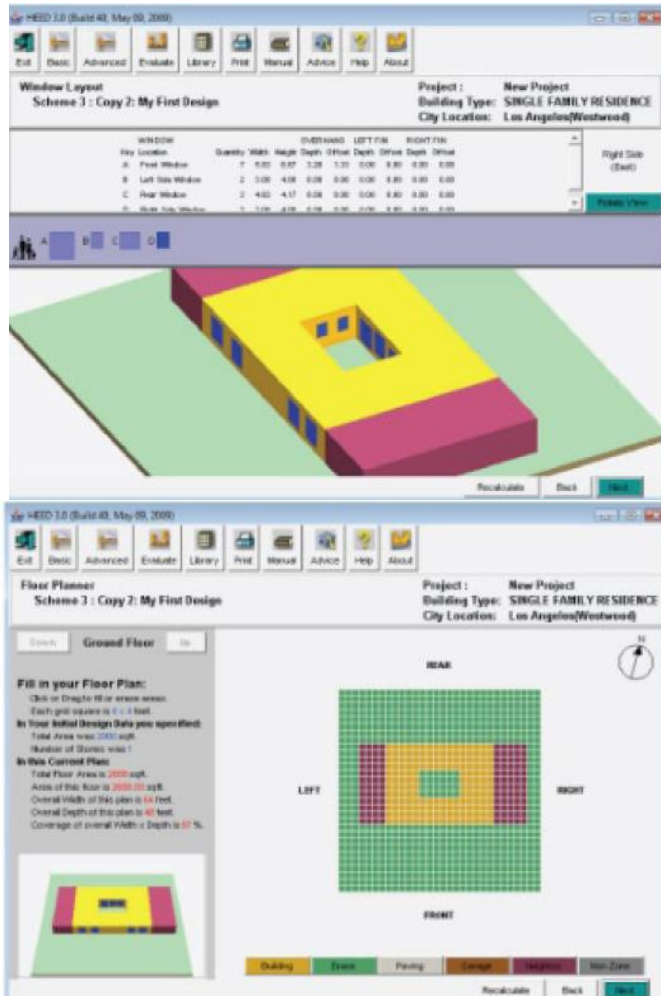

شكل (9) نموذج توضيحي لمخرجات البرنامج

المخرجات: محاكاة الحرارة، الإنارة، الصوت ومحاكاة تدفق الهواء داخل المبنى.

اسم البرنامج : **Home Energy Efficient Design (HEED)**

التعريف: هو برنامج مصمم للمباني السكنية خاصة يساعد المعماري والبناء ومالك المنزل في كيفية تصميم المبنى لتقليل أحمال الطاقة الناتجة من تكييف الهواء ويستخدم في بداية عملية التصميم. [6]

الهدف الأساسي للبرنامج : التعرف على تكلفة الطاقة للمباني السكنية والتعرف على الطاقة الفعالة للتصميم ودرجة الحرارة الداخلية واستجابة التصميم للمناخ المحيط بالمبنى [5]

المدخلات Input : البرنامج يعمل بتوفير أربع معلومات وظيفية وهي الموقع والمجموع الكلي لمساحة الأرضيات وعدد الطوابق ونوع المبنى .[6]
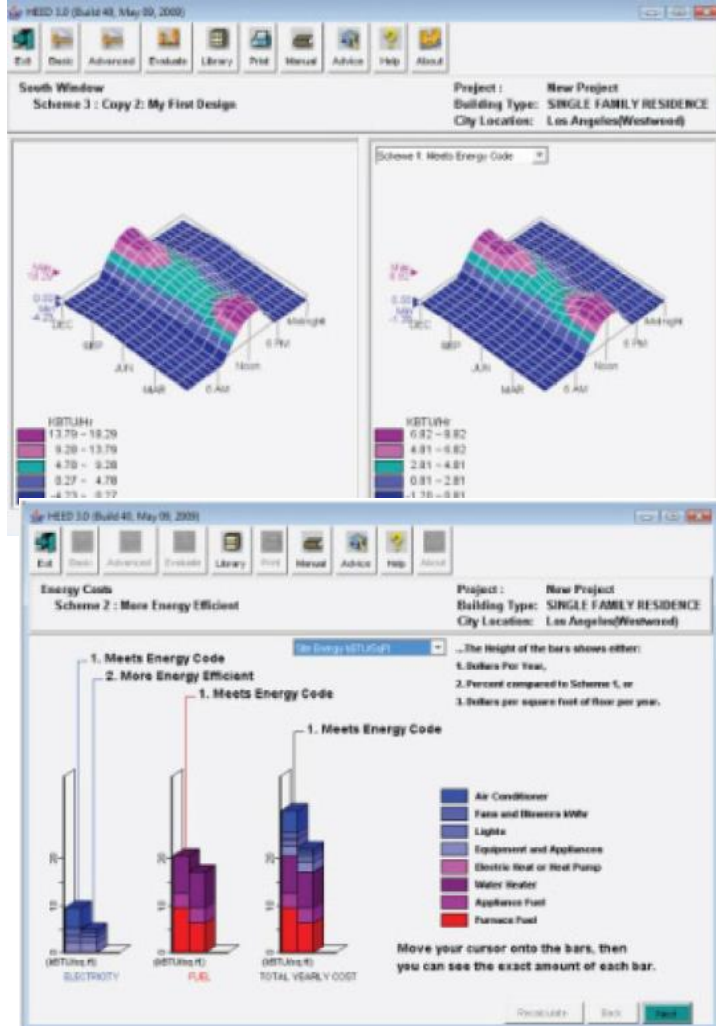

شكل (10) نموذج توضيحي لمدخلات البرنامج

المخرجات Output: يحسب الكسب في طاقة والفقد الطاقة لمكونات المبني المادية مثل الأسقف والأرضيات والجدران وألاعمدة والفتحات... الخ وتقييم أداء المبنى بيئيا مثل معرفة درجات حرارة الهواء في داخل وخارج المبنى والتغير في معدل الهواء وقوة الإضاءة وتكلفة الكهرباء.. الخ عن طريق رسومات بيانية وجداول بيانية . [7]
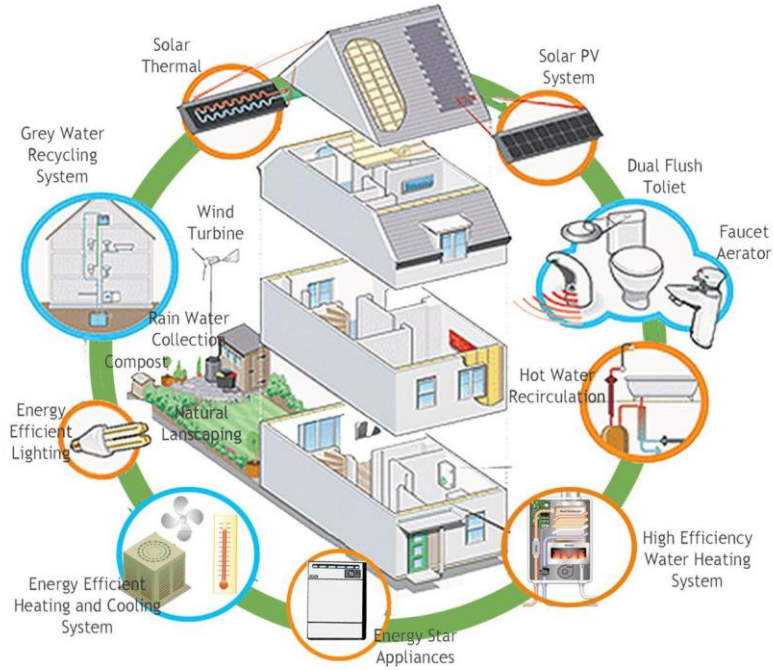
شكل (11). مخرجات تتعلق بتقييم إمكانيات المبني مثل كفاءة التبريد والتسخين وكفاءة الإضاءة والتهوية والتبريد وإمكانيات إعادة تدوير الماء البارد والساخن وتوليد طاقة نظيفة والعديد من الإمكانيات الموضحة بالشكل.
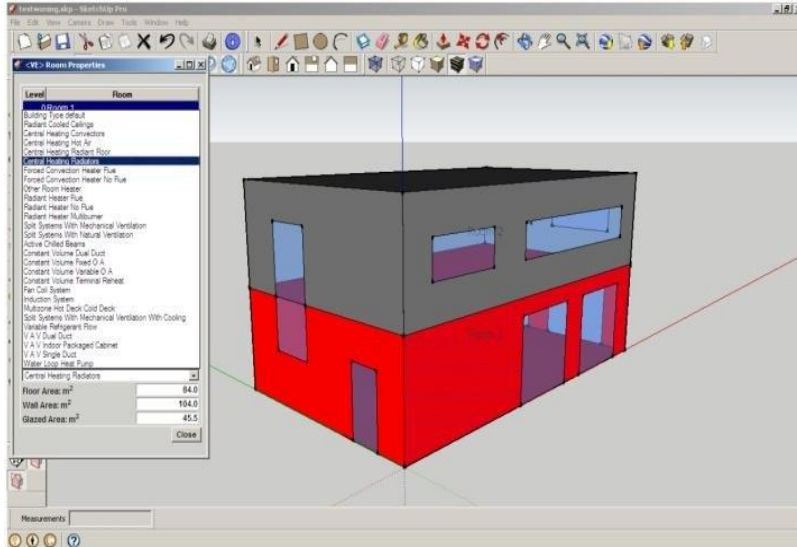
شكل (12) نموذج توضيحي لمخرجات البرنامج .

اسم البرنامج : IES VE Tool

(Integrated Environmental Solutions, 2011)

الرمز:

International Science and Technology Journal
Technology Journal
المجلة الدولية للعلوم والتقنية

العدد 26
Volume 26

المجلة الدولية للعلوم والتقنية
International Science and Technology Journal

ISTJ

تعريف : تم تطوير البرنامج الي BSP IES-VE ويحتوي على عدد من التطبيقات التي تشمل التحليل الوظيفي لأداء المبنى فالبرنامج يعرض المبنى في البعد الثالث مع وصف لعناصر المبني بشكل تفصيلي مصور[8] .

الهدف الأساسي للبرنامج : البرنامج يساعد على إخراج نتائج قياسية لكل من المتطلبات الآتية مثل أداء الطاقة ، استهلاك الطاقة ، LEED ، المحاكاة الحرارية ، HVAC ، ضوء النهار ، الأداء الحراري ، CFD ، تدفق الهواء ، اكتساب الحرارة ، فقدان الحرارة ، حساب الحمل ، التظليل الشمسي ، كثافة الطاقة الشمسية ..الخ [5]. البرنامج يعمل مع برامج هندسية ومعمارية اخري مثل ، Archi CAD و Autodesk Revit و Google Sketch Up لاستخدامها فى تصور المبنى في البعد الثالث [8]

المدخلات Input : عملية إدخال البيانات سهلة وسريعة كذلك تقنينا سهل الاستعمال للمتخصصين حيث يمكن استعمال البرنامج مع Sketch-up في تشكيل المبنى هندسيا في البعد الثالث مع قائمة الإعدادات لأنظمة الوظائف ومكونات المبنى .[6]

شكل (13) نموذج توضيحي لمخرجات البرنامج .

International Science and
Technology Journal
المجلة الدولية للعلوم والتقنية

العدد 26
Volume 26

المجلة الدولية للعلوم والتقنية
International Science and Technology Journal
ISTJ

المخرجات Output : يظهر البرنامج البيانات الإحصائية للطاقة ولضوء النهار وللتظليل الشمسي كجداول ورسومات بيانية لجميع وظائف التحليل المستنتجة للمبنى ، كذلك يظهر صور واقعية وتصور هندسي ثلاثي الأبعاد ملون لنتائج التحليل [5].
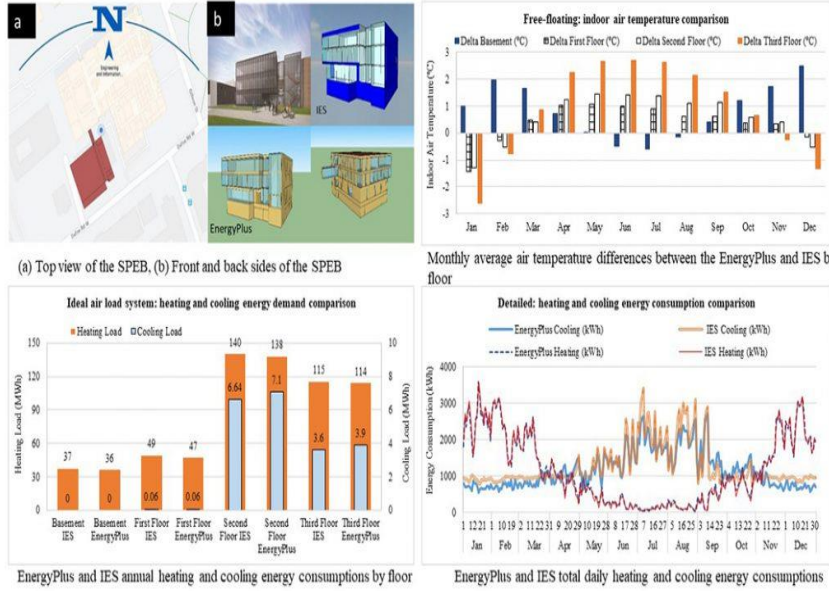
شكل (14) مخرجات للطاقة وللظلال وضوء النهار .

**البرنامج : (Bisim (Danish Building Research Institute**

الرمز : SBi

تعريف : هي محاكاة سهلة الاستخدام (User – friendly simulation) لتفاصيل المباني والمنشآت.[4]   وفي تعريف آخر للبرنامج موضح كالأتي " هي أداة كمبيوتر توفر إمكانات محاكاة متقدمة لمصممي المباني والمهندسين المعماريين وغيرهم ، عند التخطيط أو التصميم أو تحليل المناخ الداخلي واستهلاك الطاقة لأي نوع من المباني ". [5]
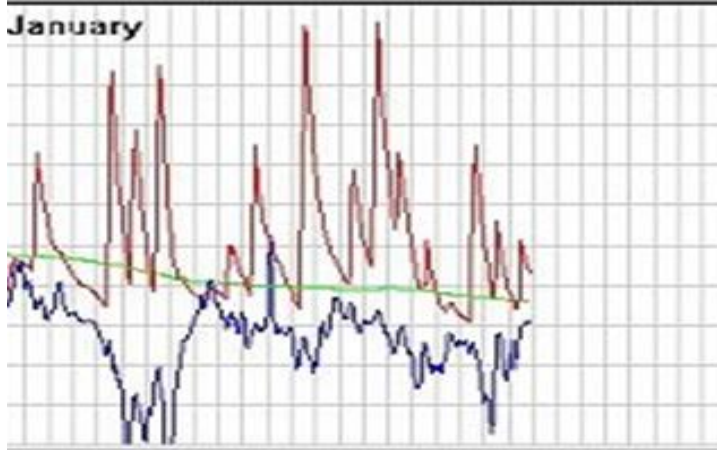
الهدف الأساسي للبرنامج :

- يستخدم لمحاكاة ضوء النهارDaylight وتسجيل الحسابات المتعلقة بضوء النهار المباشر.

- تحديد الظلال Shadowing على المبنى وتوقيت ظهور الشمس.

- يستخدم أيضا في وضع نتائج درجات الحرارة في الفضاء الداخل Thermal indoor climate ى والرطوبة والتهويةVentilation (تصميم وتحليل وقياس).[4]

مدخلات البرنامج :المحاكاة ديناميكيا للمناطق ذات التأثير الحراري داخل الغرف وتشمل المواد المستخدمة ومكونات المبنى ونوع النظام المستخدم .[5]
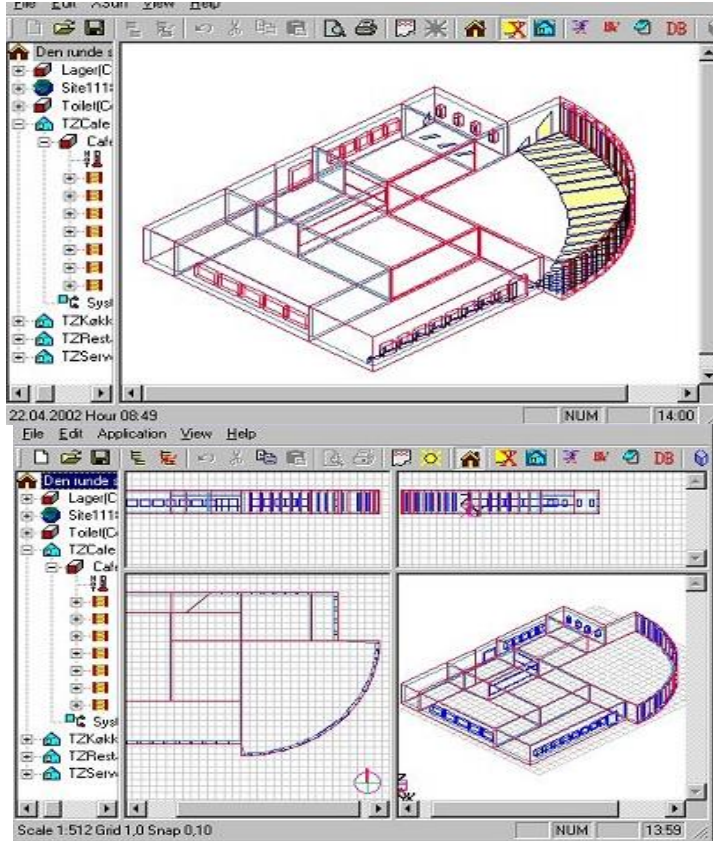
شكل (15) المدخلات : المواد المستخدمة ومكونات المبنى ونوع النظام المستخدم

مخرجات البرنامج: عرض نتائج تحليل الوظائف إلى رسوم بيانية او جداول لكل تفاصيل المبنى والنتائج قابله للنسخ والعرض من جديد [5].

شكل (17) نموذج لمخرجات البرنامج

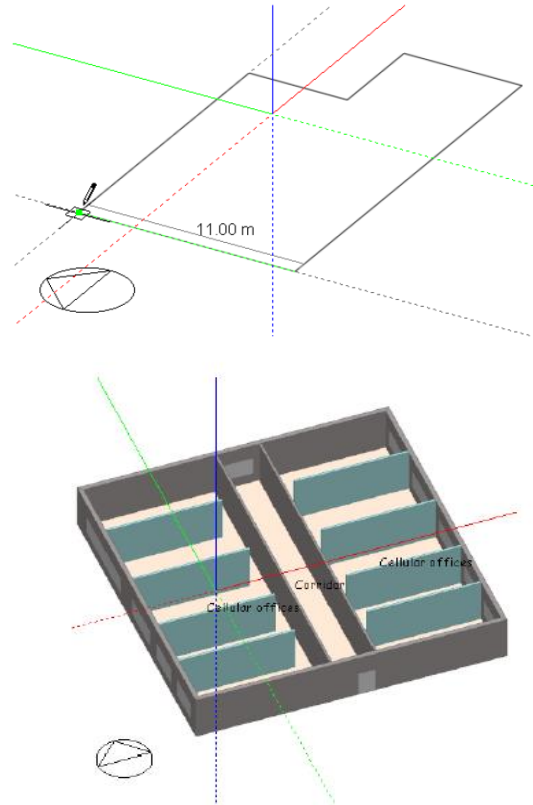**اسم البرنامج** : The DesignBuilder software

الرمز: DesignBuilder SOFTWARE

التعريف: هو برنامج متقدم مجهز محدد وهو لتسجيل محاكاة الطاقة الزائدة EnergyPlus أثناء تشغيل المبنى.[9]

الهدف الأساسي للبرنامج :

■ تسجيل استهلاك المبنى للطاقة Energy consumption

■ يستعرض خيارات للواجهات المبنى من ناحية المظهر ومن ناحية التعرض للإشعاع الشمسي .

■ المحاكاة الحرارية Thermal simulation ذات للمباني ذات التهوية الطبيعية naturally ventilated

■ يستعرض مقترحات للتحكم في الإضاءة الطبيعية وكيفية حسابها .

- يقدم مقترحات للتوفير في استهلاك الطاقة الكهربائية .

- يقدم مخططات مرسومة للتظليل الشمسي .

- يعرض حساب لأحجام معدات التدفئة والتبريد [10].

مدخلات المبنى Input: يستقبل المعلومات عن المبنى المراد تحليله وظيفيا عن طريق CAD data [10]. فهو ستخدم النماذج المعمارية في البعد الثالث مع برامج هندسية مساعدة مثل برنامج الرافيت و sketch up او الكاد Revit, ArchiCAD . [10]


شكل (18) مدخلات البرنامج : الأشكال الهندسية في البعد الثالث .

International Science and
Technology Journal
المجلة الدولية للعلوم والتقنية

العدد 26
Volume 26

المجلة الدولية للعلوم والتقنية
International Science and Technology Journal
ISTJ

مخرجات البرنامج Output : يستعرض قراءات لاستهلاك الطاقة ودرجات الحرارة والرطوبة والراحة الحرارية كذلك يقدم بيانات عن الطقس بالموقع وكيفية الانتقال الحراري من خلال الجدران والأسطح وحركة الهواء خلال الفضاءات الداخلية [5].
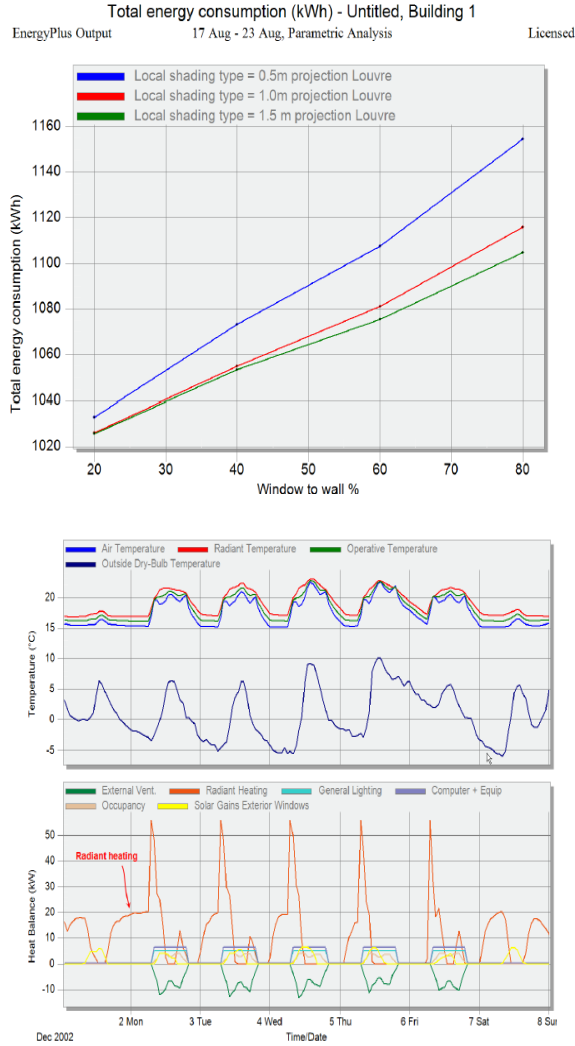
شكل (19) درجات الحرارة واستهلاك الطاقة
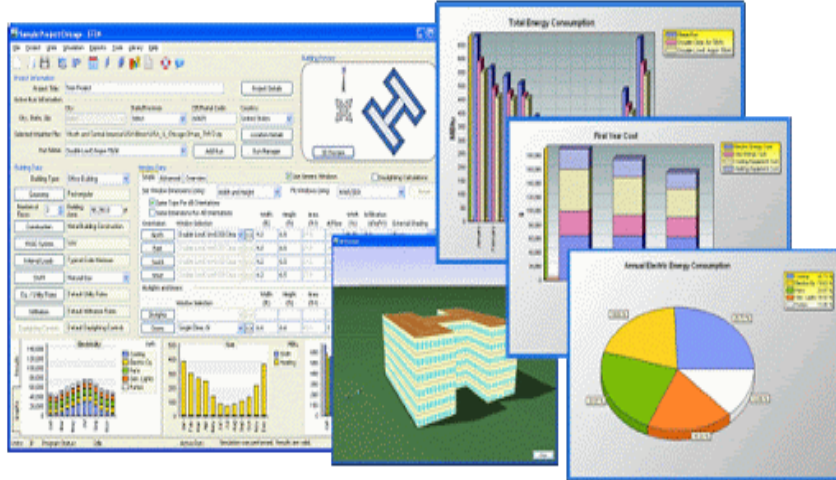
شكل (20) output مثال توضيحي لمخرجات البرنامج

4.   النتائج :

دراسة تحليلية لكل برنامج للخروج بمميزات وعيوب مستنتجه من الدراسات السابقة التي تساعد في تحديد البرنامج الأمثل وهي:

ECOTECT

مميزات:

▪ إمكانية الرجوع والتصحيح Feedback في المراحل الأولية خلال عملية تصميم المبنى. [4]

▪ يقدمECOTECT أشكال مرئية غنية في جميع مراحل التصميم [11]

▪ يساعد ECOTECT المهندسين المعماريين في المراحل الأولية لدراسة المبنى في فهم علاقة المبنى بالبيئة .[11]

▪ من السهل تطبيق أفكار المصمم في مراحل التصميم الأولى ويكون اتخاذ القرار أسهل بكثير من المراحل النهائية.[5]

▪ يقدمECOTECT رسومات بيانية تحليلية لوظائف المبنى بشكل مبسط .[5]

▪ ECOTECT أكثر البرامج فائدة بسبب السرعة وسهولة الاستخدام. [3]

■ يعطي نتائج دقيقة للبيانات الحسابية. [2]

العيوب:

■ صعوبة خلق أشكال هندسية معقدة مثل وضع النوافذ في الجدران المنحنية. .

[3]

■ يجب أن يكون المستخدمين لهذا البرنامج على دراية عالية بمتطلبات تشغيل

البيانات.[5]

HEED

المميزات :

■ يمتاز بالدقة العالية. [10]

■ سهل الاستخدام لكونها سهلة التصميم ويساعد على توفير الطاقة في المنازل

. [5]

■ لا يتخذ أجراء تقييم المبني الكثير من الوقت لكونه مصمم للمباني الصغيرة

محدودة المساحة ولقلة التفاصيل . [9]

العيوب :

■ يستخدم للمساحات الصغيرة المحدودة Single-zone buildings.[5].

• نتائج الإخراج تفتقر إلى الصفات البصرية. [5]

• مناسب فقط للمرحلة المبكرة من عملية التصميم.[10]

IES VE

المميزات:

■ عملية إدخال البيانات سهلة وسريعة. [10]

■ يسمح IES Sketch-Up للمهندسين المعماريين ليس فقط بتكوين المباني

هندسيا، ولكن أيضًا للتنبؤ بأدائها باستخدام Sketch-Up [5]

International Science and Technology Journal
Technology Journal
المجلة الدولية للعلوم والتقنية

العدد 26
Volume 26

المجلة الدولية للعلوم والتقنية
International Science and Technology Journal
ISTJ

■ تتوافق بساطة الواجهة وعملية إدخال البيانات مع طريقة عمل المهندسين المعماريين. [5]

■ بناءً على المدخلات القليلة ، تسمح هذه الأداة للمهندسين المعماريين بمحاكاة تأثير خيارات التصميم المعماري على أداء المبنى ، دون الحاجة إلى الرجوع إلى دليل. [5]

■ يسمح بمقارنة البدائل. تسمح الأداة بإدخال HVAC ومكاسب الطاقة الشمسية والتظليل والتهوية الطبيعية واستراتيجيات التعتيم. [10]

العيوب :

■ الرجوع وتعديل القرارات في تصميمات برنامج سكتش اب (Sketch-Up) غير ممكنه.

■ النتائج المستخرجة غير مناسبة ولا تدعم عملية اتخاذ القرار بسبب نقص التصور المرئي للمبنى والكثير من المعلومات النصية والجداول. [5]

BSim

المميزات :

■ يستخدم للمباني المعقدة حراريا .

■ يستخدم للمباني المشيدة لسنوات طويلة ماضية .

■ يستخدم على نطاق واسع في العالم لقدراته العالية في المحاكاة Simulation capabilities,.

■ سهل الاستخدام ولا يحتاج إلى متخصصين بقدرات عاليه لتشغيل البرنامج .

■ BSim هي أداة دقيقة للغاية لمحاكاة المناخ الداخلي الحراري في المباني. [5]

العيوب:

■ النتائج غير موحدة .

■ لا يوجد محاكاة لكافة المدخلات في نفس الوقت مجتمعه [5]

Design Builder

المميزات :

- برنامج يعطي نتائج عالية الدقة . [11]

- يوفر DesignBuilder إمكانية التشغيل البيني مع نماذج BIM من خلال إمكانية استيراد gbXML يسمح ذلك باستيراد نماذج معمارية ثلاثية الأبعاد تم إنشاؤها في Revit أو ArchiCAD أو Microstation أيضا، هندسة المبنى ، يمكن بناؤها باستخدام نموذج ثلاثي الأبعاد. [11]

- يقدم معلومات للمعماريين المتخصصين في الاستدامة لتصميم مباني صفر الطاقة NZEB. [4]

العيوب:

- يعتبر من البرامج المحاكاة المعقدة .

- جميع مخرجات عملية المحاكاة مفصلة ولا يتم فهمها وترجمتها ألا عن طريق متخصصين معماريين.

- نتائج المخرجات لا تدعم بشكل كافٍ عملية صنع القرار لدى المهندس المعماري . [11]

5. **مناقشة النتائج:**

أولا : مناقشة جدول (1) مقارنة عامه بين البرامج المختارة :
لكل أداة أو برنامج مميزات وعيوب ولكن من المهم التعرف على أفضل البرامج من حيث المميزات وهذا الجدول يوضح العديد من العناصر المهمة وهي اسم البرنامج ، الاستخدام ،هدف الاستخدام المدخلات والمخرجات والمميزات والعيوب .

أولا : من خلال تحليل الجدول رقم (1) نرى ان برنامج ECOTECT هو برنامج فعال ومفيد خلال مراحل عملية التصميم و أهم مميزاته انه أكثر دقة من البرامج

International Science and
Technology Journal
المجلة الدولية للعلوم والتقنية

العدد 26
Volume 26

ISTJ

المجلة الدولية للعلوم والتقنية
International Science and Technology Journal

الأخرى كما انه يستجيب للمراجعة Feedback وهي عملية الرجوع إلى بدايات التصميم للقيام بالتعديلات اللازمة و يعد برنامج يمتاز بسهولة تشكيل التكوينات الهندسية رغم صعوبة التعلم في بدايات التعامل معه .

ثانيا : نلاحظ من الجداول (1) إن برنامج HEED , سهل الاستخدام أكثر من البرنامج السابق ECOTECT ويماثله في الدقة ويحتاج إلي وقت قصير للتقيم التصميم ولكن يعتبر مناسب فقط للمباني ذات المساحات الكبيرة وفى يستخدم في وقت محدد من مراحل التصميم والتي تتمثل في بدايات التصميم فقط من العملية التصميمية .

ثالثا : IES VE يمتاز بالعديد من المميزات بعضها عند الاستخدام أثناء مراحل التصميم فمثلا يعتبر سهل وسريع الاستخدام خصوصا عند وضع المعلومات كمدخلات كما انه لديه أمكانية الاستخدام مع برنامج Sketch-Up الذي بدوره يساعد في تحليل وظائف التصميم بشكل سهل بالرغم من وجود صعوبة قد تواجه المتخصصين عند اتخاذ القرار نتيجة وجود الكثير من المعلومات .

رابعا : يعتبر(BSim tool)أكثر البرامج دقة عند محاكاة الفضاءات الداخلية حراريا لا توجد تقارير نتائج موحدة ، ويعتبر من البرامج التعليمية Educational user interface .

خامسا : يمتاز ايضا بالدقة العالية ويقدم معلومات مفيدة التي تدعم المعماريين فى تصميم المباني صفر الطاقة كما انه مهم فى تكوين أشكال ثلاثية الأبعاد بواسطة برامج مساعدة هيRevit, ArchiCAD or Microstation .

International Science and
Technology Journal
المجلة الدولية للعلوم والتقنية

العدد 26
Volume 26

ISTJ
المجلة الدولية للعلوم والتقنية
International Science and Technology Journal

جدول 2 : يبين اسم البرنامج ، الاستخدام ،هدف الاستخدام المدخلات والمخرجات والمميزات والعيوب (المصدر البحاث)

المتطلب	ECOTECT	HEED	IES VE	BSim	DesignBuilder
Nu of user and country of users عدد المستخدمين	**Over 2000 users approximately 60 universities mainly in Australia, UK and USA** فوق 2000 مستخدم	**14,792 users 16 % of the users in Southern California, 7% in California, 48% in the US, and 29% in another country** 14.792 مستخدم	**Global User** واسع الاستخدام	**650 users in Denmark and Germany also users in Canada, Mexico, New Zealand, Japan, France, Sweden, Norway, and Iceland** 650 مستخدم	**Global User** واسع الاستخدام
Expertise Required متطلبات الخبرة	برنامج كاد	خبرة تعلم أساسيات التصميم على البرامج	فهم كامل برامج the software	أن يكون لدى المستخدمين بعض المعرفة العامة عن تصميم المبنى وكيف تتصرف المباني حرارياً من أجل إنشاء نموذج المبنى	فهم أساسيات البرنامج Design Builder
Users المستخدمين	مهندسين المعماريين والمهندسين والاستشاريين البيئيين ومصممي المباني وبعض البنائين المالكين والمتحمسين.	مصممين ومستشاري الطاقة ، على دراية بقضايا كفاءة الطاقة ، أصحاب المنازل ودافعي الضرائب	المهندسين المعماريين والمهندسين	المهندسين والباحثين والطلاب.	لمهندسين الاستشاريين والمهندسين المعماريين وأقسام البحث الأكاديمي والتدريس الطلاب
learn التعلم	**easy-to-use(difficult for new users)** سهل الاستخدام (صعب على المستخدمين الجدد)	**easy-to-use** سهل الاستخدام	**easy-to-use** سهل الاستخدام	**easy-to-use** سهل الاستخدام	**easy-to-use** سهل الاستخدام
Speed السرعة	**v.quick** سريع جدا	يتطلب الحد الأدنى من الوقت لإجراء تقييمات التصميم	**Quick** سريع	**Quick** سريع	**Quick** سريع

International Science and
Technology Journal
المجلة الدولية للعلوم والتقنية

العدد 26
Volume 26

المجلة الدولية للعلوم والتقنية
International Science and Technology Journal
ISTJ

Accuracy الدقة	High عالي الدقة	Accurate دقيق	Accurate دقيق	Accurate دقيق	High عالي الدقة
Main aim الهدف	تستخدم للراحة، والراحة ، واستخدام الطاقة ، والمناخ وتأثيره البيئي ، والأداء الصوتي والحراري ، والإضاءة ، والتظليل ،، والتكلفة	energy costs, for home تكاليف الطاقة للمنزل	استخدام لأداء الطاقة، استهلاك الطاقة، LEED ، الحرارية ، HVAC ، الإضاءة النهارية ، الأنظمة السلبية ، التهوية الطبيعية ، ضوء النهار	سيتم محاكاة المعدات والأنظمة بشكل ديناميكي فقط في المناطق الحرارية.	Design Builder اختيارًا ممتازًا للنمذجة المبكرة لتصميمات المباني اختبر خيارات التصميم المختلفة للراحة البيئية واستهلاك الطاقة والمظهر المرئي
Programs to use يحتاج إلى برامج الموضحة بالجدول	3D CAD	--------	Archie CAD, Autodesk Revit and Google Sketch Up	Windows NT version 4, SP3, Windows 2000, Windows XP, or Windows Vista.	Archie CAD
Positive to use المميزات	يسمح للمستخدم "باللعب" بأفكار التصميم في المراحل الاولية التركيز على الملاحظات في المراحل الأولى من عملية تصميم المبنى	هي أداة تصميم بسيطة وسهلة الاستخدام ومجانية التي يمكن أن تحسب بسرعة توفير الطاقة بدائل تصميم المنزل وإعادة البناء.	مكين الفريق بأكمله التعاون في تحسين التصميم وتقليل استهلاك الطاقة	برامج مرنة (يسهل على المستخدم التعرف على أي كائن نموذج وإجراء التغييرات عليه)	يستخدم لتحليل الحرارة الداخلية للمباني المعقدة
Negative to use العيوب	صعوبات إنشاء أشكال هندسية معقدة	استخدم للمباني ذات المنطقة الواحدة.	ردود الفعل في برنامج التصميم (Sketch-Up) غير ممكنة. [5]	النماذج الاولية غير دقيقة	لا تدعم بشكل كاف عملية صنع القرار للمهندس المعماري

ثانيا : جدول (2) مقارنة من ناحية الاستخدام بين البرامج المختارة:

متطلبات الاختبار هي الخبرة المطلوبة، المستخدمون، طريقة التعلم، السرعة، الدقة، الهدف الرئيسي، برامج الاستخدام، إيجابية للاستخدام، وسلبية للاستخدام.

International Science and Technology Journal
Technology Journal
المجلة الدولية للعلوم والتقنية

العدد 26
Volume 26

المجلة الدولية للعلوم والتقنية
International Science and Technology Journal
ISTJ

جدول (3) : مقارنة بين البرامج في طريقة الاستخدام (المصدر البحاث

نوع المقارنة	ECOTECT	HEED	IES VE	BSim	DesignBuilder
Nu of user and country of users	Some country	Some country	Global User	Some country	Global User
الاستخدام العالمي	+_	+_	++	+_	++
	بعض الدول	بعض الدول	استخدام واسع	بعض الدول	بعض الدول
Expertise Required	More exp	More exp	More exp	Minimal exp	Minimal exp
مكتطلبات الخبرة	–+	_+	_+	+	+
	يحتاج خبرة عالية	يحتاج خبرة عالية	يحتاج خبرة عالية	خبرة متوسطه	خبرة متوسطه
Users	++	+	++	++	++
Learn	+_	++	+	+	+
إمكانية التعلم	متوسطة	عالية	ممكنه	ممكنه	ممكنه
Speed	++	+	+	+	+
السرعة	سريع	جيد	جيد	جيد	جيد
Accuracy	++	+	+	+	++
الدقة	عالي الدقة	جيدة	جيدة	جيدة	عالي الدقة
Main aim	Different uses	Not all	Different uses++	Not all	more uses
	++	+_		+_	+++
Programs to use	++	+	++	+	++
مدى الاستفادة	More Useful	مفيد	more useful	مفيد	More Useful
	مفيد جدا		مفيد جدا		مفيد جدا
Positive to use	+++	++	++	++	++
المميزات	more positive for use	مميز	مميز	مميز	مميز
	أكثر تميز في الاستخدام				
Negative to use	––	–––	––	–	––
السلبيات		More negative because it is very specific			
		أكثر سلبيات			

6. **الاستنتاج:**

▪ **مقارنه عامه بين البرامج المختارة :**

السمات الرئيسية لـECOTECT ، فهو يساعد المتخصصين كفريق عمل على الاندماج في مراحل التصميم المبكرة كفريق واحد، كما يمكن الرجوع والقيام بالتعديلات في مراحل التصميم، علاوة على أنه يساعد المهندسين المعماريين على فهم المبنى وعلاقته بالبيئة. لهذه الأسباب فإن ECOTECT أكثر إيجابية من البرامج الأربعة الأخرى.

▪ **مقارنة من ناحية الاستخدام بين البرامج المختارة :**

كأداة محاكاة ECOTECT تتطلب CAD وتجربة تصميم بيئي، أداة ECOTECT أكثر صعوبة للمستخدمين الجدد لإنشاء أشكال هندسية معقدة. من ناحية أخرى ، لها مزايا كبيرة للمهندسين المعماريين ، والمهندسين ، والاستشاريين البيئيين ، ومصممي المباني ، وبعض البنائين المالكين لاستخدامها ، على سبيل المثال ، ECOTECT

International Science and
Technology Journal
المجلة الدولية للعلوم والتقنية

العدد 26
Volume 26

المجلة الدولية للعلوم والتقنية
International Science and Technology Journal
ISTJ

سريع وعالي الدقة ، وهو برنامج مهم جدا في العملية المتكاملة لأنه يساعد على التعاون في العمل الجماعي في عملية التصميم ، ويركز على التغذية الراجعة في المراحل الأولى من عملية تصميم المبنى ، علاوة على ذلك فهي يتيح للفريق "اللعب" بأفكار التصميم في المراحل المفاهيمية . هذه الميزات مهمة جدًا لعملية التصميم المتكاملة، ونتيجة لذلك جعلت هذه الميزات أداة ECOTECT أكثر إيجابية في الاستخدام.

مميزات البرنامج ECOTECT :

▪ إمكانية الرجوع والتصحيح Feedback في المراحل الأولية خلال عملية تصميم المبنى. [4]

▪ يقدم ECOTECT أشكال مرئية غنية في جميع مراحل التصميم. [11]

▪ يساعد ECOTECT المهندسين المعماريين في المراحل الأولية لدراسة المبنى في فهم علاقة المبنى بالبيئة. [11]

▪ من السهل تطبيق أفكار المصمم في مراحل التصميم الأولى ويكون اتخاذ القرار أسهل بكثير من المراحل النهائية. [5]

▪ يقدم ECOTECT رسومات بيانية تحليلية لوظائف المبنى بشكل مبسط. [5]

▪ ECOTECT أكثر البرامج فائدة بسبب السرعة وسهولة الاستخدام . [3]

▪ يعطي نتائج دقيقة للبيانات الحسابية. [2]

7. التوصيات:

▪ نوصي المعماريين والمهندسين بالتعرف على كافة البرامج المتطورة مثل أدوات المحاكاة لكونها سهلة الاستخدام وليست معقدة كما وضحنا بالجداول.

▪ نوصى وزارة التعليم العالي والتقني بإدراج مثل هده البرامج بالمناهج التعليمي وتوفير إمكانيات مادية ومعامل للتدريب والتطبيق العملي داخل القاعات الدراسية بالجامعات .

International Science and
Technology Journal
المجلة الدولية للعلوم والتقنية

العدد 26
Volume 26

المجلة الدولية للعلوم والتقنية
International Science and Technology Journal
ISTJ

■ استعرضنا خمس أشهر أدوات محاكاة بالدراسة بالرغم من وجود العديد من الأدوات نوصي بالاطلاع على مميزاتها وعيوبها لان بعضها تحت التطوير .

■ إذا تم استخدام هذه البرامج قبل تنفيذ المباني وتطبيق نتائجها عمليا وخصوصا المباني السكنية سوف نتلافى العديد من المشاكل البيئية المتعلقة بالتهوية والرطوبة والحرارة والإضاءة على اقل تقدير ونبني مباني صحية خالية من المشاكل البيئية مستقبلا.

8.   المراجع:

[1] Emeritus "The Many Facets of Simulation through a Collection of about 100 Definitions Tuncer Ören" School of Information Technology and Engineering , Canada

[2] Tuncer Ören."Modeling and Simulation Body of Knowledge (M&S BoK) – Index" 2010

[3] ROBERTS, Andrew; MARSH, Andrew Cardiff University, Wales "ECOTECT: Environmental Prediction in Architectural Education" http://cebe.cf.ac.uk/ http://squ1.com/

[4] Drury B. Crawleya, _, Jon W. Handb, Michae¨ l Kummertc, Brent T. Griffithd, "Contrasting the capabilities of building energy performance simulation programs"2008

[5] http://apps1.eere.energy.gov

[6] Lieve Weytjens*, Shady Attia, Griet Verbeeck, and André De Herde "The 'Architect-friendliness' Of Six Building Performance Simulation Tools: A Comparative Study ",2011

[7] Murray Milne, Carlos Gomez, Pablo LaRoche, and Jessica Morton "A Free User-Friendly Design Tool that Shows How To Reduce Cooling Energy in Buildings" UCLA Department of Architecture and Urban Design, Los Angeles, CA 90095

[8] J-ørgen Erik Christensen1, Peder Schiønning2 and Espen Dethlefsen3"COMPARISON OF SIMPLIFIED AND ADVANCED BUILDING SIMULATION 2 TOOL WITH

International Science and Technology Journal
المجلة الدولية للعلوم والتقنية

العدد 26
Volume 26

المجلة الدولية للعلوم والتقنية
International Science and Technology Journal
ISTJ

MEASURED DATA." 13th Conference of International Building *Performance Simulation Association, Chambéry, France*,2013

[9] Design Builder Simulation ".CFD Training Guide. 2011

[10] Shady Attia, "State of the Art of Existing Early Design Simulation Tools for Net Zero EnergyBuildings: A Comparison of Ten Tools"2011.

[11] "ECOTECT friendly" 2008, www.caduser.com/register

[12] [Tobias Maile, Martin Fischer & Vladimir Bazjanac "Building Energy Performance Simulation Tools - a Life-Cycle and Interoperable Perspective" CIFE Working Paper #WP107 DECEMBER 2007, STANFORD UNIVERSITY

[13] Hema.s. Rallapalli "A Thesis Presented in Partial Fulfillment of the Requirements for the Degree Master of Science". 2010

[14] Joana Sousa1 "Energy Simulation Software for Buildings: Review and Comparison" 1 Faculdade de Engenharia da Universidade do Porto, Porto, Portugal j.bastos.sousa@gmail.com

[15] Abul Abdullah and Ben Cross, "Whole Building Energy Analysis: A Comparative Study of Different Simulation Tools and Applications in Architectural Design" 2014

[16] Rick Clyne , Steven Bodzin "Energy-10" Home Energy Magazine " September/October 1997

[17] Tuncer Ören" The Many Facets of Simulation through a Collection of about 100 Definitions" School of Information Technology and Engineering,, Canada

[18] http://apps1.eere.energy.gov/buildings/tools_directory/alpha_list.cfm

[19] http://www.solar-for-energy.com/energy-10-software.html

تقييم بعض الخصائص الفيزوكيميائية والبيولوجية لمياه الشرب المعبأة الناتجة من بعض محطات التحلية في مدينة صبراتة – ليبيا

حليمة محمد إمحمد عمر1، صلاح الدين البشير البلعزي1، طارق مفتاح2

انتصار ابوجليدة3، فوزية سمهود3، صابرين رمضان مسعود1

1 قسم علم النبات –كلية العلوم – جامعة صبراتة

1 قسم علم الكيمياء –كلية العلوم – جامعة صبراتة

2 المعهد العالي للمياه والتربة – إدارة المعاهد العليا – ليبيا

Email :–Halimah.AL–khojah@sabu.edu.ly

الملخص–:

إجريت هذه الدراسة في شهر يوليو من سنة 2017، لتقييم بعض الخصائص الفيزوكيميائية والبيولوجية لمياه الشرب المعبأة الناتجة من بعض محطات التحلية العامة في بمدينة صبراته، حيث شملت الدراسة (29) عينة مياه من هذه المحطات. أظهرت النتائج إن أغلب العينات خالية تماما من التلوث الميكروبي ماعدا العينات (5،،3، 13)، والتي ظهر فيه النمو البكتيري وبدرجات مختلفة الشدة، ومن جهة أخرى أظهرت الاختبارات الكيميائية والتي تضمنت (الرقم الهيدروجيني، الموصلية الكهربائية، الأملاح الذائبة الكلية) إن قيم الرقم الهيدروجيني للعينات (13، 12، 11، 10) هي (5.88 ،6.09، 6.19، 6.45) على التوالي، وهى تحت الحد الأدنى المسموح به في المواصفة الليبية والعالمية (WHO) للمياه المعبأة، بينما لم تتجاوز قيم الموصلية الكهربائية لجميع العينات المدروسة الحدود المسموح بها، وبالنسبة لقيم الأملاح الذائبة الكلية أظهرت النتائج أن تركيز المواد الصلبة الذائبة تراوح بين (6.11 – 188.43) مليجرام/لتر في العينات المدروسة، وبذلك تكون أغلب العينات تحت الحد الأدنى المسموح به في المواصفة القياسية العالمية (WHO) والمواصفة الليبية لمياه الشرب المعبأة وهو(500 مليجرام/لتر)

الكلمات الدليلية :– مياه الشرب، مدينة صبراتة ،محطات التحلية، البكتيريا القولونية.

Abstract:-

This study was carried out at July/ 2017, to evaluation of soma Physicochemical parameters of drink water output from purification station in **Sabratha city**, the study include (29) of drink water samples. The results showed that, the major samples were free from bacterial contamination, except (3,5,15) samples were found growing bacteria, and in another side, analysis of the physicochemical properties include (PH, EC, TDS), show that, the (PH) for (10,11,12,13) samples were (6.45, 6.19, 6.09, 5.88) respectively, they weren't limits permitted by World Health Organization (WHO).furthermore the EC values of all samples weren't limits permitted by (WHO), also the TDS values results show that, the concentration of TDS between (6.11-188.43 mg/l) in all study samples, that means of major samples weren't limits permitted by (WHO) of drink water (500mg/l) .

Key words: drink water, Sabratha city, purification station, coliform bacteria.

المقدمة introduction -:

المياه الآمنة للشرب كما جاءت وصافها في دلائل الجودة، يجب أن لا تنطوي على أي مخاطر مخيفة على الصحة بسبب استهلاكها مدى الحياة، مع مراعاة ما قد تنطوي عليه مراحل الحياة من حساسيات مختلفة وتطبق دلائل جودة مياه الشرب على المياه التي تقدم في عبوات وعلى الثلج المعد للاستهلاك البشري (منظمة الصحة العالمية ، 2004)، وتعد صناعة مياه الشرب المعبأة من أكثر قطاعات صناعة الأغذية والمشروبات ديناميكية بالرغم من التكلفة العالية بالمقارنة مع تكاليف خدمات مياه شبكة التوزيع لاسيما في المدن الصناعية وأصبحت المياه المعبأة توصف بأنها المشروب الأسرع نموا في العالم (الزروقي، 2008)، وقد رافق هذه الزيادة الملحوظة في أعداد المعامل انخفاضا حادا في النوعية (جهاز التقييس والسيطرة النوعية ،1995) الخاصة بمياه الشرب المعبأة، مما أدى إلى إغراق الأسواق بالعديد من العلامات التجارية التي تفتقر للمواصفات الصحية الخاصة بدون النظر إلى الاعتبار مطابقة المعايير القياسية لمياه الشرب وعدم الالتزام بالخصائص الكيميائية والفيزيائية المحددة لنوعية وصلاحية هذه المياه (الاميري ، 2013)، وفيما يتعلق بجودة المياه من الناحية الميكروبية،

يرجح أن يشمل التحقق إجراء اختبار للميكروبات وهو يتضمن في معظم الحالات تحليل الكائنات الحية الدقيقة المشيرة إلى حدوث تلوث بمخلفات الصرف الصحي، ولكنه قد يتضمن أيضًا في بعض الظروف تقدير كثافات عوامل ممرضة معينة (منظمة الصحة العالمية، 2004)، إن أكثر أنواع التلوث البكتيري انتشارا ينشأ عن اختلاط مياه الصرف الصحي التي تحتوي على كميات كبيرة من البكتيريا القولونية البرازية (عبدالله وآخرون،2007)، أما الخصائص الكيميائية فيجب أن لا تحتوي على املاح بتراكيز تؤثر على صحة المستهلك إضافة إلى ذلك أن ماء الشرب يجب أن يكون عديما للون والطعم والرائحة (منظمة الصحة العالمية، 2004)، ومن أهم المعايير الكيميائية (مجموع الأملاح الذائبة، التوصيل الكهربائي، الأس الهيدروجيني، العسرةِ الكلية).

وتلقى صناعة مياه الشرب المعبأة في ليبيا رواجًا كبيرًا، وتشهد بذلك هذه الصناعة انتشارا واسعًا في ظل تزايد الطلب على المنتج لأسباب تتعلق بنوعية مياه الشرب وتوافرها، ومن مظاهر توزيع المياه المعالجة في ليبيا هي محطة التنقية المنتشرة في إرجاء المدن الليبية، على الطرقات العامة الرئيسية والفرعية، وبالقرب من المدارس والأسواق والمساجد لتكون متاحة لعامة المستهلكين وهي مخصصة بشكل مباشر لاستهلاك من قبل المجتمعات السكانية والتي استعاضت بها عن شبكة المياه العامة التي تقوم الدولة بإدارتها، حيث انتشرت هذه المحطات بالمدن الليبية للحصول على الماء الصالح للشرب، وتظهر جميعها بنفس التصميم والآلية حيث تستخدم أجهزة التناضح العكسي (الفلاتر) لتحليه المياه الجوفي ، كما أن انتشار مثل هذه المحطات بالمدن يأتي بدافع الكسب المادي إذا تعتبر هذه المحطات مشاريع استثمارية يقوم بها أفراد وتخضع للمتابعة والفحوصات الفنية من قبل المجالس البلدية بالمدن. ومع ازدياد ظهور كثير من أصناف مياه الشرب تستدعي الحاجة إلى الاهتمام بإجراء الاختبارات والتحاليل للكشف عن مدى مطابقة خصائصها للمواصفات والمعايير القياسية الليبية والعالمية (المواصفة الليبية القياسية ،2016).

الدراسات السابقة cases studies:-

لقد تم الاطلاع علي العديد من الدراسات السابقة في مجال المياه المعبأة منها:−

1– قام (زاهد، 2002) بدراسة جودة مياه الشرب المعبأة المحلية والمستوردة في المملكة العربية السعودية تقييم جودة مياه 23 صنًفا منتجًا محلّيًا و 7 أصناف مستوردة من مياه الشرب المعبأة خلال النصف الأول من عام 2001 في مدينة الرياض بالمملكة العربية السعودية، ومقارنة النتائج بمواصفات مياه الشرب المعبأة الصادرة عن الهيئة العربية السعودية للمواصفات والمقاييس والجمعيّة العالمية لمياه الشرب المعبأة وإدارة الغذاء والدواء الأمريكية، تضمن التقييم المعايير الفيزيائية والكيميائية والميكروبيولوجية التالية الرقم الهيدروجيني، العكارة، المواد الصلبة الذائبة، العسر الكلي، الكالسيوم، المغنيسيوم، الصوديوم، الفلورايد، النترات، الكبريتات، الكلوريدات، الحديد، المنجنيز، وبكتريا الكوليفورم الكلية، بينت القياسات أن مستويات معايير جودة مياه الأصناف المحلية والمستوردة كانت مطابقة للمواصفات المختلفة فيما عدا الرقم الهيدروجيني في صنف محلي واحد، والفلورايد في 15 صنًفا محلّيًا، والمنجنيز في 12 صنًفا محلّيًا و 6 أصناف مستوردة كما أن تراكيز الفلورايد في صنفين محليين و 6 أصناف مستوردة لم تحقق المستوى الأدنى للفلورايد في المواصفات السعودية.

2– دراسة (العصاوي، 2007) حيث قام بدراسة تركيز الأملاح الكلية الذائبة ببعض أنواع المياه المحلية المعبأة وعينة من بحيرة قبرعون وأخرى من البحر المتوسط، أظهرت النتائج إن قيم الأملاح الذائبة الكلية للعينات (الكفرة معبأة 260)، (سفاري معبأة 65) ، (النبع معبأة 40) ، (المزن معبأة 305)، (صافيا معبأة 90)، (مياه البلدية 1100)، (بحيرة قبرعون 234500) و(البحر الأبيض المتوسط 38600).

3– دراسة (عبد الله وآخرون ،2007)، عن تقييم بكتريولوجي لبعض أنواع مياه الشرب المعبأة والمنتجة محليا مصادر هذه العينات هي مصنع مياه فزان– سبها، مصنع مياه تازربو– طرابلس، مصنع مياه الواحة – طرابلس، مصنع مياه الزهراء– طرابلس، مصنع مياه النبع– طرابلس، مصنع مياه– زليتن، مصنع طيبة– طرابلس، وقد تم في هذه الدراسة التعرف على وجود أجناس Neisseria, Pseudomonas Moraxella. Staphylococcus في بعض عينات المياه المعبأة، وجميع العينات المدروسة كانت خالية من مجموعة القولون الكلية والبرازية، بالرغم من الارتفاع في الأعداد الكلية في بعض العينات عن المواصفات القياسية الليبية.

أهداف الدراسة Objectives of Study:-

1- تقييم بعض الخصائص الكيميائية ومقارنتها بالمواصفات المحلية والعالمية لمياه الشرب المعبأة.

2- تقييم بكتريولوجي من خلال الكشف عن وجود بكتيريا *Escheriachia Coli* .

3- مقارنة مواصفات المحطات بالشروط الواجب توفرها عند إنشاء المحطة.

موقع منطقة الدراسة Rejoin of Study :-

مدينة صبراته تقع شمال غرب ليبيا كما هو مبين بالشكل رقم (1) ، بين خطي طول (12.8ً) و (12.31ً) شرقا ودائرتي عرض (32.27ً) و(32.51ً) شمالاً، ويحدها من الشمال البحر المتوسط ومن الجنوب منطقتي صرمان و العجيلات ومن الشرق منطقة صرمان ومن الغرب منطقة زواره شكل (1)، وتقدر مساحتها بـ (610 كم^2)، وهي مقسمة إلى إحدى عشر محلة متباينة من حيث المساحة (أشرف، 1996)، يبلغ سكان مدينة صبراتة حوالي 65,000 نسمة (عبدالعزيز ، 2017)، يعتمد اغلبهم على هذه المياه للشرب بسبب ملوحة مياه الآبار الارتوازية في اغلب مناطق المدينة.

شكل (1) توزيع محطات التحلية الخاضعة للدراسة

المواد وطرائق العمل Materials and Methods:-

شملت الدراسة الكشف البيولوجي عن البكتيريا القولونية *Escheriachia Coli* وتقييم الخصائص الفيزيوكيميائية (الرقم الهيدروجيني،والإيصالية الكهربائية، الأملاح الكلية) لـ 29 عينة من مياه الشرب تم جمعها من محطات تحلية المياه داخل مدينة صبراته.

شكل (2) نماذج لبعض محطات تحليه مياه الشرب المنتشرة بمدينة صبراتة

جمع العينات Collate of Samples:-

جمعت العينات وفق الطرق العلمية المتبعة، حيث أخذت قناني معقمة خاصة لجمع العينات لإجراء الكشف المجهري البكتيريا القولونية *E.Coli* ، وذلك بفتح الصنبور لمدة 5 دقائق قبل عملية تعقيم فوهة الصنبور جيدا بالكحول الإيثيلي ثم فتح صنبور الماء مرة ثانية لمدة 5 دقائق، لضمان التخلص من آثار الكحول الموجودة على فوهة الصنبور بماء العينة وحرصنا على ضمان عدم وجود إي آثار للكحول حتى لا تؤثر على الأحياء الدقيقة بالعينة، ويتم ذلك بفتح القنينة تحت تيار الماء، تغلق بإحكام

وتوضع في حافظة تبريد عند درجة حرارة 4 حتى وصولها إلى المختبر الشكل (3) ، كما أخذت عينات من المياه في قوارير بلاستيكية بحجم لتر ونصف بعد غسلها بماء العينة ثلاث مرات مع عدم رج العينة، حتى لا يفقد الماء جزء من ثاني أكسيد الكربون والذي يؤثر على مقدار الرقم الهيدروجيني حتى وصولها إلى المختبر .

شكل (3) تجميع العينات

الكشف عن بكتيريا *Escheriachia Coli* :– استخدم الوسط الغذائي الانتقائي Compact dry (E. C) لتنمية بكتيريا *Ecoli.*، وتم ملاحظة نمو المستعمرات البكتيرية بعد تنميتها في الحضانة في درجة حرارة ($37 C^o$) لمدة 24 ساعة.
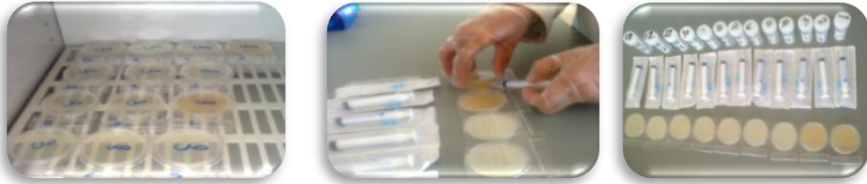
شكل (4) الكشف المجهري للعينات

التحاليل الفيزوكيميائية physicochemical analysis:-
استخدم جهاز (Multi meter) لتقدير الصفات الفيزوكيميائية (الرقم الهيدروجيني، الإيصالية الكهربائية، الأملاح الكلية).

International Science and
Technology Journal
المجلة الدولية للعلوم والتقنية

العدد 26
Volume 26

ISTJ
المجلة الدولية للعلوم والتقنية
International Science and Technology Journal

النتائج والمناقشة Result and Discussion :-

يبين الجدول (1) ،نتائج الاختبارات المجهرية وكذلك نتائج الخصائص الفيزيوكيميائية .

جدول (1) نتائج الخصائص الفيزيوكيميائية والبيولوجية للعينات

E .Coli	EC µs/cm	TDS mg / l	pH	رقم العينة
-	85.10	46.81	7.23	W1
-	141.10	77. 61	6.74	W2
+	111.60	61.38	6.77	W3
-	44.70	24.59	6.69	W4
+	53.60	29.48	6.53	W5
-	94.60	52.03	8.01	W6
-	342.60	188.43	6.80	W7
-	104.50	57.48	7.1	W8
-	325.00	187.75	6.5	W9
-	112.50	61.88	6.45	W10
-	63.90	35.15	6.19	W11
-	122.90	67.60	6.09	W12
+	78.20	43.01	5.88	W13
-	128.80	70.84	7.70	14W
-	106.3	58	7.48	15W
-	47.30	26.02	7.55	16W
-	47.60	26.18	7.13	W17
-	154.10	84.76	8.26	18W
-	22.00	12.10	7.23	W19
-	26.80	14.74	7.29	20W
-	25.60	14.08	7.13	21W
-	17.36	9.55	7.22	22W
-	34.30	18.87	6.99	23W
-	38.30	21.07	6.89	W24
-	11.10	6.11	6.94	25W
-	99.30	54.62	6.62	26W
-	56.80	31.24	6.65	27W
-	46.80	25.74	6.57	28W
/	32.00	17.60	6.64	29W
صفر	لا توجد قيمة	500-100	6.5 – 8.5	المواصفة الليبية للمياه المعبأة
-	450-1500	500-100	6.5 – 8.5	منظمة الصحة العالمية (WHO)

أولا:- مناقشة نتائج الكشف المجهري عن بكتريا   E. Coli

في نهاية الفحص الميكروبي لجميع العينات التي تم تجميعها من29 محطة تنقية، تبين إن العينات (3،5،13) ملوثة بالبكتيريا وخلو باقي العينات من التلوث البكتيري   E. Coli كما بالجدول (1)، و كان التلوث شديدا في العينة (5) حيث كان عدد المستعمرات بيها 73 مستعمرة، بينما العينتين (3،13) كانتا اقل تلوثا حيث كان عدد المستعمرات بهما (1 و 3) على التوالي، الشكل (5)، ويذكر هنا إن العينة (3) والعينة (5) ناتجة عن محطة تنقية تقع في منطقة تعرف بالسوق وهي منطقة مكتظة بالعمالة الوافدة وبتزايد فيها عدد الوافدين لاشتهارها بسوق شعبي كبير ولزيادة البناء العمراني بها مما نتج عنه عدم الاهتمام بالظروف المحيطية بهذه المحطات كما تبين إن المسافة بين خزانات هذه المحطات والآبار السوداء   (6 متر) للعينة 5 و (11 متر) للعينة 3، إذا يشكل القرب من الآبار السوداء إحدى أهم أ؟سباب التلوث البكتيري، وقد يحدث التلوث البكتيري بسبب عدم كفاءة المرشحات بالمحطة أو بسبب ظرف النخرين (عبدالله وآخرون، 2007).

و أشارت (Singla *et al*, 2014) إن تواجد بكتيريا Coliform تصل إلى 16.75 في 4 عينات من صنف المياه المعالجة المعبأة في الأكياس المستخدمة في مدينة دلهي بالهند . وهذا مؤشر هام وخطير مما يدع مجال للشك عن تدهور مستوى الجودة لمياه الشرب التي تنتجها هذه المحطات
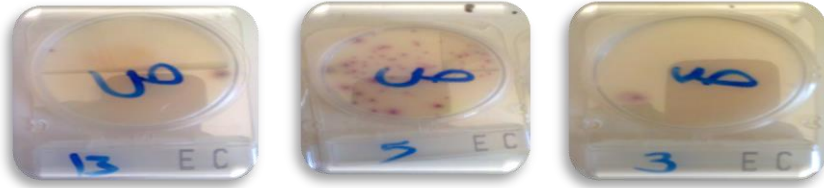
الشكل (5) التلوث البكتيري في عينات المياه الملوثة

ان التلويث الميكروبي للشبكات الحضرية الكبرى يمكن أن يسبب فاشيات واسعة النطاق للأمراض المحمولة بالماء، ولذلك يمثل ضمان الجودة في هذه النظم إحدى الأولويات، ومع ذلك فإن معظم سكان العالم نحو ٨٠ ٪ الذين لا تتوفر لهم إمكانات الحصول على إمدادات محسنة من مياه الشرب يقيمون في المناطق الريفية،   كذلك تسهم

إمدادات المياه الصغيرة والمجتمعية المحلية في معظم البلدان على نحو غير متناسب في مجمل المخاوف المرتبطة بجودة مياه الشرب، وينبغي أن يأخذ تحديد الأولويات الوطنية والمحلية في الحسبان العوامل من هذا القبيل.

ثانيا :- مناقشة نتائج التحاليل الفيزيوكيميائية

تراوحت قيم pH في الجدول (1) لكل العينات المدروسة بين (5.88 –8.26) وبالتالي فإن العينات 10، 11، 12، 13 كانت قيمها (6.45 ، 6.19 ، 6.09 ، 5.88) على التوالي وهى تحت الحد الأدنى المسموح به في المواصفة الليبية والعالمية للمياه المعبأة، في حين كانت بقية العينات ضمن الحدود المسموح بها، وقد أشار (الخير وآخرون، 2005) إن من أسباب تغير الأس الهيدروجيني هو التغير في درجات الحرارة، لذلك جمعت العينات صباحا ونقلت إلى المعمل عند درجة حرارة لا تتجاوز 25 درجة مئوية.

وبالنسبة للنتائج المتحصل عليها عن الإيصالية الكهربائية ومن مقارنة النتائج مع المحددات القياسية لمنظمة الصحة العالمية والتي حددت ب 2500 مايكروسيمينز/ سم نلاحظ إن جميع العينات المدروسة لم تتجاوز الحدود المسموح بها، وبينت نتائج تحليل العينات أن العينتين (7 و 9) هي (342.60 و 325.00) µs/cm على التوالي ، كما إن اقل قيمة كانت للعينة (25) وهي (11.10) µs/cm وهذا يدل على انخفاض محتواها الأيوني الذي هو مؤشرا غير مباشرا لمحتوى العينة من الأملاح الذائبة.

أما بالنسبة لمحتوى العينات من المواد الصلبة الذائبة فقد تراوحت النسب بين (6.11– 188.43 مليجرام/لتر) في العينات المدروسة، حيث كانت العينات (7 و 9) اعلي التراكيز والتي تزاوجت 100 مليجرام/لتر، إما باقي العينات فكانت كلها تحت 100 مليجرام/لتر، وبذلك تكون كل العينات تحت الحد الأدنى المسموح به في المواصفة القياسية الليبية والعالمية، وبحسب المواصفة القياسية الليبية فإن كل العينات تقع ضمن الحد الأعلى المسموح به بمواصفات كلا من منظمة الصحة العالمية لمياه الشرب المعبأة والمواصفة الليبية لمياه الشرب المعبأة (500 مليجرام/لتر). إلا أن التقرير الطبية تشير إلى أن انخفاض معدل الأملاح بمياه الشرب غير صحي ، كما ذكرت صحيفة

البيان الالكترونية في عددها المنشور بتاريخ (7 / 11/ 2009) إن متوسط الأملاح في مياه الشرب في ليبيا يصل إلى 63 مليجرام / اللتر ، وذلك يعني أن هذه المياه شبه مقطرة وهي ضارة بالصحة حيث تحتوي على نسب قليلة من عنصري الكالسيوم والصوديوم وكذلك باقي الأملاح الضرورية للجسم، والتي يؤدي نقصها إلى أضرار بالصحة وخاصة لدى الأطفال، كما ذكرت إن من عيوب المواصفة الليبية عدم وجود حد ادني لمحتوى المياه من الأملاح الذائبة وان محتوى 100 مليجرام / اللتر ، كحد ادني غير دقيق والأفضل اعتبار 63 مليجرام/اللتر حد ادني، وبذلك تكون العينتين (25) و (22) أكثر انخفاضا لمحتوى الأملاح الذائبة وهي غير مناسبة للشرب بتاتا ، وبنفس الحال للعينات (19، 20، 21، 29، 23، 24، 4، 28، 5، 16، 17، 16,26، 8، 25، 3، 10) التي يرتفع فيها تركيز الأملاح على التوالي إلا إنها اقل من 63 مليجرام/اللتر، وجاءت العينات (12، 14، 2، 18، 7، 9) بتراكيز أعلى من 63 مليجرام / اللتر والتي تكون أكثر ملائمة للاستهلاك البشري ، وبالنسبة لهذه النتائج يرجع أن تكون أسباب الانخفاض قيم الأملاح الذائبة الكلية هو الفلترة حيث تعمل الحديثة منها والتي تم إبدالها بجديدة نتيجة لعمليات الصيانة على طرد معظم الأملاح الذائبة وبالتالي هي ناتجة عن كفاءة هذه الأجهزة، وقد لوحظت إن معظم هذه المحطات هي حديثة الإنشاء من 6 شهور إلى 3 سنوات.
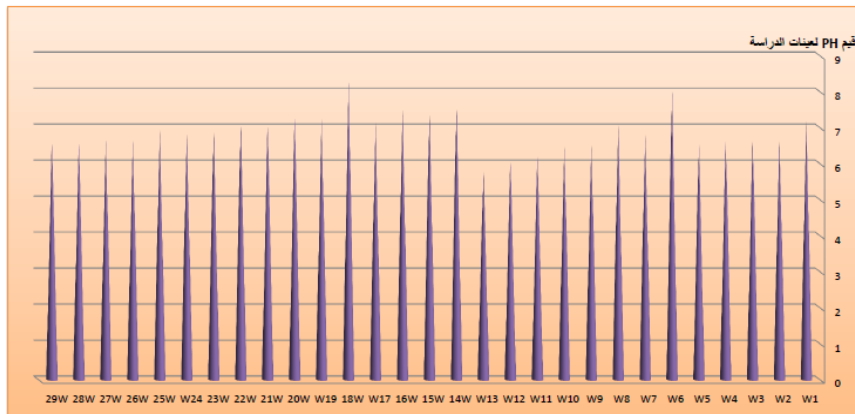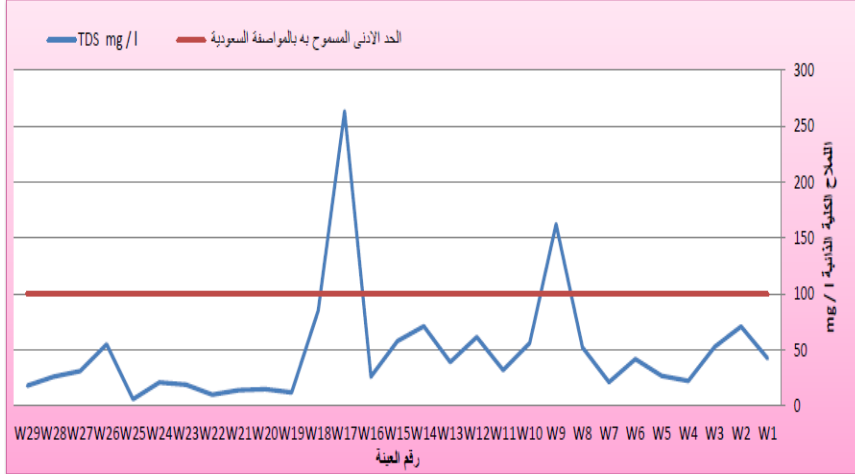

الشكل (7) يبين قيمة الأس الهيدروجيني لعينات الدراسة
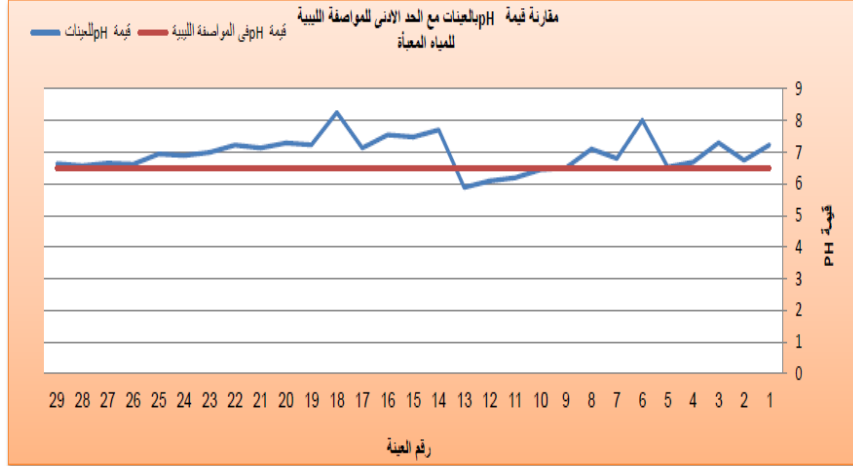
الشكل (8) يبين مقارنة الأس الهيدروجيني للعينات بالحد الأدنى للمواصفة الليبية
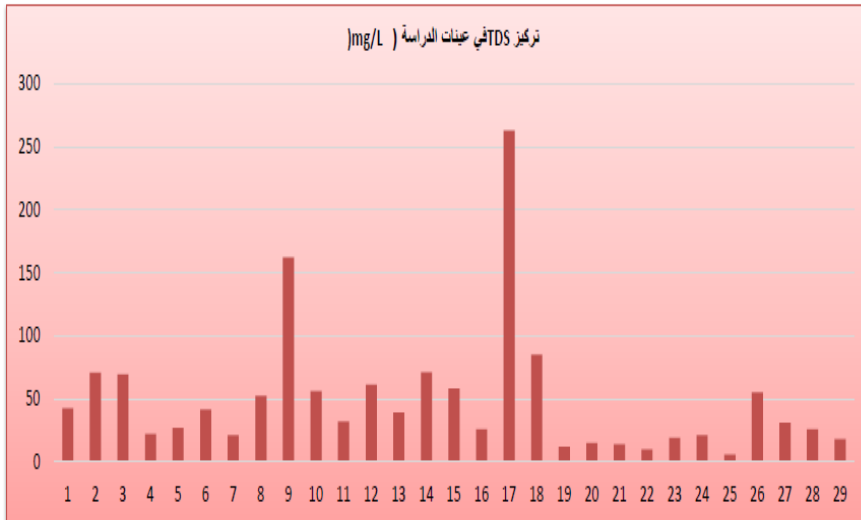
الشكل (9) يبين تركيز الأملاح الكلية الذائبة بعينات الدراسة

الشكل (10) يبين مقارنة تركيز الأملاح الكلية الذائبة للعينات بالحد الأدنى للمواصفة الليبي

نتائج المتطلبات الصحية Results of health requirements-:

يبين الشكل (8، 10) الفشل في المحطات المدروسة لتطبيق المتطلبات الصحية الواردة في المواصفة القياسية الليبية رقم 10 لسنة 2008 لمياه الشرب المعبأة والصادرة عن المركز الوطني للمواصفات والمعايير، وأظهرت نتائج الدراسة الحالية فشل 100 %من نماذج المحطات قيد الدراسة في تطبيق المتطلبات الصحية، ويعود ذلك إلى عدم التزام كل المحطات المدروسة في إتباع الاشتراطات العامة والصحية لإنشاء المحطة، وبالنظر إلى عوامل جودة المياه المعبأة هناك عدة عوامل مرتبطة قد لا تتوفر في مثل هذه المحطات، فقد أشار (Malwina *et al* ., 2013) أن من أهمها، العمليات والإنتاج النهائي، إحكام غلق العبوات، ونوعية المياه الأولية للعبوات، كما أشار إلى أهمية تمكين المستهلك من المعلومات الخاصة بمصدر المياه .

الاستنتاجات conclusion-:

بناء على النتائج المتحصل عليها في هذه الدراسة الممثلة بمياه محطات التنقية المنتشرة بمدينة صبراته يتبين تدني قيم الأملاح الكلية الذائبة لمستويات خطرة فقد وصل تركيزها 6.11 ملجم / لتر، وتدنى عام في تركيزها عن 100 ملجم / لتر بأغلب العينات،

International Science and Technology Journal
المجلة الدولية للعلوم والتقنية
Technology Journal

العدد 26
Volume 26

ISTJ
المجلة الدولية للعلوم والتقنية
International Science and Technology Journal

وهى الحد الأدنى المسموح به فى المواصفة العالمية، 82 % من العينات تحت الحد الأدنى المسموح به لتركيز الأملاح الكلية الذائبة للمواصفة السعودية مما يشير إلى خطورة هذه النوعية من المياه نظرا لانخفاض تركيز الأملاح الكلية الذائبة بها وأيضا انخفاض قيم الأس الهيدروجيني ببعض العينات 13 % من العينات تحت القيمة المسموح بها بخصوص pH فقد وصلت القيم 5.8 مما يشير لحموضة المياه و ارتفاع مستوى التلوث الميكروبي ببعض العينات إن ارتفاع مستوى التلوث في بعض العينات بمؤشرات التلوث الميكروبي التي تم دراستها، 10 % من العينات ملوثة ببكتريا *E. coli* يدل إما على استخدام مصدر مائي ملوث أو تعرض المياه للتلوث خلال مراحل التصنيع.

التوصيات Recommendation -:

نظرا للتلوث الذي تم رصده بمياه محطات تنقية مياه الشرب فإن الدراسة توصي :

1- قيام الجهات ذات العلاقة باتخاذ الإجراءات اللازمة لتشديد الرقابة والمتابعة على جميع مصانع تعبئة مياه الشرب المجازة رسميا وغيرها من قبل الجهات المختصة، وتدقيق كفاءة وجودة خطوطها الإنتاجية ومساراتها التكنولوجية وطريقة الإنتاج ومدى مطابقتها للشروط الصحية والفنية اللازمة وخاصة غير الصالحة للاستهلاك المبينة في هذه الدراسة.

2- ضرورة إلزام معامل إنتاج مياه الشرب بإنشاء مختبر لمتابعة العينات وتقييم جودتها للشرب وإخضاعها إلى مراقبة وتدقيق الجهات ذات الاختصاص.

3- إلزام مصانع تنقية مياه الشرب بتوفير مكائن لغسل وتعقيم العبوات لضمان سلامة إعادة استخدامها مرة أخرى، إذ حددت المواصفة القياسية الليبية لمياه الشرب المعبأة ، وأن تكون العبوات من النوع الصالح للاستعمال في حفظ وتعبئة المواد الغذائية ومناسبة ونظيفة تماما وخالية من التلوث ولا تسبب أي تغيير في طعم آو لون أو رائحة المياه.

4- اتخاذ الإجراءات القانونية بحق المخالفين و تحذير المستهلك عبر وسائل الإعلام المرئية والمسموعة والمقروءة عن المنتجات غير الصالحة للاستهلاك البشري.

المراجــع العربية :-

[1] منظمة الصحة العالمية (2004). دلائل جودة مياه الشرب(التوصيات)، الطبعة[1] الثالثة، المجلد (1) .

[2] المواصفة الليبية القياسية 2016 (م. م. ق. ل 10). المركز الوطني للمواصفات والمعايير القياسية، الإصدار الثاني[2].

[3] رزوقي، سراب محمد محمود (2008). دراسة واقع صناعة مياه الشرب المعبأة في العراق بين الأعوام 1995 – 2008، المؤتمر العلمي الأول، الصحة العامة استثمار لحياة أفضل، وزارة الصحة .

[4] جهاز التقييس والسيطرة النوعية (1995). المواصفة القياسية العراقية لمياه الشرب المعبأة (م ق ع /1937 /1995)، وزارة التخطيط والتعاون الإنمائي.

[5] الاميري، نجلة جبر، عصام محمد علي، صباح مالك الشطي (2013). تقييم نوعية بعض مياه الشرب المعبأة المحلية والمستوردة المعروضة بالأسواق المحلية في محافظة البصرة لأغراض الشرب، مجلة البصرة للعلوم الزراعية، المجلد 25(1): 387 – 400.

[6] عبد الله، محمد عبد الله، حسين أحمد الرشيد، منى مختار بشير، فاطمة عبد السلام سعد (2007). تقييم بكتريولوجي لبعض أنواع مياه الشرب المعبأة والمنتجة محليا، مجلة جامعة سبها (البحثية والتطبيقية)، المجلد السادس، العدد 3: 34–39.

[7] زاهد، وليد بن محمد كامل (2002). دراسة جودة مياه الشرب المعبأة المحلية والمستوردة في المملكة العربية السعودية، مجلة جامعة الملك عبد العزيز، العلوم الهندسية، مجلد 14، العدد 2، ص : 81– 104.
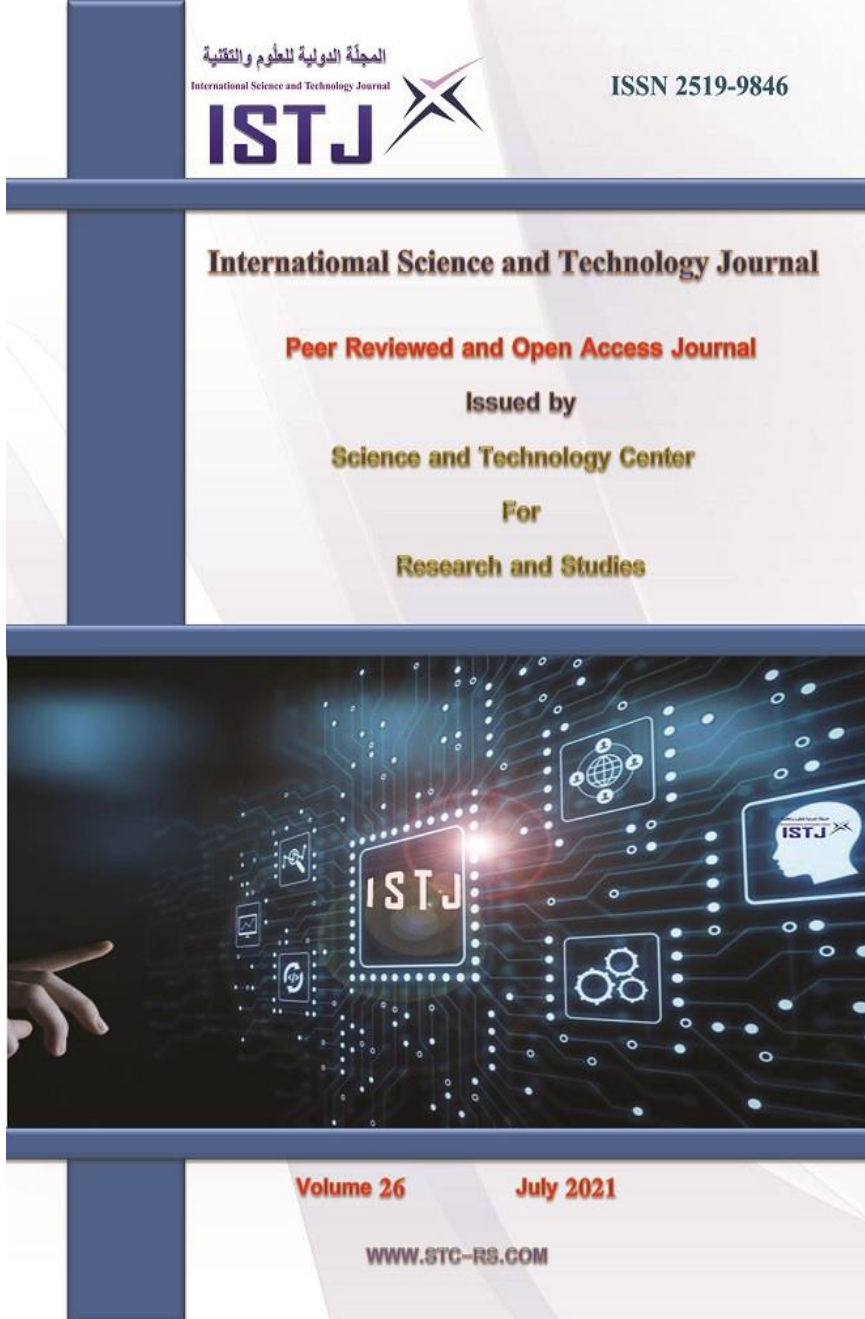
International Science and
Technology Journal
المجلة الدولية للعلوم والتقنية

العدد 26
Volume 26

المجلة الدولية للعلوم والتقنية
International Science and Technology Journal
ISTJ

[8] العصاوى، إبراهيم محمد و الضراط، فاطمة الصادق (2007). تقدير المواد الصلبة المذابة في بعض العينات من مياه الشرب (المعبأة ، المحلية) بليبيا، جامعة مصراتة – كلية العلوم – قسم الكيمياء .

[9] اشرف، عبدالعزيز طريح (1996). جغرافيا ليبيا، الطبعة الثانية، مركز الإسكندرية للكتاب، مصر .

[10] عبد العزيز، عبد الرزاق مصباح الصادق (2017). دراسة الوضع المائي لبلديتي صبراتة وصرمان، تقرير فني معد عن الوضع المائي لمدينتي صبراتة وصرمان بليبيا سنة 2017 (تقرير غير منشور).

[11] الزبيدى، عصام شاكر (2010). تركيز الأملاح الكلية الذائبة للمياه المعبأة في السوق العراقية، المجلة العراقية لبحوث السوق وحماية المستهلك، مجلد (2)، العدد (3)

[12] محمد الخير. عبدالرؤوف مونة، مفتاح داعوب. عبدالمجيد التلماني (2005). تقدير كمية المواد الصلبة المذابة والأس الهيدروجيني للمياه الجوفية في مدينة هون/ ليبيا، المجلة الليبية العالمية، المجلد (1)، العدد(2).

المراجع الأجنبية:-

[13] World Health Organization.(1986). Nitrates Blamed For Baby Death in South Dakota, Bulletin, Work Sheet 2

[14] Singla , Ashish , Hansa Kundu, Basavaraj P, Shilpi Singh, Khushboo Singh and Swati Jain (2014). Physico-Chemical and Bacterial Evaluation of Packaged Drinking Water Marketed in Delhi - Potential Public Health Implications, J Clin Diagn Res, v.8(3).

[15] WHO: World Health Organization (1996). The directives for drinking water quality, 2nd , part 2, healthy criterion and other information, Geneve, Switzerland.

[16] Mahajan , Rakesh Kumar ,T. P. S. Walia,B. S. Lark &Sumanjit (2007).   Analysis of physical and chemical parameters of bottled drinking water, Published online: 22 Pages 89-98.

[17]   Murtala Mohammed Ruma, Aziza Mohamed Ali Badr, Soliman Abd Alsattar Khater, and Attia Mahmoud Mohamed El-tantawi (2014). assessment of some physicochemical parameters levels in sachet drinking water and its effects on human health in katsina urban area, Nigeria, Science World Journal Vol 9 (No 1).

[18]   Malwina Diduch, Z˙ aneta Polkowska and Jacek Namies´nik (2013). Factors affecting the quality of bottled water, Journal of Exposure Science and Environmental Epidemiology 23, 111–119.

المجلة الدولية للعلوم والتقنية
International Science and Technology Journal

ISTJ

ISSN 2519-9846

Internatiomal Science and Technology Journal

Peer Reviewed and Open Access Journal

Issued by

Science and Technology Center

For

Research and Studies

ISTJ

Volume 26   **July 2021**

WWW.STC-RS.COM

The International Science and Technology Journal (ISTJ)

The International Science and Technology Journal (ISTJ) publishes research from all fields of academic, technical and applied sciences. The final editing and formatting of all accepted papers is done by the editorial board to ensure the consistency of the format and the quality of the product. (Please download the final editing and formatting from the website or Facebook page).

Chairman of the Editorial Board

Table of Contents

A Brief Overview of 6G Research Activities

Salim Abdallah El Hussain, Abdulhakim Ibrahim Fadlallah
College of Technical Sciences – Derna
saleemelhussain@gmail.com

الملخص

بدأ تسويق الجيل الخامس من الاتصالات المتنقلة عام 2019 م، مع توقع اعتماده على نطاق واسع في عام2021 م وما بعده. نتيجة لوباء كرونا المستجد (كوفيد−19)، دخلت المزيد من شركات على الانترنت، حيث اقبل العديد من الموظفين على تأدية أعمالهم عن بعد عن طريق الانترنت. وكنتيجة للاستخدام المتزايد للأنترنت بدأت الحاجة ملحة لتلبية الطلب المتزايد على الانترنت الذي أصبح أكثر حده. تهدف شبكات الجيل السادس لتوفير أداء متفوق على الجيل الخامس وتحقيق التطوير في الخدمات والتطبيقات مما يجعلها عامل تمكين أساسي لمجتمع المعلومات الذكي لعام 2030م. في هذه الورقة، نقدم مسحًا للتقنيات الأساسية المحتملة في G6. على وجه الخصوص، سوف نقدم الذكاء الفني والتحديات وتقنيات الاتصالات الحديثة، وتيرا هيرتز بالتفصيل، مع إعطاء مقدمة موجزة للتقنيات المحتملة الأخرى.

Abstract

Commercialization of 5G began in 2019, with widespread adoption projected by 2021 and beyond. As a result of the COVID-19 epidemic, more firms went online, ushering in a "New Normal" with a global workplace. The increased Internet usage that has resulted highlights the need for better connectivity in order to fulfill the growing demand for more severe network needs. 6G networks are intended to provide performance superior to 5G and fulfill developing services and applications, making them a crucial enabler for the intelligent information society of 2030. In this

International Science and Technology Journal
المجلة الدولية للعلوم والتقنية

العدد 26
Volume 26

ISTJ
المجلة الدولية للعلوم والتقنية
International Science and Technology Journal

paper, we present a survey of potential essential technologies in 6G. In particular, we will introduce articial intelligence, challenges and state -of- the- art, and terahertz communications technologies in detail, while giving a brief introduction to other potential technologies.

Keywords: Internet usage, better connectivity, 6G networks, intelligent information society

I.INTRODUCTION

Due to the advent of gadgets and machine-to-machine (M2M) interactions, mobile data traffic has increased exponentially during the past 10 years, the exponential expansion of mobile connectivity as shown in Figure 1, the global mobile traffic volume is also expected to increase 670 times by 2030 compared to 2010 and in general, the number of mobile phone subscriptions is expected to reach 17.1 billion [1].
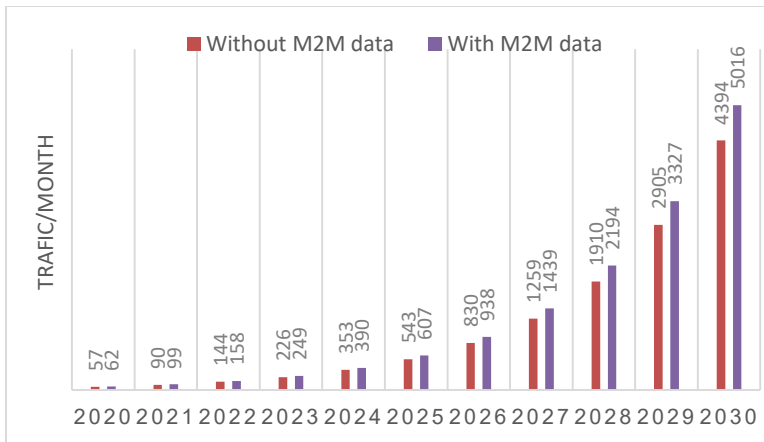
Figure 1. ITU Predictions for Global Mobile Data Traffic [1]

Data-driven adaptive and intelligent approaches have recently piqued researchers' interest. The 5G wireless networks will lay the

International Science and Technology Journal
المجلة الدولية للعلوم والتقنية

العدد 26
Volume 26

المجلة الدولية للعلوم والتقنية
International Science and Technology Journal
ISTJ

groundwork for intelligent networks that can perform Ai tasks [2]. The capacity of 5G is predicted to reach its limit by 2030 [3]. In the rest of the paper, we discuss relevant work, important difficulties, and state-of-the-art techniques and solutions.

II.LITERATURE REVIEW

A vision of 6G mobile networks is presented in several publications, which include enabling technology, prospective uses, needs, and problems. The authors of [4] focused on the important accomplishments and challenges of earlier mobile networks, ranging from 1G to 5G as showing in figure 2.

Figure 2. Shows the evolution of service kinds throughout   wireless mobile generations.

The progression of mobile networks to the 6G network was covered in [5]. The authors [6] concentrated on projected

architectural changes in 6G networks, such as 3D architecture and pervasive Ai. The authors of [7] present a complete picture of 6G, including anticipated applications, emerging trends, supporting technologies, and open research problems. The authors i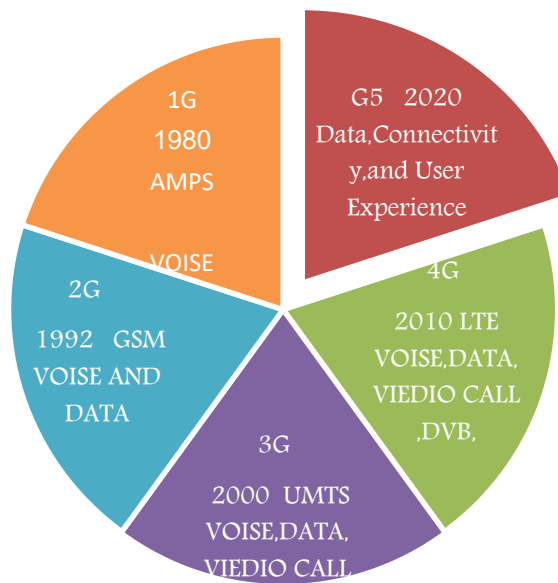n [8] explored 6G networks from an AI perspective as AI-based mobile applications grow more prevalent. The authors of this research stated that from the network core to the edge devices, 6G networks will be expected to incorporate pervasive AI solutions.[9] published one of the most recent studies on 6G networks. The writers reviewed 6G requirements and shared their vision of 6G networks. Furthermore, they hypothesized on the uses of the 6G era and highlighted the main anticipated hurdles. The authors of [10] provided a thorough analysis of 6G networks. Their analysis includes enabling technologies, possible use case scenarios, difficulties, as well as 6G's prospects and progress. Work [11] is one of the few papers that thoroughly investigates the fundamental services of the 6G network. The authors of [12] presented a list of 6G requirements based on probable future use cases (for example, augmented reality (AR)/virtual reality (VR) for industry and biosensors). Last but not least,[13] the authors emphasize the need of 6G remaining a human-centric network. In light of this, 6G networks will need to provide a high level of security and privacy.

III. CHALLENGES AND STATE-OF-THE-ARTS

 Some tough needs in 6G wireless communication must be met in order meet global technology demands. The major challenging themes are researched and discussed in this part. The THz band is the major issue in the 6G wireless communication technology. Despite the high data speeds, the high frequencies make overcoming the high path loss a significant challenge. The air absorption and propagation loss for long-distance communications are quite high. To solve the problem of frequency dispersion, new multipath channel models must be created due to the wide

International Science and Technology Journal
المجلة الدولية للعلوم والتقنية

العدد 26
Volume 26

المجلة الدولية للعلوم والتقنية
International Science and Technology Journal
ISTJ

bandwidth [14]. For the THz band, conventional modulation and coding methods are in sufficient. New transceivers should be developed to operate in the high frequency band, with very broad bandwidth, high power, high sensitivity, and low noise figure. Furthermore, not all wireless communication methods were compatible with devices. Devices should also allow users to engage with other devices via Device-to-Device D2D communication, AI, and XR [15]. Because billions of devices other than smartphones will be linked to the 6G network, efficient energy transfer techniques, particularly wireless energy transfer methods [16], should be explored, and devices connected should be designed to enable multiple charging ways. Physical layer security techniques and integrated network security strategies [17] with low cost, low complexity, and extremely high security should be studied. The high-frequency band in THz is supported by 6G wireless communication technologies, as well as spectrum and resource sharing. Transceivers should be able to support this technology if the antenna is constructed with the appropriate size; nano scale to micrometre components that meet the holographic beam forming criteria as described in [18, 19].

IV. THz COMMUNICATIONS

In general, the low-frequency spectrum band has a better propagation characteristic to enable large coverage, but because of the comparatively small bandwidth, it achieves a poor transmission rate. With the exponential growth of high-data-rate needs, 5G is expected to make advantage of the mm Wave spectrum, which can provide new bandwidths in the gigahertz range [20].

V.POTENTIALAPPLICATIONS

Some of the most important 6G wireless communication applications uMUB, uHLSLLC, mMTC, and uHDD services are used to describe 6G applications as showing in figure 3.

International Science and
Technology Journal
المجلة الدولية للعلوم والتقنية

العدد 26
Volume 26

المجلة الدولية للعلوم والتقنية
International Science and Technology Journal
ISTJ
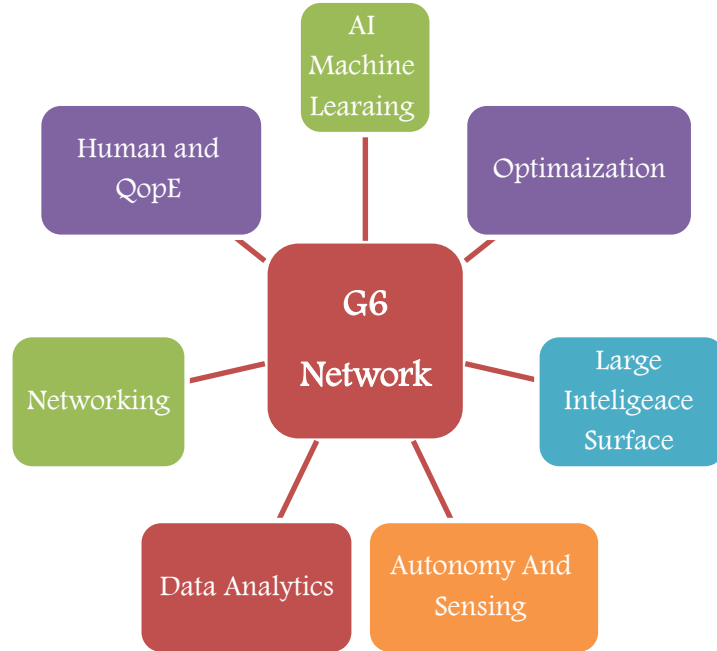
Figure 3. Depicts a summary of 6G uses.

Extended reality (XR) services, such as augmented reality (AR), mixed reality (MR), and virtual reality (VR), are critical components of 6G communication networks. All of these features rely on 3D objects and AI as their driving forces. 6G will deliver a completely immersive AR/MR/VR experience through collaborative design integration and high-quality 6G wireless connectivity, in addition to meeting perceptual computing, cognition, storage, human senses, and physiological needs [21]. Furthermore, when the cellular base station is unavailable or malfunctioning, the UAV will be employed to provide wireless broadcast and high-rate communications [22]. The brain-computer interface (BCI) is a method of controlling the brain. Home appliances and medical equipment, in particular, are commonplace

in smart societies [23]. In 6G wireless communication, the characteristics of uHLSLLC and uMTC will allow the real deployment of BCI systems for a smart life. The sensation of touch is used in haptic communication, which is a type of nonverbal communication. Remote users will be able to enjoy haptic sensations through real-time interactive systems thanks to the proposed 6G wireless connection [24].

VI. AI EMPOWERED WIRELESS COMMUNICATIONS

AI will be essential in optimizing future 6G networks by solving issues that are difficult to describe using closed-form models [25]. 6G will allow additional applications, as seen in figure 4, by utilizing Ai.

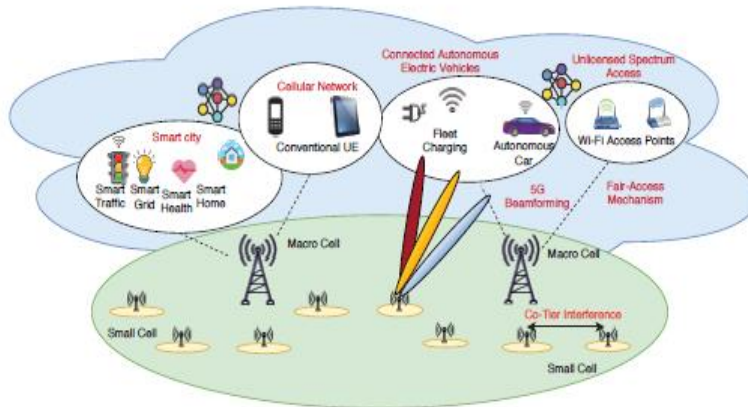Figure 4. A 6G wireless network with AI capabilities and associated applications [26].

Smart cities, cellular networks, linked autonomous electric cars, and unlicensed spectrum access are all examples of intelligent systems [27]. To ease large-scale deployment of 6G networks, this will justify a demand for the creation of new network designs and system models, as well as standardized interfaces, protocols, and

data formats [28]. Deep learning, which is regarded as a key component of AI technology, is frequently utilized in wireless networks [29]. It will be critical in a number of areas, including semantic communications, holistic communication management, control resource regions, caching, and computing, among others, all of which will contribute to the 6G paradigm change.

VII. CONCLUSIONS

Wireless communication networks of the sixth generation (6G) are planned to give global coverage. We looked at previous studies, prospective requirements and trends, enabling technologies, potential difficulties, and future research paths related to 6G.A 6G networks will rely on new technology to achieve these requirements. We have highlighted the potential applications that may be utilized for 6G communication in addition to explaining the vision and aim of 6G communications.

Reference

[1] "IMT traffic estimates for the years 2020 to 2030," Int. Telecommun. Union, ITU-Recommedation M.2370-0, Jul. 2015.

[2] S. J. Nawaz, S. K. Sharma, S. Wyne, M. N. Patwary, and M. Asaduzzaman, "Quantum machine learning for 6G communication networks: State-of-the-art and vision for the future," IEEE Access, vol. 7, pp. 46317–46350, 2019.

[3] F. Tariq, M. Khandaker, K.-K. Wong, M. Imran, M. Bennis, and M. Debbah, "A speculative study on 6G," 2019. [Online]. Available: arXiv:1902.06700.

[4] K. David and H. Berndt, "6G vision and requirements: Is there any need for beyond 5G?" IEEE Vehicular Technology Magazine, vol. 13, no. 3, pp. 72–80, Jul. 2018.

[5] T. Huang, W. Yang, J. Wu, J. Ma, X. Zhang, and D. Zhang, "A survey on green 6G network: Architecture and technologies," IEEE Access, vol. 7, pp. 175 758–175 768, Dec. 2019.

[6] ZHANG, Lin; LIANG, Ying-Chang; NIYATO, Dusit. 6G Visions: Mobile ultra- broadband, super internet-of-things, and artificial intelligence. China Communications, 2019, 16.8: 1-14.

[7] W. Saad, M. Bennis, and M. Chen, "A vision of 6G wireless systems: Applications, trends, technologies, and open research problems," IEEE Network, vol. 34, no. 3, pp. 134–142, May/June. 2019.

[8] K. B. Letaief, W. Chen, Y. Shi, J. Zhang, and Y.-J. A. Zhang, "The roadmap to 6G: AI empowered wireless networks," IEEE Communications Magazine, vol. 57, no. 8, pp. 84–90, Aug. 2019.

[9] F. Tariq, M. R. Khandaker, K.-K. Wong, M. A. Imran, M. Bennis, and M. Debbah, "A speculative study on 6G," IEEE Wireless Communications, vol. 27, no. 4, pp. 118–125, Aug. 2020.

[10] Y. Lu and X. Zheng, "6G: A survey on technologies, scenarios, challenges, and the related issues," Journal of Industrial Information Integration, vol. 19, p. 100158, Jul. 2020.

[11] [G. Gui, M. Liu, F. Tang, N. Kato, and F. Adachi, "6G: Opening new horizons for integration of comfort, security, and intelligence," IEEE Wireless Communications, vol. 27, no. 5, pp. 126–132, Oct. 2020.

[12] H. Viswanathan and P. E. Mogensen, "Communications in the 6G era," IEEE Access, vol. 8, pp. 57 063–57 074, Mar. 2020.

[13] X. Li, Q. Wang, M. Liu, J. Li, H. Peng, J. Piran, and L. Li, "Cooperative wireless-powered NOMA relaying for B5G IoT networks with hardware impairments and channel estimation errors," IEEE Internet of Things Journal, Oct. 2020.

[14] I. Akyildiz, J. Jornet, and C. Han," Terahertz band: Next frontier for wireless communications," Physical Communication, 10.1016/j.phycom.2014.01.006, 2014.

[15] M. Chowdhury, M. Shahjalal, S. Ahmed, and Y. Jang, "6G wireless communication systems: applications, requirements, technologies, challenges, and research directions," arXiv: 1909.11315, 2019.

International Science and
Technology Journal
المجلة الدولية للعلوم والتقنية

العدد 26
Volume 26

المجلة الدولية للعلوم والتقنية
International Science and Technology Journal
ISTJ

[16]   L. Pon, C. Leow, S. Abdulrahim, A. Eteng, M. Kamarudin, "Printed spiral resonator for displacement-tolerant near-field wireless energy transfer," IEEE Access, pp. 1–1, 2019.

[17]   P. Yang, Y. Xiao, M. Xiao, and S. Li, "6G wireless communications: vision and potential techniques," IEEE Network, vol. 33, no. 4, pp. 70–75, 2019.

[18]   A. Goian et al.," Fast detection of coherent signals using pre-conditioned root-MUSIC based on toeplitz matrix reconstruction," 2015 IEEE 11th International Conference on Wireless and Mobile Computing, Networking and Communications (WiMob), Abu Dhabi, pp. 168-174, 2015.

[19]   M. Alhajri et al.," Accurate and robust localization techniques for wireless sensor networks," arXiv:1806.05765, 2018.

[20]   M. Xiao et al., "Millimeter wave communications for future mobile networks," IEEE J. Sel. Areas Commun., vol. 35, no. 9, pp. 1909-1935, Sep. 2017.

[21]   W. Saad, M. Bennis, and M. Chen, "A vision of 6G wireless systems: Applications, trends, technologies, and open research problems," IEEENetw., vol. 34, no. 3, pp. 134–142, May/Jun. 2020.

[22]   [
22]. B. Li, Z. Fei, and Y. Zhang, "UAV communications for 5G and beyond:Recent advances and future trends," IEEE Internet Things J., vol. 6,no. 2, pp.2241–2263, Apr. 2019.

[23]   S. R. A. Jafri et al., "Wireless brain computer interface for smart home and medical system," Wireless Pers. Commun., vol. 106, no. 4, pp. 2163–2177, Jun. 2019.

[24]   [24]. 5G and the Haptic Internet: Emerging Technologies, Solutions and Market Opportunities, PR Newswire, New York, NY, USA, 2019.

[25]   L. Zhang, Y. Liang and D. Niyato, "6G Visions: Mobile Ultra-Broadband, Super Internetof-Things, and Artificial Intelligence," China Communications, vol. 16, no. 8, pp. 1-14, 2019.

[26]   ZHAO, Yang, et al. A survey of 6G wireless communications: Emerging technologies. arXiv preprint arXiv:2004.08549, 2020.

[27]   B. Zong, C. Fan, X. Wang, X. Duan, B. Wang, and J. Wang, \6G
technologies: Key drivers, core requirements, system architectures,
and enabling technologies," IEEE Vehicular Technology Magazine,
vol. 14, no. 3, pp. 18{27, 2019.

[28]   M. Lin and Y. Zhao, "Artificial Intelligence-Empowered
Resource Management for Future Wireless Communications: A
Survey," China Communications, vol. 17, no. 3, pp. 58-77, 2020.

[29]   Q. Mao, F. Hu, and Q. Hao, \Deep learning for Intelligent
wireless networks: Acomprehensive survey," IEEECommunications
Surveys & Tutorials, vol. 20, no. 4,pp. 2595{2621, 2018.

Calculation of the Lower Angular Excited States for Two Dimensional Finite Rectangular Well Potential Using Finite Difference Time Domain Method

Amal Hamed, Huwaida K. Elgweri and Mohamed Mansor

University of Tripoli

amal.HAMED@uot.edu.ly

Abstract

In this paper, the Schrödinger equation for two dimensional finite rectangular well potential has been solved numerically. The lower angular excited state wave functions and their corresponding energy eigenvalues are determined as well. These calculations are performed using the finite difference time domain method (FDTD) by taking advantage of the symmetric properties of the wave functions. Since there are no exact analytical solutions to the finite rectangular well potential, so in order to confirm the accuracy of our calculations, we studied different values of potential depths with certain value of potential area then we compared our results to the exact solutions of the infinite well potentials with the same area.

Kew words: finite difference time domain method, finite square well potential, finite rectangular well potentials, Schrödinger equation

الملخص

في هذا البحث تم حل معادلة شرودنجر لجهد بئر مستطيل محدود في بعدين عدديًا. حيث تم تحديد الدوال الموجية لحالات الاثارة الدنيا وقيم الطاقة الذاتية التابعة لها. تم إجراء هذه الحسابات باستخدام طريقة الفروق المحدودة في المجال الزمني من خلال الاستفادة من خصائص التماثل للدوال الموجية. ونظرًا لعدم وجود حلول تحليلية دقيقة لجهد البئر المستطيل المحدود، لذلك من أجل تأكيد دقة حساباتنا، قمنا بدراسة قيم

International Science and
Technology Journal
المجلة الدولية للعلوم والتقنية

العدد 26
Volume 26

المجلة الدولية للعلوم والتقنية
International Science and Technology Journal

ISTJ

مختلفة لأعماق الجهد مع قيمة معينة لمساحة الجهد ثم قمنا بمقارنة نتائجنا بالحلول
التحليلية لجهد بئر لانهائي له نفس المساحة .

1. Introduction

It is well known that solving Schrödinger equation for two dimensional finite rectangular well potential cannot be achieved analytically, since this potential is not separable potential. Therefore, in this case one has to resort the numerical technique. The Numerical methods have played an important role for solving many physics problems particularly in quantum mechanics. One of the most useful and powerful numerical methods is the finite difference time domain (FDTD) technique. It is successfully applied to obtain the ground state for any given system due to its diffusion behavior [1]. By modifying the boundary conditions of this method, it is easily employed to obtain some lower excited states beside to the ground state [2]. This modification involves introducing lines of zeros on the initial guess wave function and its second derivative. The only condition to apply this modification is that the potential of the studied system is symmetric, and as we will show later, the order of the excited states we can get depends on the number of symmetry axes of the potential. Therefore, applying this technique to the rectangular well potential that contains two symmetry axes allows us to extract the first three lowest angular excited states, while applying it to the square well potential leads to get extra angular excited state due to the diagonal symmetry axis of this potential.

This paper is organized into four sections including the introduction section as follows: the general theory section which introduces the (FDTD) method scheme in two-dimensions, followed by the symmetric modification scheme used to get the lowest angular excited states. In the calculations section, we apply this procedure to both the finite rectangular well potential and the finite square well potential, also the numerical results are illustrated and discussed in this section. Finally, the last section contains the summary and the conclusion.

International Science and
Technology Journal
المجلة الدولية للعلوم والتقنية

العدد 26
Volume 26

المجلة الدولية للعلوم والتقنية
International Science and Technology Journal
ISTJ

2. General Theory

The time dependent Schrödinger equation is given by

$$i\hbar \frac{\partial \psi(\vec{r},t)}{\partial t} = \hat{H} \psi(\vec{r},t) , \qquad (1)$$

where $\hat{H}$ is the Hamiltonian of the system. The dimensionless form of the Hamiltonian in two dimensions is given by

$$\hat{H} = -\left(\frac{\partial^2}{\partial x^2} + \frac{\partial^2}{\partial y^2}\right) + V(x,y). \qquad (2)$$

Applying the (FDTD) method to solve the time dependent Schrödinger equation requires transforming it into a diffusion type equation as

$$\hat{H} \psi(\vec{r},\tau) = -\frac{\partial \psi(\vec{r},\tau)}{\partial \tau}. \qquad (3)$$

This transformation is performed by replacing the real time domain to imaginary time domain i.e. $\tau = \frac{i}{\hbar}t$.

The solution of Eq. (3) in two dimensions can be written as a linear superposition of stationary states in the following form [1-4],

$$\psi(x,y,\tau) = \sum_{i=0}^{\infty} c_i \varphi_i(x,y) \, exp(-E_i\tau) , \qquad (4)$$

where c_i are expansion coefficients, $\varphi_i(x,y)$ and E_i are the complete set of eigenfunctions and their corresponding energy eigenvalues for the time-independent Schrödinger equation,

$$\hat{H}\varphi_i(x,y) = E_i\varphi_i(x,y). \qquad (5)$$

Since the (FDTD) method involves iterative procedure, so Eq. (4) can be rewritten in a convenient form as

$$\psi(x,y,n\Delta\tau) = \sum_{i=0}^{\infty} c_i \varphi_i(x,y) \, exp(-E_i n\Delta\tau) , \qquad (6)$$

where $\Delta\tau$ is the imaginary time step and n is an integer represents the number of the iterations. Applying the iterative procedure on arbitrary initial guess wave function that includes a mixture of all possible states will increase the value of the imaginary time

domain in each iteration by value equal to $\Delta\tau$ [3]. Therefore, for a large imaginary time interval the wave functions with high energy eigenvalues damp out quickly because of the factor $exp(-E_i n\Delta\tau)$ and only the lowest energy state remains which is of course the ground state in this initial guess wave function. For an ideal process the number of iterative steps n that required to obtain the lowest state wave function approaches infinity and Eq.(6) becomes

$$\lim_{n\to\infty} \psi(x, y, n\Delta\tau) = c_0 \varphi_0(x, y) \, exp(-E_0 n\Delta\tau), \qquad (7)$$

where E_0 is the smallest eigenvalue, and $c_0 \, exp(-E_0 n\Delta\tau)$ is just a constant factor which can be removed by normalizing the final wave function. It should be noted that normalizing of the wave function is done after each iteration step.

In this work, the (FDTD) method is employed to calculate the lower angular excited states by using initial guess wave function that contains lines of zeros laying on the anti-symmetric axis of the desired excited state wave function. The iterative procedure is then applied using this technique and numerically maintaining the symmetry properties of the desired wave function during the iteration, this procedure will eventually result in the appropriate lowest excited state. That is applying the iterative procedure subjected to the symmetric properties using initial guess wave function that includes no lines of zeros will approach to the ground state, while applying this procedure with the anti-symmetric properties using initial guess wave function that includes one line of zero will lead to the first angular excited state and so on.

Further details of explanation to calculate the energy eigenvalues and their corresponding eigenfunctions using symmetric properties of the potential wells in two dimensions, and the conditions those ensure continuity of symmetry of the applied initial guess wave function for both even parity and odd parity can be found in [2]. Due to the success of the (FDTD) method in applying it to two potentials that include: the simple harmonic oscillator and the finite cylindrical well with highly accurate results as demonstrated in [2], therefore, the same procedure is also applied to study the eigenvalues and eigenfunctions of a

International Science and
Technology Journal
المجلة الدولية للعلوم والتقنية

العدد 26
Volume 26

المجلة الدولية للعلوم والتقنية
ISTJ
International Science and Technology Journal

rectangular well potential in two dimensions as these potentials have no exact analytical solutions. Hence, we expect satisfying results will be obtained using similar numerical process.

In order to perform the iterative procedure involved in (FDTD) method, one has to transform the diffusion equation Eq. (3) into recursion form as follows;

Using the notation $\psi_{i,j}^n \equiv \psi(i\Delta x, j\Delta y, n\Delta \tau)$, the first order time derivative can be approximated by using the forward finite difference formula to be as

$$\frac{\partial \psi_{i,j}^n}{\partial \tau} = \frac{\psi_{i,j}^{n+1} - \psi_{i,j}^n}{\Delta \tau}. \tag{8}$$

In terms of the potential operator of the Hamiltonian in Eq. (2) it can be written as

$$V_{i,j}\, \psi_{i,j}^n = V_{i,j} \frac{\psi_{i,j}^n + \psi_{i,j}^{n+1}}{2}. \tag{9}$$

Also, the Laplacian operator can be found in two dimensions by using the central finite difference formula as

$$\nabla^2 \psi_{i,j}^n = \frac{\psi_{i+1,j}^n + \psi_{i-1,j}^n - 2\psi_{i,j}^n}{\Delta x^2} + \frac{\psi_{i,j+1}^n + \psi_{i,j-1}^n - 2\psi_{i,j}^n}{\Delta y^2}, \tag{10}$$

Where Δx is the mesh size between adjacent points $\Delta x = x_{n+1} - x_n$, and Δy is the mesh size between adjacent points $\Delta y = y_{n+1} - y_n$.

By plugging equations (8), (9) and (10) into Eq. (3) we get the recursion form equation

$$\psi_{i,j}^{n+1} = \alpha_{i,j}\psi_{i,j}^n + \beta_{i,j}\frac{\Delta \tau}{\Delta x^2}\left[\psi_{i+1,j}^n + \psi_{i-1,j}^n - 2\psi_{i,j}^n\right]$$
$$+ \beta_{i,j}\frac{\Delta \tau}{\Delta y^2}\left[\psi_{i,j+1}^n + \psi_{i,j-1}^n - 2\psi_{i,j}^n\right], \tag{11}$$

Where $\alpha_{i,j}$ is given by

$$\alpha_{i,j} = \frac{1 - \Delta \tau V_{i,j}}{1 + \Delta \tau V_{i,j}}, \tag{12}$$

and $\beta_{i,j}$ is given by

$$\beta_{i,j} = \frac{1}{1 + \Delta \tau V_{i,j}}. \tag{13}$$

International Science and Technology Journal
المجلة الدولية للعلوم والتقنية

العدد 26
Volume 26

المجلة الدولية للعلوم والتقنية
International Science and Technology Journal
ISTJ

In General, the success of the FDTD results is subjected by choosing suitable parameters of the spatial grid size and the time step. These parameters should satisfy the stability condition [5, 6], which is a very restricted condition, in order to prevent the numerical solution from diverging that is $\frac{\Delta \tau}{\Delta x^2} + \frac{\Delta \tau}{\Delta y^2} \leq 1$.

Because of the symmetric properties, the space used in these calculations is extended to the unclassical region and it is kept small by using the end formula for the second derivative at the boundaries which is given by,

$$\frac{\partial^2 \psi_{N,j}^n}{\partial x^2} = \frac{2\,\psi_{N,j}^n - 5\psi_{N-1,j}^n + 4\psi_{N-2,j}^n - \psi_{N-3,j}^n}{\Delta x^2}, \quad (14)$$

And by,

$$\frac{\partial^2 \psi_{i,N}^n}{\partial y^2} = \frac{2\,\psi_{i,N}^n - 5\psi_{i,N-1}^n + 4\psi_{i,N-2}^n - \psi_{i,N-3}^n}{\Delta y^2}, \quad (15)$$

As stated before, the iterative procedure applied on specific initial guess wave function must be subjected to the symmetric properties of this initial guess wave function, this can be achieved by giving more care in the second order derivative calculations at the axis. Therefore, if the axis includes zero line then the second derivatives along this axis using anti symmetric property will be equal to zero

$$\frac{\partial^2 \psi_{i,0}^n}{\partial x^2} = \frac{\partial^2 \psi_{i,0}^n}{\partial y^2} = 0, \quad (16)$$

$$\frac{\partial^2 \psi_{0,j}^n}{\partial x^2} = \frac{\partial^2 \psi_{0,j}^n}{\partial y^2} = 0. \quad (17)$$

If there is no zero line on the axis then the second derivative across this axis using symmetric property will be given by

$$\frac{\partial^2 \psi_{0,j}^n}{\partial x^2} = \frac{2\psi_{1,j}^n - 2\psi_{0,j}^n}{\Delta x^2}, \quad (18)$$

$$\frac{\partial^2 \psi_{i,0}^n}{\partial y^2} = \frac{2\psi_{i,1}^n - 2\psi_{i,0}^n}{\Delta y^2}. \quad (19)$$

Also, introducing zero line on the diagonal axis which presented by red points in Fig. 1 allows us to calculate the third angular excited state. This condition is performed only for the square well

International Science and
Technology Journal
المجلة الدولية للعلوم والتقنية

العدد 26
Volume 26

المجلة الدولية للعلوم والتقنية
International Science and Technology Journal
ISTJ

potential. We apply the same mesh size for this case and the second derivatives are given by

$$\frac{\partial^2 \psi_{i,j}^n}{\partial x^2} + \frac{\partial^2 \psi_{i,j}^n}{\partial y^2} = 0. \qquad if \qquad i = j. \quad (20)$$

For the end points presented in Fig.1 namely $\psi_{N,N-1}$ and $\psi_{N,N-2}$ the second derivatives with respect to x are calculated by using the end formula and anti-symmetric properties as

$$\frac{\partial^2 \psi_{N,N-1}^n}{\partial x^2} = \frac{2\psi_{N,N-1}^n - 5\psi_{N-1,N-1}^n - 4\psi_{N-1,N-2}^n + \psi_{N-1,N-3}^n}{\Delta x^2}, \quad (21)$$

$$\frac{\partial^2 \psi_{N,N-2}^n}{\partial x^2} = \frac{2\psi_{N,N-2}^n - 5\psi_{N-1,N-2}^n + 4\psi_{N-2,N-2}^n + \psi_{N-2,N-3}^n}{\Delta x^2}. \quad (22)$$

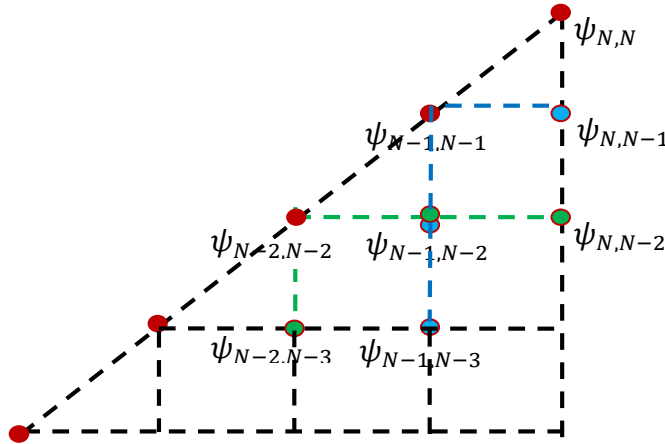Figure 1. Illustrates the second derivative calculations of the points $\psi_{N,N-1}$ and $\psi_{N,N-2}$ in the grid using the end point formula.

The energy eigenvalues are also calculated numerically by evaluating the expectation value of the Hamiltonian for their corresponding normalized eigenfunctions as [7, 8]

$$E = A \sum_{i}^{N} \sum_{j}^{N} \psi_{i,j}^* \hat{H} \psi_{i,j} \Delta x \Delta y, \qquad (23)$$

where A is a factor depends on the calculation area, in other words since the calculations of the first three lowest states are restricted to the first quarter of x-y plane then $A = 4$, whereas, the calculations of the third excited state are restricted to one eighth of x-y plane then $A = 8$.

3. Calculations

The two dimensional finite well potential is given by,

$$V(x, y) = \begin{cases} -V_0 & |x| \leq \frac{L_x}{2}, |y| \leq \frac{L_y}{2} \\ 0 & Otherwise \end{cases} , \qquad (24)$$

where V_0 is the depth of the potential, L_x and L_y are the lengths of the potential, so if $L_x \neq L_y$ we get the rectangular well potential, while if $L_x = L_y = L$ we get the square well potential.

In the distance unit a and energy unit $\frac{\hbar^2}{2ma^2}$ the dimensionless form of the time independent Schrödinger equation is given by,

$$-\nabla^2 \psi(x, y) + v(x, y)\psi(x, y) = \varepsilon \psi(x, y), \qquad (25)$$

where $v(x, y) = \frac{2ma^2}{\hbar^2} V(x, y)$, and $\varepsilon = \frac{2ma^2}{\hbar^2} |E|$.

This second order partial differential equation for finite rectangular well potential cannot be solved using separation of variables technique, therefore no exact results are offered for analytical solutions. So, we compare our numerical energy eigenvalues with the analytically eigenvalues of the infinite well potentials with the same dimensions, which are given in the reduced units by

$$\varepsilon^0\left(n_x, n_y\right) = \left(\frac{n_x^2}{L_x^2} + \frac{n_y^2}{L_y^2}\right)\pi^2 \quad , \quad n_x, n_y = 1,2,3, \dots \quad (26)$$

3.1. The finite rectangular well potential

Since there are only two symmetric axes on the rectangular well potential, then applying the symmetric techniques lead to the three lowest angular excited states beside the ground state, their

corresponding energy eigenvalues and eigenfunctions are shown in the following tables and figures. The simulation is performed using an appropriate size of mesh grids $\Delta x, \Delta y$ and the imaginary time step $\Delta \tau$. After enough number of iterations, the exact state functions are obtained. Generally, the accuracy of computed eigenvalues and eigenfunctions involve small grid space and large computational steps.

Table 1, illustrates the ground state energy eigenvalues calculated numerically for the rectangular well potential with five values of potential depths corresponding to potential area of $2X8$. For these lengths the exact ground state energy eigenvalue for the infinite well potential calculated using Eq. (26) is $\varepsilon^0(1,1) = 2.6216$. The expectation here is that $\Delta \varepsilon = \varepsilon + v_0$ approaches ε^0 for large or infinite v_0. This shift in energy amounts by changing the zero reference point to the bottom of the well and $\Delta\varepsilon$ is also expected to be less than ε^0 because of wave function spread.

TABLE 1. The Numerical Ground State Eigenvalues for Finite Rectangular Well Potential with Area 2X8

The depth	The energy eigenvalue	$\Delta\varepsilon(1,1)$	$\varepsilon^0 - \Delta\varepsilon$
100	-97.9862	2.0138	0.6078
1000	-997.7742	2.2258	0.3958
3000	-2997.6811	2.3189	0.3027
5000	-4997.5941	2.4059	0.2157
7000	-6997.4897	2.5103	0.1113

The lowest odd angular excited state energy eigenvalues are calculated for the rectangular well potential with well lengths $2X8$, in this case we can set the *x-axis* or the *y-axis* as the zero line. The numerical results are listed in Tables 2, 3. Using Eq. (26) the exact energy eigenvalues for the infinite well potential corresponding to this area are $\varepsilon^0(1,2) = 3.0843$ for the *x-axis* zero line and $\varepsilon^0(2,1) = 10.0238$ for the *y-axis* zero line.

TABLE 2. The Numerical First Angular Excited State Eigenvalues for Finite Rectangular Well Potential with Area 2X8 for Zero *x-axis*

The depth	The energy eigenvalue	$\Delta\varepsilon(1,2)$	$\varepsilon^0 - \Delta\varepsilon$
100	-97.5495	2.4055	0.6788
1000	-997.3821	2.6179	0.4664
3000	-2997.2953	2.7047	0.3796
5000	-4997.2054	2.7946	0.2897
7000	-6997.0944	2.9056	0.1787
9000	-8996.9636	3.0364	0.0479

TABLE 3. The Numerical Second Angular Excited State Eigenvalues for Finite Rectangular Well Potential with Area 2X8 for Zero *y-axis*

The depth	The energy eigenvalue	$\Delta\varepsilon(2,1)$	$\varepsilon^0 - \Delta\varepsilon$
100	-92.5498	7.4502	2.5736
1000	-991.7842	8.2138	1.8100
3000	-2991.5713	8.4287	1.5951
5000	-4991.4194	8.5806	1.4432
7000	-6991.2573	8.7427	1.2811
9000	-8991.0681	8.9319	1.0919

Finally, the third angular excited state energy eigenvalues calculated numerically with five values of potential depth corresponding to potential area $2X8$ are shown in table 4. This angular excited state contains two perpendicular lines of zeros. For these lengths the exact second angular excited state energy eigenvalue for the infinite well potential calculated using Eq. (26) is $\varepsilon^0(2,2) = 10.4865$.

TABLE 4. The Numerical Third Angular Excited State Eigenvalues for Finite Rectangular Well Potential with Area 2X8

The depth	The energy eigenvalue	$\Delta\varepsilon(2,2)$	$\varepsilon^0 - \Delta\varepsilon$
100	-92.1583	7.8417	2.6448
1000	-991.3923	8.6077	1.8788
3000	-2991.1861	8.8139	1.6726
5000	-4991.0317	8.9683	1.5182
7000	-6990.8635	9.1365	1.3500
9000	-8990.6663	9.3337	1.1528

It is clear from the results shown in the previous tables that by increasing the potential depth the results converge to the infinite well potential results which affirm our calculations. These

International Science and
Technology Journal
المجلة الدولية للعلوم والتقنية

العدد 26
Volume 26

المجلة الدولية للعلوم والتقنية
International Science and Technology Journal

ISTJ

calculations are performed with $\Delta \tau = 0.001$ and $\Delta x = \Delta y = 0.1$, with these parameters 500 iterations are sufficient to get acceptable results. Numerically, the integral calculations are used to norm the wave function and those are used to determine the energy eigenvalues are evaluated by using the trapezoidal rule.

In Fig.2 (a, b, c, d), we show the contour plot of the numerical eigenfunctions of the lowest four states for the rectangular well potential of depth 100 and dimensions 2X8 respectively.

Figure 2. The contour plot of the lowest four states wave functions of two dimensional finite rectangular well potential with depth 100 and lengths 2X8.

a. The normalized ground state wave function $\boldsymbol{\psi_{1,1}(x,y)}$.
b. The normalized first angular excited state wave function $\boldsymbol{\psi_{1,2}(x,y)}$.
c. The normalized second angular excited state wave function $\boldsymbol{\psi_{2,1}(x,y)}$.
d. The normalized third angular excited state wave function $\boldsymbol{\psi_{2,2}(x,y)}$.

3.2. The finite square well potential.

The usual square well potential could become special case for the rectangular well with similar initial conditions. In addition, the

same mathematical model was used in order to demonstrate the usefulness of the (FDTD) method to study the wave equation of the square well potential. Because of the symmetric properties of the square well we can extract the third angular excited state beside the three lowest states by introducing a diagonal zero line.

The results in table 5, show the numerically calculated energy eigenvalues for the four lowest states for the square well potential with depth 100 and length $4X4$ which has the same area of the previously studied rectangular well potential.

TABLE 5. The Numerical Lowest Four States Energy Eigenvalues for Square Well Potential with Depth 100 and Dimensions 4X4

The state	Energy eigenvalue
Ground state (no zero line)	-98.9285
1st angular excited state (one line of zero)	-97.3547
2nd angular excited state (two lines of zero)	-95.7816
3rd angular excited state (three lines of zero)	-89.5083

The contour plots of the numerical normalized wave functions associated with the energy eigenvalues presented in table 5 are shown in Fig 3. The ground state wave function is presented in Fig 3a, while Fig 3b. presents the degenerated first angular excited state wave function that contains one zero line laying on $y - axis$, Fig 3c. presents the second angular excited state wave function, and Fig 3d. presents the third angular excited state wave function.

International Science and Technology Journal
المجلة الدولية للعلوم والتقنية

العدد 26
Volume 26

المجلة الدولية للعلوم والتقنية
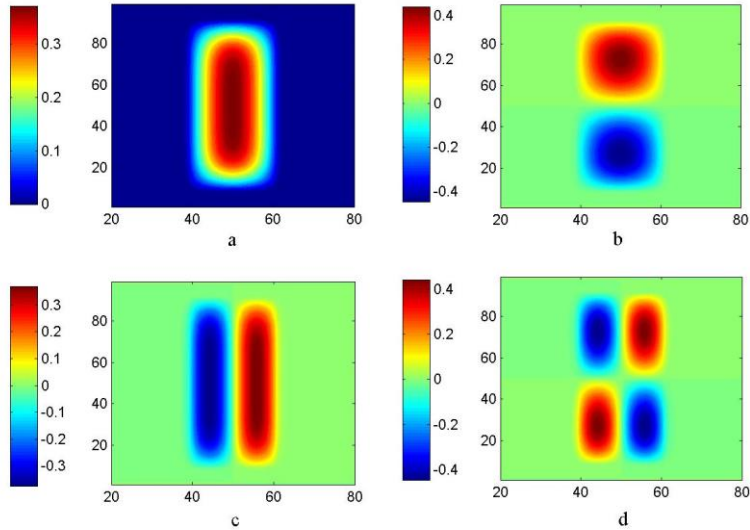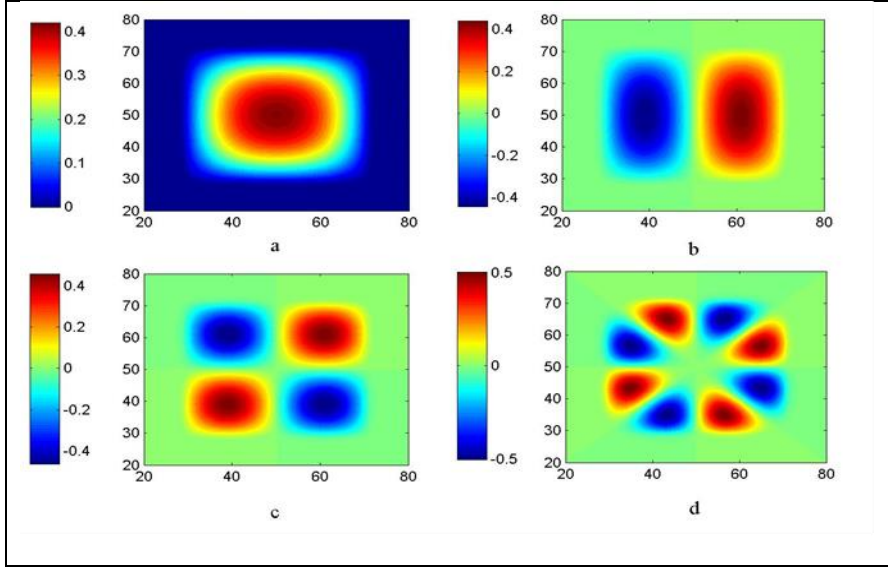International Science and Technology Journal
ISTJ

Figure 3. The contour plot of the four lowest states wave functions of two dimensional finite square well potential with depth 100 and lengths 4X4.
   a.   The normalized ground state wave function.
   b.   The normalized first angular excited state wave function.
   c.   The normalized second angular excited state wave function.
   d.   The normalized third angular excited state wave function

Conclusion

In this paper we presented the numerical solutions of the lowest angular excited states for a particle trapped in two-dimensional finite well potential. These solutions are produced by applying the (FDTD) method using the appropriate symmetric arguments, because of the symmetry of the potential, the wave functions can always be classified into symmetric or anti-symmetric wave functions. Also, these symmetry arguments reduce the computing cost to 25 % by using only the first quadrant. Further reduction of computing cost is obtained by using the end formula for the second derivative restricting the calculations to even a smaller region in the first quadrant. Two different shapes of the finite well potentials are studied in this investigation, the first shape is the rectangular well which involves two symmetric axes allowing us to calculate

the lowest angular excited states that contain two perpendicular axes, either both of them are symmetric axes, or only one of them is zero axis, or both of them are zero axes. The second shape is the square well which includes four symmetric axes that allows us to calculate extra angular excited state that contains diagonal zero axis. In the first example we checked our results by comparing it with those corresponding to the exact energy eigenvalues of the infinite rectangular well potential with the same area, such comparison gave us good guide for the accuracy of our numerical results.

References

[1] Wayan Sudiarta, I, Wallace Geldart, D.J, 2007, Solving the Schrödinger equation using the finite difference time domain method, Journal of Physics A: Mathematical and Theoretical, 1885-1896.

[2] Elgweri, H.K, Hamed, A, Mansor, M, 2021, Calculating the lower angular excited states in two dimensions using Finite Difference Time Domain method, in press.

[3] Elgweri, H.K, Mansor, M, 2015, First excited solutions of Schrödinger equation by the diffusion method applied to various one dimension problem, Journal of Academy for Basic and Applied Science, 14(1),1-4.

[4] Mansor, M, Sherif, T. S, Swedan, S. A, 2004, Improved simple numerical method using the diffusion equation applied for central force bound quantum systems, Journal of basic and applied science. 14,72-81.

[5] Grimm, R, Storer, R. G, 1969, A new method for the numerical solution of the Schrödinger equation, Journal of Computational Physics, 4,230-249.

[6] Mitchell, A.R and Griffiths, D.F, 1980, The finite difference method in partial differential equations, John Wiley and Sons, New York.

[7] Schiff, L, 1955, Quantum Mechanics, Mc Graw-Hill, New York.

[8] Merzbacher, E, 1970, Quantum Mechanics, 2nd edition, John Wiley and Sons, New York.

Effects of Indole Butyric Acid concentrations Study on the Growth of Vicia Faba Plant Under Salt Stress

Safa Y. M. Ragab   **Hend M. E. Emhemed**

Botany department, Faculty of Science, Tobruk Univesity

Yassen_Ragab@yahoo.com   Hand9454@gmail.com

Abstract

To recognize the validity of plant type for the soils that characterized by high salinity, it is important to study how much the plants suffered from growth rate at different concentration of salt stress. This study was performed on the effect of Indole Butyric Acid (IBA) on the growth of *Vicia Faba* plant under two different concentration (4 gm & 9 gm) of sodium chloride and the control treatment without (IBA and NaCl2). Shoot and root length were effectively improved under the thedifferent levels of indole 3 acetic acid .The data regarding root length are showed that the length of root is significantly affected by IBA at the two different levels comparing with the control sample of distilled water. The values show that maximum root length at R1 (13.2 cm) for the treated samples at concentration (4 gm), while (4.5 cm) for untreated samples. On the other hand, R3 display different values, whereas, it was (12.4 cm) for treated samples and (7.5 cm) for untreated samples. At the concentration (9 gm) seams to more affected by salt stresses, whereas, the root length was (10.9 cm) and (6.3 cm) for treated and untreated samples respectively. Also, it is obviously that the number of lateral roots have been affected by the salty stresses. The obtained results reflect this affecting, whereas, R1, R2 and R3 showing variable values for the two concentration levels (4 & 9 gm) for both treated and untreated samples. The values are (15 & 12), (16& 10), (14 & 13) and (19 & 9), (14 & 11) and (12 & 8) respectively.

The obtained measurements exhibit more or less the same behavior of leaves lengths. Whereas, the plants more affected at high concentration (9 gm) comparing with concentration (4 gm). The

highest value was recorded at R2 (2.6 cm) for the treated sample (4 gm).

From the obtained results it is observed that, the salinity at different concentration causes clear decreasing in the plant growth for the investigated samples.

The changing of measurements parameters mainly related to the nature of soil salinity. The results exhibit a wide variation of these parameters for both treated and untreated samples.

Plant growth strongly affected at high concentration of salt stresses (9 gm). The increasing of salinity in the soil may be leads to the increase of accumulation in plant tissues which affected negatively on growth rate.

Keywords: Vicia Faba, salt stress, IBA, concentration, growth.

الملخص

لمعرفة مدى صلاحية النباتات الملائمة للترب ذات الخصائص الملحية فقد أجريت هذه الدراسة على نبات الفول. *Vicia faba*

لمعرفة مدى تأثير الإجهاد الملحي عند تركيزات مختلفة على معدلات النمو في أجزاء النبات المختلفة التي شملت كل من طول الريشة، طول الجذير، طول الورقة، عرض الورقة، وذلك خلال فترة زمنية استغرقت ثلاثة أسابيع. حيث اشتملت الدراسة على 12عينة لنبات الفول، 6 منها معالجة بحامض IBA و6غير معالجة في ثلاث حالات وهي الماء المقطر (الخالي من أي إضافات)، والمعالج بتركيز 4 جرام والآخر المعالج بتركيز 9 جرام. أظهرت البيانات المتعلقة بطول الجذر أن طول الجذر يتأثر بشكل كبير بـ IBA على مستويين مختلفين مقارنة بعينة التحكم من الماء المقطر. أظهرت القيم أن أقصى طول للجذر R1 (13.2 سم) للعينات المعالجة بتركيز (4 جم) بينما (4.5 سم) للعينات غير المعالجة. من ناحية أخرى أظهرت قيم R3 مختلفة حيث كانت (12.4 سم) للعينات المعالجة و (7.5 سم) للعينات غير المعالجة. عند التركيز (9 جم) كانت أكثر تأثراً بضغوط الملح بينما كان طول الجذر (10.9 سم) و (6.3 سم) للعينات المعالجة وغير المعالجة على التوالي. أيضا ، من الواضح أن عدد الجذور

International Science and
Technology Journal
المجلة الدولية للعلوم والتقنية

العدد 26
Volume 26

ISTJ
المجلة الدولية للعلوم والتقنية
International Science and Technology Journal

الجانبية قد تأثر بالإجهادات المالحة. النتائج التي تم الحصول عليها تعكس هذا التأثير ، بينما أظهرت R1 و R2 و R3 قيمًا متغيرة لمستويي التركيز (4 و 9 جم) لكل من العينات المعالجة وغير المعالجة. القيم هي (15 و 12) و (16 و 10) و (14 و 13) و (19 و 9) و (14 و 11) و(12 و 8) على التوالي.

تظهر القياسات التي تم الحصول عليها نفس سلوك أطوال الأوراق إلى حد ما. في حين أن النباتات أكثر تأثرا بتركيز عال (9 جم) مقارنة بالتركيز (4 جم). سجلت أعلى قيمة عند R2 (2.6 سم) للعينة المعالجة (4 جم).

لقد أظهرت النتائج المتحصل عليها عن وجود تأثير واضح في كل المعاملات التي تمت دراستها في الحالات المختلفة على كلٍ من طول الريشة وطول الجذير وأبعاد الورقة، وذلك مقارنةً بالعينات التي لم يتم معالجتها. كما أسفرت الدراسة أيضاً عن زيادة تأثير معدلات النمو والإنبات على النبات بزيادة التركيز في المحلول وذلك عند التركيز 9 جرام مقارنة بالتركيز 4 جرام في كافة الحالات عند مقارنتها بالعينات غير المعالجة.

وقد خلُصت الدراسة إلى أن معدل النمو في كافة أجزاء النبات تتأثر سلبياً مع زيادة التركيز الملحي والذي بدوره يكون نتيجة تزايد الإجهاد في التربة عند مستويات ليس بمقدور النبات تحملها، وعليه يتعين تحديد نسب الملوحة في الترب وذلك لاختيار النباتات الملائمة لها التي لديها القدرة على تحمل هذه الإجهادات الملحية.

الكلمات المفتاحية: الإنبات، معدل النمو، التركيز، الإجهاد الملحي، العينات المعاملة، العينات غير المعاملة، الفول.

1. Introduction

Vicia faba is an important food legume crop grown for human and animal consumption globally especially in china north African countries parts of Europe as well as north and south Americas, is a species of flowering plant in the pea and bean family f*abaceae*.
In Egypt among the most important legumes *faba bean* which used on a large scale as tradional human diet because it contain high percentage of proteins so it is important to increase maximize yield of faba bean on the other hand faba bean is important for

agriculture because of its high protein content and symbiosis with rhizobium bacteria in Egypt mature seeds of faba bean are good sources of protein starch cellulose vitamin c and minerals biostimulants are an organic material that has been shown to influence several metabolic processes such as respiration photosynthesis and nucleic acid synthesis and ion uptake and when applied in small quantities enhances plant growth and development.

Faba bean is an annual legume botanically known as *Vicia faba* [8] the crop is known by many names most of which refer to a particular subgroup rather than the whole species. faba bean fava bean broad bean horse bean windsoe bean tick beans(small types) Bakela (Ethiopia) body kumouvje (former USSR) faveira (Portugal).[9,10].

Indole 3 -butyric acid (IBA) is an auxin precursor that is converted to IAA which considered an important player in controlling the growth of lateral roots [1,2]. Moreover, the enlargement of root systems is caused by branching via lateral root formation and the extent of root branching is dependent on the growth state of the plant [3]. IBA has long been used in agriculture to promote root initiation growth from plant cutting .However, IBA inhibits primary root elongation and stimulates lateral root formation [4]. It has been established that Indole-3-butyric acid (IBA) is an endogenous compound in a variety of plant species when applied exogenously, IBA has a variety of different effects on plant growth and development, However, the compound of IBA used for the induction of adventitious roots (Ludwig- Muller, 2000) [5].

Further analysis demonstrate that IBA- derived IAA plays an essential role in root hair and cotyledon cell expansion [6]. The discovery of auxin as a plant growth hormone, its physiological effects and practical application attracting story of horticultural research [7]. It has been reported that the synthetic Indole-3-butyricacid IBA has the capacity of forming roots which more effective than IAA for rooting. All the growth regulators are not equally stable for rooting growth. However, the growth regulators Indole Butyric acid is one of the most widely used in order to achieve high percentage of rooting growth success for the

ornamental species. The current investigation was carried out in order to enhance the rooting system ability by using different concentration of IBA (Indole Butyric acid [7]. The main aim of this study is to find out the best concentration of IBA for the growth and rooting of beans plant , We aim to investigate the mechanisms underlying the growth of lateral roots, which may lead to the enhancement of crop agriculture, through the production of better yields or by increasing resistance against adverse environmental conditions such as low nitrogen, low phosphate, and drought. This will aid in the production of food for the growing global population.

2. Objective of Study

The main target of this study is to investigate the effect of Indole Butyric Acid (IBA) on the growth of *Vicia Faba* Plant under different concentration of salt stresses in soils.

3. Materials and Methods

An experiment was conducted in the laboratory of the Faculty of Science, Department of Botany, University of Tobruk according to the method described in [13] This study was carried out through December-January months of 2021 year. The experiment was performed to know the effect of Indole-3-Butyric acid and sodium chloride salt on the rooting and growth of beans (*Vicia faba*) seeds, and the experiment was carried out in a laboratory in plastic pots with a diameter of 25 centimeters and a depth of 30 centimeters. where each treatment was repeated 3 times and each pot contained 2 kg of soil after being washed well by distilled water.

to get rid of the salts in it, then dried and sterilized under the sun for 24 hours to see the effect of soaking the seeds with Indole -3-butyric acid IBA at a concentration of (300) ppm for 24 hours and another soaked in distilled water. For the same period on the germination and growth of seeds in saline media different resulting from dissolving quantities of 99.9% NaCl in distilled water and distilled water only (watch) (400, 900) ppm, equivalent to (9, 4, 0) grams per liter and its efficiency in improving germination and seedling growth characteristics under the influence of salt stress of

International Science and Technology Journal
المجلة الدولية للعلوم والتقنية

العدد 26
Volume 26

المجلة الدولية للعلوم والتقنية
International Science and Technology Journal
ISTJ

beans. Measurements were taken for the seedling growth stage for each pot containing five (5) seeds that were superficially sterilized with 5% sodium hydrochlorate solution.

4. Results and Discussion

The results of the experimental works of four parameters were measured the period of the investigation of effect of IBA (Indole Butyric Acid) levels on the growth and rooting of *Vicia faba* plant. This study was performed to assessment IBA levels for achieving growth at the different concentrations; these concentrations are 4gm and 9gm at three cases R1, R2 and R3 for treated and untreated samples. The obtained results were presented in **Table (1).**

4.1. Length radical (cm)

The data regarding root length are presented in **Table (1**).

 The results showed that the length of root is significantly affected by IBA at the two different levels comparing with the control sample of distilled water. The values show that maximum root length at R1 (13.2 cm) for the treated samples at concentration (4 gm), while (4.5 cm) for untreated samples. On the other hand, R3 display different values, whereas, it was (12.4 cm) for treated samples and (7.5 cm) for untreated samples. At the concentration (9 gm) seams to more affected by salt stresses, whereas, the root length was (10.9 cm) and (6.3 cm) for treated and untreated samples respectively. This is attributed to the role of indole 3 acetic acid in *viciafaba* plant , because it encourages the creation of cellular enzymes. It has been proven with certainty that indole 3 acetic acid encourages the formation of enzymes, and they also found that indole 3 acetic acid encourages the formation of enzymes for protein, and that this causes the release of amino tryptophan, which is the nucleus or precursor to the formation of auxin. This auxin performs its work in the cell wall, and it is found that it performs the action of indole 3 acetic acid in the plant and this is in agreement with what was found by [11] that

Treatments at $10-7$ and $10-9$ M IAA tended to increase the leaf number and leaf area compared with other IAA treatments and the control. IAA's primary efficiency was to stimulate the

International Science and Technology Journal
المجلة الدولية للعلوم والتقنية

العدد 26
Volume 26

المجلة الدولية للعلوم والتقنية
International Science and Technology Journal
ISTJ

development of stems and roots, lateral root production, and root elongation by extending the new cells in the meristem .

It was noticed that the concentration of IBA affecting on the root length comparing with the control samples. **Figure (1)** a bar char depicted this variation of the results, while **Figure (2**) is a radar chart.

Table1. Measured values of root length Length radical

Root length (cm)						
Replication	**Treated**			**Untreated**		
	Distilled water	**Concentration (4 gm)**	**Concentration (9 gm)**	**Distilled water**	**Concentration (gm 4)**	**Concentration (gm 9)**
R1	4.4	13.2	6.2	5.4	4.5	4.2
R2	6.3	10.8	8.4	6.8	5.5	4.4
R3	8.4	12.4	10.9	7.5	7.4	6.3

Fig. 1 Bar chart of root length values

International Science and
Technology Journal
المجلة الدولية للعلوم والتقنية

العدد 26
Volume 26
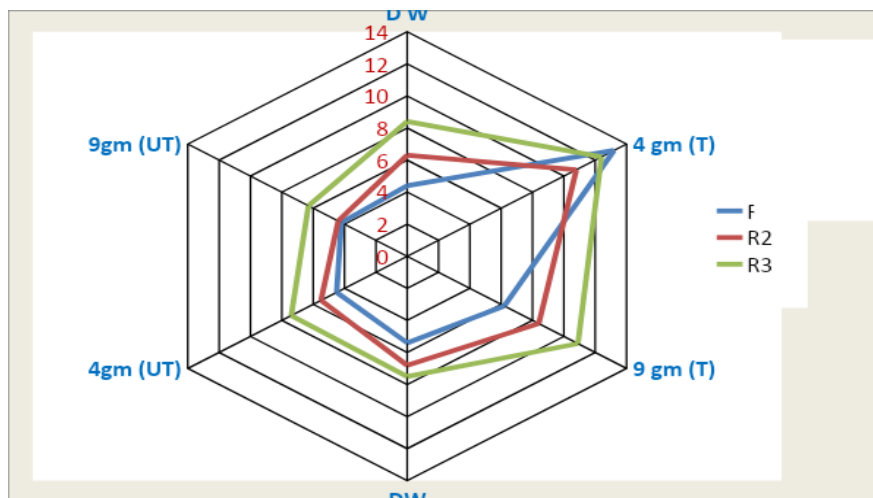
ISTJ
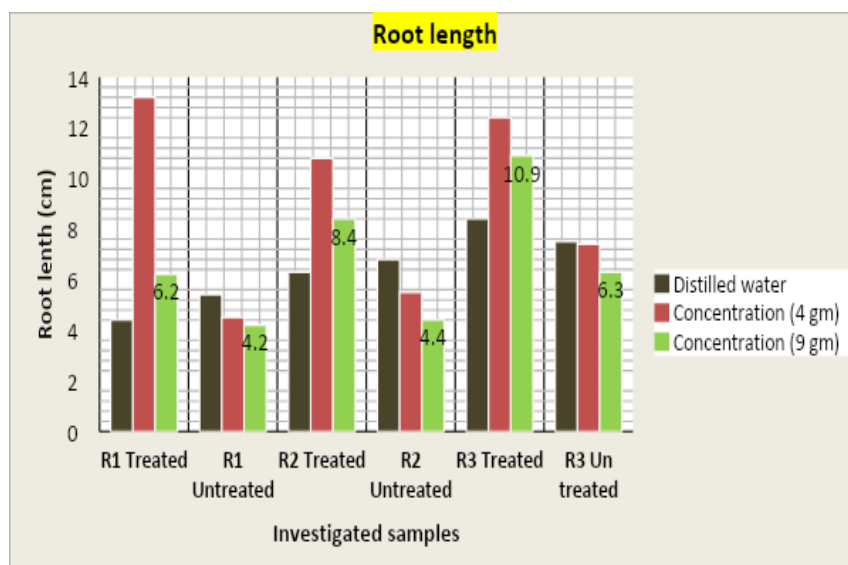
Fig. 2 Radar chart of root length values

4.2. Lateral Roots Number

Also, it is obviously that the number of lateral roots have been affected by the salty stresses. The obtained results reflect this affecting, whereas, R1, R2 and R3 showing variable values for the two concentration levels (4 & 9 gm) for both treated and untreated samples. The values are (15 & 12), (16 & 10), (14 & 13) and (19 & 9), (14 & 11) and (12 & 8) respectively **Table (2).** This variation more clearly depicted through bar charts in **Figure (3)** and radar chart in **Figure (4).**

Table 2 Measured values of lateral roots number

Number of lateral roots					
Replication	Treated			Untreated		
	Distilled water	Concentration (4 gm)	Concentration (9 gm)	Distilled water	Concentration (gm 4)	Concentration (gm 9)
R1	9	15	16	16	12	9
R2	12	16	14	14	10	11
R3	13	14	12	17	13	8

International Science and
Technology Journal
المجلة الدولية للعلوم والتقنية

العدد 26
Volume 26

المجلة الدولية للعلوم والتقنية
ISTJ
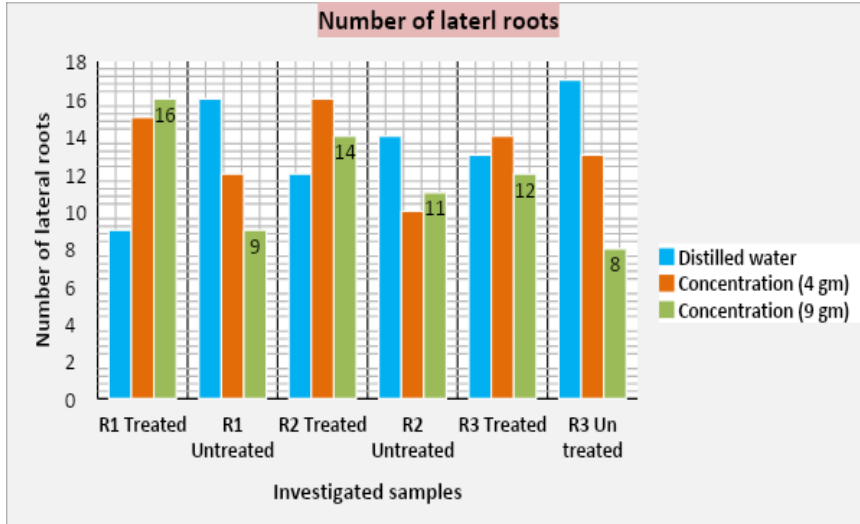
Fig. 3 Shows the variation of lateral roots number
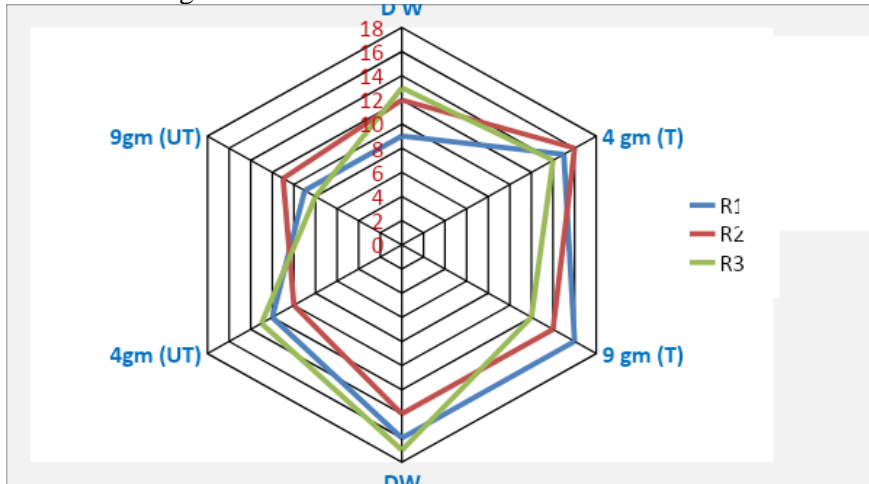
Fig. 4 Radar chart for lateral roots number

4.3. Leaf Length

To recognize so far the salty stresses soil how much affecting on the rate of plant growth, the investigation study was conducted on the plant leaves. From the reported data it is clearly that the leaf length also affected by salty stresses. From **Table (3)** we can observed that at level two of concentration (9 gm) is lower values comparing with the concentration (4 gm). The highest value was

International Science and
Technology Journal
المجلة الدولية للعلوم والتقنية

العدد 26
Volume 26

المجلة الدولية للعلوم والتقنية
ISTJ
International Science and Technology Journal

recorded at (4 gm) for treated sample of R3 (5.2 cm). On the other hand, **Figure (5**)

display the variation between these values through the bar chart representation and radar chart in **Figure (6**). However, this an argument without results that leaf length and width were increased at low IAA concentration ($10-11$ M) compared to the control.

Table 3 Measured values of leaf length

Leaf length (cm)						
Replication	**Treated**			**Untreated**		
	Distilled water	**Concentration (4 gm)**	**Concentration (9 gm)**	**Distilled water**	**Concentration (gm 4)**	**Concentration (gm 9)**
R1	2.2	4.3	4.2	2.3	1.5	1.4
R2	1.9	4.8	4.5	2.2	1.4	1.2
R3	3.1	5.2	4.9	2.9	1.7	1.3
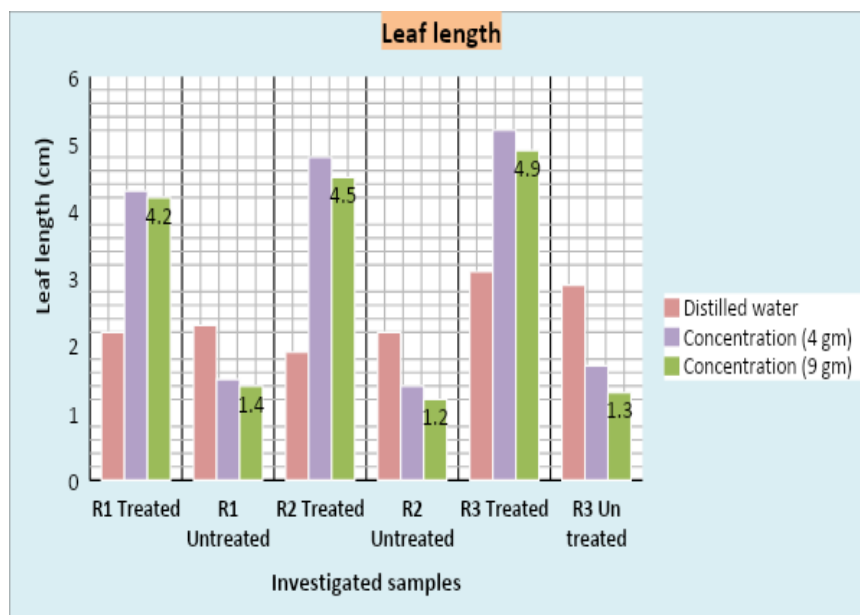
Fig. 5 Depicts the variation of leaf length

International Science and
Technology Journal
المجلة الدولية للعلوم والتقنية

العدد 26
Volume 26

المجلة الدولية للعلوم والتقنية
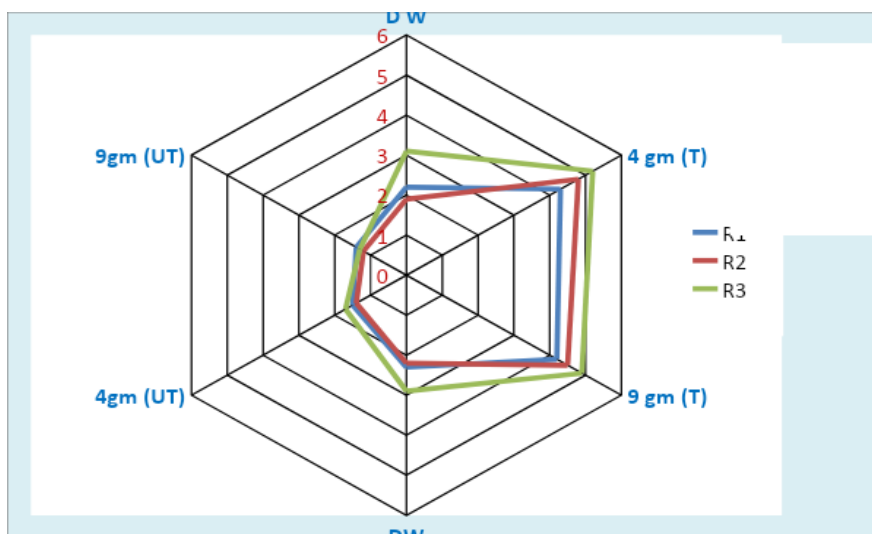International Science and Technology Journal
ISTJ

Fig. 6 Radar chart for leaf length

However, to make sure the affecting of salt stresses on the plant growth, leaves wide have been measured. The obtained measurements exhibit more or less the same behavior of leaves lengths. Whereas, the plants more affected at high concentration (9 gm) comparing with concentration (4 gm). The highest value was recorded at R2 (2.6 cm) for the treated sample (4 gm) as shown in **Table (4)**.

Table4. Measured values of leaf wide.

	Leaf wide (cm)					
Replication	**Treated**			**Untreated**		
	Distilled water	Concentration (4 gm)	Concentration (9 gm)	**Distilled water**	Concentration (gm 4)	Concentration (gm 9)
R1	1.1	2.4	2.1	1.2	2.0	1.1
R2	1.4	2.6	2.2	1.3	2.3	1.2
R3	1.6	2.3	2.0	1.6	2.2	1.3

Figure (7) a bar chart gives a clear view for the range of variation between the measured data of leaves wide, whereas, Figure 8 of radar chart emphasize this variation. In general, this reflected the affecting of plant under variable concentration of salt stresses.
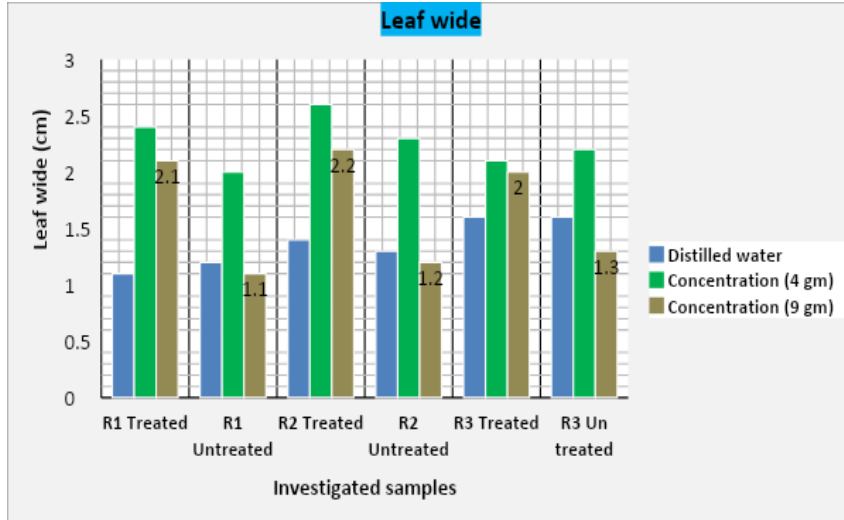

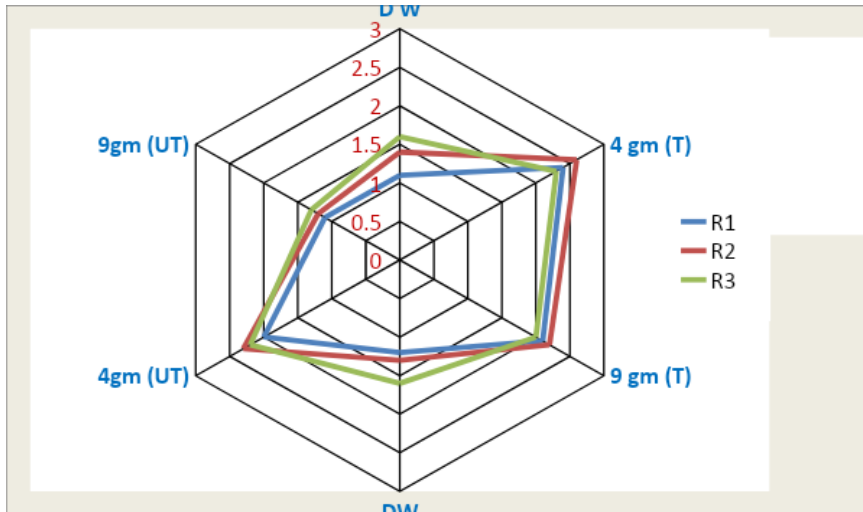Fig. 7 Illustrates the variation of leaf wide

Fig. 8 Radar chart for leaf wide

5. Conclusion

From the previous study, the following conclusion can be drawn:

1. The salinity at different concentration causes clear decreasing in the plant growth for the investigated samples.
2. The changing of measurements parameters mainly related to the nature of soil salinity.
3. The results exhibit a wide variation of these parameters for both treated and untreated samples.
4. Plant growth strongly affected at high concentration of salt stresses (9 gm).
5. The increasing of salinity in the soil may be leads to the increase of accumulation in plant tissues which affected negatively on growth rate.

References

[1] Blakely, L. M., Durham, M., Evans, T. A., & Blakely, R. M. (1982). Experimental studies on lateral root formation in radish seedling roots. I. General methods, developmental stages, and spontaneous formation of laterals. *Botanical Gazette*, *143*(3), 341-352.

[2] Laskowski, M. J., Williams, M. E., Nusbaum, H. C., & Sussex, I. M. (1995). Formation of lateral root meristems is a two-stage process. *Development*, *121*(10), 3303-3310.

[3]]Celenza, J. J., Grisafi, P. L., & Fink, G. R. (1995). A pathway for lateral root formation in Arabidopsis thaliana. *Genes & development*, *9*(17), 2131-2142

[4] Jiang, Z., Li, J., & Qu, L. J. (2017). Auxins. *Hormone Metabolism and Signaling in Plants*, 39-76.

[5] Ludwig-Müller, J. (2000). Indole-3-butyric acid in plant growth and development. *Plant Growth Regulation*, *32*(2), 219-230.

[6] Strader, L. C., & Bartel, B. (2011). Transport and metabolism of the endogenous auxin precursor indole-3-butyric acid. *Molecular plant*, *4*(3), 477-486.

[7] Jamal, A., Ayub, G., Rahman, A., Rashid, A., Ali, J., & Shahab, M. (2016). Effect of IBA (Indole Butyric Acid) levels on the growth and rooting of different cutting types of Clerodendrum splendens. *Pure and Applied Biology*, *5*(1), 64.

[8] Hanelt, P., & Mettin, D. (1989). Biosystematics of the genus Vicia L.(Leguminosae). *Annual review of ecology and systematics*, *20*(1), 199-223.

[9] Hawtin, G. C., & Hebblethwaite, P. D. (1983). Background and history of faba bean production. *The faba bean*, 1-21.

[10] Singh, A. K., Bharati, R. C., Ch, N., & Pedpati, A. (2013). An assessment of faba bean (Vicia faba L.) current status and future prospect. *African Journal of Agricultural Research*, *8*(50), 6634-6641.

[11] Lam, V. P., Lee, M. H., & Park, J. S. (2020). Optimization of Indole-3-Acetic Acid Concentration in a Nutrient Solution for Increasing Bioactive Compound Accumulation and Production of Agastache rugosa in a Plant Factory. *Agriculture*, *10*(8), 343.

[12] Fässler, E., Evangelou, M. W., Robinson, B. H., & Schulin, R. (2010). Effects of indole-3-acetic acid (IAA) on sunflower growth and heavy metal uptake in combination with ethylene diamine disuccinic acid (EDDS). *Chemosphere*, *80*(8), 901-907.

[13] Mona Abdullah and Kholoud Farag. (2021). Effect of gibberellic acid GA3 on germination and seedling growth characteristics under salt stress conditions in wheat. Al-Bayan Journal, Sirte University. number (9).

FREEZE-THAW AND SULFATE RESISTANCE OF GEOPOLYMER MORTAR MADE OF WASTE MATERIAL

Abdoslam Alnkaa
Higher Institute of Sciences and Technology Yefren
nankaa@rocketmail.com

ABSTRACT

The aim of the present experimental study is to investigate the resistance of little cementitious value-based geopolymer mortars subjected to sulfate resistance (3 months) and freeze-thaw cycles (150 cycles). Waste material was used as the base material to produce geopolymer mortar. Three types of waste material, namely Slag (GGBFS), fly ash (FA) and glass powder (GP), all of which can be activated with an alkali agent, were selected to study the effect of the steam-cured (SC) and water-cured (WC) methods on the mechanical proporties of the geopolymer mortar with a constant concentration (12M) of sodium hydroxide. Upon the analysis of the modulus of sodium silicate ($Na_2SiO_3/NaOH = 1$) and the different proportions amounts of geopolymer in these three materials - GGBFS, FA, and GP – the results indicate that the compressive strength value of all specimens was higher than the values obtained for them once not subjected to any freeze-thaw resistance test, except for those containing GGBS and GP. It can be inferred that the investigated geopolymer FA materials possess an highly acceptable freeze resistance under water-cured conditions. In addition, all these specimens exhibit high levels of resistance to magnesium sulfate immersion and again their compressive strength values under WC conditions are found to be higher than those under SC settings.

Keywords: Fly ash, Geopolymer mortar, Sodium silicate, Sodium hydroxide, Slag, Compressive strength and flexural strength, sulfate exposure.

International Science and Technology Journal
المجلة الدولية للعلوم والتقنية

العدد 26
Volume 26

ISTJ
المجلة الدولية للعلوم والتقنية
International Science and Technology Journal

الملخص

تهدف هذه الدراسة التجريبية التحقيق في مدى مقاومة عجنة الجيوبوليمر عند غمرها في محلول الكبريتات المغنيسيوم لمدة (3 أشهر) و كذلك دورات التجميد و الذوبان حتى (150 دورة). تم استخدام النفايات كمواد أساسية لإنتاج عجنة الجيوبوليمر و تم اختيار ثلاثة أنواع من مواد النفايات المثمثلة في (الخبث والرماد المتطاير و مسحوق الزجاج) والتي يمكن تنشيطهما جميعًا باستخدام عامل قلوي المثمثل في هيدروكسيد الصوديوم بتركيز (12مولاري) و سيليكات الصوديوم و النسبة بينهما 1:1 و تم إختيار نوعان من المعالجة و هما المغالجة بالبخار و الغمر في المياه و دراسة الحواص الميكانيكية لعجنة الجيوبوليمر. تشير النتائج إلى أن قيمة مقاومة الانضغاط لجميع العينات كانت أعلى من القيم التي تم الحصول عليها للعينات التي لم تخضع لدورات التجميد و الذوبان ما عد العينات التي تحتوي على (الخبث و مسحوق الزجاج). يمكن القول ان عجنة الجيوبوليمر التي تحتوي على الرماد المتطاير لها مقاومة عالية لدورات التجمد و الذوبان التي تمت معالجتها بالغمر بالمياه. . بالإضافة إلى ذلك ، تُظهر جميع هذه العينات مستويات عالية من المقاومة للغمر في كبريتات المغنيسيوم مع أن قيم مقاومة الانضغاط تحت المعالجة بالغمر بالمياه كانت أعلى من تلك التي تمت معالجتها بالبخار.

INDREDUCTION

Producing geopolymer mortar can help to decrease negative environmental impacts in case of Portland cement (OPC). By merely substituting this material, the amount of CO_2 released can be brought down significantly. To provide an example, making 1 ton forms roughly the same amount of CO_2, which finds its way into the atmosphere [1-3], not to mention the need for about 2800Kg of raw materials apart from fuel and others and the release of another 5–10 percent of airborne dust [4].

A number of nations are signatory to the UN's Framework Convention on Greenhouse Gases of 1992 held in Rio. Two years later, the Convention was made effective and accepted by 196 countries, including Turkey, with the aim to decrease greenhouse

International Science and
Technology Journal
المجلة الدولية للعلوم والتقنية

العدد 26
Volume 26

المجلة الدولية للعلوم والتقنية
ISTJ
International Science and Technology Journal

gas emissions and help to bring down the rate of global warming by 2 ° C until the year 2100 [5].

For this reason , reducing CO_2 emission has become a need and can be achieved by developing, for one, different cement folders – for example, ground-granulated blast furnace slag and fly ash which is considered very well documented and efficient in order to make better mortar from OPC [6, 7]. A benefit of these waste materials is that a great number of different alumina-silicate sources are formed as industrial residues, such as fly ash, slag, etc., able to be activated by adding an amorphous phase (this is myt understanding of the original vague statement. Also, numerous activators including alkali sulfate, carbonate, hydroxide or silicate can be utilized in this process. Alkali, in particular Na or K silicates, are ingredients that help to create better-performing materials [8, 9] and have significant industrial importance in the activation process [10].

Considering other research efforts in this respect, one can see that geopolymers ahvce so far been primarily based on fly ash class F(FA) or ground granulated blast furnace slag (GGBFS). These previous attempts have laso been mostly focused on geopolymer concrete and mortars as regard the engineering properties of FA and GGBFS based-geopolymer concrete [11-13]. Apart from this, few defects are associated with the impact of alkaline activating ratios (Na_2SiO_3 / NaOH) on the mechanical properties of geopolymer mortar [14, 15]. Yet, studies are rare as far as the effects of different types of curing are concerned on the element of resistance to freezing-Thawing and sulfate resistance of geopolymer mortars.

Given this background, in the present study, class F (FA), GGBS, and (GP) which is rich in silica and alumina are used as primary materials for the geopolymer mortar as described in Table 3. The motivation behind this experiment is that there has always been a future initiative to come up with the best mortars using only 100% industrial byproducts at low cost, power consumption, and

International Science and Technology Journal
المجلة الدولية للعلوم والتقنية

العدد 26
Volume 26

ISTJ
المجلة الدولية للعلوم والتقنية
International Science and Technology Journal

environmental impact with improved engineering properties and superior durability.

This research primarily focuses on investigating the effect of water-cured and steam-cured techniques on the freeze-thaw and sulfate resistance of geopolymer mortars based on FA, GGBFS, and GP. A major challenge to producing successful geopolymer mortars is determining the right mechanics at low temperatures. Like Portland cement, the geopolymer interaction is more easily achieved at ambient temperatures and, while it may be possible to examine test samples at high temperatures under laboratory settings, it is more difficult to do so in the site itself.

Geopolymer materials are regarded as possessing high degrees of resistance to sulfate solutions and low temperatures in general thanks to high freeze-thaw levels. Mortar from the materials can stand freezing and maintain its properties. Freezing-Thawing resistance is quite essential in the construction sector as buildings are meant to stay the influence of varying temperatures for extended periods of time. Reports are available on freeze work applied to waste materials such as F-class FA and GGBFS. According to studies, compressive strengths value of geopolymer mortar samples after 150 freeze-thaw cycles tend to decrease by just 30% before the freeze-thaw cycles test. [18].

Sun et al[16] reports on the durability of freeze-thaw in fly ash-based alkali-activated mortars under normal conditions and sulfate and hydrogen sulfate (H_2SO_4) resistance of fly ash-based geopolymer mortars cured under normal conditions. The results are compared with OPC mortars, concluding continuous increases in mass, dynamic modulus and compressive strength with time as well as resistance of FA mortars to 5% Na_2SOi_4 solution being better than that of OPC.

Thokchom et al. studied the effect of magnesium sulphate solution on fly ash-based geopolymer mortar samples. They immersed the samples in 10% by weight MgSO4 solution for 168 days, after which period the samples showed very little increase in weight and

decrease in compressive strength by about 56%[17]. The results show that fly ash has acceptable resisting properties against $MgSO_4$ solutions and, thus, may be used in fire-prone constructions such as tunnels and skyscrapers.

EXPERIMENTAL WORK

Materials:

At this stage, tested mixtures were based on class F fly ash (FA), ground granulated blast-furnace slag (GGBFS), and glass powder(GP) and tested as to variations in the proportion of waste material and basic alkali activator (sodium silicate-sodium hydroxide) to improve the mechanical properties of the geopolymer mortar.

Fly ash FA:

Most of the fly ash available worldwide is a low-calcium by-product obtained from burning anthracite and bituminous coal. The substance isconsidered one of the most important source materials for geopolymer cement. In general, the value of CaO content is less than 10%, while that of $SiO_2 + Al_2O_3 + Fe_2O_3$ exceeds 70 %, thereby creating the potential for alkali reaction. Most of the fly ash consists of coal combustion from a heterogeneous mixture of aluminosilicate and fused silica as well as small amounts of crystalline materials including molybdate, quartz, hematite and magnetite. This degree of heterogeneity means that additional care is needed to ensure a perfect mix design and a consistent final product. The study was conducted at the Çatalağzi Thermal Power Station in Zonguldak, Turkey. The specific gravity of the FA was 2.39g/cm^3 and the fineness was $6000 \text{ cm}^2/\text{g}$.

Ground Granulated Blast-Furnace Slag (GGBFS):

Ground granulated blast furnace slag (GGBFS) is another industrial by-product resulting from rapid water cooling of molten steel. It is known to have beneficial properties for the concrete industry due to being relatively inexpensive, resistance to chemical reactions and maintaining excellent thermal properties. In general, the value of $SiO_3 + Al_2O_3 + Fe_2O_3$ exceeds 84 %. In this study, the

GGBFS was provided from the Ereğli Iron–Steel Factory in Oyak, Turkey, with a specific gravity (S.G) of 2.81 g/cm3 and a fineness of 4250. The chemical composition is shown in Table 1.

Glass Powder (GP).

The glass powder is grounded using a Los Angles machine and to produce finer ash, further grounded with a small mill. The mean diameter of particle size is about 13 μm with a specific gravity of 2.56 g/cm3 and the fineness of 5320 cm^2/g.

Table 1. Chemical composition of GGBFS, GP and FA (%)

Oxide	SiO$_2$	Al2O3	Fe2O3	CaO	MgO	SO3	K2O	Na2O
GGBFS	36.7	5.20	0.98	32.61	10.12	0.99	0.76	0.42
FA	61.81	9.54	7.01	1.77	2.56	0.31	0.99	2.43
GP	72.66	1.57	0.39	11.41	1.24	0.07	0.54	12.89

Standard Aggregate:

The aggregate used in the study was standard and in accordance with the TS EN196-1. The sieve analysis is given in Table 2.

Table 2. Sieve analysis

Sieve Size (mm)	Remaining cumulative (%)
2,0	0
1.6	7±5
1	33±5
0.5	67±5
0.16	87±5
0.08	99±1

Alkali Activator:

The alkaline activator used in this experiment was a combination of sodium silicate and sodium hydroxide solution. Also, the activator from the sodium silicate solution (Na$_2$O = 11%, SiO$_2$ = 31% and water = 57% by mass) and the sodium hydroxide (NaOH) solution was prepared by dissolving small, compressed mass of sodium hydroxide in water with a concentration of 12M.

Preparation of Specimen Mixtures:

Blended slag, glass powder and fly ash alkali-activated mortars are the subject of tests in this study, where we used standard aggregate, GGBFS, GP, FA, water, NaOH, and Na_2SiO_3 so as to achieve conformity with the TS-EN196-1 standards [18]. The water-to-binder ratio (W/B) is a well-known factor that affects mortar properties. Thus, a constant value of 0.33 was adopted for this factor again in accordance with TS-EN196-1[18]. Sodium Metasilicate/ binder ratio[S/B] is 0.4 and also standard aggregate/binder ratio [A/B] is 1.23. The mortars were cured at different temperatures and under two different conditions: In the first water-cured (WC) series the specimens were placed into a water tank and curing remained to the age of test. The temperature of water curing was kept at the range of $20 \pm 2°C$. This method is similar to that used for curing Portland. In the second steam cured (SC) series, steam water curing took place at 85 °C for 12h, followed by standard curing at 20 ± 3 °C until testing. The design of the mixtures was simplified by replacing 5% GGBFS (by weight) with FA and GP in order to reach an optimum ratio for each curing condition. The ingredients of the mortar mixtures are given in Table 3[19].

Table 3. Mortar mixture ingredients

specimens N0	GGBFS %	FA %	GP %
S0	100	0	0
S1	90	0	10
S2	85	0	15
S8	90	10	0
S12	85	15	0
S15	70	15	15

Testing:

Freezing-thawing and sulfate resistance of geopolymer mortar specimens were investigated in terms of visual appearance, weight loss, and loss of compressive strength.

International Science and
Technology Journal
المجلة الدولية للعلوم والتقنية

العدد 26
Volume 26

المجلة الدولية للعلوم والتقنية
ISTJ

Freezing-Thawing Resistance:

Freezing-thawing of slag, fly ash and glass powder-based geopolymer mortars were carried out to determine weight loss, compressive strength, and ultrasonic. Freeze-thaw resistance was tested on the 40*40*160 mm specimens after 90 days with two types of curing. In this test, the mortar specimens were put in freezer at -20°C for 4h for freezing and in water at room temperature for 4 h for the thawing period. The freezing-thawing test cycle was repeated for 150 cycles and then a compressive strength test was conducted. Also, the same specimens from each type of the mixture were kept at the same curing condition during the freezing-thawing test of the other specimens and all mortar specimens were tested at the same age. Before starting to test the specimens for the freeze and thaw cycles, they are weighed and then measured by ultrasonics. The Freeze-thaw specimens after these tests are shown in Figures 1 and 2.
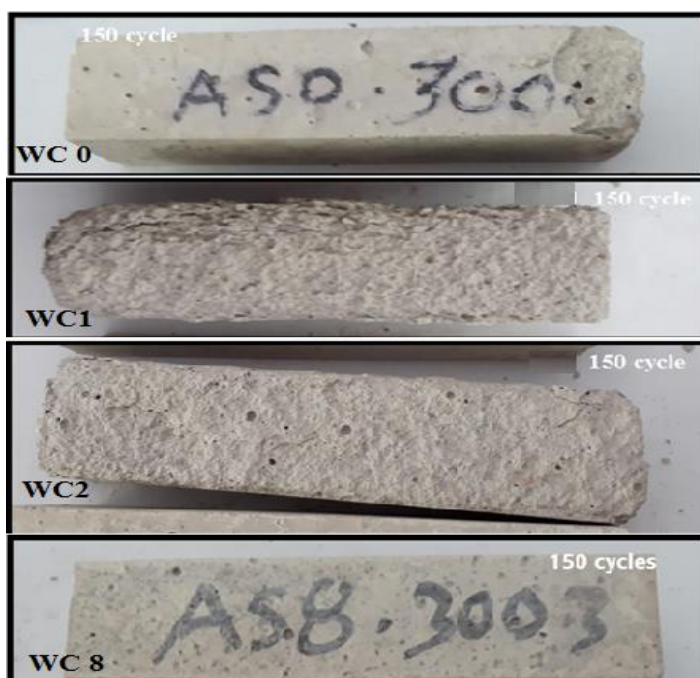

Figure 3 Weight loss results after freeze-thaw test with 150 cycles for WC.

International Science and
Technology Journal
المجلة الدولية للعلوم والتقنية

العدد 26
Volume 26

المجلة الدولية للعلوم والتقنية
International Science and Technology Journal
ISTJ

Figure 2. Geopolymer Mortar after 150 cycles for SC.

The freeze resistance of the geopolymer mortar specimens with steam curing were investigated using 150 freezing and thaw cycles. As per Figure 2, the mass of the samples did not change – that is, no disintegration occurred - during the freeze and Thaw cycles testing. The values of the compressive strength of samples were smaller after freeze-thawing cycles as compared with those obtained for the samples after 90 days. No damage or deformation could be detected after 150 cycles. The strength of the samples after 150 Freeze-Thaw cycles is lost between 4% to 27% of that determined after the same period of time (Figures 6). Also, except for SC8, SC12 the strength of these samples after 150 freezing cycles increased to about 13 percent of that determined after the same period of time. It is evident from the results obtained that the investigated geopolymer FA materials possess a very high level of freeze resistance. From Figure 6, it can be observed that the weight losses are ranged from 0.29% to 3.19%.

International Science and Technology Journal
المجلة الدولية للعلوم والتقنية

العدد 26
Volume 26

المجلة الدولية للعلوم والتقنية
ISTJ

The freeze resistance values of geopolymer mortar specimens with WC were investigated using 150 freezing and thaw cycles. The mass of the specimens (WC0, WC1, and WC2) was changed and surface disintegration occurred. That is, this effect can actually be seen in the figure 1. The weight losses were 6.44%, 11.75%, and 7.52% for WC0, WC1, WC2, respectively where does this fig 3 belong. The losses of the compressive strength of specimens were 52%, 42% after freeze-thawing cycles as compared with the values obtained for the samples after 90 days for WC1, WC2, respectively (see Fig 4). No damage or deformation could be detected after 150 cycles for other specimens WC8 to WC15. The strength of this sample after 150 freezing cycles increased to range from 13% to 18% of that determined after the same period of time, and the maximum compressive strength was 92.1 MPa at WC8. It is evident from the results obtained that the investigated geopolymer FA materials possess a very high and promising level of freeze resistance.

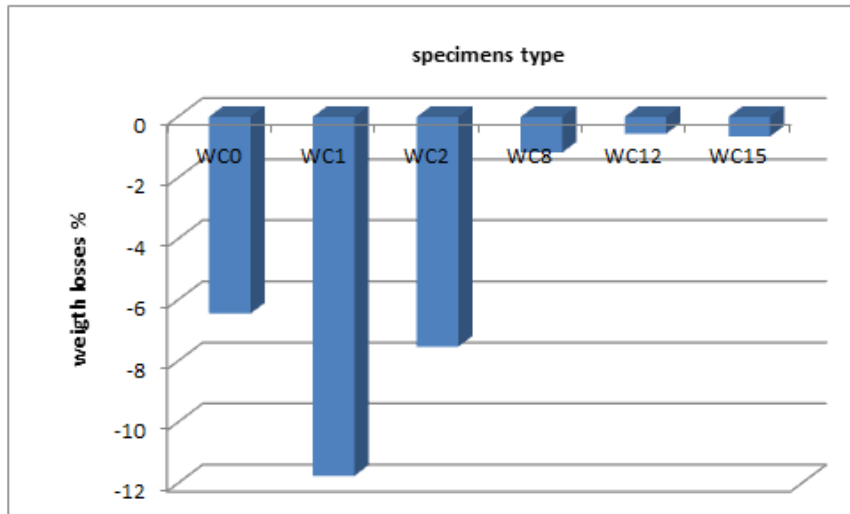
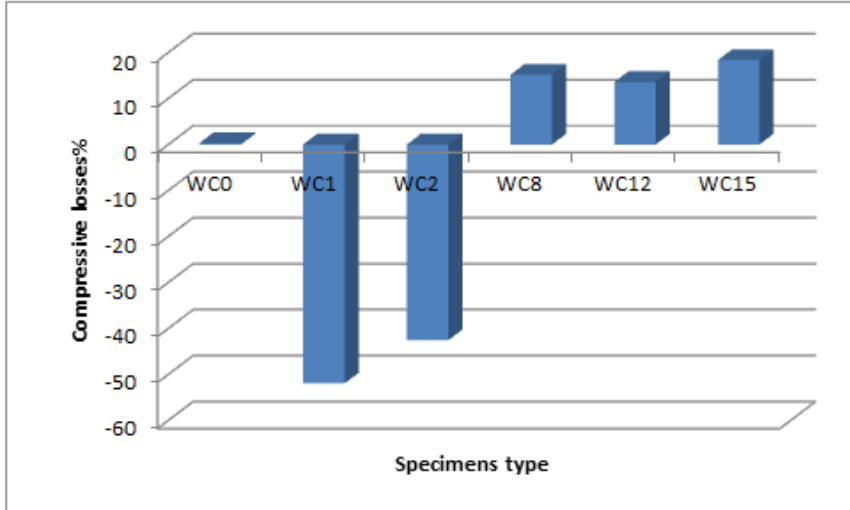Figure 3Weight loss results after freeze-thaw test with 150 cycles for WC.

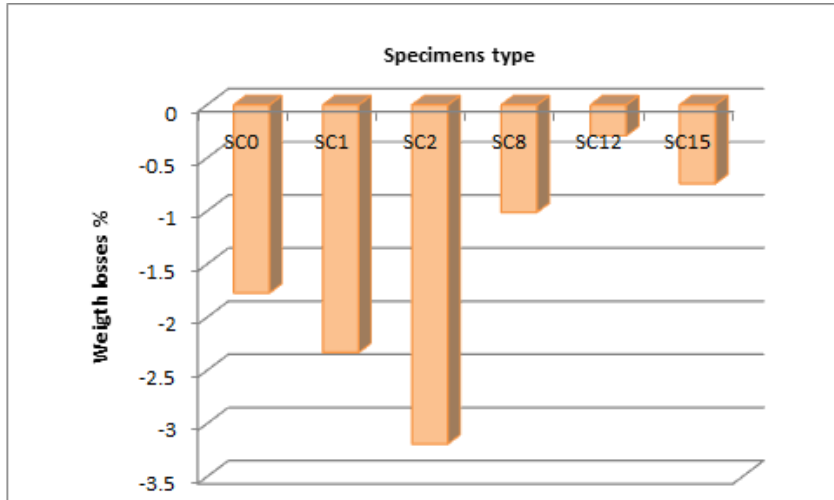Figure 4. Compressive strength loss results after freeze-thaw test with 150 cycles for WC.

Figure 5. Weight loss results after freeze-thaw test with 150 cycles for SC.
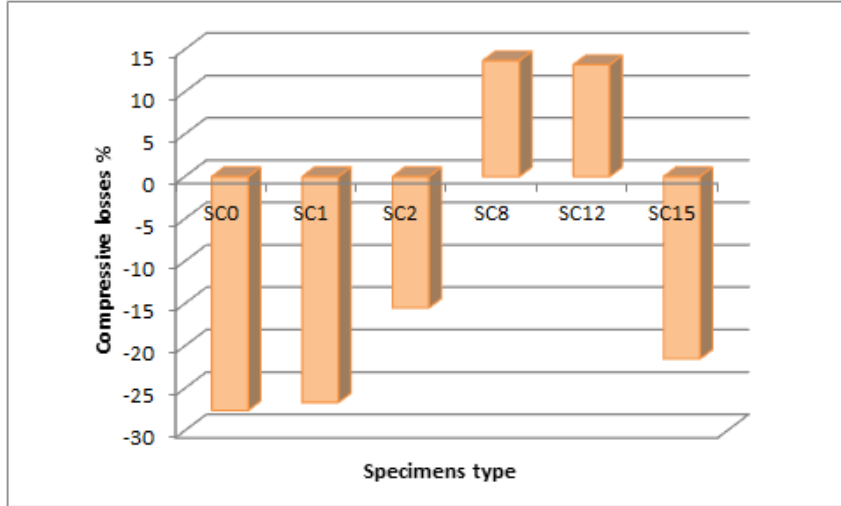
International Science and
Technology Journal
المجلة الدولية للعلوم والتقنية

العدد 26
Volume 26

ISTJ

Figure 6.　　　Compressive strength loss results after freeze-thaw test
with 150 cycles for SC.

Ultrasonic pulse velocity test:
Ultrasonic pulse velocity (UPV) was used to measure the travel
time (t) of an ultrasonic pulse passing through the geopolymer
specimen length (L).　The electronic timing device determines the
interval between the onset and reception of the pulse electronically
in µs. The sample length between transducer divided by the travel
time of gives the average velocity (v) of wave propagation. The
results of the geopolymer specimens UPV measurements are given
in Table 6.

**Table 6. Results of ultrasonic pulse velocity (UPV) for 150 cycles
under (SC) and (WC).**

specimens No	avg. velocity after testing	comp.str. Mpa after 150 cycle	specimens No	avg. velocity after testing	comp.str. Mpa after 150 cycle
SC0	2.609	42.84	WC0	2.792	59.8
SC1	2.421	30.4	WC1	2.46	57.8
SC2	2.087	30	WC2	2.47	56.7
SC8	3.481	92.15	WS8	3.385	75.3
SC12	3.089	87.8	WC12	3.387	76.3
SC15	3.105	82.6	WC15	2.595	60

Accordingly, WC achieved the highest values followed by SC which has a higher slag/fly ash+ glass powder ratio). All of the steam-cured geopolymer mortar mixes observed lower ultrasonic pulse velocities than those water-cured, even with the same or higher compressive strength. The results indicate that an increased velocity corresponds to the same compressive strength.

In this section, the UPV values against compressive strength are plotted in Figures 7 and 8. The relationship between pulse velocity, V (km/sec), and compressive strength after the Freeze-Thaw test (MPa) fitted equations as follows:

For WC: $f_c = 54.723V - 92.186$ $\qquad$ $R^2 = 0.908$ $\qquad$ (4.2)

For SC: $f_c = 20.341V + 6.3819$ $\qquad$ $R^2 = 0.9628$ $\qquad$ (4.3)

The equations obtained reveal acceptable correlation values in both cases of geopolymer (SC, WC) and UPV in the geopolymer mortar. Therefore, the UPV technique can be successfully used for the estimation of the compressive strength of the geopolymer mortar mixes made with alkali-activated GGBFS, FA, and GP.
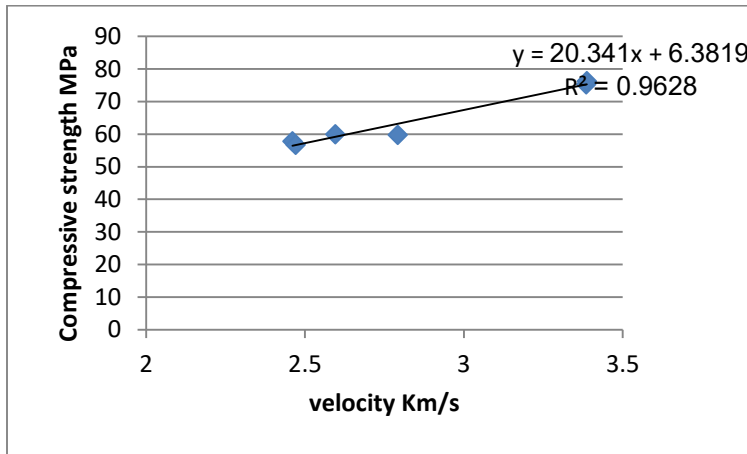

Figure 7. Relationship between Compressive Strength and Ultrasonic Pulse Velocity after Freeze-Thaw test with 150 cycles under SC.
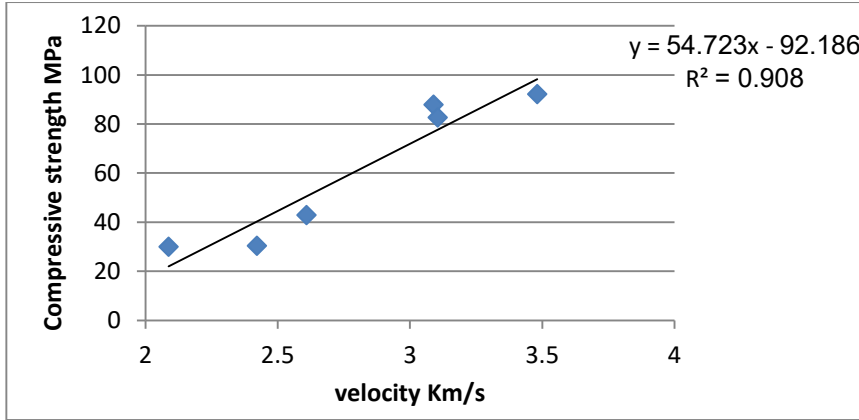
International Science and Technology Journal
المجلة الدولية للعلوم والتقنية

العدد 26
Volume 26

المجلة الدولية للعلوم والتقنية
International Science and Technology Journal
ISTJ

Figure 8.   Relationship between Compressive Strength and Ultrasonic Pulse Velocity after Freeze-Thaw test with 150 cycles under WC

Sulfate Resistance:

After de-moulding, the samples were mixed according to the same proportion ingredients stated earlier and using the two different curing conditions. Then, the specimens were immersed in a solution consisting of 10% $MgSO_4$ by weight of water for 3 months. The containers were left in a room controlled at 20°C until testing. The solutions in containers were replaced every month. Before subjecting the specimens to the $MgSO_4$ solution, they are weighed. The specimens after end immersion in $MgSO_4$ solution are seen in Figures 9.

Table 7. Results of weight losses and compressive strength After 90 days Exposure to MgSO₄ for WC.

specimens No	losses wt. % 3 month	compr. strength after test	compressive stre. at 90 days	losses in compressive %
WC0	0.40	77.9	76.30	2.05
WC1	-0.20	71.1	74.20	-4.36
WC2	2.50	58.5	67.06	-14.64
WC8	0.90	65.75	65.00	1.14
WC12	-0.10	73.5	66.23	9.90
WC15	1.40	51.6	72.92	-41.31

International Science and Technology Journal
المجلة الدولية للعلوم والتقنية

العدد 26
Volume 26

المجلة الدولية للعلوم والتقنية
ISTJ

Table 8. Results of weight losses and compressive strength 90 days Exposure to MgSO4 for SC.

specimens No	losses wt. % 3 month	compr. strength after test	Compressive stre. at 90 days	losses in compressive%
SC0	2.72	56.3	42.71	24.14
SC1	1.16	61.45	46.20	24.82
SC2	0.79	54	42.77	20.80
SC8	1.14	83	78.15	5.84
SC12	0.38	77.5	75.87	2.11
SC15	-0.38	84.8	67.42	20.50

Figure 9. Geopolymer Mortar After 90 days of Exposure to MgSO₄ for SC and WC.

Figure 10. Geopolymer Mortar After 90 days of Exposure to MgSO4 for WC.
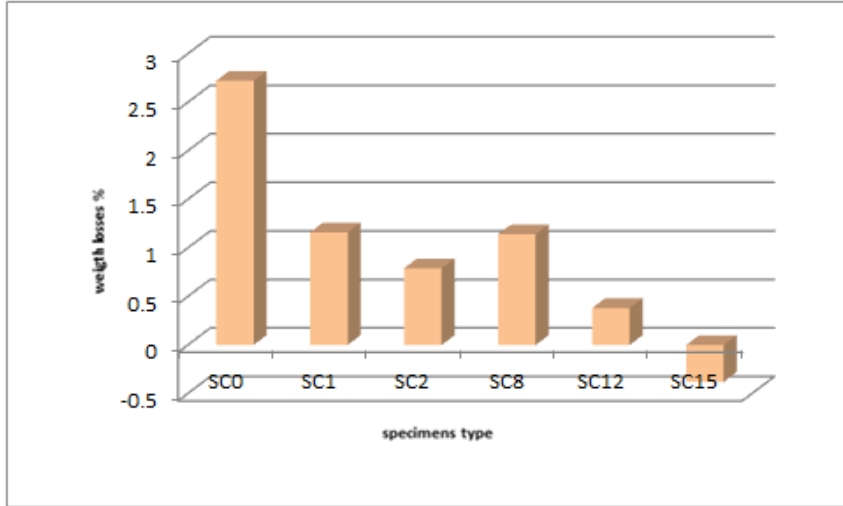
Figure 11. Weight loss After 90 days of Exposure to MgSO$_4$ for SC
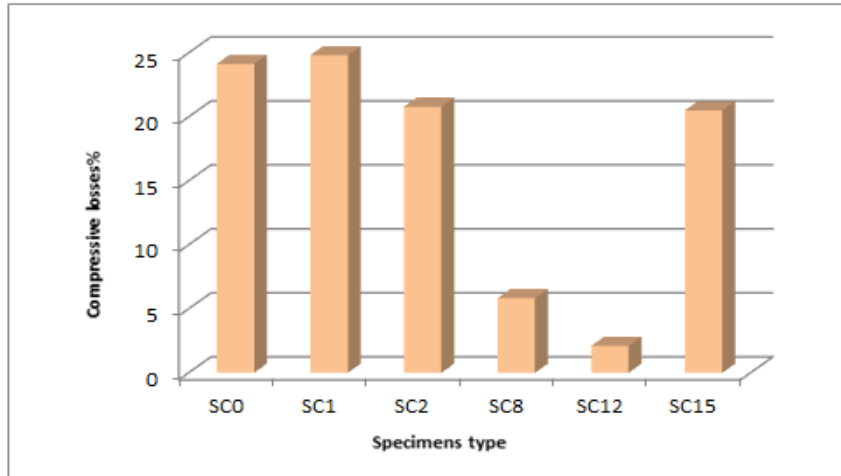
Figure 12. Compressive strength loss after 90 days of Exposure to
MgSO4 for SC.

International Science and Technology Journal
المجلة الدولية للعلوم والتقنية

العدد 26
Volume 26

المجلة الدولية للعلوم والتقنية
International Science and Technology Journal
ISTJ
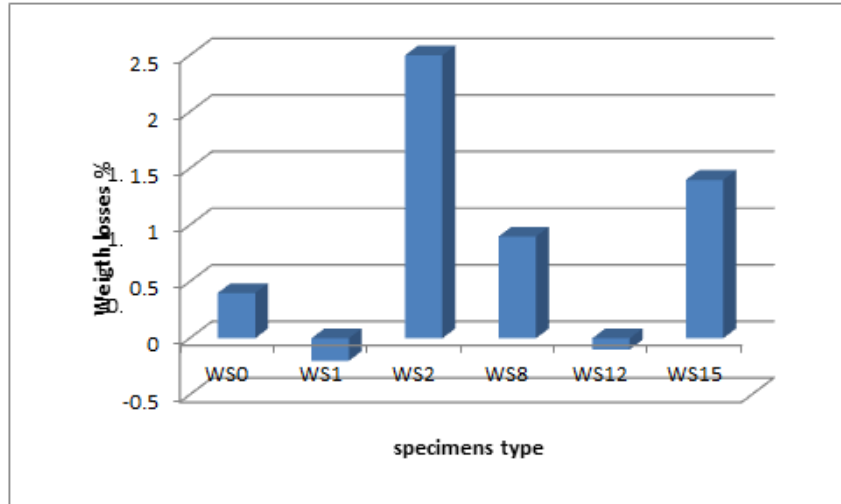
Figure 13. Weight loss after 90 days of Exposure to MgSO4 for WC.

Figure 14. Compressive strength loss after 90 days of Exposure to $MgSO_4$ for WC.

According to visual observations steam-cured, fly ash class F, GGBFS, and GP-based geopolymer mortar exhibits high resistance to magnesium sulfate immersion. Slag/fly ash specimens exposed to $MgSiO_4$ for up to six months showed no visual signs of surface deterioration, cracking or spalling (see Fig 9). Also, compressive

strength values increased up to 10% those obtained after immersion (you mean in up to 10% of the specimens after immersion). Moreover, weight losses remained nearly equivalent to those obtained prior to immersion, measuring less than 0.1 percent and exceeding 0.9% from initial geometry, as can be seen in Figure 11. Also, geopolymer mortar based on slag/glass powder specimens, showed no visual signs of surface deterioration, cracking or spalling, as Figure 9 depicts. Compressive strength losses decreased up to 10% those obtained after immersion. Moreover, weight loss remained nearly equivalent prior to imm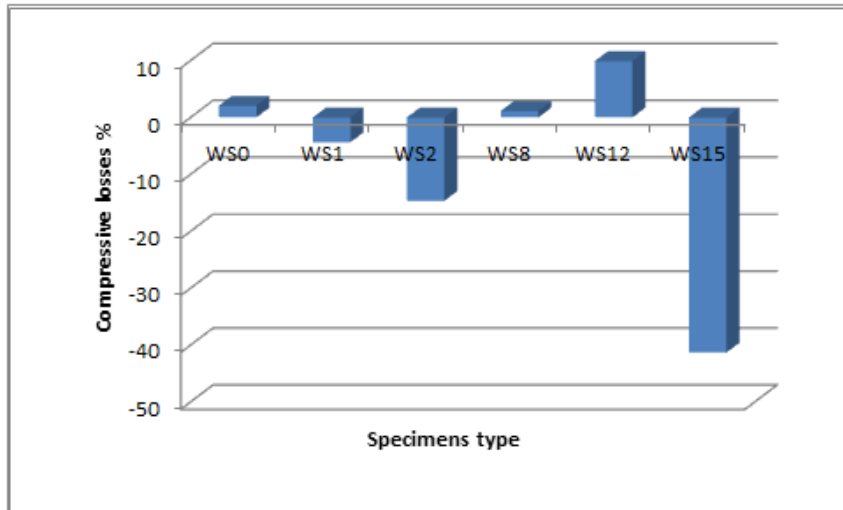ersion, measuring less than 0.2 percent and exceeding than 2.5%, as can be seen from the initial geometry in Figure 12; whereas, in WC15 the weight was increased by 1.4% and the compressive strength was decreased by 41%.

Figure 10 shows the compressive strength development of the various hardened geopolymer mortar with different percentage of glass powder content under WC conditions. From the figure, it is observed that the glass powder (GP) has a significant influence on compressive strength, which increases with GP content up to 10%. Beyond this percentage, the compressive strength begins to decrease. The 90-day compressive strength obtained for water-cured geopolymer mortar was 61MPa, and for 15% content of glass powder the compressive strength was 54MPa. The decrease in strength was 10.7%. Though, when compared to compressive strength at 90 days without immersion in sulfate the values stood at 24.8%, which is 20.8% bigger than 90 days compressive strength. In this way, the increase in glass powder content is shown to have a significant effect on the weight of geopolymer mortar. The weight of the specimen decreases under WC conditions with the increase in the quantity of GP, whereas it increases under SC conditions with the increase in the proportion of GP.

CONCLUSION

In this experimental study, we investigated sulfate and freeze-thaw resistance of geopolymer mortars using FA, GGBS, and GP. Based on the test results, the following conclusions can be reached:

International Science and
Technology Journal
المجلة الدولية للعلوم والتقنية

العدد 26
Volume 26

المجلة الدولية للعلوم والتقنية
International Science and Technology Journal

ISTJ

- Water-curing is better than steam-curing for slag and fly ash-based geopolymer mortar.
- No visual signs of surface deterioration, cracking, spalling, disintegration, or deformation could be detected after 150 of freeze-thaw cycles for specimens under steam-cured conditions.

- The effect of freeze and thaw test on the weight loss of GGBFS and GP-based geopolymer mortar is larger than that on the weight loss of GGBS- and FA-based geopolymer mortars.

- The GGBS- and FA- based geopolymer mortar is important for water-cured, it's showed greater compressive strength in comparison and after freeze-thaw test.
- The minimum compressive strength was obtained in the GGBFS and GP -based geopolymer mortar under water-cured settings.
- The GGBFS and GP -based geopolymer mortar lost the most compressive strength in comparison to the other specimens.
- Fly ash class F, GGBFS, and GP-based geopolymer mortar exhibits high resistance to magnesium sulfate immersion.
- Sulfate resistance in geopolymer mortars has an effect on the weight and compressive strengths of the specimens subjected to water-curing.
- Pulse velocity techniques can be successfully used to estimate the compressive strength of the geopolymer mortar mixes made with alkali-activated.

REFERENCES

[1] Peng, J.X., et al. Modeling of carbon dioxide measurement on cement plants. in Advanced materials research. 2013. Trans Tech Publ.
[2] Li, C., et al. CO2 emissions due to cement manufacture. in Materials Science Forum. 2011. Trans Tech Publ.

International Science and Technology Journal
المجلة الدولية للعلوم والتقنية

العدد 26
Volume 26

المجلة الدولية للعلوم والتقنية
International Science and Technology Journal
ISTJ

[3] Huntzinger, D.N. and T.D. Eatmon, A life-cycle assessment of Portland cement manufacturing: comparing the traditional process with alternative technologies. Journal of Cleaner Production, 2009. **17**(7): p. 668-675.

[4] Buchwald, A. and M. Schulz, Alkali-activated binders by use of industrial by-products. Cement and concrete research, 2005. **35**(5): p. 968-973.

[5] Yamin, F. and J. Depledge, The international climate change regime: a guide to rules, institutions and procedures. 2004: Cambridge University Press.

[6] Wang, S.-D., et al., Alkali-activated slag cement and concrete: a review of properties and problems. Advances in cement research, 1995. **7**(27): p. 93-102.

[7] Yang, K.-H., et al., Properties of cementless mortars activated by sodium silicate. Construction and Building Materials, 2008. **22**(9): p. 1981-1989.

[8] Fernández-Jiménez, A. and A. Palomo, Composition and microstructure of alkali activated fly ash binder: Effect of the activator. Cement and concrete research, 2005. **35**(10): p. 1984-1992.

[9] Palomo, A., M. Grutzeck, and M. Blanco, Alkali-activated fly ashes: a cement for the future. Cement and concrete research, 1999. **29**(8): p. 1323-1329.

[10] Provis, J., Activating solution chemistry for geopolymers, in Geopolymers. 2009, Elsevier. p. 50-71.

[11] Bakharev, T., Geopolymeric materials prepared using Class F fly ash and elevated temperature curing. Cement and concrete research, 2005. **35**(6): p. 1224-1232.

[12] Atiş, C.D., et al., Influence of activator on the strength and drying shrinkage of alkali-activated slag mortar. Construction and building materials, 2009. **23**(1): p. 548-555.

[13] Degirmenci, F.N., FREEZE-THAW AND FIRE RESISTANCE OF GEOPOLYMER MORTAR BASED ON NATURAL AND WASTE POZZOLANS. Ceramics–Silikáty, 2018. **62**(1): p. 41-49.

[14] Omer, S.A., R. Demirboga, and W.H. Khushefati, Relationship between compressive strength and UPV of GGBFS based geopolymer mortars exposed to elevated temperatures. Construction and Building Materials, 2015. **94**: p. 189-195.

[15] Yahya, Z., et al., Effect of solids-to-liquids, Na2SiO3-to-NaOH and curing temperature on the palm oil boiler ash (Si+ Ca) geopolymerisation system. Materials, 2015. **8**(5): p. 2227-2242.

[16] Sun, P. and H.-C. Wu, Chemical and freeze–thaw resistance of fly ash-based inorganic mortars. Fuel, 2013. **111**: p. 740-745.

[17] Thokchom, S., P. Ghosh, and S. Ghosh, Performance of fly ash based geopolymer mortars in sulphate solution. Journal of engineering science and technology review, 2010. **3**(1): p. 36-40.

[18] Enstitüsü, T.S., Çimento deney metotlari-Bölüm 1: Dayanim tayini. TS EN, 2009: p. 196-1.

[19] Abdoslam Alnkaa., FARKLI KÜR KOġULLARININ GEOPOLĠMER HARÇÖZELLĠKERĠNE ETKĠSĠ; KASTAMONU ÜNĠVERSĠTESĠN, 2019.

Influence of post processing techniques on surface texture of selective laser melting parts

Akram Alqurayd[1] , Khalid Alrbaey[2] , Mousa Shagan[3]

[1,3]Higher institute of marine sciences techniques Sabratha

[2]College of Engineering Technology – Surman

eswei0077@gmail.com, moga_kh2001@yahoo.com, mousa.shagan@gmail.com

الملخص

في هذا العمل تم دراسة تأثير تقنيات مختلفة لمعالجة و تحسين خشونة الاسطح للاجزاء المصنعة بطريقة الإضافة لتقنية الليزر . في هذة الدراسة تم استخدام الالة نوع رينيشو (125) بالتعاون مع مركز البحوث الصناعية بمدية كوفنتري (MTC) لتصنيع قطع من معدن الستانلس ستيل المقاوم للصدأ (المملكة المتحدة). علي الرغم من أن هذه التقنية قادرة على إنتاج نماذج ثلاثية الأبعاد دقيقة وذات كثافة عالية مماثلة لتلك المصنوعة من الأساليب التقليدية مباشرة من بيانات CAD. الا أن ، هناك بعض العيوب التي تعاني منها هذه التقنية، وهي إن القطع المصنعة بهذه التقنية تعاني من خشونة في الاسطح والتي تتراوح بين 10 إلى 45 ميكرومتر، بسبب المتغيرات في مستوي الطاقة لإستخدام الالة . ولعل الهدف من هذا العمل هو مقارنة تحسين خشونة الاسطح المنتجة من الفولاذ المقاوم للصدأ 316L، وقد أظهرت جميع التقنيات المستخدمة تحسنا جيدا في خشونة الاسطح مع بعض العيوب على نسيج حواف الاسطح كما هو مبين في النتائج النهائية.

1-   ABSTRACT

In this work, the effects of different post processing techniques on surface texture improvement of additive manufactured parts made by Selective Laser Melting powder bed. In this investigation Renishaw's SLM 125 was employed to produce 3D parts by using stainless steel 316L, at Manufacturing Technology Centre (MTC) Coventry (UK). SLM is techniques capable to produce fully dense functional 3D models direct from CAD data, similar with those

International Science and Technology Journal
المجلة الدولية للعلوم والتقنية

العدد 26
Volume 26

المجلة الدولية للعلوم والتقنية
ISTJ

made with traditional methods. On the other, hand the major drawback is that the parts have granular poor surface finish, which ranges from 10 to 45 μm due to machine adjustment parameters.

The aim of this work is to compare surface finish improvement of SLM parts several post processing methods have been applied using Stainless Steel 316L. All techniques showed good improvement of surface finish with some drawback on surface texture as showed in followed results.

Keywords, selective laser melting, surface roughness, pot processing

2-   Introduction.

Additive manufacturing is an overall term that is used to describe all the technologies that are used to manufacture parts by addition of material in layer by layer to obtain the final model, enhanced by using three dimension cad model (CAD) date, as opposed to the traditional subtractive methods or processes that involved the removal of material according [1].

AM techniques have a challenge of producing parts with a stepped surface finish and many researchers have identified this problem since the existence of this technology. Metal power bed methods such as SLS and SLM are suffering from a granular poor surface finish because of powder particle size, layer thickness, laser power etc..[2].

Figure.1.shows the effect of angle on surface finish characterizations, Results show that increase angle lade to decries surface finish, many researchers have proved that; surface roughens improvement using in process techniques under the influence and knowledge of the machine parameters.

Figure 1: Showing poor surface finish

Some of the most important variables that can adjusted include using fine powder, thin layers, laser energy, incorporating hatch spacing, building period of parts, part orientation and scan spacing ets. Figure (2) illustrates the basic parameters during additive manufacture [3] [4].
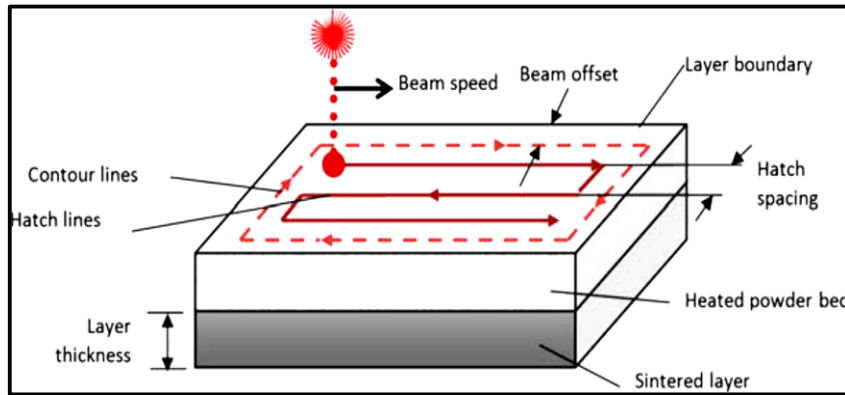
Figure 2: Showing in process parameters

Over the previous years, several approaches have been put in place in order to improve the surface finish of layer manufactured components companies such as Best in class, Extrude hone, Taylor Hobson, Keyence, Renishaw Plc etc.

Several surface modifications methods from other companies are being implemented to solve this problem such as re-melting, shot peening, hand polishing, laser ablation, sandblasting, machining, chemical, thermal processes etc. while, the cost price of components manufactured are increasing due to the post processing techniques[2][5] [6]

2.1- Surface finish characterisation and improvement on Layer manufactured Parts

Surface roughness measurement has been described as one of the most significant area of study in engineering scope and layer manufacturing parts. Thus, a number of surface measurement methods and equipment have been entered in this field for period of time to be more precise. The worth mentioned in this case there

are two way of describe surface data, which namely respectively two dimensions and three dimension surface measurement [7].

Nowadays, three dimensional is being more preferred because it is illustrated more data to describe surface characterizations. The equipment's for characterization are available in wide range of versions such as in laboratories and some of them are also portable, to be used in the field.

Therefore, there are two techniques currently have been used to measure characterization of surface roughness such as:[8]

- Contact (stylus profiling)
- Non-contact (optical)

Gnarly, surfaces are normally composed of the following features as you showing in figure below. In hence, some are flat, some may be afflicted with waviness, some may vary from fine to coarse, some may be perfectly smooth etc.[9] [10].

Figure (3) shows surface texture connected with additive manufacture technique. Generally there are two methods that are currently being used to improve the surface finish of layer manufactured parts, which respectively namely in process techniques and post processing methods.
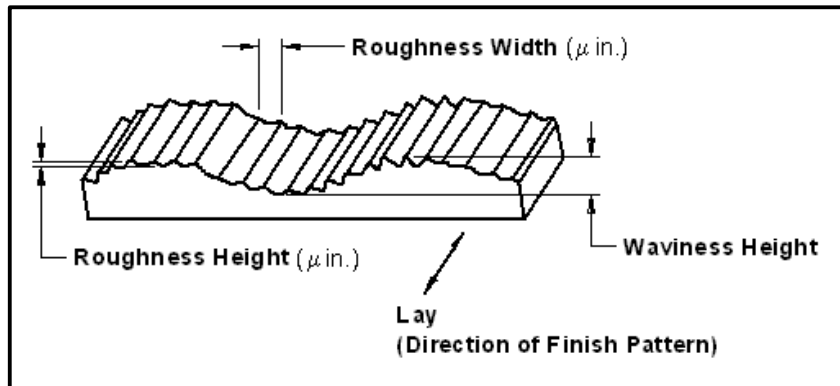
Figure 3: surface characteristics [11]

Most of the parts manufactured by SLM improved by using a variety of surface modifications methods available on the market today, several mechanical post processing have been completed, in

order to improve surface finish of SLM Stainless Steel 316L parts and its influence's on surface textures[3][12][13].

3. . Experimental work Plan

The work was carried out according to the scheme shown in the following below **(Figure.4)**

1- Design of the benchmark

↓

2- Printing of the part

↓

3- Surface characterisation
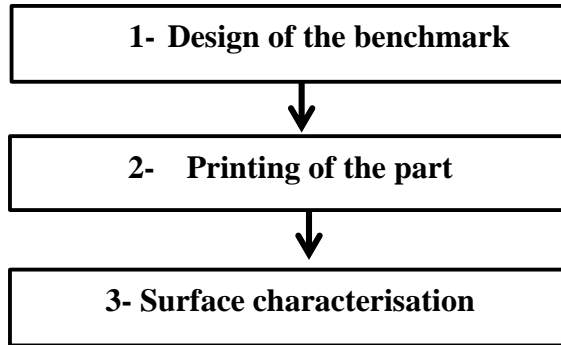
Figure 4: Experimental methodology flowchart

3.1- The Benchmark design and manufacture procedure.

The samples were made on the Renishaw SLM125. The experiment was carried out by setting up the machine and implementing the optimal parameters as in the following table(table.1).

Table 1: Selected process parameters

Laser power	layer thickness	Exposure	Point Distance
200W	50μm	50μs	75mm

Stainless steel powder was used to build the samples, with different geometry surfaces and four identical samples were built using SS 316L to complete this investigation.

The benchmark below was designed in to characterize surface roughness in different surfaces such as top surface, interior surfaces, round; sloping plane etc., then will be used for post processing methods as shown in figure .5, and figure.6.
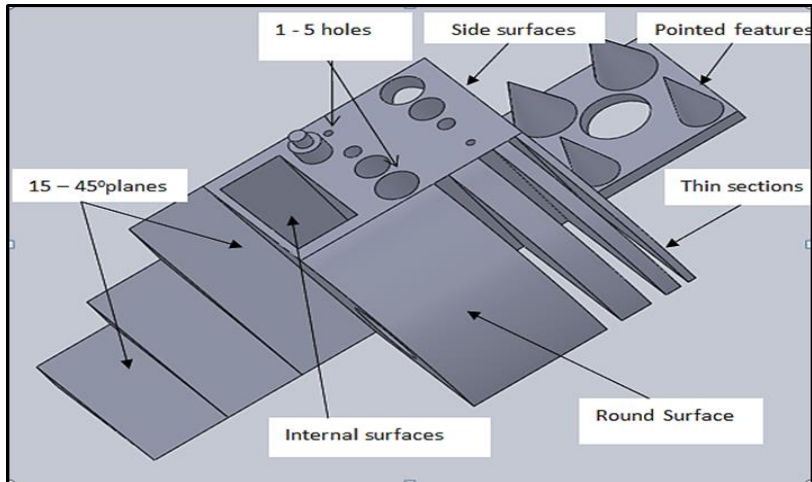
Figure 5: Benchmark model with different views
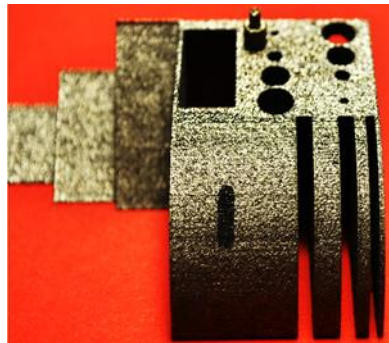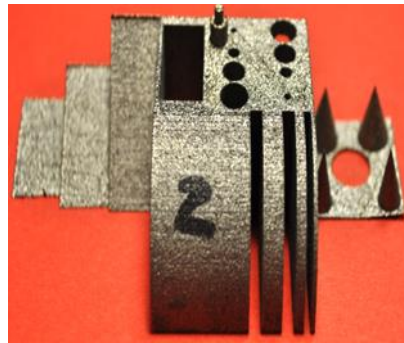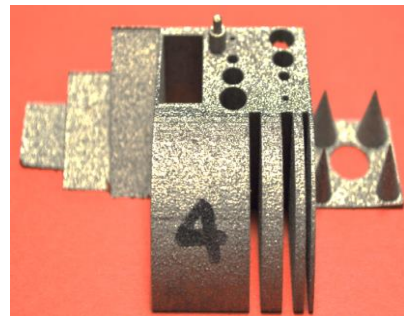
Figure 6: Separated samples from the substrate

All the benchmarks were made and removed carefully from the substrate using the band saw machine.

3.2- Surface Roughness and Characterization

After separating the models from the substrate, the surface finish was analysed using contact profilometer , as shown in figure (7).
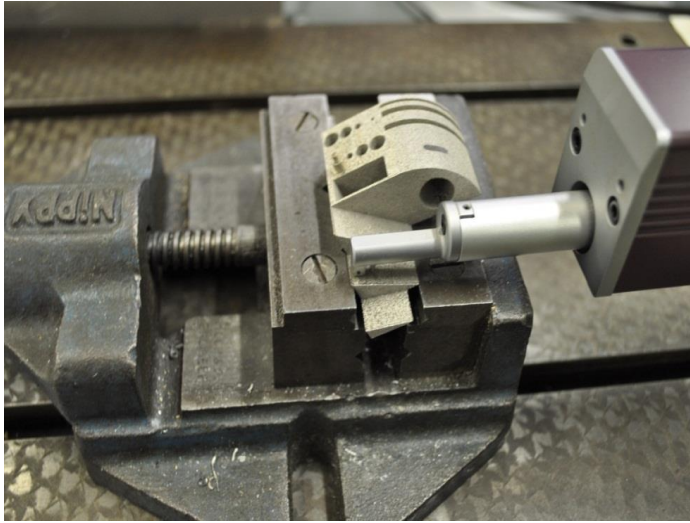
Figure 7: Surface measuring – contact method

4.- Results and Discussion

This section shows analysis of the manufactured benchmark using 3D digital microscope form Talysurf instrument and accuracy using a Vernier caliper. (Figure 8 below)

International Science and
Technology Journal
المجلة الدولية للعلوم والتقنية

العدد 26
Volume 26

المجلة الدولية للعلوم والتقنية
International Science and Technology Journal
ISTJ
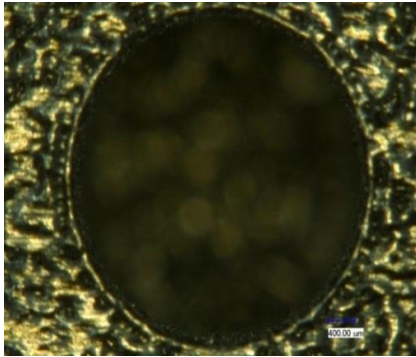
A
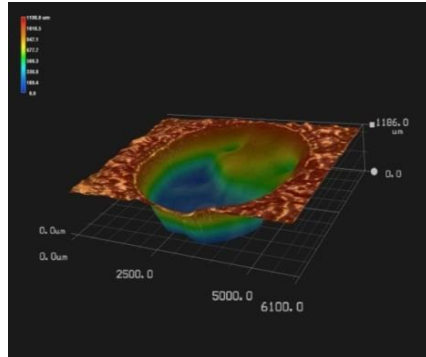
B
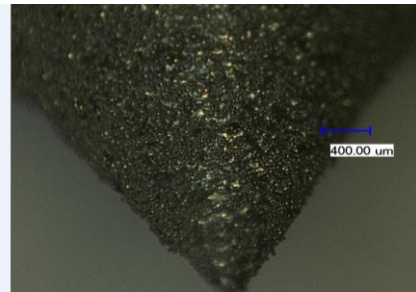
C
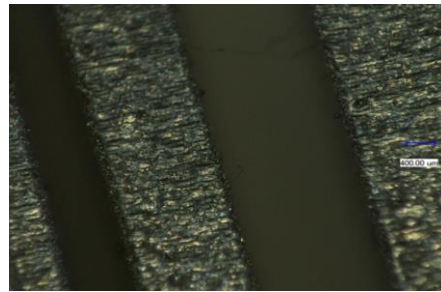
D
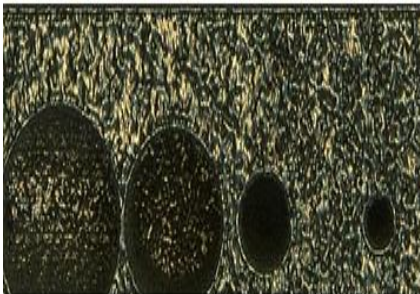
E
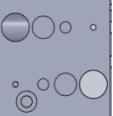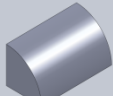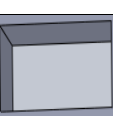
F
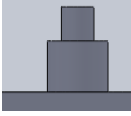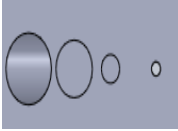
Figure 8: 2D micrographs showing balling on thin sections, on cones, holes etc.

International Science and
Technology Journal
المجلة الدولية للعلوم والتقنية

العدد 26
Volume 26

ISTJ

Figure 8 shows geometrical features of the benchmark (**A**) internal surfaces are filled with balling and discolouration, (**B**) is a 3D view of the hole showing agglomeration and balling, (**C**) – cone with porosity around the surface, (**D**) thin walls with balling,(**E**) – top surface holes with bad edges on different diameters and (**F**) angle planes with stair effect.

After building the benchmark, analyses and measured of defects on every feature wear been completed as showed in the below table.

Table 2: Results on manufactured sample.

	Geometry	Accuracy	Ra	Rv	Rq	Rp	Defects
15º plane		98%	25.6	83.9	32.7	104.3	Balling, Porosity
30º plane		100%	21.4	55.3	66.6	66.6	Balling, Porosity
45º plane		100%	21.9	58.1	26.4	93.9	Balling, sharp edges
Top surface		100%	26.5	77.4	33	101	Balling, Over melting
Round Surface		100%	18.3	63.2	24.1	76.5	Balling, Porosity
Side Walls		99%	17	52.9	21.2	63.8	Porosity
Internal Surface		98%					Powder sticking

International Science and Technology Journal
المجلة الدولية للعلوم والتقنية

العدد 26
Volume 26

المجلة الدولية للعلوم والتقنية
International Science and Technology Journal
ISTJ

Thin sections		100%					Balling
Small features		99%					Sharp edges
Holes		98%					Powder sticking
Pointed corners		97%					Balling
Cones		99%	16.4	35.8	20	51.7	Balling

As can be seen the blue area indicates that no surface characterisation was done when using contact instrument because it was too big to fit into internal surfaces.

5. Selection of the Post Processing Methods

There are several post processing techniques available on the market today and been one of the important steps required in SLM parts. The following methods in Figure 9 were selected to improve the surface texture of benchmarks because of the geometry and feature complicated of parts.

The criteria of methods are to improve the surface texture within a low cost and short time.

International Science and Technology Journal
Technology Journal
المجلة الدولية للعلوم والتقنية

العدد 26
Volume 26

المجلة الدولية للعلوم والتقنية
International Science and Technology Journal

ISTJ

```
┌─────────────────────────────────────────────┐
│      Selection of post processing methods    │
└─────────────────────────────────────────────┘
     │            │              │          │
     ▼            ▼              ▼          ▼
Grit blasting  Vapour blasting  Shot blasting  Electro polishing
                      │
                      ▼
┌─────────────────────────────────────────────┐
│  Analysis of Results and comparison of processes │
└─────────────────────────────────────────────┘
```
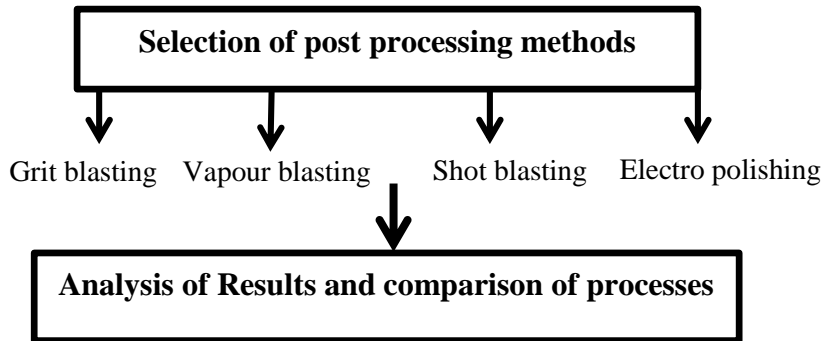
Figure 9: Experimental methodology overview flowchart 2

5.1. Grit Blasting Process

This method used an abrasive high pressure in order to smooth the surface. The method has some drawbacks due its can destroy small features such as sharp corners and small surface. The part below was processed by **Blast master machine** and the process took about ten minutes.

Figure10 shows a comparison of the benchmarks before and after

the process. It shows that the surface has improved but there are

some destruction on thin section and plane.

A   **B**
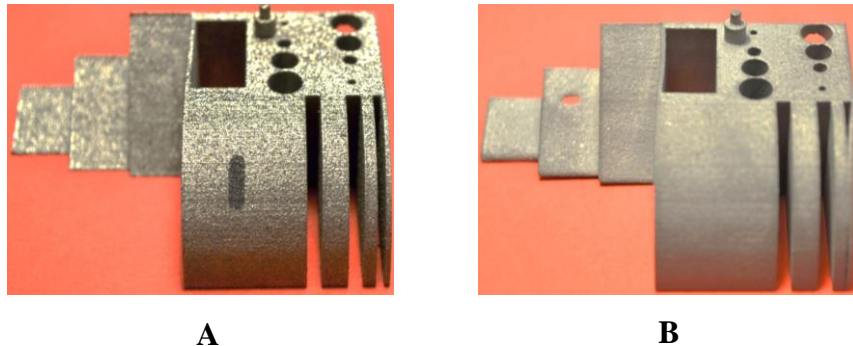
Figure 10: A before and B after grit blasting.

International Science and
Technology Journal
المجلة الدولية للعلوم والتقنية

العدد 26
Volume 26

المجلة الدولية للعلوم والتقنية
International Science and Technology Journal
ISTJ

5.2. Vapour Blasting Process

The technique uses water and glass bead media to polish the surface. Gyson blast cleaner machine was used to polish the part and the process only took approximately ten minutes.

Figure 11 shows a comparison of the two benchmarks before and after the process and **B** shows that the benchmark is well polished but there is deformation on plate cones
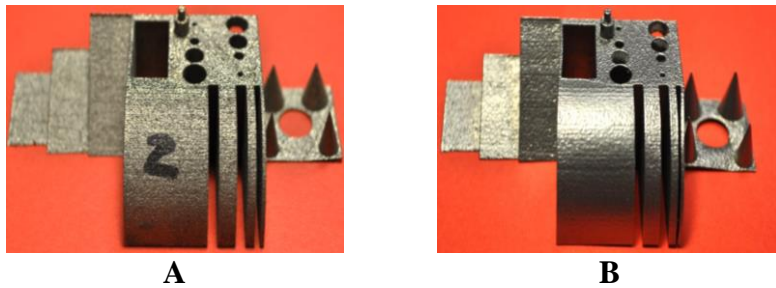
Figure 11: A before and B after vapour blasting

5.3. Shot Blasting Process

The benchmark was post processed at Newtech Powder Coaters using pressure pot shot blasting machine. The model was ATO 101015 (G, E) and the process took approximately ten minutes. Steel shots were used as media for blasting.

Figure 12 shows a comparison of the benchmark before and after the process and **B** shows some deformation on thin section due to high pressure exerted during the process
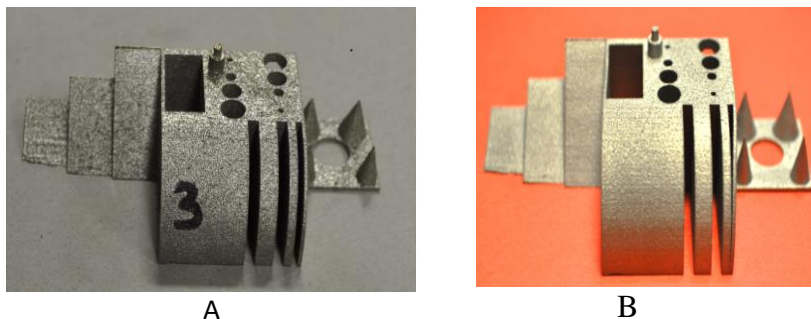
Figure 12: A before and B after shot blasting

International Science and
Technology Journal
المجلة الدولية للعلوم والتقنية

العدد 26
Volume 26

المجلة الدولية للعلوم والتقنية
ISTJ

5.4 Electro Polishing.

The benchmark was post processed using ionic liquid for ten minutes, then rinsed in water and finally in HCL to remove surface oxide.

After that it was dipped in ionic liquid for electro polishing for twenty minutes.

Figure 13 shows a comparison of the two benchmarks before and after electro polishing. B shows that the benchmark is well polished and a shiny texture. There is no deformation.

A

B
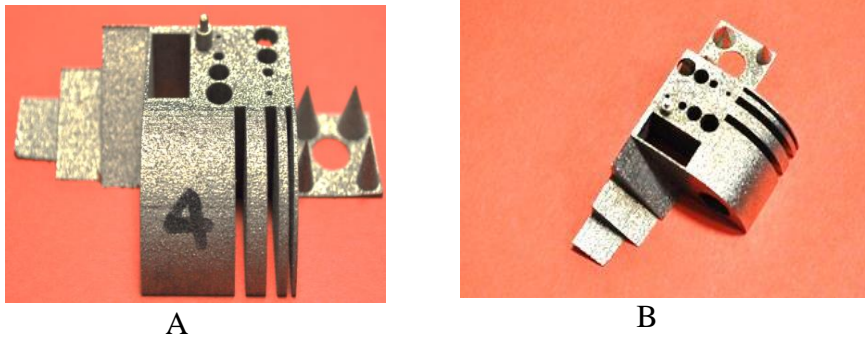
Figure 13: Before electro polishing.

6. Surface Characterization, Results and Discussions

This section displays surface roughness results measured on the processed benchmarks from four different methods. Tables, graphs and micrographs below shows the results of amplitude parameters measured using the Form Talysurf PGI instruments. All these amplitude parameters are based on overall height.

6.1. Shot Blasting Process.

Table3 shows several surface parameters measured on vertical characteristics of the surface deviations at 5*2.5mm cut-offs. The table shows parameters R_t, R_v, R_p R_z on the shot blasted benchmark measured. It shows the maximum depth and maximum height below and above the mean line within the same sampling span

Amplitude Parameters measured on shot blasted benchmark

Table 3: Amplitude of parameters measured after shot blasting

	Top surface	Round surface	Side Walls	15º plane	30º plane	45º plane	Cone/surface
Ra	11.228	9.845	6.260	12.365	11.614	8.228	7.362
Rp	31.360	31.727	22.114	34.420	37.632	25.103	26.163
Rv	37.864	28.713	22.470	34.149	42.034	23.904	25.343
Rt	93.865	98.435	66.162	90.621	162.719	68.103	51.506
Rz	69.225	60.441	44.584	68.569	79.666	49.008	51.506
Rd	24.14	21.86	26.89	26.68	27.27	25.10	23.08
Pq	14.432	13.209	8.161	15.191	17.021	10.482	9.137

6.2 Vapour Blasting Process

Table 4 shows several amplitude parameters measured on the benchmark on different surfaces from vapour blasting process. Side walls shows an average roughness of 3.9μm compared to 30º with 109μ

Amplitude Parameters measured on vapour blasted benchmark

Table 4: Amplitude of parameters measured after shot blasting

	Top surface	Round surface	Side Walls	15º plane	30º plane	45º plane	Cone /surface
Ra	9.815	5.246	3.907	12.171	10.945	6.888	4.388
Rp	28.670	13.919	11.045	29.369	29.290	15.77	11.02
Rv	23.707	12.662	11.274	32.823	29.536	19.756	14.408
Rt	72.628	41.785	33.774	81.664	109.987	60.444	25.429
Rz	52.178	26.582	22.320	62.192	58.827	35.348	25.429
Rdq	7.72	5.56	7.36	12.73	9.63	7.73	13.01
Pq	12.662	6.536	4.899	14.732	15.045	8.937	5.422

International Science and Technology Journal
المجلة الدولية للعلوم والتقنية

العدد 26
Volume 26

المجلة الدولية للعلوم والتقنية
International Science and Technology Journal
ISTJ

6.3. Grit Blasting Process

Table 5 shows all the surface parameters measured on all the surfaces of the benchmark as indicated on the table above after grid blasting process.

Amplitude Parameters measured on grit blasting benchmark						
Table 5: Amplitude of parameters measured after grit blasting						
	Top surface	Round surface	Side Walls	15º plane	30º plane	45º plane
Ra	8.829	7.810	5.508	7.559	7.169	7.565
Rp	26.496	23.421	16.814	24.035	22.329	24.832
Rv	25.091	27.390	17.993	9.361	28.826	27.483
Rt	59.240	86..461	50.150	55.513	69.522	83.467
Rz	51.587	50.812	34.807	47.964	51.156	52.315
Rdq	24.36	20.57	18.43	24.25	24.57	23.39
Pq	10.851	10.237	6.999	9.361	9.210	9.992

6.4 Electro Polishing Process

Table 6 shows a collection of surface results on the benchmark after post processing and the minimum Ra is found on the side wall surface 5.9 µm as compared to the top surface with 16.5µm. This shows that electro polishing does not subtract a lot of materials compared to other methods used

Amplitude Parameters measured on electro polishing benchmark							
Table 6: Amplitude of parameters measured after electro polishing.							
	Top surface	Round surface	Side Walls	15º plane	30º plane	45º plane	Cone/surface
Ra	16.588	9.965	5.907	17.915	9.231	8.406	5.909
Rp	46.958	31.413	11.045	45.723	24.659	26.912	26.931
Rv	72.184	40.400	11.274	71.356	31.870	22.277	14.258
Rt	160.293	176.163	33.774	155.43	97.712	85.624	41.190

International Science and
Technology Journal
المجلة الدولية للعلوم والتقنية

العدد 26
Volume 26

المجلة الدولية للعلوم والتقنية
International Science and Technology Journal
ISTJ

Rz	119.142	71.813	22.320	117.07	56.529	49.189	41.190
Rdq	19.78	15.93	7.36	24.49	11.58	9.29	8.14
Pq	22.535	14.326	4.899	24.175	11.865	10.748	7.706

6.5 Comparison of Surface Topology

As can be seen on the micrographs below, Figure. shows that all the blasting methods subtract a substantial amount of material as compared to electro polishing technique. From the results found electro polishing is not suitable for polishing SLM metal powder parts.

Shot Blasting

Vapour Blasting

Grid Blasting

Electro Polishing
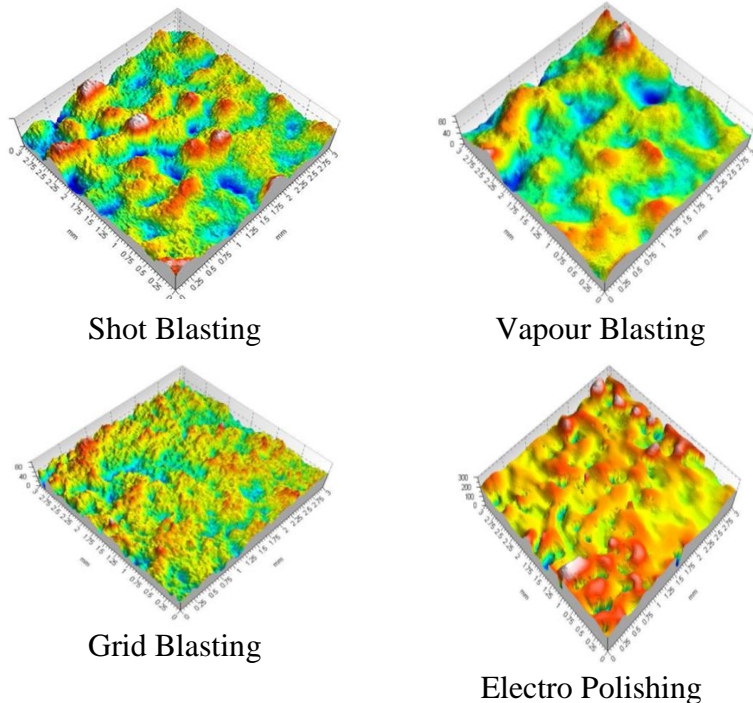
Figure 14: Surface morphology of the top surface area.

International Science and Technology Journal
المجلة الدولية للعلوم والتقنية

العدد 26
Volume 26

المجلة الدولية للعلوم والتقنية
International Science and Technology Journal
ISTJ

From all the post processing methods carried out, they are all very effective in surface finishing of SLM parts and the Table 7 below summarizes some of the data collected.

Table 7: Comparison table of post processing methods

.Comparison table of the post processing methods used				
Processes	**Ra**	**Accuracy**	**Defects**	**Time – (minutes)**
Shot blasting	Good	Poor	Yes	5-10
Grit/bead blasting	Good	Poor	Yes	5-10
Vapour polishing	Better	Good	Yes	10-15
Electro polishing	Good	Good	No	10-20

Figure 15 shows a radar or spider chart used to compare the post processing methods used since they are different. Percentages are shown in Table 8

Table 8: *Table of comparison post processing in percentages*

Process	Ra%	Accuracy %	Defects %	Time %	Rt %	Rz %
Shot blasting	70	80	80	80	40	65
Grid blasting	75	70	60	80	80	90
Vapour blasting	80	90	95	70	60	80
Electro polishing	65	95	95	60	30	50

International Science and
Technology Journal
المجلة الدولية للعلوم والتقنية

العدد 26
Volume 26

المجلة الدولية للعلوم والتقنية
International Science and Technology Journal
ISTJ
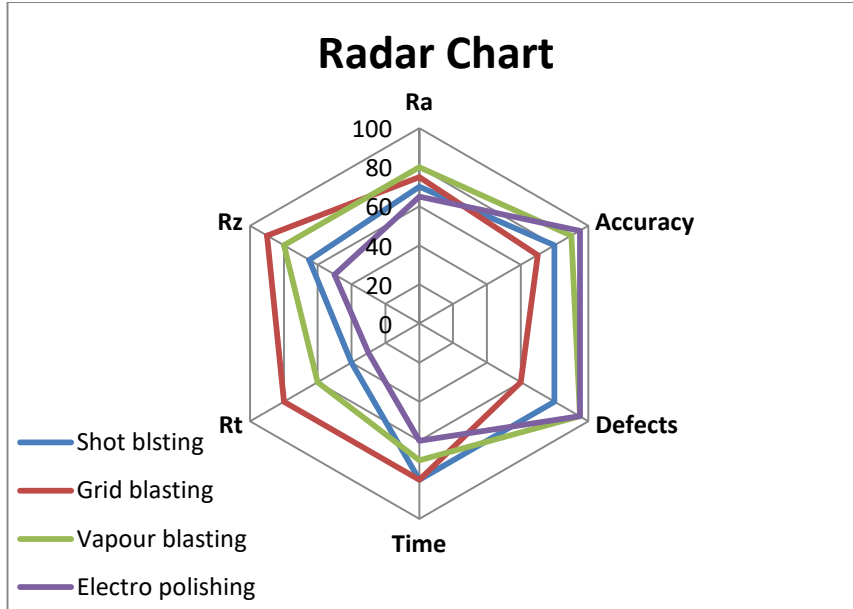
Figure 15: Radar chart

7. Conclusion

The aim of this work was researching on how to improve the surface finish of SLM metal powder parts.

Four benchmark models were built on SLM 125 machine using layer by layer method and they were all post processed successfully. It is concluded that average roughness (Ra) has been improved by the different mention methods. Ra has been reduced on side walls from 17 - 3.9µm by vapour blasting process and followed by grit blasting with 5.5µm. All the results were carefully analysed and presented in the form of figures, tables and graphs. Some of the methods also need to consider the geometry of the part e.g. complex shapes are very difficult to machine but processes like sand blasting and electro polishing are preferred. On the other hands, Electro polishing method is not very effective in internal surfaces because from the results obtained internal surfaces were still very rough and other techniques have their own advantages and limitations as well.

Although, Post processing is a very important technique to (SLM) parts because it will improve the functionality of the components span. Some of the methods are too harsh because they destroy thin sections and small features.

References

[1] D. Thomas, "The Development of Design Rules for Selective Laser Melting," University of Wales. Cardiff Institute, 2009.

[2] V. Alfieri, P. Argenio, F. Caiazzo, and V. Sergi, "Reduction of surface roughness by means of laser processing over additive manufacturing metal parts," Materials (Basel)., vol. 10, no. 1, pp. 1–11, 2017, doi: 10.3390/ma10010030.

[3] D. a Hollander et al., "Structural, mechanical and in vitro characterization of individually structured Ti-6Al-4V produced by direct laser forming.," Biomaterials, vol. 27, no. 7, pp. 955–963, Mar. 2006, doi: 10.1016/j.biomaterials.2005.07.041.

[4] J. Kranz, D. Herzog, and C. Emmelmann, "Design guidelines for laser additive manufacturing of lightweight structures in TiAl6V4," *J. Laser Appl.*, vol. 27, no. S1, p. S14001, Feb. 2015, doi: 10.2351/1.4885235.

[5] B. Sagbas, "Post-Processing Effects on Surface Properties of Direct Metal Laser Sintered AlSi10Mg Parts," *Met. Mater. Int.*, vol. 26, no. 1, pp. 143–153, Jan. 2020, doi: 10.1007/s12540-019-00375-3.

[6] E. Brandl, U. Heckenberger, V. Holzinger, and D. Buchbinder, "Additive manufactured AlSi10Mg samples using Selective Laser Melting (SLM): Microstructure, high cycle fatigue, and fracture behavior," *Mater. Des.*, vol. 34, pp. 159–169, Feb. 2012, doi: 10.1016/j.matdes.2011.07.067.

[7] B. T. Chi, T. Ballinger, R. Olds, and M. Zecchino, "Surface Texture Analysis Using Dektak Stylus Profilers."

[8] C. Sanz, V. G. Navas, O. Gonzalo, and G. Vansteenkiste,

International Science and Technology Journal
المجلة الدولية للعلوم والتقنية

العدد 26
Volume 26

المجلة الدولية للعلوم والتقنية
ISTJ
International Science and Technology Journal

"Study of surface integrity of rapid manufacturing parts after different thermal and finishing treatments," *Procedia Eng.*, vol. 19, pp. 294–299, Jan. 2011, doi: 10.1016/j.proeng.2011.11.115.

[9] Y. Sun, A. Moroz, and K. Alrbaey, "Sliding wear characteristics and corrosion behaviour of selective laser melted 316L stainless steel," *J. Mater. Eng. Perform.*, vol. 23, no. 2, 2014, doi: 10.1007/s11665-013-0784-8.

[10] K. Alrbaey, D. Wimpenny, R. Tosi, W. Manning, and A. Moroz, "On optimization of surface roughness of selective laser melted stainless steel parts: A statistical study," *J. Mater. Eng. Perform.*, vol. 23, no. 6, pp. 2139–2148, 2014, doi: 10.1007/s11665-014-0993-9.

[11] P. M. Lonardo and a. a. Bruzzone, "Measurement and Topography Characterisation of Surfaces Produced by Selective Laser Sintering," CIRP *Ann. - Manuf. Technol.*, vol. 49, no. 1, pp. 427–430, Jan. 2000, doi: 10.1016/S0007-8506(07)62981-3.

[12] O. Piiroinen, "Improving surface quality in vacuum infused parts of composite laminates produced using vacuum," no. March, pp. 26–29, 2008.

[13] K. Alrbaey, D. I. Wimpenny, A. A. Al-Barzinjy, and A. Moroz, "Electropolishing of Re-melted SLM Stainless Steel 316L Parts Using Deep Eutectic Solvents: 3×3 Full Factorial Design," *J. Mater. Eng. Perform.*, vol. 25, no. 7, pp. 2836–2846, Jul. 2016, doi: 10.1007/s11665-016-2140-2.

Investigation of the Effect of Magnetic Field on some Physical Properties of Water

Najat Khalifa Boufa
Zawia University, Faculty of Medical Technology, Medical Engineering Department, Zawia, Libya
Email: n.boufa@zu.edu.ly

Abstract

The main purpose of this study was to investigate whether or not a water treatment by magnetic field could change the physical properties of water as reported in some scientific literature, the properties which were studied such as density, electrical conductivity, total dissolved solids, pH value, and NaCl concentration. The water sample which tested in this study was well water, the magnetically treatment of well water samples was by two types of magnets; first type was electromagnet of low fixed intensity (900 G=90mT), where the water samples were exposed to this magnetic field at various times (5, 10, 15, 20, 25, 30) min. The second type was permanent magnet, the exposing time to permanent magnetic field was 7 days.

It was found that these examined physical properties of well water samples were changed following the magnetic treatment, the changes depend on the magnetization conditions, and the magnetic field causes changing in the electrical conductivity due to the ability to dissolve and dissociate salts; influence on solubility of salts was remarkable. As well as a positive effect on the pH value, the water samples become less acidic.

The results of this study suggested that the magnetic treatment improve quality of water, therefore, the magnetization process submits improvements on water applications in several areas such as industry, agriculture and medicine.

Keywords: Permanent magnetic field; Electromagnetic field; Electrical conductivity; Total dissolved salts; pH.

International Science and Technology Journal
Technology Journal
المجلة الدولية للعلوم والتقنية

العدد 26
Volume 26

المجلة الدولية للعلوم والتقنية
International Science and Technology Journal
ISTJ

Abbreviations: MF: Magnetic field, PMF: Permanent magnetic field, EMF: Electromagnetic field, EC: Electrical conductivity, TDS: Total dissolved salts, T: Tesla, G: Gauss.

الخلاصة:

الهدف الرئيسي من هذه الدراسة هو التحقق من أن معالجة المياه بالمجال المغناطيسي يمكن أن يغير الخواص الفيزيائية للماء كما أشارت إليه بعض الدراسات والأبحاث العلمية، حيث تمت دراسة الكثافة، والموصلية الكهربائية، والأملاح الكلية الذائبة، والأس الهيدروجيني، ونسبة تركيز كلوريد الصوديوم في الماء، العينة التي أجريت عليها الدراسة هي ماء بئر.

تمت عملية المغنطة بنوعين من المجال المغناطيس، النوع الأول مجال كهرومغناطيسي ثابتة شدته منخفضة (900 جاوس = 90 ملي تسلا)، عرضت العينات للمجال الكهرومغناطيسي في أزمنة مختلفة (5، 10، 15، 20، 25، 30) دقيقة، النوع الثاني من المجال مجال مغناطيسي دائم، حيث عرضت العينات لهذا المجال لمدة 7 أيام متواصلة.

من خلال النتائج المتحصل عليها لوحظ تغير في الخواص الفيزيائية لعينات المياه بعد معالجتها مغناطيسيا، وان هذه التغييرات تعتمد على ظروف المغنطة، فقد تسبب المجال المغناطيسي في تغير الموصلية الكهربائية بسبب قدرته على إذابة الأملاح وتفككها، فقد كان تأثير المجال على ذوبان الأملاح ملحوظًا، بالإضافة إلى تأثيره الإيجابي على الأس الهيدروجيني، فالمياه المعالجة مغناطيسيا أصبحت أقل حامضية.

أظهرت نتائج هذه الدراسة أن المعالجة المغناطيسية للماء تعمل على تحسين جودته، وبالتالي فإن عملية المغنطة تقدم تحسينات على تطبيقات المياه في العديد من المجالات مثل الصناعة والزراعة والطب.

1. Introduction

Water is classified as a diamagnetic substance. A water molecule is composed of an oxygen atom and two hydrogen atoms, with the chemical formula H_2O, they are bonded by covalent bond, via a

International Science and
Technology Journal
المجلة الدولية للعلوم والتقنية

العدد 26
Volume 26

المجلة الدولية للعلوم والتقنية
International Science and Technology Journal
ISTJ

shared pair of electrons, as an isosceles triangle with its upper angle of 104.45°, figure1 shows a molecule of normal water, this is because the oxygen atom, carries two pairs of unshared electrons [1], where the oxygen is slightly negative, whereas the hydrogen is slightly positive. This structure of water molecule will have similar qualities of a magnetic dipole. Due to that, water molecules will attract each other in the opposite end, by a hydrogen bond, this bond allows the water molecules to form a group of water molecules (clusters), as seen in figure2. The hydrogen bonds between water molecules give water four features; it is denser in liquid state than solid state, it has cohesion and a high boiling point, it has a good solubility [2].
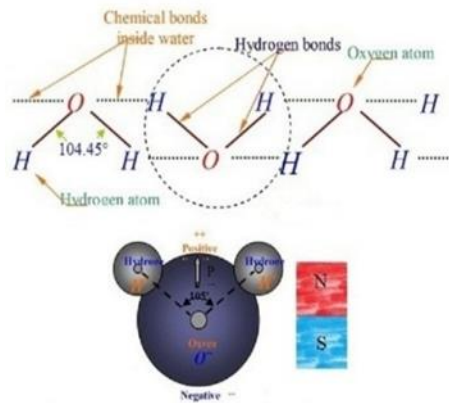
Figure 1. Normal Water molecule
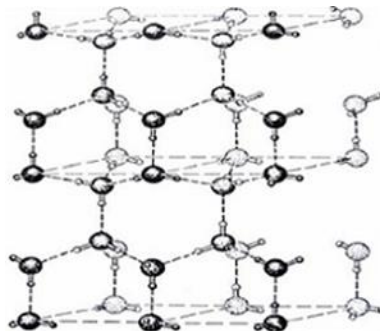
Figure 2. Structural group of water molecules

International Science and
Technology Journal
المجلة الدولية للعلوم والتقنية

العدد 26
Volume 26

المجلة الدولية للعلوم والتقنية
International Science and Technology Journal
ISTJ

When water is exposed to MF, magnetization can affect the two forces that control the water structure, chemical hydrogen bond and Van der Waal's forces, where magnetization can break hydrogen bonds between water clusters, and the water molecules will arrange in one direction as illustrated in figure3, this mode of arrangement causes reducing the bond angle from 104.45° to 103°, leading to decrease in the consolidation degree between water molecules, also decrease in clusters sizes by converted into single molecules or smaller ones, that is why the magnetic water viscosity is less than ordinary water viscosity. These changes in water molecules composite cause changes in some physical and chemical properties [1-5].
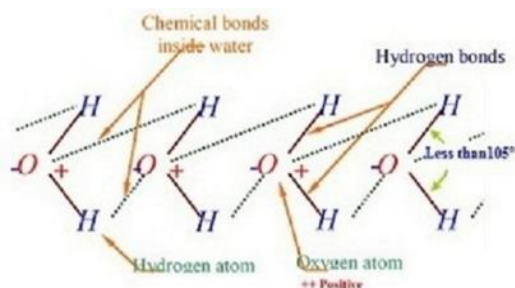
Figure 3. Water molecule under effect of MF

Magnetic water does not mean that it has a magnetic force that can attract things. It's water different from ordinary water in its properties. It is water which is passed through a MF at specific speed, or by placing the magnet inside or near the water, for period of time. The magnetization degree of water depends on the following parameters [1, 3, 6, 7,8, 9]:
1. Magnetic field intensity.
2. Duration of exposing water to MF.
3. The amount of exposing water to the field.
4. Velocity of water flow.
Although the effect of MF on the water is a controversial issue, however, magnetic water has several applications in different aspects. For example, it can purify wastewater, promote plant growth, inhibit the scaling of metallic surfaces and improve the

International Science and Technology Journal
المجلة الدولية للعلوم والتقنية

العدد 26
Volume 26

المجلة الدولية للعلوم والتقنية
International Science and Technology Journal
ISTJ

performance of concrete, in addition using it in medical fields [10, 11].

The objective of this study is to investigate the effect of magnetic field on properties of water by exposure the water samples to different magnetic field intensities at variable exposure times.

2. Literature Review

Many studies were carried out to probe the effect of the magnetic field on water. The reported effects of magnetic water treatment are varied. Some studies reported no significant magnetic treatment effect on the properties of water. While others have shown that magnetic treatment has no effect on the chemical properties of water, such that its composition remains unchanged after treatment, on the other hand, it influences the physical parameters [12]. In other cases, studies reported that the MF could change the physicochemical water properties [1]. The changes in the physical parameters such as viscosity, surface tension and evaporation enthalpy, cause molecular interactions and thus changes in the chemical properties of water [13].

Amiri and Dadkhah conducted a series of experiments to investigate that the magnetic water treatment reduces the surface tension, the test results showed a decrease in surface tension of water [6]. A similar result was obtained by Holysz et al. the MF could increase the electrical conductivity, and decrease the surface tension of water [14]. Alwediyani et al and Khudiar et al. also reported reducing in surface tension and density, while increased pH value, and electrical conductivity of magnetic water [15,16]. Alkhazan et al. studied the magnetized lake water, found increasing in the pH value and decreasing in its odor and electric conductivity, dissolving oxygen, and dissolving minerals by a higher rate than un-magnetized water, in addition to water clearness [17]. Esmaeilnezhad et al. said that the properties of magnetized water are useful in industries associated with its surface tension, pH, viscosity and electrical conductivity, they found decreasing in electrical conductivity and surface tension, while pH, and the shear viscosity increase in water upon the application of a MF [18]. Huan-Xiao Hu and Chao Deng tested the

electrical conductivity and evaporation of magnetized water at different temperatures. The results showed that the conductivity and evaporation of the magnetized water increase to different degrees compared with regular tap water [8]. Also, Wang tested the evaporation of magnetic water, reported the increase of evaporation amount, the decrease of specific heat and boiling point of tap water after magnetization, the changes depend on the magnetic intensity [10]. The researcher also reported in another study, the effect of a static MF on liquid water using frictional experiments, the result suggested the friction coefficient was smaller in the MF [19].

Gaafar M, Moosa measured the TDS at different MF strength (3000-5000G) at exposure time varied from (2-30) min, reported that at two minutes with higher MF its better in dissolving the salts that used in making kidney stone [20]. Studies reported that MF impacts on hydrogen bonds between water molecules and found some exchange which happened in the properties of water such as light absorption, surface tension, EC and pH [21].

On the contrary, other researchers reporting negative results such as; Hasson and Bramson studied the effectiveness of commercial MF device in suppressing calcium carbonate, found that the magnetic exposure had no effect on suppress the scale formation of $CaCO_3$ [22]. Also Limpert and Raber reported that the magnetic treatment device has no significantly to prevent scale formation in a heat exchanger system [23].

Based on these facts, this study aims to investigate the effect of MF on water properties, by subjected it to the MFs, and examined the following parameters:

-**Density**which is the ratio of the mass to the volume of a substance, i.e. it's a measurement of how tightly matter is packed together. The exact density of water is about 0.999 g/ml at 4°C, the rounded value of 1 g/ml. It can be calculated by using the following formula:

$$\rho = \frac{m}{V} \qquad\qquad (1)$$

Where : ρ is density, m is mass, and V is volume of a substance [24].

International Science and
Technology Journal
المجلة الدولية للعلوم والتقنية

العدد 26
Volume 26

المجلة الدولية للعلوم والتقنية
ISTJ

-**Electrical Conductivity (EC)** it is a measure of a material's ability to conduct an electric current, has SI unit of Siemens per meter (S/m) [24].

-**pH Balance** it is a measure of how acidic/basic water is, indicated to relative amount of free hydrogen and hydroxyl ions in the water [25].

-**Total Dissolved Salts (TDS)** is made up of inorganic salts and organic matter, that dissolved in water, such as calcium, magnesium, potassium, sodium, bicarbonates, chlorides, iron, lead, and sulfates [26].

-**Sodium Chloride** is an inorganic chloride salt, has chemical formula NaCl, which is most responsible for the salinity of water, by giving drinking water a salty taste at a concentration greater than 180 milligrams per liter [26].

3. Materials and Methods
3.1. Setup Experimental
The well water was divided into three samples, a control group as an untreated sample of 200 ml, a 200 ml sample exposed to a PMF, and a 120 ml sample, which was divided into six samples each sample of them has 20 ml, each of them were exposed to the EMF at different times. Each period of exposure for each sample was repeated five times. And each sample was taken immediately after each exposure time to MF, to examine the parameters like density, EC, pH, NaCl concentration, and TDS, which initially measured before magnetic treatment of all water sample. The experiments were performed at 28±5°C.

The pH value of water samples was measured by using pH meter model 80. Hanna instruments HI 2300 EC/TDS/NaCl meter was used to measure TDS, EC, and NaCl of each sample. In addition, Microsoft Office Excel 2016 was used to analyze all data obtained.

3.2. Generation method of MF
MF is generated, when an electric current passing through a wire of coil, this type of MF disappears when the electric current is turned off, which called electromagnetic field. The strength of the EMF is various, depends on the amount of electric current, and

number of coil turns [25, 27]. Ampere's law uses to calculate the MF inside the coil is as follows:

$$B = \mu_0 \frac{N \times I}{L}$$ (2)

Where: B is magnetic field, measured in Tesla = 10^4 Gauss

N is number of coil turns, I is electric current, measured in Amperes, L is length of the coil, measured in meter, and $\mu_0 = 4\pi \times 10^{-7}$ is vacuum permeability, measured in Newton per square ampere N/A^2.

Permanent magnet is made from ferromagnetic materials such as iron, nickel and cobalt, these ferromagnetic materials create an intense persistent magnetic field without the need for any electrical power.

In this work, firstly, the EMF was generated by 1.6 Amp of electrical current passing through a coil of 8.5cm length, inner diameter 1.7cm, outer diameter 2cm, number of turns 3900, where the coil connected to 2 V of DC power supply, the intensity of EMF that created was calculated by using equation 2. It was found equal to (900G = 0.09 T = 90mT). Although electromagnets can produce MFs of high intensity, however, in this study, we used low MF intensity. Then, each sample of the six samples which contain 20 ml of tested water is in the test tube was subjected to this MF for variable time (5, 10, 15, 20, 25, 30) min.

The second treatment of the well water sample was by PMF, which produced by two bar of magnets, dimension of each magnet was $10 \times 1.5 \times 0.5$ cm (length, width, height). 200 ml of tested water is in 250 ml Pyrex beaker, then the magnets were placed vertically on both sides of the beaker, where the top and bottom was without MF and the magnets remained for 7 days at room temperature.

4. Results
4.1. Effects of Magnetization on Density
To measure the density of the well water sample, 200ml of the sample was placed in a 250 ml Pyrex beaker, then the mass was measured before and after the magnetic treatment by using sensitive balance, then the density was calculated using equation 1. Figure 4a shows the decrease in the density of well water samples

when 900 G of EMF was applied at variable exposure time, the highest decrease was 0.715g/ml at 30 min of exposing time, while the untreated well water sample has a density of 0.972 g/ml. In case of PMF, the density of the magnetic water dropped to 0.799 g/ml, as shown in figure 4b, the decrease in the density is due to amount of dissolved salts, that cause an increase in the mass of water sample.

Figure 4a. Effect of 900 G of EMF on well water density at variation times.
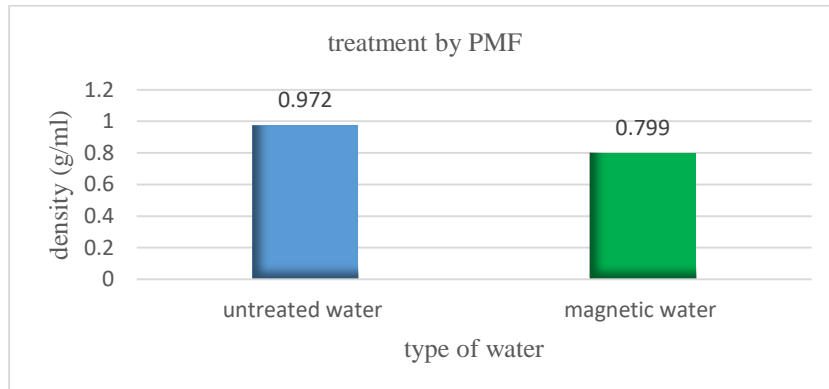
Figure 4b. Effect of PMF on well water density for 7 days of exposure time.

4.2. Effects of Magnetization on pH

Figure 5a reveals that variation of pH value of the well water samples under EMF of 900 G at different exposure times, slightly increased by 3%, 6%, 4.5%, 6%, 9%, 1.5% at exposure time (5, 10, 15, 20, 25, 30) min respectively. In case of PMF: The pH value of magnetic water increased significantly from 6.6 (untreated sample) up to 8.2, by 24% as shown in figure 5b. This increase in pH value leads to reduce the acidic and arise the base, due to increasing the hydroxyl ions and decreasing in the hydrogen ions concentration. The influential of PMF on pH value was greater than electromagnetic field.
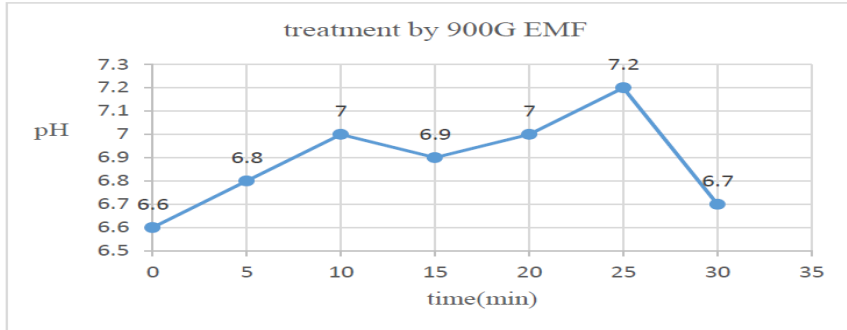
Figure 5a. Effect of 900 G of EMF on well water pH at variation times
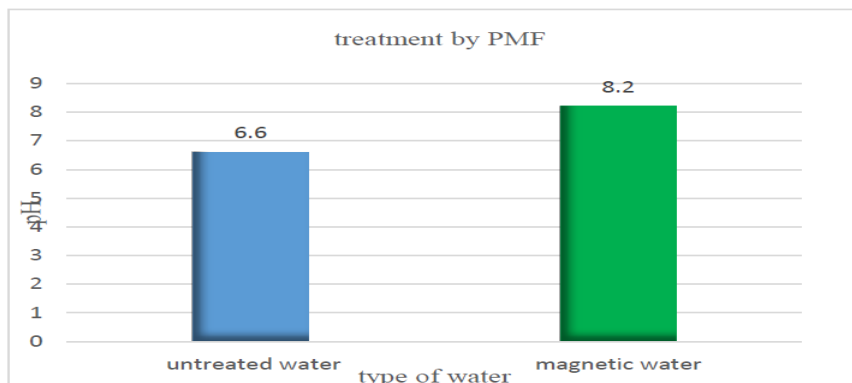
Figure 5b. Effect of PMF on well water pH for 7 days of exposure time

International Science and Technology Journal
المجلة الدولية للعلوم والتقنية

العدد 26
Volume 26

المجلة الدولية للعلوم والتقنية
ISTJ

4.3. Effects of Magnetization on TDS

It's clear that the MF impacts on TDS of experimented well water, but the effectiveness may depend on the intensity of the MF. A significant decrease on the TDS of the treated well water samples was observed by 900 G of EMF, while the TDS was increased significantly when PMF was applied.

For EMF; It is clear that difference of exposing time has a different influence on the TDS of magnetic water, the results as illustrated in figure 6a shows a significant decrease in the TDS for the treated well water, the decrease was more remarkable at 15 min which recorded 990 ppm = 0.99g/l, as compared with TDS for the untreated sample 1570ppm =1.57g/l where the decrease rate is about 36%. This decreasing in TDS proved that the low magnetic field could dissociate the constituent salts. Whereas, the TDS increased from 1570ppm=1.57g/l for untreated water sample to 1960ppm=1.96g/l for treated water sample by about 24.8%, when treatment was by PMF for 7 days, as illustrated in figure 6b.
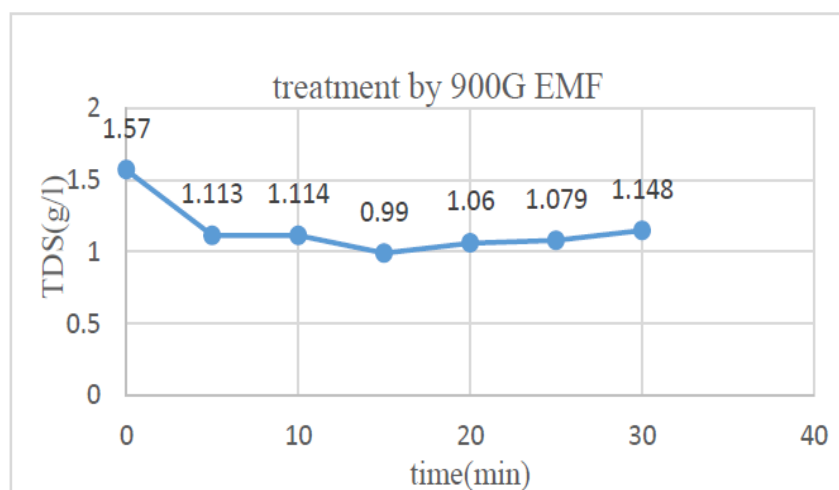
Figure 6a. Effect of 900 G of EMF on well water TDS at variation times
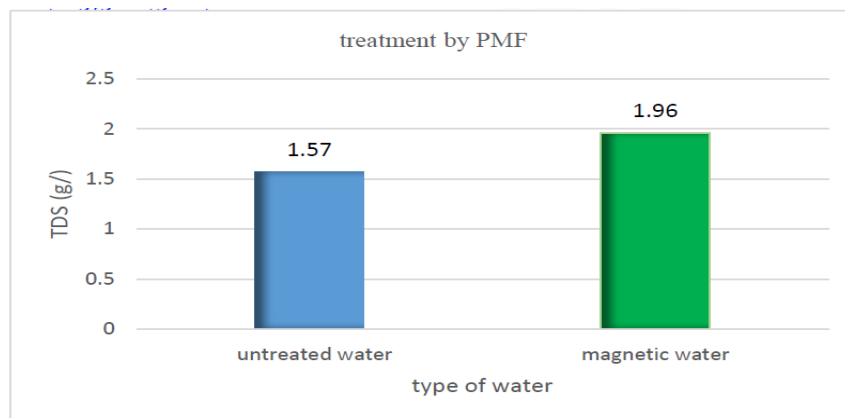
Fig.6b. Effect of PMF on well water TDS for 7 days of exposure time

4.4. Effects of Magnetization on EC

As mentioned previously; the well water sample was subjected to two types of MFs of different intensities. When an EMF was used to magnetized the well water samples, the obtained results in figure 7a, shows that there is a significant decrease in EC of all well water samples under different magnetization time. EC decreased from $2662\mu S = 2.662mS$ for untreated sample to 1.882, 1.845, 1.518, 1.613, 1.475, and 1.91 mS for treated samples at exposure time 5, 10, 15, 20, 25, and 30 min respectively. The reduction in EC agree with the reduction in TDS for all samples, when treated by EMF. This indicates that the low MF can reduce the EC and TDS which is a good for the removal of salinity from the water.

In case of PMF, The EC is higher than that of untreated sample, where EC was increased up to 3.27mS, as indicated in figure 7b. In this magnetic treatment the EC is also higher than that of EMF of 900 G. Whether the EC increases or decreases after the magnetic treatment. This change indicates that the electrical property of the water has changed due to the MF.

International Science and
Technology Journal
المجلة الدولية للعلوم والتقنية

العدد 26
Volume 26

المجلة الدولية للعلوم والتقنية
International Science and Technology Journal
ISTJ
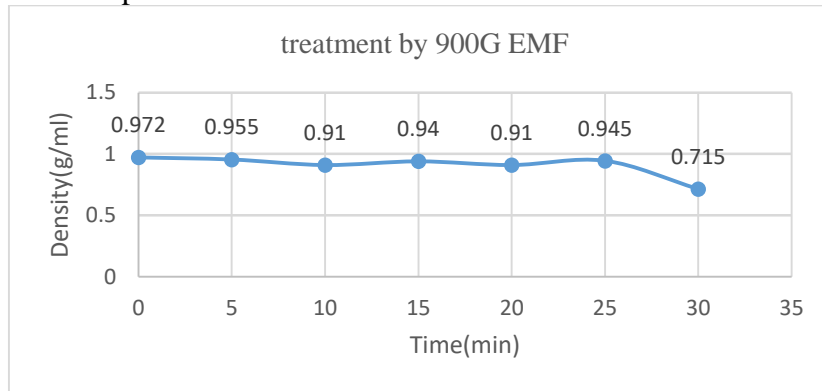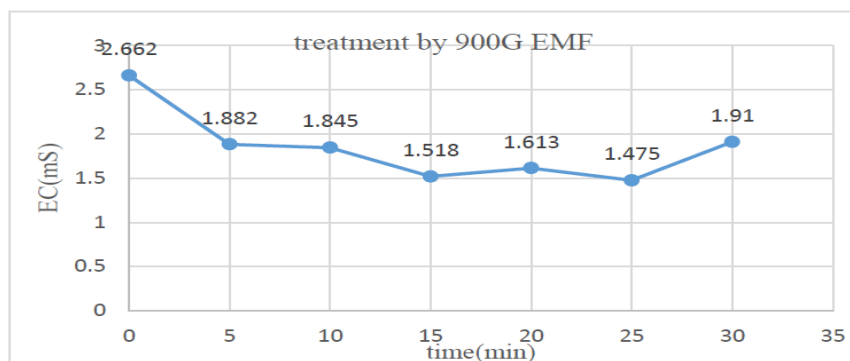

Figure 7a. Effect of 900 G of EMF on well water EC at variation times
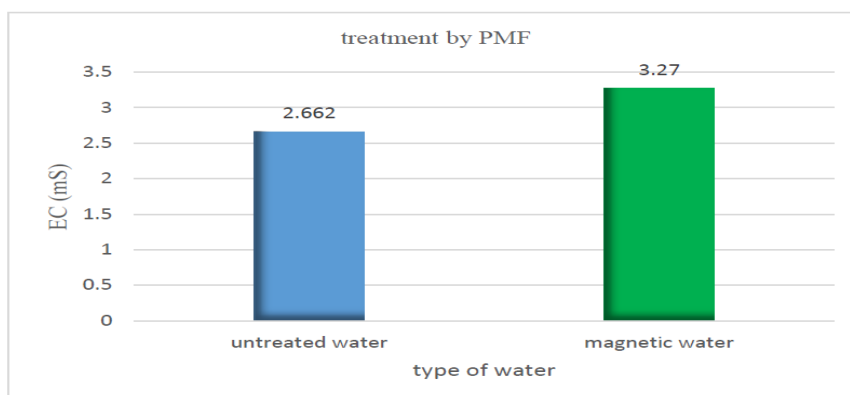
Figure 7b. Effect of PMF on well water EC for 7 days of exposure time

4.5. Effects of Magnetization on NaCl

It observed that in figure 8a the concentrations of NaCl are clearly decreased at different exposure times when EMF was applied, the NaCl concentrations were decreased from 5.2 (untreated sample) to 3.7, 3.5, 3, 3.6, 3.2, 3.7% at exposure time 5, 10, 15, 20, 25 ,30 min respectively. Otherwise, the result obtained by exposure water to the PMF was different, where NaCl concentration increased from 5.2 for the untreated sample to 6.3 for the magnetic water sample, as indicated in figure 8b.

حقوق الطبع محفوظة
للمجلة الدولية للعلوم والتقنية

International Science and
Technology Journal
المجلة الدولية للعلوم والتقنية

العدد 26
Volume 26

المجلة الدولية للعلوم والتقنية
International Science and Technology Journal
ISTJ
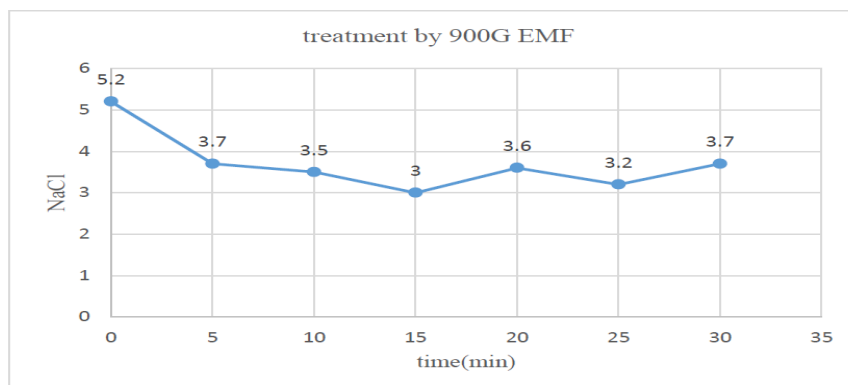
Figure 8a. Effect of 900 G of EMF on well water NaCl concentrations at variation times.
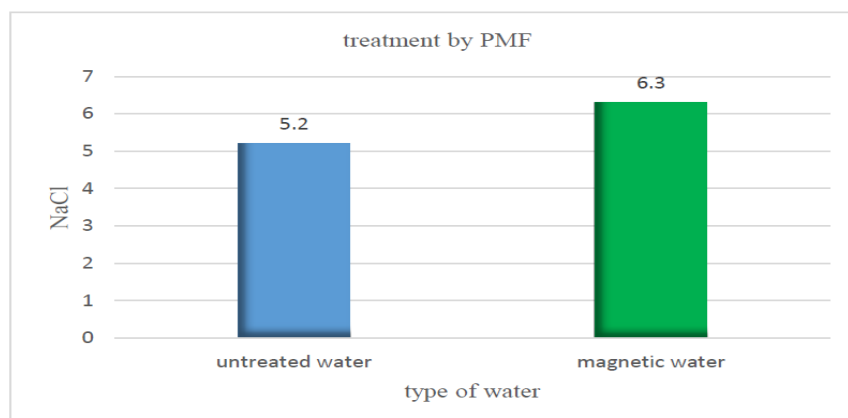
Figure 8b. Effect of PMF on well water NaCl concentrations for 7 days of exposure time.

5. Discussion and Conclusion

This study aimed to investigate whether the MF affects the properties of water. The study finding is consistent with many studies have proved that, properties of water are changed when subjected to MF. The results obtained when the samples of well water subjected to the EMF (900 G) suggested that EC, TDS, and NaCl concentration of magnetized water are decreased, compared

International Science and Technology Journal
المجلة الدولية للعلوم والتقنية

العدد 26
Volume 26

المجلة الدولية للعلوم والتقنية
International Science and Technology Journal
ISTJ

to untreated sample. This result is similar with data in [17, 24] who pointed out the decrease in EC, TDS, Na, Cl in static magnetic treatment. In contrast, when PME was applied, EC, TDS, and NaCl concentration are increased. The increasing in NaCl concentration is similar with the result which reported in [5].

The MF has a positive effect on pH values. When water samples were treated by both MFs (EMF, PMF), an increment in the pH values occurred, which is beneficial to reduce the acidic. This result is in conformity with the most previous studies. The density of all treated samples decreased after magnetically treatment, either the MF intensity is low or high. This result is in accordance with [15], they reported reducing in the density of magnetic water, wherever the magnetic treatment was done by a neodymium magnet for 7 days, and the water sample was static.

Whether decreased or increased tested parameters after the magnetization process. This suggests that the MF has impact on the water properties. From these results, it can be deducing that the role of magnetization on changing water properties is depending on the hydrogen bonds between water molecules, and impurity atoms and ion which contained in water. If the magnetization causes increases or decreases the hydrogen bonds between water molecules, so it reduces or increases the ability of electrolysis [3]. Also the variation in results may be due to a magnetic type, the experimental setup, such as exposure time, the condition of water, whether static or flowing through magnetic field where the experiments in this study were done statically. Thus that, a full understanding of magnetized water remains an open issue, which still needs to be discussed in further experiments.

References.

[1] Ahmed. S, Effect of Magnetic Water on Engineering Properties of Concrete. College of Engineering. Feb(2009) AREJ Vol.17 No.1.

[2] C. Quiun, T. Molden, C. Sanderson, Magnetic Treatment of Water Prevents Mineral Buildup (1997) www.Superiorawaterconditioner.com

[3] Mothafer Dawood, Magnetic Water, Electronic book. https://www.researchgate.net/publication/337481523_alma_al mmghnt_-_mzfr_ahmd_almwsly

[4] AL-Sinjary Z, AL-Talib A. Effect of magnetizing water on uniform of sprinkle irrigation, AREJ (2009) Vol17, Issue 1, pp 68-79

[5] Karkush. M, Ahmed. M, AL-Ani. S, Magnetic Field Influence on The Properties of Water Treated by Reverse Osmosis, Vol. 9, No. 4, (2019), 4433-4439 4433

[6] Amiri. M, Dadkhah. A, On reduction in the surface tension of water due to magnetic treatment. Colloids Surf A (2006), 278(1):252–5.

[7] Jianshu. L, Experimental study on the surface tension of magnetized water. International Communications in Heat and Mass Transfer Volume 121(68):105091.

[8] Huan-Xiao Hu, Chao Deng, Effect of Magnetized Water on the Stability and Consolidation Compressive Strength of Cement Grout Materials (2021), 14(2), 275.

[9] Emil. C, Aleksandra. S, Lucyna. H, Influence of Magnetic Field on Evaporation Rate and Surface Tension of Water. Colloids Interfaces (2018), 2(4), 68.

[10] Wang, et al. Effect of magnetic field on the physical properties of water. DOI:10.1016/j.rinp.2017.12.022

[11] McMahon, C, Investigation of the quality of water treated by magnetic field, B. Sc. Thesis Toowoomba University of

Southern Queensland Faculty of Engineering and Surveying, (2009).

[12] Hassan. K, Magnetic Treatment of Brackish Water for Sustainable Agriculture, M.Sc. Thesis, The American University in Cairo, (2015).

[13] Szatyłowicz. E, Skoczk. I, Magnetic Field Usage Supported Filtration Through Different Filter Materials. Water (2019), 11(8), 1584.

[14] Holysz. L, Szczes. A, Chibowski. E. Effects of a static magnetic field on water and electrolyte solutions. J Colloid Interface Sci (2007);316(2):996.

[15] Alwediyani. H, Almasoudi. A, et al. The Change in Physical Properties of Magnetic Water, B. Sc. Thesis.Umm Al Qura University Makkah- Kingdom of Saudi Arabia.

[16] Khudiar. K, Ali. A, Effect of magnetic water on some physiological aspects of adult male rabbits. In Proceeding of the Eleventh Veterinary Scientific Conference, (2012), Pp.120-126

[17] Alkhazan. K., Sadddiq. A, The effect of magnetic field on the physical, chemical and microbiological properties of the lake water in Saudi Arabia. Journal of Evolutionary Biology Research, (2010), 2(1), 7-14.

[18] Esmaeilnezhad. E, et al, Characteristics and applications of magnetized water as a green technology, Journal of Cleaner ProductionVol 161, 10 Sep 2017, Pag 908-921

[19] Wang. Y, Zhang. B, et al, The effect of a static magnetic field on the hydrogen bonding in water using frictional experiments. J Mol Struct (2013) ;1052(11):102–4.

[20] Gaafar. M, et al, Effect of Magnetic Water on Physical Properties of Different Kind of Water, and Studying Its Ability to Dissolving Kidney Stone, B.Sc. Journal of Natural Sciences Research, Vol.5, No.18, 2015.

International Science and
Technology Journal
المجلة الدولية للعلوم والتقنية

العدد 26
Volume 26

المجلة الدولية للعلوم والتقنية
International Science and Technology Journal
ISTJ

[21] Joshi. K, Kamat. P, Effect of Magnetic Field on the Physical Properties of Water, J. Ind. Chem. Soc. 43 (1966), Pages (620-622).

[22] Hasson. D, Bramson. D, Effectiveness of magnetic water treatment in suppressing calcium carbonate scale deposition (1985). Eng. Chem. Process Design and Development, 24; 588.

[23] Limpert. G, Raber. J, Tests of nonchemical scale control devices in a once-through system. Materials Performance, (1985), 24 (10); 40-45.

[24] F. Sears, Electricity and magnetism, 5th printing, (1974) Wesley Publishing Company. Hand book.

[25] [25]. Kennan. W, General Chemistry, 2ndEdition (1993), Translated by Saad Wasef Arab Development Institute.

[26] El‑Shamy. A, Abdo-Elshafe. A, The consequence of magnetic field on the parameters of brackish water in batch and continuous flow system. Dec (2021)Bulletin of the National Research Centre 45(1).

[27] J. Jackson, Classical Electrodynamics, 2nd Edition (1975), John Wily and sons, Inc.

[28] Hilal. M, Helal. M, Application of magnetic technologies in desert agriculture, II Effect of magnetic treatments of irrigation water on salt distribution in olive and citrus fields and induced changes of ionic balance in soil and plant, Egyptian J. soil. Sci. (2000) Vol. 40, No. 3 PP. 423- 435.

[29] Umidjon. M, Shoazimova. K, Influence of the Magnetic Field on the Viscosity Coefficient of Lubricoolant that is used in the Cutting Process. Dec 2020 DOI:10.17683/ijomam/issue8.50

Measurement of Activity concentrations levels of natural radionuclide in soil sample collected from Ajmail city, Libya

[1]Muna. M. Aoneas, [2]Eldakli Mohsan
[1]University of Zawia, Faculty of Science, Physics department, Al Ajaylat, Libya.
[2]University of Zawia, Faculty of Science, Physics department, Az Zawiyah, Libya.
E-mail address: m.aoneas@zu.edu.ly

الملخص

في هذه الدراسة تم قياس النشاط الاشعاعي للنويدات المشعة الطبيعية لعينات من التربة السطحية جمعت من خمسة وعشرون موقع فى مدينة الجميل – دولة ليبيا فى مارس سنة الفان وواحد وعشرون باستخدام كاشف الجرمانيوم عالي النقاوة ولقد وجد ان تركيز النويدات تتراوح للراديوم [226]Ra بين 5.01 و 23.35 بيكريل/كغم، والبوتاسيوم K[40] بين 61.42 و 251.42 بيكريل/كغم، والثوريوم [232]Th بين 0.90 و 12.63 بيكريل/كغم. وكل هذه القياسات تقع ضمن الحدود المسموح بها عالميا. وكذلك تم حساب معدل الجرعة الممتصة لأشعة جاما في الهواء و مكافيء الراديوم و مستوى الخطورة الخارجي و الداخلي.

Abstract

In this work, we measured the activity concentrations of naturally radioactive materials in soil samples collected from 25 locations from Ajmail city on March 2021, which were measured by gamma ray spectrometry system using a High Purity Germanium (HPGe) detector.

The activity concentrations of natural radionuclides were varying from 5.01 to 23.35 Bq.kg^{-1} for ^{226}Ra, for ^{40}K vary from 61.42 to 251.42 Bq.kg^{-1}, and for ^{232}Th vary from 0.90 to 12.63 Bq.kg^{-1} The average of the concentration levels for all inspected nuclides are

generally found to be lower than the assigned international radioactivity concentration levels [1].

Absorbed dose rates in air, and the Radium Equivalent Activity were calculated. The external and internal hazard index for the soil samples are also investigated.

Keywords: Natural radiation, activity concentrations, High Purity Germanium (HPGe) detector.

Introduction

Radionuclides are unsteady isotopes which go through radioactive decay for example they discharge beta particles, alpha particles and gamma rays. some radionuclides occur normally in air, soils and plants, rocks and some are created artificially as in atomic weapon testing, industrial supply, medicine, and nuclear technology [2][3].

The main external source of irradiation of the human body is Gamma radiations emitted from naturally occurring radioactive materials such as ^{232}Th, ^{238}U, and ^{40}K, which known as terrestrial background radiation [4]. The measurements of natural radioactivity in soil samples are required to determine any changes of natural background activity with time as the result of any nuclear activity. Many surveys have been done in the last decade to measure the activity concentrations of natural radionuclides in soil [5][6][7].

In this work the soil samples were collected from 25 locations in Ajmail city. The Activity concentrations of natural radionuclides were measured by using HPGe detector, dose rates in air, Radium Equivalent Activity, the external and internal hazard index were calculated.

Materials and methods
Sample Collection and Preparation.

The samples were collected from the soil surface (3-5 cm depth), where the coordinates of each sampling location were recorded. Table 1 shows the locations from which the soil samples were collected.

The samples were left to dry, and each of the samples was weighed using an electronic balance. These samples are kept in Marinelli Beakers and stored for one month to reach the secular radioactive equilibrium condition.

Table 1: GPS location of the sampling points.

Sample no.	Sample ID	Latitude	Longitude
1	A	32.856356N	12.116775E
2	B	32.862976N	12.103541E
3	C	32.862793N	12.092794E
4	D	32.870012N	12.070891E
5	E	32.856874N	12.067230E
6	F	32.863019N	12.047417E
7	G	32.861137N	12.024088E
8	H	32.846151N	12.008133E
9	I	32.819937N	11.991301E
10	J	32.801235N	11.975806E
11	K	32.774178N	11.972161E
12	L	32.740948N	11.946293E
13	M	32.739932N	12.000721E
14	N	32.763058N	12.015026E
15	O	32.774702N	12.065032E
16	P	32.792004N	12.130587E
17	Q	32.799482N	12.155671E
18	R	32.815088N	12.110201E
19	S	32.806584N	12.092596E
20	T	32.824735N	12.075307E
21	U	32.817888N	12.050455E
22	V	32.833852N	12.039830E
23	W	32.820830N	12.029158E
24	X	32.839159N	12.015838E
25	Y	32.849068N	12.045101E

Energy and Efficiency Calibrations of the Detector

High Pure Germanium Detector (HPGe) with relative Efficiency 90% and an energy resolution of 1.92 Kev for the 1332.5 Kev of ^{60}Co gamma lines Fig 1. HPGe detector is provides sufficient information to radionuclides from their gamma ray emissions.

The energy and efficiency calibrations were determined before the activity concentrations of ^{232}Th, ^{40}K, and ^{226}Ra radionuclides in the samples were determine.

The energy calibration of the detector was carried out by using the following gamma lines obtained from some gamma standard sources as ^{137}Cs (661.62KeV), and ^{60}Co (1173.23 and 1332.51 Kev). The detector efficiency calibration curve as a function of energy for solid matrix is shown in Fig.2.

Figure 1: gamma ray spectrometer system with High Purity Germanium (HPGe) detector.
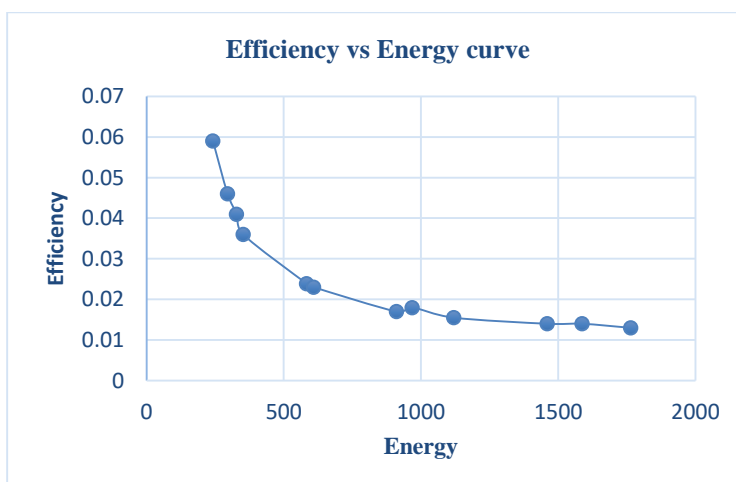
Figure 2: The efficiency calibration curve for HPGe detector as a function of energy.

International Science and
Technology Journal
المجلة الدولية للعلوم والتقنية

العدد 26
Volume 26

المجلة الدولية للعلوم والتقنية
International Science and Technology Journal
ISTJ

Activity concentrations

The Activity concentrations of ^{40}K, ^{226}Ra, and ^{232}Th in soil samples were determined directly by using a HPGe detector.

The ^{226}Ra activity concentrations of natural radionuclides were determined by using the 295.2 and 351.9 Kev photopeaks of ^{214}Pb, the 609.3, 1120.3 Kev photopeak of ^{214}Bi. The ^{232}Th activity concentration was determined using the 583.14 Kev photopeak of ^{208}Tl, the 911.07, and 968.9 Kev photopeaks of ^{228}Ac, and 238.6Kev photopeaks of ^{212}Pb. And the activity concentration of ^{40}K was determined directly from the 1460 Kev gamma line.

The activity concentration of a certain radionuclide of each sample were calculated using the following formula [8].

$$A = \frac{net\ CPS}{Eff.M.I_\gamma} \qquad (1)$$

Where A is the net gamma counting rate (counts per second) for a peak at energy E, $net\ CPS$ is the (net gamma counts per second = cps for sample – cps for background), Eff is the efficiency of the detector at energy E (Kev), I_γ is Absolute intensity of the gamma ray, and M is the mass of the soil sample under consideration measured in kilograms.

Calculation of absorbed dose rate

The contribution of the natural radionuclides to the absorbed dose rate in air D_r depends on the concentration of the radionuclides in the soil. The dose can be calculated at 1 meter above the ground level from the measured activity concentrations of ^{226}Ra, ^{232}Th, and ^{40}K radionuclides using the following formula [9][10]:

$$D_r(nGyh^{-1}) = 0.462\ A_{Ra} + 0.604 A_{Th} + 0.0417 A_K \qquad (2)$$

where D_r is the dose rate, 0.462, 0.604 and 0.0417, are the dose conversion factors, A_{Ra}, A_{Th}, and A_K are the activity concentrations of ^{226}Ra, ^{232}Th, and ^{40}K in Bq. kg^{-1}, respectively.

Calculation of Radium Equivalent Activity

The radium equivalent activity is defined as a common radiological index that represents the activity concentrations and existing of natural radionuclide of ^{226}Ra, ^{232}Th, and ^{40}K in the terrestrial. The radium equivalent activity Ra_{eq} calculated according to the following formula [11]:

$$Ra_{eq} (Bq.Kg^{-1}) = A_{Ra} + 1.43A_{Th} + 0.077A_{K} \qquad (3)$$

Calculation of External and Internal Hazard Index

The external and internal hazard index due to the emitted gamma rays for each sample was calculated according to the following formula [12][13]:

$$H_{ex} = \frac{A_{Ra}}{370} + \frac{A_{Th}}{259} + \frac{A_{K}}{4810} \leq 1 \qquad (4)$$

$$H_{ein} = \frac{A_{Ra}}{185} + \frac{A_{Th}}{259} + \frac{A_{K}}{4810} \leq 1 \qquad (5)$$

Where H_{ex}, H_{in} are the external and internal hazard index, respectively. The value of H_{ex}, and H_{in} must be lower than or equal to unity in order to keep the radiation hazard insignificant.

Results and discussion

The specific activity of natural radionuclides of ^{232}Th, ^{226}Ra, and ^{40}K for a total of 25 soil samples were presented in Table 2, and figures 3, 4, and 5.

The maximum value of the activity concentration of ^{40}K radionuclide was 263.31 Bq.kg^{-1}, and the minimum concentration value was 61.42 Bq.kg^{-1}, with an average 143.44 Bq.kg^{-1}. The maximum value of the activity concentration of ^{226}Ra radionuclide was 23.35 Bq.kg^{-1}, and the minimum concentration value was 5.01 Bq.kg^{-1}, with an average 9.84 Bq.kg^{-1}.

The maximum value of the activity concentration of ^{232}Th radionuclide was Bq.kg^{-1}, and the minimum concentration value was Bq.kg^{-1}, with an average 4.25 Bq.kg^{-1}.

International Science and
Technology Journal
المجلة الدولية للعلوم والتقنية

العدد 26
Volume 26

المجلة الدولية للعلوم والتقنية
International Science and Technology Journal
ISTJ

Clearly, the results in all samples show that the activity concentration of ^{226}Ra is higher than the activity concentration of ^{232}Th. The average activity levels of ^{226}Ra are about 2.3 times higher than that of ^{232}Th in the soil sample.

Table 2 The specific activity of natural radionuclides of ^{232}Th, ^{226}Ra, and ^{40}K for a total of 25 soil samples.

Sample no.	Soil simple	Activity		
		^{40}K (Bq.kg^{-1})	^{232}Th (Bq.kg^{-1})	^{226}Ra (Bq.kg^{-1})
1	A	145.08±2.57	1.47±0.01	7.36±1.10
2	B	61.42±1.09	8.42±0.28	10.60±0.13
3	C	75.17±1.33	5.63±0.09	7.02±0.10
4	D	75.69±1.34	4.80±0.08	7.70±0.12
5	E	172.66±3.06	6.42±0.10	15.03±0.03
6	F	123.00±2.178	0.90±0.01	7.64±0.17
7	G	173.65±3.07	6.43±0.10	8.74±0.13
8	H	136.29±2.41	4.44±0.04	14.40±0.19
9	I	96.61±1.71	5.07±0.05	6.94±0.06
10	J	169.03±2.99	1.50±0.01	7.79±0.10
11	K	263.31±4.66	12.63±0.18	10.48±0.13
12	L	190.23±3.37	5.53±0.12	6.72±0.07
13	M	251.42±4.45	1.42±0.01	7.73±1.72
14	N	150.83±2.67	9.27±0.14	5.01±0.06
15	O	133.30±2.36	B.D.L	7.98±0.09
16	P	152.04±2.69	B.D.L	6.45±0.06
17	Q	109.92±1.95	9.84±0.15	23.35±0.29
18	R	100.77±1.78	1.23±0.01	13.25±0.15
19	S	165.76±2.93	B.D.L	5.47±0.19
20	T	123.38±2.18	0.90±0.00	7.67±0.18
21	U	152.14±2.69	8.35±0.13	8.07±0.13
22	V	175.26±3.10	3.25±0.03	7.54±0.09
23	W	156.56±2.77	1.56±0.01	8.56±0.08
24	X	139.80±2.47	7.17±0.11	14.35±0.16
25	Y	92.80±1.64	B.D.L	20.11±0.24
Average+ S.D		143.44±2.49	4.25±0.07	9.84±0.23

It was also show that the calculation of activity concentrations of ^{40}K were exceeded the calculation of the activity concentrations for ^{232}Th, and ^{226}Ra. This is an indication that the measurement of

the activity concentration of ^{40}K radionuclide is a more abundant than the measurement of the activity concentration of other elements in the soils samples.

A good thing that there are no any activity concentrations of ^{137}Cs found in all samples, and the average of the concentration levels for all inspected nuclides are generally found to be lower than the assigned international radioactivity concentration levels [1].
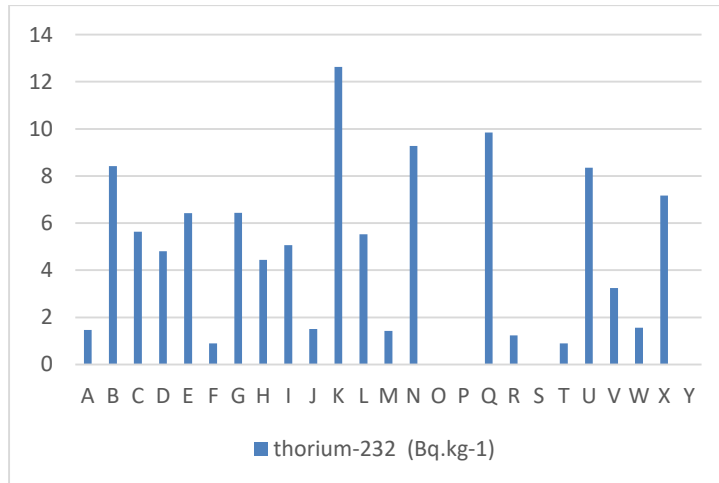
Figure 4: The specific activity of radionuclides ^{232}Th for the soil samples.

Also the results of the absorbed dose rate, the radium equivalent activity, the external and internal hazard index were presented in Table 3, and Figures 6,7.

The absorbed dose rates were varying from 9.25 to 23.45 nGyh^{-1} with an average 13.09 nGyh^{-1}, these values lower than the average value mentioned in UNSCEAR report [1]. The radium equivalents were varying from 2.86 to 48.82 $Bq.Kg^{-1}$ with an average 26.24 $Bq.Kg^{-1}$, these values are lower than the assigned international allowed limit of 370 $Bq.Kg^{-1}$. the external hazard indices were varying from 0.049 to 0.132 with an average 0.067, These values are much less than unity. The internal hazard indices were varying from 0.010 to 0.708 with an average 0.148, These values are much less than unity.

International Science and
Technology Journal
المجلة الدولية للعلوم والتقنية

العدد 26
Volume 26

ISTJ
المجلة الدولية للعلوم والتقنية
International Science and Technology Journal
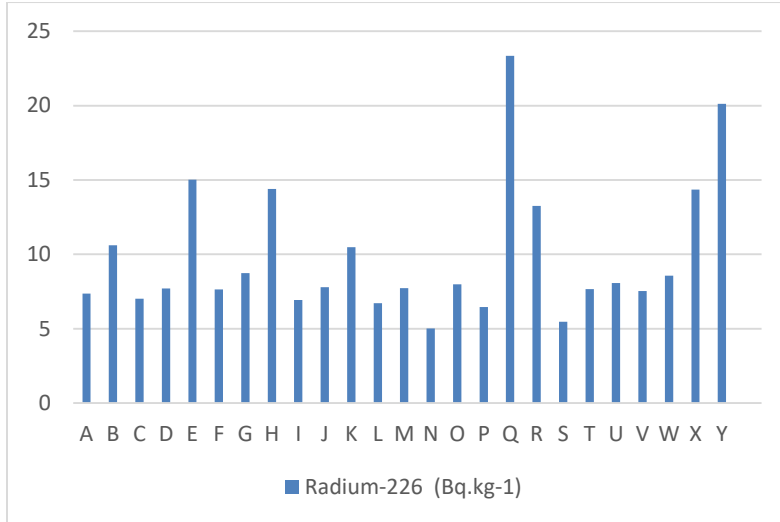
Figure 5: The specific activity of radionuclides ^{226}Ra for the soil samples.
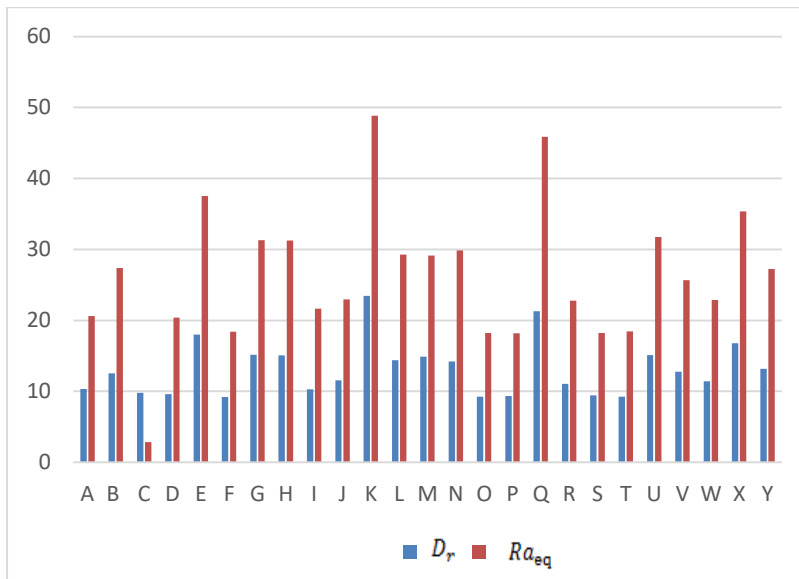
Figure 6: The dose rate D_r(nGyh^{-1}), and the radium equivalent activity Ra_{eq} $(Bq.Kg^{-1})$ for the soil samples.

International Science and
Technology Journal
المجلة الدولية للعلوم والتقنية

العدد 26
Volume 26

ISTJ

Table 3: The absorbed dose rate, the radium equivalent activity, and the external and internal hazard index for the soil samples.

Sample no	Code sample	D_r(nGyh^{-1})	$Ra_{eq}\ (Bq.Kg^{-1})$	H_{ex}	H_{ein}
1	A	10.34	20.63	0.055	0.076
2	B	12.54	27.37	0.074	0.010
3	C	9.78	2.86	0.056	0.075
4	D	9.61	20.39	0.055	0.076
5	E	18.02	37.51	0.101	0.142
6	F	9.20	18.40	0.050	0.070
7	G	15.16	31.31	0.085	0.108
8	H	15.08	31.24	0.084	0.123
9	I	10.30	21.63	0.058	0.077
10	J	11.55	22.95	0.062	0.083
11	K	23.45	48.82	0.132	0.160
12	L	14.38	29.28	0.079	0.097
13	M	14.91	29.12	0.079	0.100
14	N	14.20	29.88	0.081	0.094
15	O	9.25	18.24	0.049	0.708
16	P	9.32	18.16	0.049	0.066
17	Q	21.31	45.86	0.124	0.87
18	R	11.067	22.77	0.062	0.097
19	S	9.44	18.23	0.049	0.064
20	T	9.23	18.46	0.050	0.071
21	U	15.12	31.73	0.086	0.107
22	V	12.75	25.68	0.069	0.090
23	W	11.43	22.85	0.062	0.085
24	X	16.79	35.37	0.096	0.134
25	Y	13.16	27.26	0.074	0.128
Average		13.09	26.24	0.067	0.148

Conclusion

In this study, the activity concentrations for soil samples which collected from 25 locations in different areas chosen randomly around Ajmail city were calculated by using HPGe detector. The average activity concentrations for ^{40}K was 143.44 Bq.kg^{-1}, for ^{232}Th was 4.25 Bq.kg^{-1}, for ^{226}Ra was 9.84 Bq.kg^{-1}.

The activity concentrations of ^{40}K were exceeded markedly the activity concentrations of ^{232}Th, and ^{226}Ra. It was also show that

International Science and
Technology Journal
المجلة الدولية للعلوم والتقنية

العدد 26
Volume 26

المجلة الدولية للعلوم والتقنية
International Science and Technology Journal
ISTJ

the measured activity concentrations of ^{40}K exceeded markedly the values for both radium and thorium.
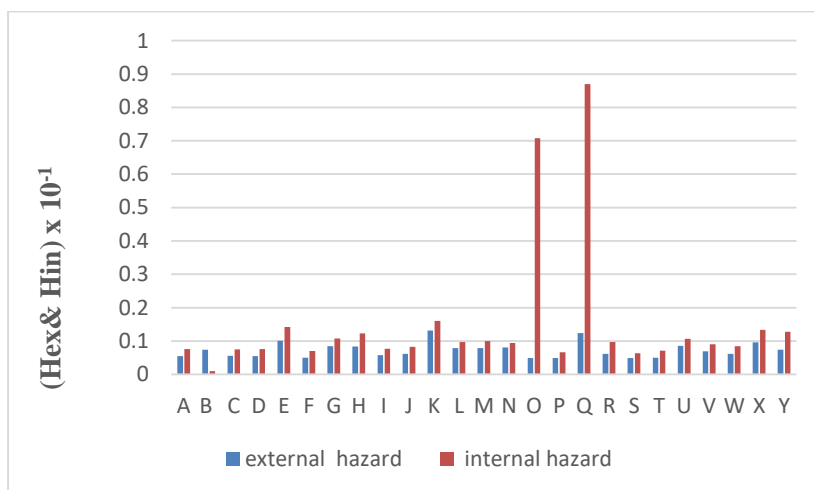
Figure 7: The external and internal hazard index for the soil samples.

A good thing that there are no any activity concentrations of ^{137}Cs found in all samples, and the average of the activity concentration for all nuclides are generally found to be lower than the assigned international radioactivity concentration levels [1].
the absorbed dose rate, the radium equivalent activity, the external and internal hazard index were also lower than the average value mentioned in UNSCEAR report [1].
This study can be considered a useful resource for future studies on natural radioactivity.

References
[1] UNSCEAR, Sources and Effects of Ionizing Radiation, United Nations Scientific Committee on the Effects of Atomic Radiation. United Nations, New York, USA, (2000). Annex

[2] EHSAN, M…, RAHMAN, M. F., TABASSUM, N., PRODHAN, M. M., PERVIN, S., MAHFUZ SIRAZ, M. M., MAHAL, S. F. (2019). THE ACTIVITY CONCENTATION

International Science and Technology Journal
المجلة الدولية للعلوم والتقنية

العدد 26
Volume 26

المجلة الدولية للعلوم والتقنية
International Science and Technology Journal
ISTJ

OF RADIONUCLIDES (226Ra,. *J. Bangladesh Acad. Sci*-169-180.

[3] Khan A.J, Prasad R . and Tyagl R.K, " Nuclear Tracks and Radiation Measurements", Vol. 20, No. 4, pp: 609-612, (1992).

[4] UNSCEAR. Report to the General Assembly. New York, NY, USA: UNSCEAR, 2000.

[5] Alazemi, N., Bajoga, A., Bradley, D., Regan, P., Shams, H., 2016. Soil radioactivity levels, radiological maps and risk assessment for the state of Kuwait. Chemosphere 154, 55e62.

[6] Darko, G., Faanu, A., Akoto, O., Acheampong, A., Goode, E.J., Gyamfi, O., 2015. Distribution of natural and artificial radioactivity in soils, water and tuber crops. Environ. Monit. Assess. 187 (6), 339.

[7] Milenkovic, B., Stajic, J., Gulan, L., Zeremski, T., Nikezic, D., 2015. Radioactivity levels and heavy metals in the urban soil of Central Serbia. Environ. Sci. Pollut. Res. 22 (21), 16732e16741.

[8] S. Harb, A. H. El-Kamel, A. I. Abd El-Mageed, A. Abbady, and Wafaa Rashed"CONCENTRATION OF U-238, U-235, RA-226, TH-232 AND K40 FOR SOME GRANITE SAMPLES IN EASTERN DESERT OF EGYPT", Proceedings of the 3rd.

[9] United Nations Scientific Committee on the Effects of Atomic Radiation (UNSCEAR), 2008. Sources and effects of ionizing radiation. Report to the General Assembly. New York, United Nation.

[10] Varshney R,Mahur AK, Sonkawade RG, Suhail M, Azam A, and Prasad R, 2010, "Evaluation and analysis of ^{226}Ra, ^{232}Th, ^{40}K and radon exhalation rate in various grey cements". Indian J Pure Appl Sci Physics , 48, 473–477.

 حقوق الطبع محفوظة
للمجلة الدولية للعلوم والتقنية

[11] José A. dos Santos J., Jorge J. R.Ferreira C., Cleomacio M.da Silva, S. Vita S. and Romilton dos Santos A., 2005, "Analysis of the ^{40}K Levels in Soil using Gamma Spectrometry", Brazilian Archives Of Biology And Technology, 48, Special : 221-228.

[12] Xinwei L, 2005, "Natural radioactivity in some building materials of Xi'an, China". Radiat Meas,40(1),94–97.

[13] Beretka, J.; Mathew, P. J., 1985, "Natural Radioactivity of Australian Building Materials, Industrial Wastes and By-products". Health Physics, 48(1):87-95.

MECHANICAL PERFORMANCE OF QUARRY DUST FINE POWDER (QDFP) BRICKS

ABUBAKER FATHI M. YAHYA
Almergib University - Faculty of Engineering- Department of Civil Engineering
Al khoms – Libya
Afy00218@gmail.com

الملخص

يتزايد إنتاج الإسمنت على نطاق واسع وذلك لأن الإسمنت يدخل في معظم مشاريع البناء. يخلق إنتاج الإسمنت أيضًا مشكلة بيئية فيما يتعلق بانبعاثات ثاني أكسيد الكربون وتلوث الغبار والضوضاء أثناء عملية التفجير للحصول على مواد خام جديدة. حاليًا في هذه الدراسة تم استخدام مسحوق غبار المحاجر الناعم (QDFP) كبديل جزئي للإسمنت في الطوب. لذلك ركزت هذه الدراسة على الأداء الميكانيكي من حيث مقاومة الانضغاط للطوب المصنوع من طوب OPC و QDFP بنسبة 0.5 (ماء \ إسمنت). تم اعتماد الخليط المحتوي على نسب رمل إسمنتية 1: 3.

أكدت النتائج أن نسبة مقاومة الانضغاط للطوب QDFP بنسب خلط مختلفة انخفضت مع زيادة نسبة استبدال الاسمنت بـ QDFP. بالإضافة إلى ذلك ، وجد أن الاستبدال الأمثل لـ QDFP هو استبدال 40٪ من الإسمنت المصنوع من خليط بنسبة 1: 3.0 من نسبة رمل الإسمنت ، والتي كانت مقاومة الانضغاط فيها 28.37 نيوتن / مم 2 و 37.65 نيوتن / مم 2 في 28 و 60 يوم من العمر على التوالي.

ABSTRACT

Cement production is widely increasing as it involved in most of the construction projects. Cement production also create problem to the environmental regarding to CO_2 emissions, dust pollution, and noise during blasting process for getting new the raw materials. Currently, many studies have been conducted on the application of quarry dust as a partial replacement of sand. Nevertheless, the utilization of quarry dust in the practice of quarry dust fine powder (QDFP) as a partial replacement of cement in brick still limited. Therefore, this study concentrated on the

International Science and
Technology Journal
المجلة الدولية للعلوم والتقنية

العدد 26
Volume 26

المجلة الدولية للعلوم والتقنية
International Science and Technology Journal
ISTJ

mechanical performance in terms of compressive strength of bricks made of OPC and QDFP bricks with 0.5 water cement ratio (w/c). The mix designed for (60) samples of bricks and tested after 28 and 60 days of air-dried curing. There were six (6) batches of which vary in QDFP replacement of cement content. The replacement percentage ranges between values of 0%, 15%, 20%, 25%, 30%, and 40%. Each percentage has ten (10) samples. The size of bricks cube is 215mm x 100mm x 65mm. The mixture containing cement-sand ratios of 1:3 was adopted. The results confirmed that, the percentage of compressive strength for QDFP bricks decreased with increasing the replacement percentage of cement with QDFP. In addition it was found that, the optimum replacement of QDFP is at 40% replacement of cement made of mix proportion of 1:3.0 of cement sand ratio, which the compressive strength was 28.37 N/mm^2 and 37.65 N/mm^2 in 28 and 60 days of age respectively.

Keywords: Cement production, the environmental, CO_2 emissions, quarry dust fine powder (QDFP), compressive strength.

1-INTRODUCTION

Bricks are one of the oldest types of building materials. It is an ideal building material because it is relatively cheap to make.

The production of cement reported to contribute to a bad impact on the environment since it contributes to the emission of carbon dioxide (CO_2) accounting for proximately 7% to 8% of CO_2 globally (Kartini, 2010). It was reported that produce 1 ton of clinker, it releases 1 ton of CO_2, which means about 0.95 to 0.97 ton of CO_2 per ton of Portland cement produced (Glasser, 1998). The extractions of raw materials such as limestone and clay from the natural resources also contribute to the changing of the natural landscape. Due to highly demand of raw materials in the production of cement, it has created a serious damage to the environment. To reduce the impact of cement production to the environment, the Supplementary Cementitious Materials (SCMs) was introduced (Scheffer, 2009).

Supplementary Cementitious Materials (SCMs) are these materials that can replaced the cement in making concrete with

good mechanical properties and good durability. Nowadays, many materials have been used as SCMs and most of these materials are considered as waste materials. As a matter of fact, when some of these SCMs are used in making concrete, it can produce concrete with better strength and durability properties such as concrete made with fly ash (Meyer, 2009). SCMs can be produced from natural resources or by artificial production. Most of the SCMs were selected from the industrial waste production (NRMCA, 2000).

Furthermore, waste materials are a very sensitive issue these days and their impact on the environment is pushing researchers to conduct studies on these waste materials and try to utilize them in way that help reducing their impact on the environment. This research was carried out with attention to identify the alternative materials in reducing the utilization of natural resources in the production process of cement.

In this study, the quarry dust fine powder (QDFP) was used for bricks mixture as a partial replacement of cement. QDFP source is from quarry dust (QD) taken from Negri Roadstone Quarry Nilai, Negri Sembilan.Malaysia It is expected that, the use of QDFP can reduce the demand for cement as well as the environmental problems. QD is obtained after grinding process to become fine particles and then sieve passing 90 µm sieve size. In addition, this research also investigated the effect of QDFP on compressive strength by conducting compressive strength test.

2 METHODOLOGY

The main objective of the laboratory work of this study was to investigate and compare the mechanical performance of the QDFP bricks in term of compressive strength for various replacements of cement content with QDFP with cement-sand ratios 1:3 and 0.5 w/c.

The mixture which contains cement, sand, and QDFP were studied. The cement type that was used is OPC, type of sand is river sand of sieve passing 5mm sieve size, and QDFP with size of sieve passing 90µm were used.

2.1 Preparation of bricks samples

This study involves laboratory investigation on six (6) batches of QDFP bricks. There were (60) samples of bricks prepared for this study. Samples were tested after 28 and 60 days of air drying. Basically, there were six (6) batches of which vary in QDFP replacement percentage of cement content. The replacement percentage ranges between values of 0%, 15%, 20%, 25%, 30%, and 40%. Each percentage has ten (10) samples divided to two groups each one five (5) samples for 28 and 60 days. The samples were subjected to air curing. For mix proportion 1:3, with replacement of 0%, 15%, 20%, 25%, 30%, and 40%, they are denoted as MB1, MB2, MB3, MB4, MB5 and MB6 respectively.

The size of brick is 215 mm length, 100 mm wide, and 65 mm height.

Table 1. the preparation of bricks samples needed in this study.

Mixture Designation	Replacement of Cement Content with QDFP	Cement-Sand Ratio	Compressive Strength Test	
			28 days	60 days
			No. of Samples	
MB1	0 %		5	5
MB2	15%		5	5
MB3	20%	1:3.0	5	5
MB4	25%		5	5
MB5	30%		5	5
MB6	40%		5	5

Total number of samples = 60

2.2 Materials Selection

In this research, the materials were collected and stored in a good condition in the Concrete Laboratory of Civil Engineering Faculty, UiTM, Shah Alam. The main materials in this investigation were:

2.3.1Cement (OPC) , Ordinary Portland Cement was the cement used in this study with type of 'Buaya' brand and fulfilling the

standards of BS EN 196-6. the chemical composition of OPC is shown in Table 2.

Table 2.Chemical composition of OPC used in this study

1. Chemical Composition	2. Percentage (%)
3. SiO_2	4. 15.05
5. Al_2O_3	6. 2.56
7. Fe_2O_3	8. 4.00
9. TiO_2	10. 0.12
11. MgO	12. 1.27
13. CaO	14. 72.17
15. Na_2O	16. 0.08
17. K_2O	18. 0.41
19. P_2O_5	20. 0.06
21. MnO	22. 0.06
23. SO_3	24. 2.90
25. Loss of Ignition	26. 1.33

2.3.2QDFP

QDFP was product obtained from grinding process of the QD which has fraction passing 63μm with size of sieve passing 90μm. In this investigation, the QDFP was the SCMs which have been used to supplement the cement. Quarry dust was collected from Negeri Roadstone Quarry Nilai. Malaysia

2.3.2.1Preparation of QDFP

The preparation of QDFP was carried out through three stages named as collecting, grinding and sieving. Collection stage was from Negeri Roadstone Quarry Nilai and in Figure 1. shows the QD collected before grinding. Grinding stage was done by using the Los Angeles (LA) Abrasion Machine as shown in Figure 2. the machine was set for 5000 revolutions with 33.3 rpm for each 5 kg of quarry dust with 16 nos. of ball bearings for about two and half (2 ½) hour. The crushed quarry dust specimens shown in Figure 3 were then sieved by using 90micron sieve size. The QDFP was stored in a good condition at the concrete laboratory until the time has been used.

Figure 1: QD before grinding by LA Abrasion Machine

Figure 2: LA Abrasion Machine

Figure 3: QD after grinding by LA Abrasion Machine

International Science and Technology Journal
المجلة الدولية للعلوم والتقنية

العدد 26
Volume 26

المجلة الدولية للعلوم والتقنية
ISTJ
International Science and Technology Journal

2.3.3 Sand

River sand is the type of sand that was used in this investigation with sieving passes 5mm sieve size.

2.3.4Water

Tap water was used in this investigation as it contains no substance and free from impurities which could affect the cement mix and can have an appreciably harmful effect upon strength of cement.

2.3.4.1Water to Cement Ratio

In this investigation water-cement ratio of 0.5 was used.

2.4Mix Proportion

Six different mixes was prepared in this study. Each mix had different amount of QDFP as a cement replacement. The six mixes are showed in Table 3 and detail of materials mix proportion for each mix type is shown in Table 4.

Table 3: The different types of mix proportions

Mixture Designation	Cement-Sand Ratio	OPC (%)	QDFP (%)
MB1		100	0
MB2		85	15
MB3	1:3	80	20
MB4		75	25
MB5		70	30
MB6		60	40

Table 4: Materials mix proportions for each mix

International Science and Technology Journal
المجلة الدولية للعلوم والتقنية

العدد 26
Volume 26

المجلة الدولية للعلوم والتقنية
ISTJ

Mixture Designation	Cement-Sand Ratio	MOULD VOLUME (M3)	CEMENT (KG)	SAND (KG)	WATER (KG)	QDFP (KG)
MB1			0.72	2.15	0.36	0.00
MB2			0.61	2.15	0.36	0.11
MB3			0.57	2.15	0.36	0.14
MB4	1:3	0.0014	0.54	2.15	0.36	0.18
MB5			0.50	2.15	0.36	0.22
MB6			0.43	2.15	0.36	0.29

2.4.1.Preparation of Mortar

The mixing was done in mixing machine as shown in Figure 4 to ensure that the process of batching is done effectively to give the mortar better strength. Thorough mixing is important for the production of uniform and high quality mix.

Cement and sand was mixed in dry condition with a trowel for a minute and then water was added. The preparation of the mortar is according to the BS EN 196-1, water cement ratio of 0.5, and the mixture is mixed until it is homogeneous

Figure 4: Cement paste mixer

2.4.2.Casting

The process of casting is where the mix is poured into cube mould. The size of 215mm x 100mm x 65mm for cube mould is

shown in Figure 5. The mortar was placed in the cube mould and then the mix compacted using the vibrator machine shown in Figure 6 to eradicate the air hole to give the maximum density to the mix. The vibrator machine was used in order to improve the quality of compaction rather than using conventional method that is by using rod. If the compaction is not thorough, the mix will be weaker and less dense.

Then the cube moulds were air dried in the lab with temperature of 27 ± 2° C and 90% relative humidity for 24 hours. After 24 hours the cubes are removed from the mould and then placed in well-ventilated area until testing as shown in Figure 7. Only one size of cube mould was used to cast the mix for testing purposes. Total of 60 cubes were prepared and placed in the ventilated area at the concrete laboratory.

Figure 5: Bricks mould of 215mm x 100mm x 65mm

Figure 6: Vibrator machine

International Science and Technology Journal
المجلة الدولية للعلوم والتقنية

العدد 26
Volume 26

المجلة الدولية للعلوم والتقنية
ISTJ

أ.

Figure 7: Air dried of samples at the ventilation area

2.4.3 Compressive Strength Test

The aim of this test was to determine the compressive strength of bricks based on BS EN 772-1:2000, *Methods of Testing for Masonry Units*, Part 1: Determination of compressive strength.

After air dried of 28 and 60 days each specimens are placed in the Compression Testing Machine as shown in Figure 8.

Figure 8: Compression Testing Machine

The specimen is placed with flat face horizontal in the centre of the machine pressure after placing two sheets of iron top and bottom of the sample to make sure the distribution of the load on the sample evenly. The load was applied axially at rate of 14

N/mm^2 per minute till failure occurs and maximum load at failure was noted and then reading of compressive strength was taken. The averages result of five (5) specimen were reported.

3 RESULT AND DISCUSSION

This study was carried out to investigate the potential of QDFP as a SCMs for bricks. In this research presenting the results obtained from the tests conducted at Civil Engineering Lab, UiTM, Shah Alam. Malaysia Discussions for these results were done to evaluate the mechanical performance of QDFP as a SCMs. Compressive strength test was conducted on the QDFP bricks.

3.1 Compressive strength of QDFP bricks

The results from compressive strength test were accordance to BS EN 772-1:2000 using 60 samples of bricks in size of 215 mm, 100 mm, and 65 mm at different level of QDFP cement replacement 15%, 20%, 25%, 30%, and 40%, of cement-sand ratio 1:3. All the samples contain w/c ratio of 0.5. The average compressive strength was obtained from the five (5) specimens for air dried at 28 and 60 days.

The results obtained from compressive strength test were summarized in Table 5, cement–sand ratio contain in the mixture. The graphs of compressive strength versus age of samples, and compressive strength versus mixture description were taken from the tables. In this phase the effect of cement replacement percentage with QDFP was discussed.

International Science and
Technology Journal
المجلة الدولية للعلوم والتقنية

العدد 26
Volume 26

المجلة الدولية للعلوم والتقنية
International Science and Technology Journal
ISTJ

Table 5: Compressive strength of QDFP bricks taken at 28 and 60 days of ventilation with cement-sand ratio of 1:3

27. Mixture 28. Designation	29. QDFP (%)	30. Compressive strength (N/mm^2)			
		31. After 28 Days		32. After 60 Days	
33. MB1	34. 0	35.	42.57	36.	52.85
37. MB2	38. 15	39.	36.63	40.	45.51
41. MB3	42. 20	43.	33.77	44.	43.11
45. MB4	46. 25	47.	32.15	48.	38.40
49. MB5	50. 30	51.	29.18	52.	38.65
53. MB6	54. 40	55.	28.37	56.	37.65
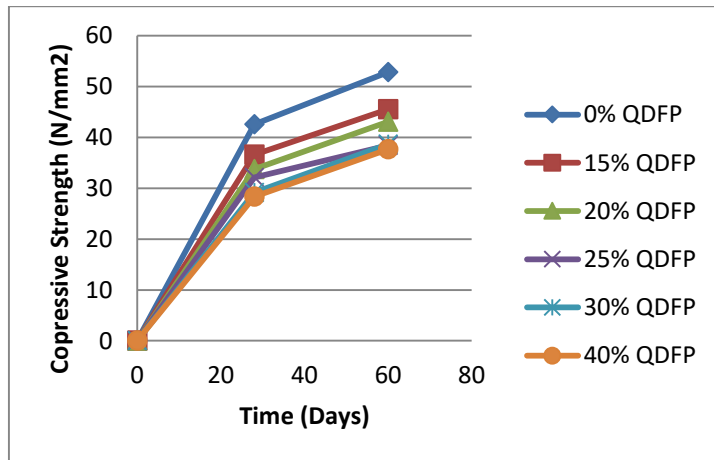
Figure 1: Compressive strength of QDFP bricks versus age of ventilation with cement-sand ratio of 1:3.0 taken at 28 and 60 days

International Science and
Technology Journal
المجلة الدولية للعلوم والتقنية

العدد 26
Volume 26

المجلة الدولية للعلوم والتقنية
International Science and Technology Journal
ISTJ
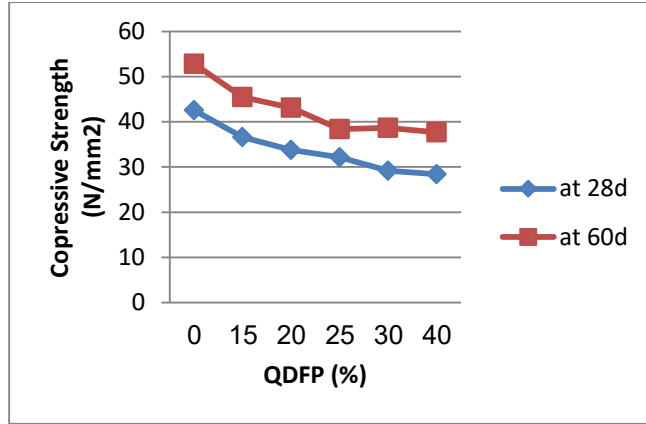
Figure 2: Compressive strength of QDFP bricks with respect to QDFP replacement level taken at 28 and 60 days made of cement-sand ratio 1:3.0

From that it can be concluded that, the compressive strength of bricks for 60 days of ventilation shown higher compressive strength compared to 28 days of ventilation. Hence, the compressive strength for this mix (cement-sand ratio 1:3.0) increased when the ventilation day was prolonged.

From Table 3.1 and Figure 2 it can be seen that the compressive strength of OPC bricks was higher than compressive strength of QDFP bricks. The compressive strength decreases with increasing in the QDFP cement replacement of 15%, 20%, 25%, 30%, and 40% with QDFP. Hence, the compressive strength decreases with increasing percentage of cement replacement with QDFP. However, the values of compressive strength were all above the acceptable standard of 20N/mm^2 which is considered as to be used in external non load bearing wall.

From all of the above, the compressive strength for brick that made of different mix proportion decreases with increasing the amount of cement replacement with QDFP. This is due to the reaction of QDFP in order to form calcium silicate hydrate (C-S-H) which occur at slower rate than the main chemical reaction. However, the compressive strengths of QDFP bricks were higher than the significant in the BS EN 772-1:2000.

The compressive strength of QDFP bricks increases with increasing in the days of ventilation from 28 to 60 days due to the time taken to replace calcium hydroxide to increase the C-S-H.

Now, the optimum cement replacement with QDFP for each proportion mix is taken to study the effect of different mix composition. Since the compressive strength for all mixes was higher than 20 N/mm^2 which indicated a good quality of bricks, stated by Neville (2002), 40% was selected to be the best replacement of cement with QDFP for each mix proportion.

Conclusion

1- compressive strength for QDFP bricks of cement – sand ratio of 1:3.0 and 0.5 (W/C) decreased with increasing the percentage replacement of cement with QDFP.

2- the replacement of QDFP selected was 40% replacement of cement with QDFP.

3- The compressive strength of QDFP bricks increases with increasing in the days of ventilation from 28 to 60 days due to the time taken to replace calcium hydroxide to increase the C-S-H.

4- Utilization of QDFP can contribute into sustainable development, which can be utilised in brick mixtures as good substitute for cement.

5- The demand, cost, and environmental effect of dust pollution and CO_2 emissions can be reduced.

References

BS EN 196-3:2005, *Method of Testing Cement*, Determination of Sitting Time and Soundness. British Standard Institution (BS).

BS EN 196-6:2010, *Method of Testing Cement*, Determination of Fineness. British Standard Institution (BS).

BS EN 772-1:2000, *Methods of Testing for Masonry Units*, Part 1: Determination of compressive strength.

Kartini, K. (2010), *Rice Husk Ash in Concrete*, University Publication Centre (UPENA), UiTM, IBSN 978-976-363-052-7.

Meyer, A. (2009), *Experiences in the Use of Superplasticizers in Germany in Superplasticizers in Concrete*, Detroit, Michigan, ACI SP-62, pp. 21-36.

Neville, A. M. (2002), *prope rties of concrete, 4th Edition*, ISBN 0-582- 23070-5, Longman, England, pp. 1-632

Nur Hanani Binti Abdul Rahim (2010) Durability Properties Of Superplasticized Quarry Dust Fine Powder (QDFP) Concrete With 0.6% W/C, Dissertation submitted as partial requirement for the degree of Master of Science in Civil Engineering, Faculty of Civil Engineering UNIVERSITI TEKNOLOGI MARA, Shah Alam Malaysia

ON BOUNDEDNESS OF SOLUTION OF NONLINEAR FUNCTIONAL DIFFERENTIA SYSTEMS

HUDA FARG ALSPIHE
College of Science and Technology Qaminis, Libya
E-mail:houda_frag@qi.edu.ly

HALA ALI SHELO
Department of Mathematics, Faculty of Science, Benghazi University, Libya
E-mail: halaali22@yahoo.com

Abstract:
Non-negative definite Lyapunov functions are employed to obtain sufficient conditions that guarantee boundedness of solutions of nonlinear functional differential systems.
The theory is applied to nonlinear volterra integral-differential equation with infinite delay.
Keywords: Nonlinear differential system, Boundedness; Uniform roundedness; Lyapunov functional; Volterra integro-differential equations.

المخلص:

في هذا البحث تماستخدام دالة ليبانوف(Lyapunov)   الغير سالبه و المحددة للحصول علي شروط كافيه تضمن حدود حلول الأنظمة التفاضلية الغير خطيه، و تطبيق النظرية علي معادلة فولتير(Volterra) التفاضلية التكاملية الغير خطيه مع التأخير الا نهائي.

الكلمات المفتاحية : النظام التفاضلي الغير خطي ، المحدوديه، المحدودية المنتظمة، دالة ليبانوف ، معادلة فولتير التفاضلية التكاملية.

I. Introduction
In this paper, we utilize non-negative definite Lyapunov functions and obtain sufficient conditions that guarantee the boundedness of all solutions of the system of functional differential equations

$$x'(t) = G(t, x(s); \ -\infty < s \le t) \overset{\text{def}}{=} G(t, x(.)) \qquad (1.1)$$

International Science and
Technology Journal
المجلة الدولية للعلوم والتقنية

العدد 26
Volume 26

المجلة الدولية للعلوم والتقنية
International Science and Technology Journal
ISTJ

where $x \in \mathbb{R}^n$, $G : \mathbb{R}^+ \times \mathbb{R}^n \to \mathbb{R}^n$ is a given nonlinear continuous function in t and x. For a vector $x \in \mathbb{R}^n$ we take $\| x \|$ to be the Euclidean norm of x. Let $t_0 > -\infty$, the n for each continuous function $\varphi : (-\infty, t_0] \to \mathbb{R}^n$, there is at least one continuous function $x(t) = x(t, t_0, \varphi)$ on an interval $[t_0, I]$ satisfying (1.1) for $t_0 \le t \le I$ and such that $x(t, t_0, \varphi) = \varphi(t)$ for $-\infty < t \le t$. It is assumed that at $t = t_0$, $x'(t)$ is the right hand derivative of $x(t)$. For conditions ensuring existence, uniqueness and continuability of solutions of (1.1) we refer the reader to [1] and [5].

In [10], Raffoul researched the use of non-negative definite Lyapunov functions to obtain sufficient conditions that guarantee the boundedness of all solutions of the system of functional differential equations

$$x'(t) = G(t, x(s); \ 0 < s \le t) \overset{\text{def}}{=} G(t, x(.))$$

This paper extends the research of Raffoul in [10] to a system of functional differential equations with different boundary conditions (i.e. $-\infty < s \le t$ instead of $0 < s \le t$)

In [9], Raffoul studied the boundedness of solutions of thein itial value problem

$$x'(t) = G(t, x(t)); t \ge 0$$
$$x(t_0) = x_0$$

by making use of Non-negative definite Lyapunov functions.

A stereotype of equation (1.1) is the Volterra Integro-differential equation

$$x'(t) = Ax(t) + \int_{-\infty}^{t} B(t,s) f\big(x(s)\big) ds. \tag{1.2}$$

We are mainly interested in applying our results to Volterra Integro-differential equations of the forms of (1.2) with $f(x) = x^n$ where n is positive and rational. It is important to notice that the results of [9] do not apply to equations similar to (1.2). In [1] Burton and the others proved general theorems using Lyapunov functionals of convolution types and obtained conditions for boundedness of solutions and stability of the zero solution of (1.1). However, in this paper our conditions are different and offer a new perspective at looking at the notion of boundedness. To provide an application to our Theorems, we will apply our obtained results to

International Science and
Technology Journal
المجلة الدولية للعلوم والتقنية

العدد 26
Volume 26

المجلة الدولية للعلوم والتقنية
International Science and Technology Journal
ISTJ

nonlinear Volterra integro-differential equations. At the end of the paper we will compare our Theorems to those obtained in[12] and show that our results are different when it comes to applications. For more on the boundedness and stability of solutions of(1.1), we refer the interested reader [3], [4], [7], [8], [13], [6] and [11].

II. Boundedness of Solutions

In this section we use non-negative Lyapunov type functionals and establish sufficient conditions to obtain boundedness results on all solutions $x(t)$ of (1.1). Let φ: $(-\infty, t] \to \mathbb{R}^n$be continuous, we define$|\phi| = sup\{\|\phi(s)\|: -\infty < s \le t\}$.

From this point forward, if a function is written without its argument, then the argument is assumed to be *t*.

Definition 2.1 We say that solutions of system (1.1) are bounded, if any solution $x(t, t_0, \phi)$ of (1.1) satisfies

$\|x(t, t_0, \phi)\| \le c(|\phi|, t_0), \ for \ all \ t \ge t_0,$

Where $c : \mathbb{R}^+ \times \mathbb{R}^+ \to \mathbb{R}^+$ is a constant that depends on t_0 and $\phi$is a given continuous and bounded initial function. We say that solutions of system (1.1) are uniformly bounded if cis independent oft_0.

If $x(t)$ is any solution of system (1.1), then for a continuously differentiable function

$V: \mathbb{R}^+ \times \mathbb{R}^n \to \mathbb{R}^+,$

We define the derivative $V^{'}$ of V by

$$V'(t, x) = \frac{\partial V(t,x)}{\partial t} + \sum_{i=1}^{n} \frac{\partial V(t,x)}{\partial x_i}.$$

A continuous function $W: [0, \infty) \to [0, \infty)$with$W(0) = 0, W(s) > 0ifs>0$ and W strictly increasing is called a wedge. (In this paper wedges are always defined by $W \ or \ W_i$ where i is a positive integer).

Theorem 2.1 Let D be a set in$\mathbb{R}^n$. Suppose there exist a continuously differentiable Lyapunov functional $V: \mathbb{R} \times D \to \mathbb{R}^+$ that satisfies

International Science and Technology Journal
المجلة الدولية للعلوم والتقنية

العدد 26
Volume 26

المجلة الدولية للعلوم والتقنية
International Science and Technology Journal
ISTJ

$$\lambda_1 W_1(|x|) \leq V(t,x)$$
$$\leq \lambda_2 W_2(|x|)$$
$$+ \lambda_2 \int_{-\infty}^{t} \varphi_1(t,s) W_3(|x(s)|)\, ds \qquad (2.1)$$

And

$$V'(t,x) \leq -\lambda_3 W_4(|x|) - \lambda_3 \int_{-\infty}^{t} \varphi_2(t,s) W_5(|x(s)|)ds$$
$$+ L \qquad (2.2)$$

for some positive constants $\lambda_1, \lambda_2, \lambda_3$ and L, where $\varphi_i(t,s) \geq 0$ is a scalar function for
$-\infty < s \leq t < \infty, i = 1,2$, such that for some constant $\gamma \geq 0$ the inequality

$$W_2(|x|) - W_4(|x|)$$
$$+ \int_{-\infty}^{t} \big(\varphi_1(t,s) W_3(|x(s)|)$$
$$- \varphi_2(t,s) W_5(|x(s)|)\big)ds \leq \gamma \qquad (2.3)$$

Holds. Moreover, if $\int_{-\infty}^{t} \phi_1(t,s)ds \leq B$ for some positive constant B, then all solutions of (1.1) that start in D are uniformly bounded.

Proof let $M = \lambda_3/\lambda_2$ for any initial time t_0, let $x(t)$ be any solution of (1.1) with $x(t) = \phi(t), for -\infty < t \leq t_0$. Then,

$$\frac{d}{dt}\big(V\big(t,x(t)\big)e^{M(t-t_0)}\big) = \Big[V'\big(t,x(t) + MV\big(t,x(t)\big)\big)\Big]e^{M(t-t_0)}.$$

For $x(t) \in \mathbb{R}^n$ using (2.2) we get

International Science and Technology Journal
Technology Journal
المجلة الدولية للعلوم والتقنية

العدد 26
Volume 26

المجلة الدولية للعلوم والتقنية
International Science and Technology Journal
ISTJ

$$\frac{d}{dt}\left(V\big(t,x(t)\big)e^{M(t-t_0)}\right)$$

$$\leq \left[-\lambda_3 W_4(|x|) - \lambda_3 \int_{-\infty}^{t} \varphi_2(t,s)W_5(|x(s)|)ds \right.$$
$$+ L + M\lambda_2 W_2(|x|)$$
$$\left. + M\lambda_2 \int_{-\infty}^{t} \varphi_1(t,s)W_3(|x(s)|)ds\right] e^{M(t-t_0)}$$

$$=\lambda_3 \left[W_2(|x|) - W_4(|x|) + \int_{-\infty}^{t}\big(\varphi_1(t,s)W_3(|x(s)|) - \varphi_2(t,s)W_5(|x(s)|)\big)ds + L\right] e^{M(t-t_0)}$$

$$\leq (\lambda_3\gamma + L)e^{M(t-t_0)}$$

$$:= Ke^{M(t-t_0)} \qquad (2.4)$$

Integrating (2.4) from t_0 to t we obtain,

$$V\big(t,x(t)\big)e^{M(t-t_0)} \leq V(t_0,\phi) + \frac{K}{M}e^{M(t-t_0)} - \frac{K}{M}$$

$$\leq \lambda_2 V(t_0,\phi) + \frac{K}{M}e^{M(t-t_0)}.$$

Consequently,

$$V\big(t,x(t)\big) \leq \lambda_2 V(t_0,\phi)e^{M(t-t_0)} + \frac{K}{M}.$$

From condition (2.1) we have $\lambda_1 W_1(|x|) \leq \lambda_2 V\big(t,x(t)\big)$, which implies that

$$|x| \leq W_1^{-1}\left[\left\{\frac{1}{\lambda_1}\right\}\left(\lambda_2 W_2(|\phi|) + \lambda_2 W(|\phi|)_3 \int_{-\infty}^{t} \varphi_1(t_0,s)ds + \frac{K}{M}\right)\right]; \text{ for all } t \leq t_0$$

This completes the proof.

Example 2.1 Consider the scalar nonlinear Volterra integro-differential equation

$$x' = \sigma(t)x(t) + \int_{-\infty}^{t} B(t,s)x^{2/3}(s)ds. \quad t \geq t_0 ; x(t) = \phi(t)\text{for}-\infty < t \leq t_0 (2.5)$$

If

$$2\sigma(t) + \int_{-\infty}^{t} |B(t,s)|ds + \int_{t}^{\infty} |B(u,t)|\, du \leq -1,$$

$$(*) \int_{-\infty}^{t} \int_{t}^{\infty} |B(u,s)|\,du\,ds \,,\, \int_{t}^{\infty} |B(t,s)|\,ds < \infty,$$

And

$$(**)\frac{|B(t,s)|}{3} \geq \int_{t}^{\infty} |B(u,s)|\,du$$

Then all solution of (2.5) are uniformly bounded.
To see this we let

$$V(t,x) = x^2 + \int_{-\infty}^{t} \int_{t}^{\infty} |B(u,s)|\,du\,x^2(s)\,ds.$$

Then along solution of (2.5) we have

$$V'(t,x) = 2xx' + \int_{t}^{\infty} |B(u,t)|x^2(t)\,du - \int_{-\infty}^{t} |B(t,s)|\,x^2(s)\,ds$$

$$\leq 2\sigma(t)x^2 + 2\int_{-\infty}^{t} |B(t,s)|\,|x(t)|x^{2/3}(s)\,ds$$

$$+ \int_{t}^{\infty} |B(u,t)|x^2(t)\,du - \int_{-\infty}^{t} |B(t,s)|x^2(s)\,ds.$$

Using the fact that $ab \leq a^2/2 + b^2/2$, the above inequality simplifies to

$$V'(t,x) \leq 2\sigma(t)x^2 + \int_{-\infty}^{t} |B(t,s)|\big(x^2(t) + x^{3/4}(s)\,ds\big)$$

$$+ \int_{t}^{\infty} |B(u,t)|x^2(t)\,du$$

$$- \int_{-\infty}^{t} |B(t,s)|\,x^2(s)\,ds. \qquad (2.6)$$

To further simplify(2.6) we make use of Young's inequality, which says for any two nonnegative real numbers w and z, we have

$$wz \leq \frac{w^e}{e} + \frac{z^f}{f} \,,\, with\ 1/e + 1/f = 1.$$

Thus, for $e = 3/2$ $and\ f = 3$, we get

International Science and
Technology Journal
المجلة الدولية للعلوم والتقنية

العدد 26
Volume 26

المجلة الدولية للعلوم والتقنية
International Science and Technology Journal

ISTJ

$$\int_{-\infty}^{t} |B(t,s)| x^{3/4}(s)ds = \int_{-\infty}^{t} |B(t,s)|^{1/3} |B(t,s)|^{2/3} x^{3/4}(s)ds$$

$$\leq \int_{-\infty}^{t} \left(\frac{|B(t,s)|}{3} + \frac{2}{3}|B(t,s)|x^2(s) \right) ds$$

By substituting the above inequality into (2.6), we arrive at

$$V'(t,s) \leq \left(2\sigma(t) + \int_{-\infty}^{t} |B(t,s)|ds + \int_{-\infty}^{t} |B(u,t)| du \right) x^2(t)$$

$$- \int_{-\infty}^{t} \left(|B(t,s)| - \frac{2}{3}|B(t,s)| \right) x^2(s)ds + L$$

$$\leq -x^2(t) - \int_{-\infty}^{t} \frac{|B(t,s)|}{3} x^2(s)ds + L ,$$

Where $L = \frac{1}{3}\int_{-\infty}^{t}|B(t,s)|ds$. By taking $W_1 = W_2 = W_{4=}x^2(t)$, $W_3 = W_5 = x^2(s)$, $\lambda_1 = \lambda_2 = \lambda_3 = 1$ And $\varphi_1(t,s) = \int_{t}^{\infty}|B(u,s)| du$, $\varphi_2(t,s) = \frac{|B(t,s)|}{3}$, We see that all the conditions of theorem (2.2) are satisfied. Hence all solutions of (2.5) are uniformly bounded.

Note that $B(t,s) = e^{-k(t-s)}$, $k = 3$ will satisfy all requirements of Example (2.1)

$$(*) \int_{-\infty}^{t} \int_{t}^{\infty} |B(u,s)| du ds < \infty$$

$$\int_{-\infty}^{t} \int_{t}^{\infty} |e^{-3(u-s)}| du ds \leq \frac{1}{9}$$

$$(*) \int_{-\infty}^{t} |B(t,s)| ds = \int_{-\infty}^{t} |e^{-3(t-s)}| ds \leq \frac{1}{3}$$

$$(**) \int_{t}^{\infty} |B(u,s)| du = \int_{t}^{\infty} |e^{-3(u-s)}| du = \frac{1}{3} e^{-3(t-s)}$$

$$\frac{|B(t,s)|}{3} = \frac{e^{-3(t-s)}}{3}$$

$$= \int_{t}^{\infty} |B(u,s)| du = \int_{t}^{\infty} e^{-3(u-s)} du = \frac{1}{3} e^{-3(u-s)}$$

Also, we assert that Example (2.1) can be easily generalized to handle nonlinear Volterra equations of the form

$$x' = \sigma(t)x(t) + \int_0^t B(t,s) f\big(s, x(s)\big)ds,$$

Where $\left|f\big(t, x(t)\big)\right| \leq x^{2/3}(t) + M$, for some positive constant M. condition (2.3) did not come into play, which was due to the fact that $r = q = 2$. In the next example, we consider a nonlinear system in which condition (2.3) naturally comes into play.

Example 2.2 let $D = \{x \in \mathbb{R}: \|x\| \geq 1\}$. Let $\phi(t)$ be a given bounded continuous initial function such that $\|\phi(t)\| = 1$, for $-\infty < t \leq t_0$. Consider the scalar nonlinear Volterra integro-differential equation

$$x' = \sigma(t)x^3(t)$$
$$+ \int_{-\infty}^t B(t,s)x^{1/3}(s)ds \, , t \geq t_0 \, , x(t)$$
$$= \phi(t) \, for \, -\infty < t \leq t_0 \qquad (2.7)$$

If $\qquad 2\sigma(t) + \frac{1}{2}\int_{-\infty}^t |B(t,s)|^{\frac{1}{2}} + \int_t^\infty |B(t,s)| \, du \leq -1$

$* \quad \int_{-\infty}^t \int_t^\infty |B(u,s)|duds \, , \int_{-\infty}^t \left(|B(t,s)| + |B(t,s)|^{\frac{3}{2}}\right) ds < \infty,$

$$** \quad \frac{5|B(t,s)|}{6} \geq \int_t^\infty |B(u,s)|du$$

Then all solution of (2.7) that are in the set D are uniformly bounded.

To see this , we consider the Lyapunov function $V(t,s): \mathbb{R} \times D \to \mathbb{R}^+$

$$V(t,s) = x^2 + \int_{-\infty}^t \int_t^\infty |B(u,s)| \, dux^4(s)ds.$$

Then along solution of (2.7) we have

$$V'(t,x) = 2xx' + \int_t^\infty |B(u,s)|x^4(t)du - \int_{-\infty}^t |B(t,s)| \, x^4(s)ds$$

$$\leq 2\sigma(t)x^4 + 2\int_{-\infty}^{t}|B(t,s)|\,|x(t)||x(s)|^{1/3}ds$$
$$+ \int_{t}^{\infty}|B(u,t)|x^4(t)du - \int_{-\infty}^{t}|B(t,s)|x^4(s)ds.$$

By noting that $\quad 2|x(t)||x(s)|^{1/3} \leq x^2(t)x^{2/3}(s)\quad$ we have from the above inequality that

$$V'(t,x) \leq 2\sigma(t)x^4 + \int_{-\infty}^{t}|B(t,s)|\big(x^2(t) + |x(s)|^{2/3}\big)\,ds$$
$$+ \int_{t}^{\infty}|B(u,t)|x^4(t)du - \int_{-\infty}^{t}|B(t,s)|x^4(s)ds.$$

Next we note that

$$\int_{-\infty}^{t}|B(t,s)|x^2(t)dt = \int_{-\infty}^{t}|B(t,s)|^{1/2}|B(t,s)|^{1/2}x^2(t)ds$$
$$\leq \int_{-\infty}^{t}|B(t,s)|^{1/2}\left[\frac{|B(t,s)|}{2} + \frac{x^4(t)}{2}\right]ds.$$

Also, using Young's inequality with e = 6 and f = 6/5, we get

$$x(s)^{2/3}|B(t,s)| = x(s)^{2/3}|B(t,s)|^{1/6}|B(t,s)|^{5/6}$$
$$\leq \frac{x^4(s)|B(t,s)|}{6} + \frac{5}{6}|B(t,s)|.$$

$$V'(t,x) \leq \left(2\sigma(t) + \frac{1}{2}\int_{-\infty}^{t}|B(t,s)|ds + \int_{t}^{\infty}|B(u,t)|du\right)x^4(t)$$
$$- \int_{-\infty}^{t}\left(|B(t,s)| - \frac{|B(t,s)|}{6}\right)x^4(s)ds + L$$

$$\leq -x^4(t) - \int_{-\infty}^{t}\frac{5|B(t,s)|}{6}x^4(s)ds + L$$

Where $\quad L = \frac{5}{6}\int_{-\infty}^{t}|B(t,s)|\,ds + \frac{1}{2}\int_{-\infty}^{t}|B(t,s)|^{3/2}ds$. By taking $W_1 = W_2 = x^2(t), \quad W_3 = W_5 = x^4(s), \lambda_1 = \lambda_2 = \lambda_3 = 1 \quad$ and $\varphi_1(t,s) = \int_{t}^{\infty}|B(u,s)|du, \quad \varphi_2(t,s) = \frac{5|B(t,s)|}{6} \quad$ we see that condition (2.1) and (2.2) of theorem 2.2 are satisfied. Left to show that condition (2.3) hold. Since $\frac{5|B(t,s)|}{6} \geq \int_{t}^{\infty}|B(u,s)|\,du\quad$ we have, for $x \in D$ that

International Science and
Technology Journal
المجلة الدولية للعلوم والتقنية

العدد 26
Volume 26

المجلة الدولية للعلوم والتقنية
ISTJ
International Science and Technology Journal

$$W_2(|x|) - W_4(|x|)$$
$$+ \int_{-\infty}^{t} (\varphi_1(t,s)W_3|x(s)| - \varphi_2(t,s)W_5|x(s)|)ds$$
$$= x^2(t) - x^4(t) + \int_{-\infty}^{t} \left(\int_{t}^{\infty} |B(u,s)|\, du - \frac{5|B(t,s)|}{6} \right) x^4(s)ds$$
$$\leq x^2(1-x^2) \leq 0.$$

Thus, condition (2.3) is satisfied for $\gamma = 0$. An application of theorem (2.4) yields

$$|x(t)| \leq \left[|\phi^2(t_0)| + W_3\left(|\phi| \int_{-\infty}^{t} \varphi_1(t_0,s)ds + \frac{K}{M} \right) \right]^{1/2}$$
$$\leq \left[1 + \int_{-\infty}^{t_0} \int_{t_0}^{\infty} |B(u,s)|du + \frac{K}{M} \right]^{1/2}, for\ all\ t \geq t_0$$

Hence, every solution $x\ with\ x(t) \in D$ satisfied

$$1 \leq |x(t)| \leq \left[1 + \int_{-\infty}^{t_0} \int_{t_0}^{\infty} |B(u,s)|\, du + \frac{K}{M} \right]^{1/2}; for\ t \geq 0.\ \square$$

Note that $B(t,s) = e^{-k(t-s)}, k = 6/5$ will satisfy all requirements of Example 2.2.

$$* \quad \int_{-\infty}^{t} \int_{t}^{\infty} |B(u,s)|\, duds < \infty$$
$$\int_{-\infty}^{t} \int_{t}^{\infty} |e^{-6/5(u-s)}|duds \leq \frac{25}{36}$$
$$* \quad \int_{-\infty}^{t} |B(t,s)|\, ds = \int_{-\infty}^{t} |e^{6/5(t-s)}|ds \leq \frac{5}{6}$$
$$** \quad \int_{t}^{\infty} |B(u,s)|\, du = \int_{t}^{\infty} |e^{-6/5(u-s)}|\, du = \frac{5}{6}e^{-6/5(t-s)}$$
$$** \quad \frac{5|B(t,s)|}{6} = \frac{5e^{-6/5(t-s)}}{6} = \int_{t}^{\infty} |B(u,s)|\, du$$
$$= \int_{t}^{\infty} e^{-6/5(t-u)}du = \frac{5}{6}e^{-6/5(t-s)}$$

In the next theorem we show that solutions are bounded.

Theorem 2.2

Let D be a set in $\mathbb{R}^n$. Suppose there exist a continuously differentiable Lyapunov function
$V: D \to R^+$ that satisfies

$$\lambda_1(t)W_1(|x|) \leq V(t,x)$$
$$\leq \lambda_2 W_2(|x|)$$
$$+ \lambda_2(t)\int_{-\infty}^{t} \varphi_1(t)W_3(|x(s)|)ds \qquad (2.8)$$

and

$$V'(t,x) \leq -\lambda_3(t)W_4(|x|)$$
$$- \lambda_3(t)\int_{-\infty}^{t} \varphi_2(t,s)W_5(|s|)ds$$
$$+ L \qquad (2.9)$$

for some positive continuous function $\lambda_1(t), \lambda_2(t), \lambda_3(t)$ and positive constant L, where $\lambda_1(t)$ is non decreasing and $\varphi_i(t,s) \geq 0$ is a scalar function continuous for $-\infty < s \leq t < \infty, i = 1,2$ such that for some constant $\gamma \geq 0$ the inequality
$$W_2(|x|) - W_4(|x|)$$
$$+ \int_{-\infty}^{t} \big(\varphi_1(t,s)W_3(|x(s)|)$$
$$- \varphi_2(t,s)W_5(|x(s)|)\big)ds \leq \gamma \qquad (2.10)$$

hold. Moreover, if $\int_{-\infty}^{t} \phi_1(t,s)ds \leq B$ and $\lambda_3(t) \leq N$ for some positive constants B and N, then all solution of (1.1) that stay in D are bounded.

Proof

Let $M = inf_{t \in \mathbb{R}^+} \frac{\lambda_3(t)}{\lambda_2(t)}$

For any initial time t_0, let $x(t)$ be any solution of (1.1) with $x(t_0) = \phi(t_0)$. By calculating
$$\frac{d}{dt}\big(V(t,x(t))e^{M(t-t_0)}\big)$$

And then by a similar argument as in Theorem 2.1 we obtain,

$$V(t,x(t)) \leq \lambda_2(t_0)V(t_0,\phi) + \frac{K}{M}e^{-M(t-t_0)}$$
$$+ \frac{K}{M} \qquad (2.11)$$

International Science and
Technology Journal
المجلة الدولية للعلوم والتقنية

العدد 26
Volume 26

المجلة الدولية للعلوم والتقنية
ISTJ
International Science and Technology Journal

Where $K = N\gamma + L$. Consequently,

$$V(t, x(t)) \leq \lambda_2(t_0)V(t_0, \phi) + e^{-M(t-t_0)} + \frac{K}{M}.$$

Since $\lambda_1(t)$ is nondecreasing we have for $t \geq t_0 \geq -\infty$

$$W_1(|x|) \leq \frac{1}{\lambda_1(t)}\left(\lambda_2(t_0)V(t_0, \phi)e^{-M(t-t_0)} + \frac{K}{M}\right)$$

$$\leq \frac{1}{\lambda_1(t_0)}\left(\lambda_2(t_0)V(t_0, \phi)e^{-M(t-t_0)} + \frac{K}{M}\right)$$

Hence,

$$||x|| \leq W_1^{-1}[\frac{1}{\lambda_1(t_0)}\left(\lambda_2(t_0)V(t_0, \phi)e^{-M(t-t_0)} + \frac{K}{M}\right)]$$

This completes the proof.

$\square$

The proof of the next theorem can be found in [9].

Theorem 2.3 Suppose that there a continuously differentiable Lyapunov functional$V: \mathbb{R}^+ \times \mathbb{R}^n \to \mathbb{R}^+$ that satisfies

$$\lambda_1||x||^p \leq V(t, x), \quad V(t, x) \neq 0 \text{ if } x \neq 0 \quad (2.12)$$

and

$$V'(t, x) \leq -\lambda_2(t)V^q(t, x) \quad (2.13)$$

for some positive constants $\lambda_1, p, q > 1$ where $\lambda_2(t)$is a positive continuous function such that

$$c_1 = \inf_{t \geq t_0 \geq 0} \lambda_2(t) > 0. \quad (2.14)$$

Then all solutions $x(t)$ of (1.1) satisfy

$$||x|| \leq 1/\lambda_1^{1/p}\{[V^{1-q}(t_0, \phi) + c_1(q-1)(t-t_0)]^{-1/(q-1)}\}^{1/p}.$$

As an application of the previous theorem, we furnish the following example.

Example 2.3 To illustrate the application of Theorem 2.3, we consider the following two dimensional system of nonlinear Volterra integro-differential equations

$$y_1' = y_2 - y_1|y_1| - y_1y_2^2 \int_{-\infty}^{t} |B(t,s)|f(y_1(s), y_2(s))ds$$

$$y_2' = y_1 - y_2|y_2| - y_1^2y_2 \int_{-\infty}^{t} C(t,s)g(y_1(s), y_2(s))ds$$

International Science and Technology Journal
Technology Journal
المجلة الدولية للعلوم والتقنية

العدد 26
Volume 26

المجلة الدولية للعلوم والتقنية
International Science and Technology Journal
ISTJ

$$(y_1(t), -y_2(t)) = (\varphi_1(t), \varphi_2(t)),$$

For some given initial continuous and bounded functions $\varphi_1(t), \varphi_2(t)$, $-\infty \le t \le t_0$.

The scalar functions $|B(t,s)|$, $C(t,s)$ are continuous in t and s and $|B(t,s)| \ge |C(t,s)|$. Also, the scalar $f(y_1(s), y_2(s))$ and $g(y_1(s), y_2(s))$ are continuous in y_1 and y_2. We assume that $f(y_1(s), y_2(s)) > 0, |g(y_1(s), y_2(s))| \le f(y_1(s), y_2(s))$, for all $y_1, y_2 \in R$.

Let us take $V(y_1, y_2) = \frac{1}{2}(y_1^2 + y_2^2)$. Then

$$V'(y_1, y_2) = y_1^2|y_1| - y_2^2|y_2|$$

$$-y_1^2 y_2^2 (\int_{-\infty}^{t} |B(t,s)| f(y_1(s), y_2(s)) ds$$

$$- \int_{-\infty}^{t} C(t,s) g(y_1(s), y_2(s)) ds)$$

$$\le -(|y_1|^3 + |y_2|^3) + y_1^2 y_2^2 \int_{-\infty}^{t} (|C(t,s)|$$

$$- |B(t,s)|) f(y_1(s), y_2(s)) ds$$

$$\le -2[\frac{|y_1|^3}{2} + \frac{|y_2|^3}{2}]$$

$$= -2[\frac{(|y_1|^2)^{3/2}}{2} + \frac{(|y_2|^2)^{3/2}}{2}]$$

$$\le -2(|y_1|^2 + |y_2|^2)^{3/2} 2^{-3/2}$$

$$= -2V^{3/2}(y_1, y_2)$$

where we have used the inequality

$$(\frac{a+b}{2})^l \le \frac{a^l}{2} + \frac{b^l}{2}, \qquad a, b > 0, \qquad l > 1.$$

Hence, by Theorem 2.3 all solutions of the above two dimensional system are uniformly bounded.

References

[1] Burton, A., Quichang, H, and Mahfoud, W. E., Liapunovfunctionals of convolution type, J. Math. Analy. Appl. 106(1985), 249-272.

[2] Burton, T., Volterra Integral and Differential Equations. Academic Press, New York, 1983

[3] Caraballo, D., On the decay rate of solutions of non-autonomous differential systems, Electron. J. Di. Eqns., Vol. 2001(2001), No. 05, pp. 1-17.

[4] Cheban, D., Uniform exponential stability of linear periodic systems in a Banach space , Electron. J. Di. Eqns., Vol. 2001(2001), No. 03, pp. 1-12.

[5] Driver, D., Ordinary and Delay Differential Equations. Sprinmger Publ., New York, 1977.

[6] J. K. Hale, Theory of Functional Differential Equations, Springer-Verlag, Berlin, (1977).

[7] Lakshmikantham V., Leela S. and Martynyuk A., Stability Analysis of Non-linear Systems. Marcel Dekker, New York, 1989 Linh, N., and Phat, V., Exponential stability of nonlinear time-varying differential equations and applications, Electron. J. Di. Eqns., Vol. 2001(2001), No. 24, pp. 1-13.

[8] Linh, N., and Phat, V., Exponential stability of nonlinear time-varying differential equations and applications, Electron. J. Di. Eqns., Vol. 2001(2001), No. 24, pp. 1-13.

[9] Raffoul. Y. , Boundedness in nonlinear differential equations, Nonlinear Studies, Vol. 10. No. 4, pp. 343-350, (2003).

[10] Raffoul.Y., Boundedness in nonlinear functional differential equations with applications to volterraintegrodifferntailequations, Journal of Integral Equations and Applications, Vol. 16, No. 4, (2004).

[11] S. Kato, Existence, uniqueness and continous dependence of solutions of delay differential equations with innite delay in a Banach space, Journal of Mathematical Analysis and Applications, Vol. 195, No 1, (1995).

[12] Vanualailai. J.,Some stability and boundedness criteria for a class of Volterra integro-differential systems, Electronic Journal of Qualitative Theory of Differential Equations, No. 12, pp. 1-20, (2002).

[13] Yoshizawa T., Stability Theory by Lyapunov Second Method. The Math. Soci. of Japan, Tokyo, 1966.

SYNTHESIS OF GEOPOLYMER BINDER FROM TREATED PALM OIL FUEL ASH

M. J. A. Mijarsh [1,2] , M.A. Megat Johari[1]*, S. M. Alburki [3], M.O. M. Mashri[1,4], A. O.Alsawehli[3]

mjalmijarsh@elmergib.edu.ly [1] , cemamj@eng.usm.my [2],
smalburki@Elmergib.edu.ly [3], mashriomar@gmail.com[4],
adnan0102a@gmail.com[3]

[1] School of Civil Engineering, Universiti Sains Malaysia, Malaysia
[2] Civil Engineering Department, Faculty of Engineering, El-Mergib University, Al-Khums, Libya
[3] Chemical Engineering Department, Faculty of Engineering, El-Mergib University, Al-Khums, Libya
[4] College of Technical Sciences-Bani Walid, Libya.

*Corresponding author email: cemamj@ eng.usm.my (M.A. Megat Johari)

ABSTRACT

This study deals with the ability of geopolymers mortar synthetized from industrial waste of treated palm oil fuel ash (TPOFA) containing aluminosilicate activated with alkaline activator solution. Geopolymers are inorganic polymers formed by the activation of amorphous aluminosilicate ($Al_2O_3.SiO_2$), which react in a strongly alkaline medium. 10M NaOH, Na2SiO$_3$:NaOH with a 2.5 weight ratio, and alkali-activator: solid-material with a 0.47 weight ratio were used as the alkaline medium. The production of geopolymer mortar synthesized from TPOFA is currently underway at Universiti Sains Malaysia (USM); the results of the experiments that are in progress show that the TPOFA-geopolymer mortar achieved a compressive strength of 19 MPa after only 1 day of curing. The properties of the TPOFA-based geopolymer mortar were further analyzed via Fourier transform infrared spectroscopy (FTIR), X-ray diffractography (XRD), thermogravimetry (TGA/DTA) , field emission scanning electron microscopy (FESEM), and energy dispersive spectroscopy (EDS) analysis. All results of the analyses show that

International Science and Technology Journal
Technology Journal
المجلة الدولية للعلوم والتقنية

العدد 26
Volume 26

ISTJ
المجلة الدولية للعلوم والتقنية
International Science and Technology Journal

the main binding phases are the tridimensional tecto-aluminosilicate type gel.

Keywords: Geopolymer, TPOFA, tecto-aluminosilicate.

الملخص

تهدف هده الدراسة الى التعامل مع قدرة الجيوبولمر والتي تم تكوينها من النفايات الصناعيةِ من زيت النخيل المعالج الذي يحتوي على سيليكات الالومينا ولتي تم تنشيطها بستخدام المنشطات القلوية. وهي مركبات كيميائية لا عضويةَ تم تكوينها بتنشيطِ سيليكات الالومينا$(Al_2O_3.SiO_2)$ ، والتي تكون نشطة في الوسط قلوي بقوة 10 مول من هيدروكسيد الصوديوم، مَع نسبة الصوديوم هيدروكسايد إالي الصوديوم سليكات2.5 نسبة وزنية، ونسبة المنشّط قلوي 0.47 نسبة وزنية إستعملتْ كوسط قلوي. يجري حاليًا إنتاج ملاط جيوبوليمر المُصنّع من معالجة رماد زيت النخيل في جامعة العلوم الماليزية ؛ تظهر نتائج التجارب الجارية أن ملاط جيوبوليمر المُصنّع من معالجة رماد زيت النخيل حقق قوة ضغط تبلغ 19 ميجا باسكال بعد يوم واحد فقط من المعالجة. جميع العيناتتم تحليلها عن طريق أشعة تحت الحمراءِ وتم استخدام اجهزة مزيد من التحليل عبر مطيافية الأشعة تحت الحمراء لتحويل فورييه (FTIR) و حيود الأشعة السينية (XRD) و قياس الوزن الحراري (TGA/DTA)، المسح المجهري الإلكتروني للانبعاثات الميدانية (FESEM) ، والتحليل الطيفي المشتت للطاقة (EDS). كُل تظهر جميع نتائج التحليلات أن مراحل الربط الرئيسية هي هلام النوع ثلاثي الأبعاد من نوع Tecto−aluminosilicate.

1. Introduction

Geopolymer is formed by dissolving aluminosilicate materials in a highly alkaline solution, to produce tridimensional tecto-aluminosilicate binder [1]. Nonetheless, not all source materials used for geopolymer synthesis could be able to produce the tridimensional tecto-aluminosilicate binder, except kaolinite [2]. Therefore, geopolymer synthesis is dependent on the use of material rich in aluminum-silicate glass activated with alkaline solutions [3]. Most of the research commonly used source

International Science and Technology Journal
Technology Journal
المجلة الدولية للعلوم والتقنية

العدد 26
Volume 26

المجلة الدولية للعلوم والتقنية
International Science and Technology Journal
ISTJ

materials rich in Si and Al such as kaolin [4]. Research has also been conducted on industrial wastes such as fly ash and slag due to their high silica and alumina contents with little or high CaO contents, respectively [4]. The potential of POFA, as a source material for geopolymer synthesis has not been adequately explored and most of the previous research studies were limited only in a few countries in particular Malaysia and Thailand compared to other waste materials [5].

POFA is a by-product from the burning of empty fruit bunches, kernel shells, and fibers to heat up boiler for generating electricity in palm oil mills [5]. Large amounts of POFA are produced in Malaysia, Thailand, and Indonesia, and it is expected to increase annually [6]. Most of the POFA are disposed in landfills which may contribute to environmental problems in the future [7]. Therefore, many research works have been conducted to find suitable solutions for the proper disposal of POFA [8-10].

Recently, Megat Johari et al. [5] utilized grinding and heating processes in order to remove the excess carbon content and to reduce the median particle size of POFA to about 2.06 µm. A highly efficient pozzolan was obtained through the treatment processes. The treated POFA (TPOFA) was utilized to improve the engineering and transport properties of high performance concrete (HPC). TPOFA in amounts of up to 60% of the overall binder content   was used to produce green HPC but the remaining 40% of Portland cement (OPC) still causes emission of greenhouse gases. The use of geopolymer to substitute OPC in the production of HPC can potentially reduce CO_2 emissions by 0.836 ton of CO_2 per ton of binder replaced (OPC generates 1 ton CO_2 per ton of binder; geopolymer generates 0.164 ton CO_2 per ton of binder) [11]. So far, no research has reported the synthesis of geopolymers using TPOFA as the source material, indicating the innovative nature of this research.

Ariffin et al. [12] reported the production of geopolymers using untreated POFA combined with pulverized fuel ash (PFA) which was reacted with an alkaline activator at a ratio of 30:70 (POFA :PFA); producing geopolymer with compressive strength of 30 MPa after 28 days of curing. Therefore, this work presents the first

International Science and Technology Journal
Technology Journal
المجلة الدولية للعلوم والتقنية

العدد 26
Volume 26

المجلة الدولية للعلوم والتقنية
International Science and Technology Journal
ISTJ

effort to explore and quantify the potential application of TPOFA-based geopolymer mortar. The use of high amounts of TPOFA will also help reduce CO_2 emission, preserve natural resources as well as protect human health. Thus, the motivation of this research can be summarized as follows: [i] innovation by synthesizing geopolymers using high volume of TPOFA which has not been reported in the existing literature, and [ii] reuse industrial waste i.e. TPOFA through geopolymer technology to convert industrial by-products into useful materials. Subsequently, this effort could be very useful for environmental protection purposes by minimizing the burden of landfills as well as providing alternative binders to meet the increase in demand for ordinary Portland cement. This scenario has created great interest among researchers, especially those from palm oil producing countries.

One of the biggest advantages of geopolymer synthesis, which may very likely be its greatest weakness as well, is that the raw materials used in synthesizing geopolymers are incredibly diverse as it can be produced using different materials [13, 14] and there are only few restrictions imposed on the purity, particle size, composition or morphology of the materials. As suggested by previous researchers e.g. Duxson et al. [15], more efforts should be made to investigate the geopolymers induced under some particular reaction conditions, such as utilization of new raw materials and low temperature synthesis. Therefore, this research is focused on geopolymer development by utilizing cheap and plentiful aluminosilicate material or industrial by-products (TPOFA) to fabricate products with excellent mechanical and physical properties. This green geopolymer (TPOFA-based geopolymer mortar) is currently being developed at Universiti Sains Malaysia (USM) based on the most acceptable synthesis properties.

2. Materials and Methods
2.1.1 Source material
The collected raw POFA from a palm oil mill in Nibong Tebal, Penang, Malaysia was treated to form (TPOFA). The treatment process was followed as per previous research [10]. The final form of TPOFA as dry source material is shown in Fig. 1. The chemical

International Science and
Technology Journal
المجلة الدولية للعلوم والتقنية

العدد 26
Volume 26

المجلة الدولية للعلوم والتقنية
International Science and Technology Journal
ISTJ

and physical properties of the TPOFA in this study are provided in Table 1. TPOFA particles are mostly crushed particles, irregular and angular in shape, as shown in Fig 2. The particle size distribution curve of TPOFA is shown in Fig.3. Treated POFA is classified as a class F mineral admixture according to ASTM C618 [16].

Table 6: Chemical compositions analysis using XRF technique and physical properties of TPOFA [10].

Chemical	Component (%)
SiO_2	61.33
Al_2O_3	7.018
Fe_2O_3	5.11
CaO	8.20
MgO	4.69
P_2O_5	4.55
K_2O	6.50
SO_3	0.27
TiO_2	0.25
MnO	0.097
Na_2O	0.123
C	1
Physical properties	
Specific surface area (m^2/g)	1.775
Loss on ignition (%)	2.53
Median particle size (µm)	2.06

Figure 1: The treated POFA (TPOFA)

International Science and Technology Journal
المجلة الدولية للعلوم والتقنية

العدد 26
Volume 26

المجلة الدولية للعلوم والتقنية
ISTJ
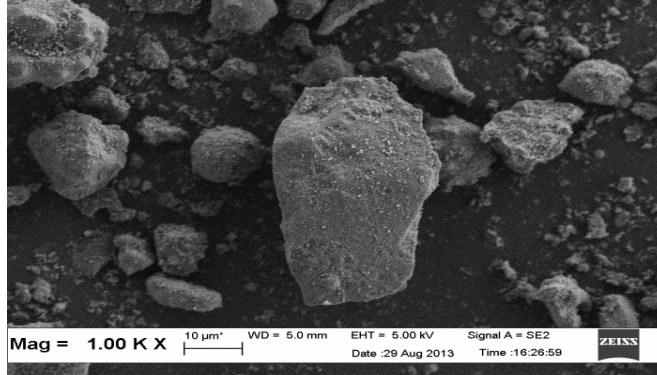
Figure 2: TPOFA particle shape analysed using SEM technique
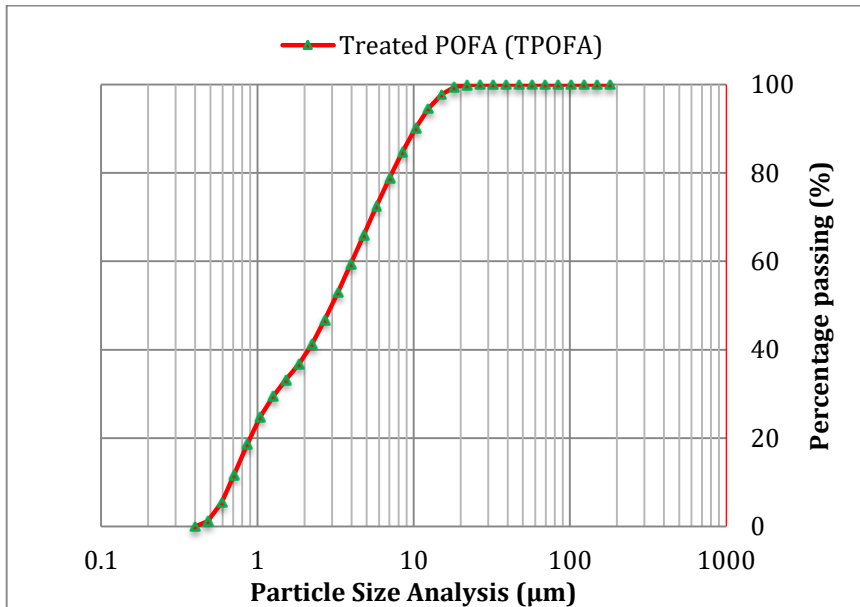
Figure 3: Particle size analysis of TPOFA

2.1.2 Alkaline activator

The NaOH pellets and Na_2SiO_3 were utilized to prepare a composite of alkaline activator solution. The NaOH as an analytical grade in pellet form, with 98% purity. The commercial Na_2SiO_3 with less transparent in viscous liquid form, consists of 14.7% Na_2O, 29.4% SiO_2, and 55.9% H_2O with a specific gravity

of 1.53 g/cm^3 at 20°C and a silica modulus (Ms, where Ms = SiO$_2$/Na$_2$O) of 2 was used.

2.1.3 Aggregate

The river sand passing through a 1.18 mm sieve and retained on a 150 μm sieve, with a fineness modulus of 2.8 and specific gravity of 2.65 was used for the mixes

2.2 Design of Mixtures

The mixture consists of dry source material TPOFA, alkaline activator, and sand. The ratio and the concentration of the alkaline activator preparation were chosen based on previous researches [10]. The prepared alkaline activator was more viscous, which make the fresh mix cohesive and sticky. Therefore, the fresh properties of the mix were enhanced via added water was used with a 5% by weight ratio of geopolymer paste [17]. However, an increase in water content in the mix increases the workability and reduces the compressive strength results. To solve this matter the calculated amount of additional water was prepared as 8 M NaOH concentration. All of the geopolymer mortar samples were made with sand to solid material weight ratios of 1.5, as described in Table 2.

Table 2: Mixture proportions of TPOFA-based geopolymer mortar (Kg/M^3)

TPOFA (kg)	Sand (kg)	Na-silicate (kg)	10 M NaOH (kg)	Add water (kg)
761.831	1,142.745	253.757	102.303	55.994

2.3 Specimens Preparation

The mixture consist of source material and alkaline activator solution. The dry source material of TPOFA was weighed. Then, the alkaline activator solution was prepared as described in our previous research work [10] and measured as per the design mixture described in Table.2. After the solution was prepared, the sand was weighed. Thereafter, a Hobart N50 paddle mixer was

used to produce the geopolymer as illustrated ASTM C305 [18]. Two speed selection transmission i.e. low speed and medium speed of 140± 5 and 285 ± rpm, with a planetary motion of approximately 62 rpm and 125 rpm, respectively. The TPOFA was mixed for 30 seconds at low speed to evenly distribute it in the bowl. Then, the activator solution was added and mixed for 30 seconds at low speed. Sand was slowly added into the mix and followed by 30 seconds mixing at low speed. The mixer was stopped, change to medium speed and mixing process continued for 1.5 Minutes. The mixing was stopped for 15 seconds and the mix was manually scraped from the bowl sides and paddle. The mixing process was continued at medium speed for 1 minute. Right after the mixing, the workability of the fresh geopolymer mortar was determined using a Flow Table. The Flow test was carried out as per ASTM C1437 [19].

After the flow test, the fresh mortar was cast into 50 mm x 50 mm x 50 mm steel molds in two layers. The specimen was compacted using the method described in ASTMC109 [20]. This was followed by an additional vibration of 10 s using a vibrating table. The specimens were wrapped with cling film to avoid moisture evaporation, allowed to stand for 1 h at 25 °C and then cured at 70ºC for 24h [21]. Finally, the specimens were left under room temperature maintained at 23±2 °C, 70% relative humidity until it was time for testing.

2.4 Specimens analysis

The specimens were tested for compressive strength according to ASTM C109M [20]. The test was performed on three specimens from each mixture. The specimen at age of 28 days was also analyzed by X-ray diffraction (XRD), Fourier transforms infrared spectroscopy (FTIR), Thermogravimetric analysis/Differential thermal analysis TGA/DTA analysis, and Field Emission Scanning Electron Microscopy (FESEM) with energy dispersive X-ray (EDX) analysis. XRD was used to determine the phases present in the specimen. Analysis was carried out using XRD machine (Bruker D8 Advance) with CuKα radiation (1.5406 Å) from 10 to 90 of 2θ°. Diffraction patterns were then analysed using Expert HighScorePlus software. FTIR was used to identify the different

International Science and Technology Journal
المجلة الدولية للعلوم والتقنية

العدد 26
Volume 26

المجلة الدولية للعلوم والتقنية
International Science and Technology Journal
ISTJ

types of chemical bonds in the materials on a molecular level. For FTIR, the equipment used was Perkin-Elmer Spectrum One. Approximately 5 mg of powdered specimen was mixed with 95 mg of potassium bromide (KBr) and ground using an agate mortar and pestle. The powder was pressed for 2 min under 2.758 MPa using hydraulic pressing to prepare the translucent pellets which were then inserted into the infrared spectrometer. The infrared spectra were recorded in the range of 400-4000 cm^{-1}. FESEM with EDX analysis was performed on the fractured surface of the specimen. The FESEM machine (model Zeiss Supra 35 VP) was used to characterize the specimen. Each specimen was mounted on a specimen holder using carbon tape. The specimen was then coated with gold to enhance image resolution and avoid electrostatic charging. The coated specimen was then placed inside the FESEM specimen chamber for character analysis. TGA/DTA analysis was used to analyze the thermal behaviors of TPOFA-based geopolymer mortar powdered specimen to ensure the achievement of thermal equilibrium during transient heating [22]. Simultaneous TGA and DTA were performed using an instrument called Shimadzu DTG-60/60H. 15-20 mg of the specimen was placed in a platinum pan and heated to nitrogen atmosphere from 25 °C to 1000 °C at 10 °C/min in the same gas environment.

3. Results and discussion
3.1 Workability and Strength of TPOFA-based geopolymer mortar

Fig. 4 shows that the flow of TPOFA-based geopolymer mortar (TPOFAGM) was in the range of 155 ± 5%. In contrast, several other authors reported placement difficulties related to the low workability of geopolymeric mortars which were produced using different source materials such as metakaolin, slag, fly ash, and lignite bottom ash with flow ranges between 110 ± 5%–135 ± 5% [17, 23-26]. Therefore, this could be linked to the particle shape which has a significant effect on particle-fluid interaction. The dispersion and turbulence modulation characteristics for non-spherical particles may be significantly different from spherical particles.

International Science and
Technology Journal
المجلة الدولية للعلوم والتقنية

العدد 26
Volume 26

ISTJ

Figure 4: Flow table used to measure the workability of TPOFA-based geopolymer mortar

The compressive strength development with curing time of TPOFA-based geopolymer mortar is shown in Fig 5. The compressive strength increased with the increase in curing age. The strength at 1 day curing time was 19 MPa which is about 70% of the total strength. High compressive strength observed in TPOFA-based geopolymer mortar was linked to the advantages of flow of mixture obtained in the range of $155 \pm 5\%$. This value is far better than those obtained when using other source materials to produce geopolymer. For example, kaolin-based geopolymers only gained 6 MPa at 180 days of curing [27], while other recent research which used kaolin-based geopolymers only gained 15 MPa after 28 days curing [28]. In addition, geopolymers produced using tungsten mine waste mud gained only 1-3 MPa after 42 days [29] curing. Moreover, the synthesis of geopolymer from mixture of red mud and rice husk ash only gained compressive strength in the ranges from 3.2 to 20.5 MPa between the ages of 14-49 days [30] and the synthesis of geopolymer from biomass fly ashes gain a compressive strength of 18 MPa after 10 days [31]. Hence, the geopolymerization result from the TPOFA-based geopolymer mortar as compared to geopolymerization resulted from different raw materials is far better, owing to the fact that the starting raw materials play a significant role in the geopolymerization result and affect the mechanical properties and microstructure of the final

geopolymer products. Theoretically, the Si–O–Si bonds are stronger than those of Si–O–Al and Al–O–Al [32], implying that the strength of geopolymers should increase with the Si/Al ratio because the density of the Si–O–Si bonds increases with the Si/Al ratio [30].
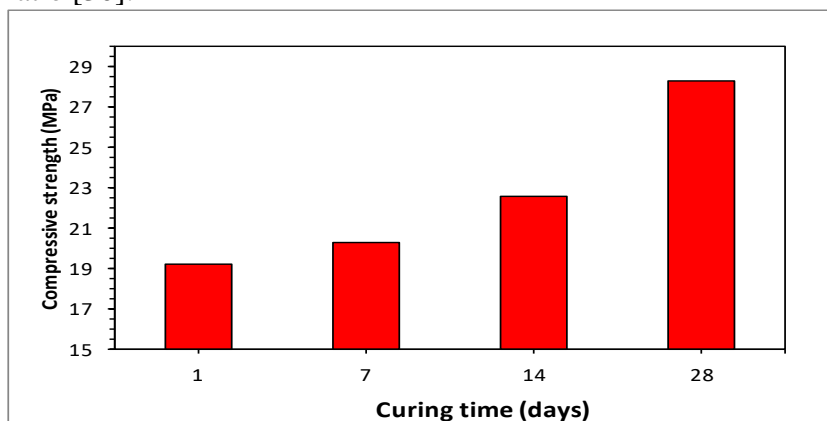
Figure 5: Compressive strength of the investigated specimens TPOFA-based geopolymer mortar

3.2 Chemical Bond Development Analysis Using FTIR

Fig. 6 is the FTIR analysis for the source material TPOFA (Fig.6a) and alkali-activated TPOFA products (Fig. 6b). The two different spectra can be easily distinguished from one another. TPOFA exhibiting a broad band around ~1,103 cm^{-1} is associated with the asymmetric stretching of Si–O–Si bonds of SiO$_2$, along with a vibration mode at ~474 cm-1 attributed to the bending of Si–O–Si and O–Si–O bonds [33]. A band at 693 and 713 cm^{-1} is associated with the asymmetric vibration mode of the quartz double band [34], a band at 795 cm-1 is attributed to the bending vibration mode of the Si–O–Si bonds [35], a band at 875 cm-^{1} is associated with the asymmetric vibration mode of the Al-O-H [36], a band at ~1,445 cm^{-1} is associated with the asymmetric vibration mode of the O–C–O bonds in carbonates, while a band at 3600–2200 cm^{-1} is attributed to the stretching vibration mode of the (–OH, HOH) [37].

The differences between the FTIR absorption frequencies for the source material TPOFA and TPOFA-based geopolymer mortar

International Science and Technology Journal
المجلة الدولية للعلوم والتقنية

العدد 26
Volume 26

المجلة الدولية للعلوم والتقنية
International Science and Technology Journal
ISTJ

products could provide evidence of effective geopolymerization in this study, as indicated in Fig. 6 (a,b). The vibration band at 474 cm^{-1} shifted to a lower frequency in the ~455 cm^{-1} region and is attributed to Si–O bending vibrations (N-A-S-H) which provides an indication of the degree of ''amorphisation'' of the material, since its intensity does not depend on the degree of crystallisation [38, 39]. New weaker vibration bands at ~604 cm^{-1} and ~ 776 cm^{-1} are attributed to the bending vibration mode of the Si–O–Al [38]. While the vibration band at ~880 cm^{-1} is attributed to sodium bicarbonate deformation band [34]. The strongest vibration at 1103 cm^{-1} in TPOFA shifts to lower frequencies at 1012 cm^{-1} due to asymmetric stretching (Si–O–Si and Al– O–Si) bonds , Si–O stretching, and OH bending (Si–OH) in TPOFA-based geopolymer mortar products [40]. FTIR spectroscopy is, however, a possible and simple method for the monitoring of geopolymerization reactions and formation of hard structure. The common atmospheric carbonation of the geopolymer was revealed by the band centered at 1500–1400 cm^{-1}, which indicated the appearance of O–C–O stretching vibrations. Another interesting finding related to geopolymerization includes the significant bands located at approximately 3467 cm^{-1} and 1648 cm^{-1} for the O–H, H-O-H stretches and H–O–H bending, respectively [37].
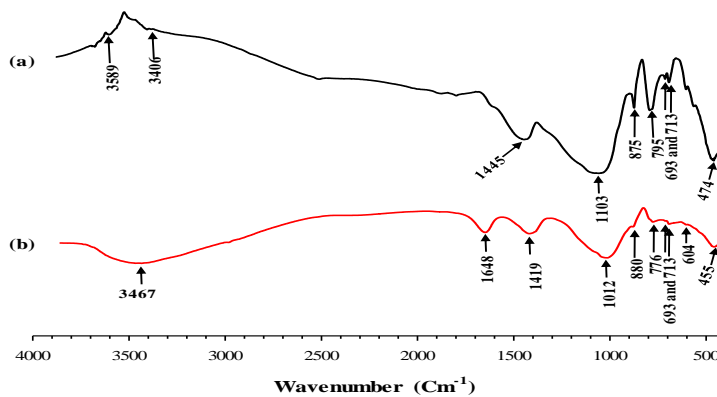
Figure 6: The FTIR analysis for (a) TPOFA and (b) TPOFA-based geopolymer mortar

3.3 Mineralogical analysis

X-ray diffraction patterns irrespective of the material studied (original or activated TPOFA) are shown in Fig. 7. The phases found in raw TPOFA are similar to those in XRD patterns observed by previous researchers [10, 21]; they contain quartz, cristobalite, and $K_3Al_2(PO_4)_3$ as shown in Fig. 7a. However, the XRD diffractograms of the alkali-activated TPOFA, as shown in Fig. 7b, indicate the formation of two phases during the geopolymer synthesis. The characteristic peaks observed corresponded to quartz (ICSD no. 98-010-7204) and anorthite (ICSD no. 98-002-1580). An important deduction that can be made from the presence of the main significant phase i.e. anorthite is that it indicates the formation of high quality binder [41]. A binding matrix derived from the tecto-aluminosilicate containing Na and Ca obtained by reacting source material TPOFA with alkaline activator characterized by the chemical formula $(Na_{.45}Ca_{.55})(Al1_{.55}Si_{2.45}O_8)$ (sodium calcium tecto-alumosilicate) 3-dimensional structures. Preferably, the tecto-aluminosilicate cement should contain at least one alkali hydroxide [42].

XRD analysis indicated that the dissolution of calcium promoted an ion exchange process with sodium from the 3D aluminosilicate network; this explains the formation of gel binder sodium calcium tecto-alumosilicate in the TPOFA-based geopolymer mortar. The calcium dissolution behaviour was also reported by Rowles and O'Connor [43] who observed the solubility of Ca in the Na_2SiO_3 activating solution and the consequent presence of this element in the geopolymeric gel. Indeed, the TPOFA contains calcium and during the dissolution/polycondensation phase, Ca leached out of the Ca-containing precursor particles readily and was incorporated into the matrix. This is generally attributed to the 3D aluminosilicate gel [44].

International Science and
Technology Journal
المجلة الدولية للعلوم والتقنية

العدد 26
Volume 26

المجلة الدولية للعلوم والتقنية
ISTJ
International Science and Technology Journal
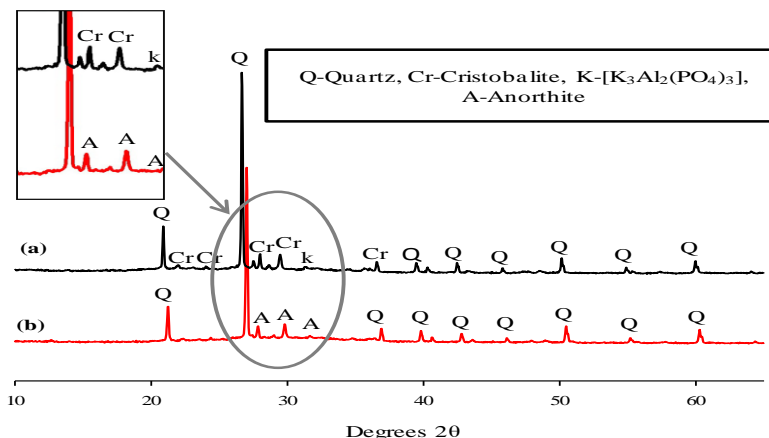
Figure 7: X-ray diffraction patterns of (a) source material TPOFA, and
(b) TPOFA-based geopolymer mortar

3.4 FESEM-EDX analysis

Fig 8a. shows a micrograph of the surface of TPOFA-based geopolymer mortar specimen at 28 days. It is clear that the geopolymer microstructure is quite dense with minimal microcracks. EDX microanalyses on specific specimen indicate the presence of various elements i.e. Na, Ca, Si, Al, and O. Therefore, the binder gel was the result of the bond-formation between all of these elements.

The micrograph also shows the formation of needle crystals. As shown in Figure 8b, the SEM analysis for the needle-like crystals containing mainly SiO_2 with small amount of Ca and Na. However, previous work [44] reported that these are mainly rich in Na and Ca by EDX analysis and they are probably carbonates. The needle crystals were also indicated in other research and there was no explanation provided [45].

The observation from XRD, FTIR, and FESEM-EDX is very well correlated and explains the formation of gel binder sodium calcium tecto-aluminosilicate in the TPOFA-based geopolymer mortar. This gel binder is responsible for the high compressive strength which was proven in the experimental works.

International Science and Technology Journal
المجلة الدولية للعلوم والتقنية

العدد 26
Volume 26

المجلة الدولية للعلوم والتقنية
International Science and Technology Journal
ISTJ
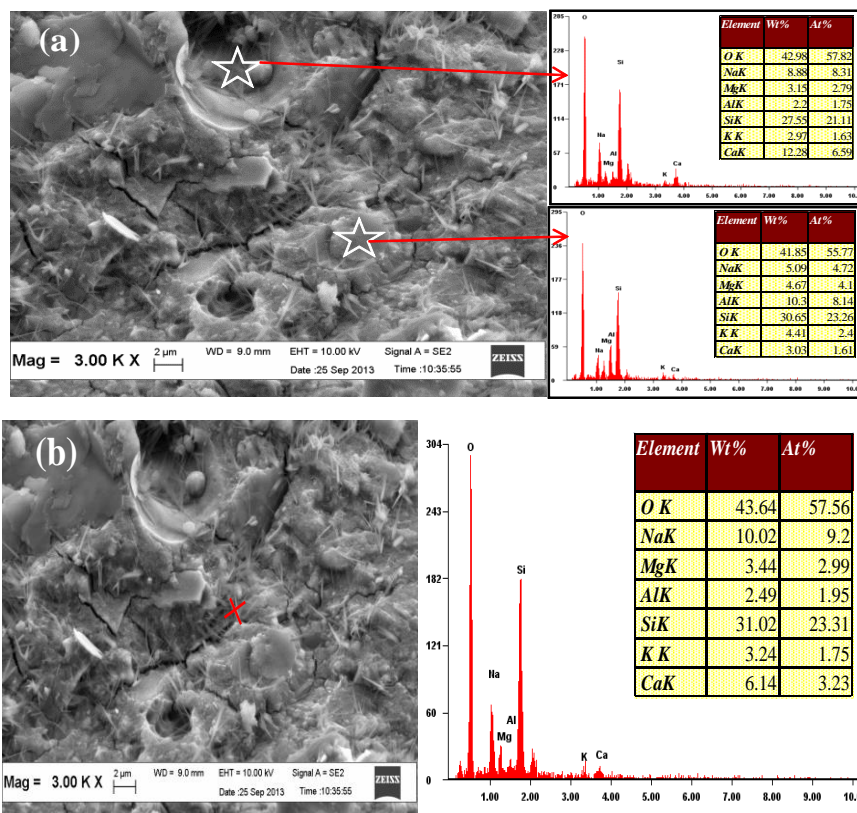
Figure 8 (a and b): SEM-EDX results of TPOFA based geopolymer mortar

3.4 Thermogravimetry result

TGA/DTA was used to determine water evaporation rates and predict damage of inorganic polymer structure under specific heating conditions. Fig 9 shows the results of the TGA/DTA analysis of the TPOFA-based geopolymer mortar specimen cured at 70 °C for 24 hours followed by 28 days curing at room temperature. The decrease in weight peaked at the 72 °C , as indicated by the DTG curve, belongs to the loss of some volatile materials from the dehydration/dehydroxylation process. The derivative weight loss curves in the range of 25-100 °C indicated by TGA was approximately 17.5%. Additional weight loss at the thermal interval between 100 °C and 600°C with a weight loss

International Science and
Technology Journal
المجلة الدولية للعلوم والتقنية

العدد 26
Volume 26

المجلة الدولية للعلوم والتقنية
International Science and Technology Journal
ISTJ

percentage of 8.9%, belongs to organic matter volatilization, and dehydration/dehydroxylation process [46]. Total deterioration of tecto-aluminosilicate main gel binder occurs at the region between 600-800 °C, as indicated by the DTA curve. The percentage of weight loss for the tecto-aluminosilicate gel binder was 3.3%, as calculated by TGA. The total percentage of weight remaining after exposure at 1000 °C was ~69%. The details of weight loss are given in Table 3.

These results reflect the high quality of TPOFA-based geopolymer mortar binder production and its thermal stability under exposure to temperatures up to 600 °C [10]. It should be emphasized that TGA curves in Fig. 9 are of a smooth nature. No peaks were observed which proves the absence of hydrates in the crystalline form, e.g. $Ca(OH)_2$ or $CaCO_3$.

Table 3: Mass loss at different temperature ranges based on TGA analysis

Temperature (ºC)	25-100	100-200	200-300	300-400	400-500	500-600	600-800	800-1000
Wt. Loss (%)	17.490	3.667	1.657	1.431	1.196	0.873	3.295	0.588
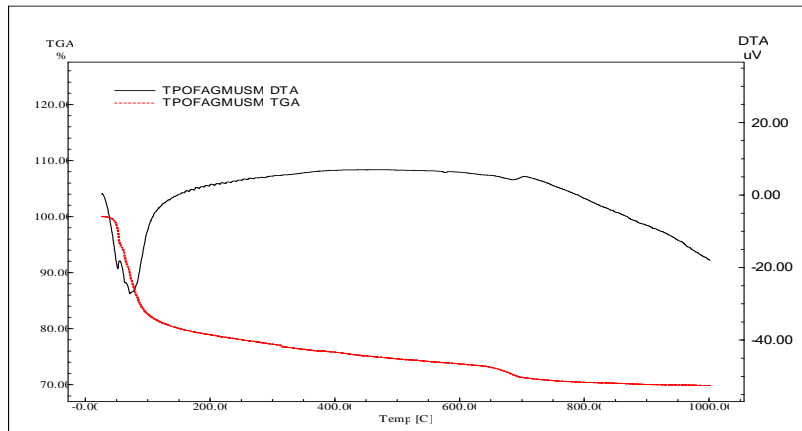
Figure 9: TGA and DTA results of TPOFA-based geopolymer mortar

International Science and Technology Journal
المجلة الدولية للعلوم والتقنية

العدد 26
Volume 26

المجلة الدولية للعلوم والتقنية
International Science and Technology Journal
ISTJ

4. CONCLUSION

The production of TPOFA-based geopolymer mortar in this research achieved greater utilization of industrial waste (TPOFA) to produce a green geopolymer with highly workable mixture and high compressive strength (19 MPa) in only 1 day. The use of analytical techniques (XRD, FESEM-EDX, and FTIR) provided useful information regarding the quality, morphology, and characteristics of the gel formation of the tecto-aluminosilicate binder. In addition, the stability of this tecto-aluminosilicate binder at elevated temperature of up to 800 ℃ was confirmed by DTA/TGA analysis.

References

[1] M.S. Salwa, A.M. Al Bakri, H. Kamarudin, C. Ruzaidi, M. Binhussain, S.S. Zaliha, Review on Current Geopolymer as a Coating Material, Australian Journal of Basic and Applied Sciences 7(5) (2013) 246-257.

[2] J. Davidovits, 30 years of successes and failures in geopolymer applications. Market trends and potential breakthroughs, Keynote Conference on Geopolymer Conference, 2002.

[3] J. Van Jaarsveld, J. Van Deventer, L. Lorenzen, The potential use of geopolymeric materials to immobilise toxic metals: Part I. Theory and applications, Minerals Engineering 10(7) (1997) 659-669.

[4] M. Ibrahim, M. Maslehuddin, An overview of factors influencing the properties of alkali-activated binders, Journal of Cleaner Production (2020) 124972.

[5] M.A. Megat Johari, A.M. Zeyad, N. Muhamad Bunnori, K.S. Ariffin, Engineering and transport properties of high-strength

green concrete containing high volume of ultrafine palm oil fuel ash, Construction and Building Materials 30(0) (2012) 281-288.

[6] N.M. Altwair, M.A. Megat Johari, S.F. Saiyid Hashim, Flexural performance of green engineered cementitious composites containing high volume of palm oil fuel ash, Construction and Building Materials 37(0) (2012) 518-525.

[7] W. Tangchirapat, T. Saeting, C. Jaturapitakkul, K. Kiattikomol, A. Siripanichgorn, Use of waste ash from palm oil industry in concrete, Waste management 27(1) (2007) 81-88.

[8] O.M.M. Elbasir, M.A. Megat Johari, Z.A. Ahmad, Effect of fineness of palm oil fuel ash on compressive strength and microstructure of alkaline activated mortar, European Journal of Environmental and Civil Engineering 23(2) (2019) 136-152.

[9] M. Ibrahim, M.A. Megat Johari, M. Maslehuddin, M.K. Rahman, B.A. Salami, H.D. Mohamed, Influence of composition and concentration of alkaline activator on the properties of natural-pozzolan based green concrete, Construction and Building Materials 201 (2019) 186-195.

[10] M.J.A. Mijarsh, M.A. Megat Johari, B.H. Abu Bakar, Z.A. Ahmad, A.M. Zeyad, Influence of SiO2, Al2O3, CaO, and Na2O on the elevated temperature performance of alkali-activated treated palm oil fuel ash-based mortar, Structural Concrete 22 (2021) E380-E399.

[11] J.P. Hos, P.G. McCormick, L.T. Byrne, Investigation of a synthetic aluminosilicate inorganic polymer, Journal of materials science 37(11) (2002) 2311-2316.

[12] M. Ariffin, M. Bhutta, M. Hussin, M. Mohd Tahir, N. Aziah, Sulfuric acid resistance of blended ash geopolymer concrete, Construction and Building Materials 43 (2013) 80-86.

[13] A.M. Rashad, A comprehensive overview about the influence of different additives on the properties of alkali-activated slag – A guide for Civil Engineer, Construction and Building Materials 47(0) (2013) 29-55.

[14] A.M. Rashad, Alkali-activated metakaolin: A short guide for civil Engineer – An overview, Construction and Building Materials 41(0) (2013) 751-765.

International Science and
Technology Journal
المجلة الدولية للعلوم والتقنية

العدد 26
Volume 26

المجلة الدولية للعلوم والتقنية
International Science and Technology Journal
ISTJ

[15] P. Duxson, J.L. Provis, G.C. Lukey, S.W. Mallicoat, W.M. Kriven, J.S. Van Deventer, Understanding the relationship between geopolymer composition, microstructure and mechanical properties, Colloids and Surfaces A: Physicochemical and Engineering Aspects 269(1) (2005) 47-58.

[16] ASTM-C618, Standard Specification for Coal Fly Ash and Raw or Calcined Natural Pozzolan for Use as a Mineral Admixture in Concrete, Annual Book of ASTM Standards 04(02) (2005) 310-313.

[17] P. Chindaprasirt, T. Chareerat, V. Sirivivatnanon, Workability and strength of coarse high calcium fly ash geopolymer, Cement and Concrete Composites 29(3) (2007) 224-229.

[18] A.-C. 305, Standard Practice for Mechanical Mixing of Hydraulic Cement Pastes and Mortars of Plastic Consistency, AMERICAN SOCIETY FOR TESTING AND MATERIALS 1-3.

[19] ASTMC1437, Standard Test Method for Flow of Hydraulic Cement Mortar, (2013).

[20] ASTM-C109/C109M, Standard Test Method for Compressive Strength of Hydraulic Cement Mortars (Using 2-in. or [50-mm] Cube Specimens), Annual Book of ASTM Standards 04(01) (1999) 1-6.

[21] M.J.A. Mijarsh, M.A. Megat Johari, Z.A. Ahmad, Synthesis of geopolymer from large amounts of treated palm oil fuel ash: Application of the Taguchi method in investigating the main parameters affecting compressive strength, Construction and Building Materials 52(0) (2014) 473-481.

[22] A.M. Al Bakri, H. Kamarudin, M. Bnhussain, I.K. Nizar, A. Rafiza, Y. Zarina, THE PROCESSING, CHARACTERIZATION, AND PROPERTIES OF FLY ASH BASED GEOPOLYMER CONCRETE, Rev. Adv. Mater. Sci 30 (2012) 90-97.

[23] D. Moura, E. Vasconcelos, F.P. Torgal, Y. Ding, Concrete repair with geopolymeric mortars: influence of mortars composition on their workability and mechanical strength, (2011).

[24] A. Sathonsaowaphak, P. Chindaprasirt, K. Pimraksa, Workability and strength of lignite bottom ash geopolymer mortar, Journal of hazardous materials 168(1) (2009) 44-50.

[25] M. Palacios, F. Puertas, Effect of superplasticizer and shrinkage-reducing admixtures on alkali-activated slag pastes and mortars, Cement and concrete research 35(7) (2005) 1358-1367.

[26] J.I. Escalante-García, A.V. Gorokhovsky, G. Mendoza, A.F. Fuentes, Effect of geothermal waste on strength and microstructure of alkali-activated slag cement mortars, Cement and concrete research 33(10) (2003) 1567-1574.

[27] C.Y. Heah, H. Kamarudin, A.M. Mustafa Al Bakri, M. Bnhussain, M. Luqman, I. Khairul Nizar, C.M. Ruzaidi, Y.M. Liew, Study on solids-to-liquid and alkaline activator ratios on kaolin-based geopolymers, Construction and Building Materials 35(0) (2012) 912-922.

[28] A.D. Hounsi, G.L. Lecomte-Nana, G. Djétéli, P. Blanchart, Kaolin-based geopolymers: Effect of mechanical activation and curing process, Construction and Building Materials 42(0) (2013) 105-113.

[29] I. Silva, J.P. Castro-Gomes, A. Albuquerque, Effect of immersion in water partially alkali-activated materials obtained of tungsten mine waste mud, Construction and Building Materials 35 (2012) 117-124.

[30] J. He, Y. Jie, J. Zhang, Y. Yu, G. Zhang, Synthesis and characterization of red mud and rice husk ash-based geopolymer composites, Cement and Concrete Composites 37(0) (2013) 108-118.

[31] R. Rajamma, J.A. Labrincha, V.M. Ferreira, Alkali activation of biomass fly ash–metakaolin blends, Fuel 98(0) (2012) 265-271.

[32] B.H.W.S. De Jong, G.E. Brown Jr, Polymerization of silicate and aluminate tetrahedra in glasses, melts, and aqueous solutions—I. Electronic structure of H6Si2O7, H6AlSiO71−, and H6Al2O72−, Geochimica et Cosmochimica Acta 44(3) (1980) 491-511.

[33] S. Bernal, E. Rodríguez, R. Mejia de Gutiérrez, J. Provis, S. Delvasto, Activation of Metakaolin/Slag Blends Using Alkaline Solutions Based on Chemically Modified Silica Fume and Rice Husk Ash, Waste Biomass Valor 3(1) (2012) 99-108.

[34] M. Criado, A. Palomo, A. Fernández-Jiménez, Alkali activation of fly ashes. Part 1: Effect of curing conditions on the

carbonation of the reaction products, Fuel 84(16) (2005) 2048-2054.

[35] T. Bakharev, Durability of geopolymer materials in sodium and magnesium sulfate solutions, Cement and concrete research 35(6) (2005) 1233-1246.

[36] Z. Yunsheng, S. Wei, L. Zongjin, Preparation and microstructure of K-PSDS geopolymeric binder, Colloids and Surfaces A: Physicochemical and Engineering Aspects 302(1–3) (2007) 473-482.

[37] Q. Li, H. Xu, F. Li, P. Li, L. Shen, J. Zhai, Synthesis of geopolymer composites from blends of CFBC fly and bottom ashes, Fuel 97 (2012) 366-372.

[38] V.F.F. Barbosa, K.J.D. MacKenzie, C. Thaumaturgo, Synthesis and characterisation of materials based on inorganic polymers of alumina and silica: sodium polysialate polymers, International Journal of Inorganic Materials 2(4) (2000) 309-317.

[39] I. García-Lodeiro, A. Fernández-Jiménez, A. Palomo, D.E. Macphee, Effect of calcium additions on N–A–S–H cementitious gels, Journal of the American Ceramic Society 93(7) (2010) 1934-1940.

[40] I. García Lodeiro, D.E. Macphee, A. Palomo, A. Fernández-Jiménez, Effect of alkalis on fresh C–S–H gels. FTIR analysis, Cement and concrete research 39(3) (2009) 147-153.

[41] S. Kumar, R. Kumar, S. Mehrotra, Influence of granulated blast furnace slag on the reaction, structure and properties of fly ash based geopolymer, Journal of materials science 45(3) (2010) 607-615.

[42] W. Schwarz, A. Lerat, TECTOALUMINOSILICATE CEMENT AND PROCESS FOR PRODUCING IT, EP Patent 0,500,840, 1999.

[43] M.R. Rowles, B.H. O'Connor, Chemical and Structural Microanalysis of Aluminosilicate Geopolymers Synthesized by Sodium Silicate Activation of Metakaolinite, Journal of the American Ceramic Society 92(10) (2009) 2354-2361.

[44] M.C. Bignozzi, S. Manzi, I. Lancellotti, E. Kamseu, L. Barbieri, C. Leonelli, Mix-design and characterization of alkali

activated materials based on metakaolin and ladle slag, Applied Clay Science 73(0) (2013) 78-85.

[45] A. van Riessen, E. Jamieson, C.S. Kealley, R.D. Hart, R.P. Williams, Bayer-geopolymers: An exploration of synergy between the alumina and geopolymer industries, Cement and Concrete Composites 41(0) (2013) 29-33.

[46] V.N. Castaldelli, J.L. Akasaki, J.L. Melges, M.M. Tashima, L. Soriano, M.V. Borrachero, J. Monzó, J. Payá, Use of Slag/Sugar Cane Bagasse Ash (SCBA) Blends in the Production of Alkali-Activated Materials, Materials 6(8) (2013) 3108-3127.

Overview Study of Cloud Computing and Mobile Cloud Computing

Nuri Abrahem Elshamam

Asmarya Islamic University
nurishammam67@gmail.com

Mohamed Almahdi Eshtawie

Libyan Academy Misurata
eshtawie@yahoo.com

الملخص

تعتبر الحوسبة السحابية المتنقلة مزيج بين الحوسبة السحابية والحوسبة المتنقلة بالإضافة إلى الشبكات اللاسلكية حيث توفر الهواتف الذكية موارد حسابية واسعة لمستخدمي الأجهزة المحمولة، هذا بالإضافة إلى استخدام الحوسبة السحابية لتوصيف مراكز البيانات المتاحة لعديد المستخدمين عبر شبكة الإنترنت. وبذلك أصبحت، الحوسبة السحابية المتنقلة هي السائدة اليوم ، ولها وظائف موزعة على مواقع عديدة من خوادم مركزية. ولهذا رأينا أن نقدم من خلال هذه الورقة دراسة عامة عن الحوسبة السحابية والحوسبة السحابية المتنقلة. على أن تغطي هذه الدراسة نماذج التسليم والنشر للحوسبة السحابية ، بالإضافة إلى السمات الرئيسية للحوسبة السحابية المتنقلة.

Abstract

Mobile cloud computing (MCC) is a combination of cloud computing, mobile computing, and wireless networks. However; due to their capabilities, mobiles bring rich computational resources to mobile users. On the other hand, cloud computing is used to describe data centers available to many users over the internet. Today, large clouds predominant have functions distributed over multiple locations from central servers. This paper presents an overview study of cloud computing and mobile cloud computing. The study covers delivery and deployment models of cloud computing, as well as the main features of mobile cloud computing.

Keywords: cloud computing, MCC, mobile cloud applications.

1. INTRODUCTION

New data storage, processing and display technologies have allowed mobile devices to do nearly anything that had previously been traditionally done with larger personal computers. Moreover; these devices day by day improved in their capabilities, and get dropped in their prices. In contrast, due to mobile devices portability nature, they have limited resources such as computation power, screen size and battery power when compared with personal computers. In recent times, however, the cloud applications have been gaining popularity and there are some really good reasons for the same. It is natural for a beginner or an application novice to be befuddled by the technical jargons that are thrown around, while talking about Mobile Cloud Applications and mobile Cloud Computing. Figure 1 below shows the growth of mobile cloud applications.
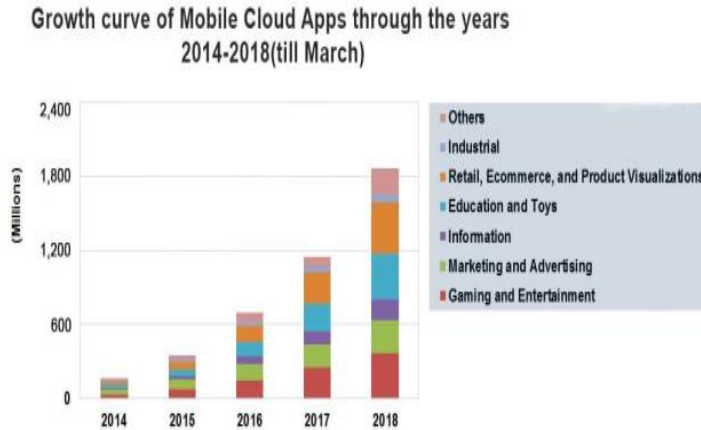
Fig. 1 The growth of mobile cloud applications

2. CLOUD COMPUTING

Cloud computing dates back to the 1950s. It is not a technology, rather it is one of the computing models, and considered as another version of internet technology. Over the years, it has evolved through many phases including grid and utility on-demand

computing. While cloud computing brings great opportunity, it can also introduce challenges for business leaders and IT departments. Inconsistent performance and security problems are the most common disadvantages that continue to affect the perceptions about cloud. It is another version of internet technology. It can provide network resources, CPU, RAM, Storage and Software resources over the web. Cloud computing is characterized with two main models i.e., the delivery models and the deployment models. Figure 2 shows these characteristics.
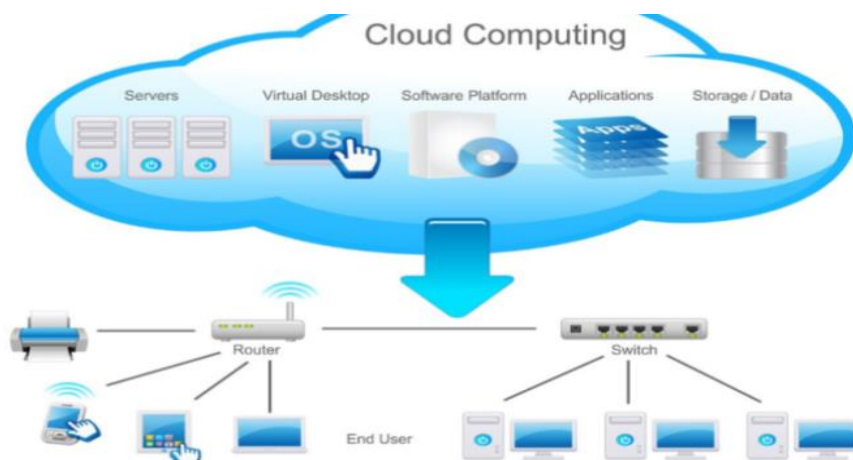
Fig. 2 Cloud computing Characteristics

2.1 DELIVERY MODELS

In cloud computing, delivery models or types are classified into three models based on service delivery.

2.1.1 Infrastructure-as-a-Service (IaaS)

In this model, the service providers allow the client to access the virtual servers in their data center. The clients are able to use virtual servers i.e., the row hardware, in its all without the need of infrastructure maintenance [1].

When compared with the other two delivery service models, IaaS shows the most flexibility inspired from its architecture and usage in other words, the client can enjoy the flexibility as well as the

International Science and
Technology Journal
المجلة الدولية للعلوم والتقنية

العدد 26
Volume 26

المجلة الدولية للعلوم والتقنية
ISTJ

scalability without having to worry about the physical server's maintenance or hardware addition to the existing infrastructure.
Benefits of using IaaS model are:
- No Capital Investments
- Expand as You Grow
- Flexible Options
- Focus on What You Do Best
- Latest and Greatest Technology
- Get Started Immediately
- Anytime, Anywhere Access
- Tight Security Controls

2.1.2 Platform-as-a-Service (PaaS)

This model is different from IaaS in terms of software tools i.e., operating system, database, and some other necessary software tools, that are used to develop and run the software in the cloud. It does not support the client hardware maintenance too. However, the trade off with the PaaS model is that the service providers will lock down the service, and the clients will not be able to use their own developer tools [1].
Benefits of using PaaS model are:
- Innovate Faster
- Focus Resources
- Save Money
- Get the Best Technology
- Stay Up to Date
- Maximize Uptime
- Scale Easily
- Strengthen Security
- Get the Best Support

2.1.3 Software-as-a-Service (SaaS)

Similar to the previous models, the clients in this model does not have to perform any maintenance for the hardware, platform or software. The clients access and use the application software provided. However, this model provides the least flexibility in

comparison with the two other models since the clients can only use the applications and software provided by the provider. The capability provided to the consumer is to use the provider's applications running on a cloud infrastructure. The applications are accessible from various client devices such as a web browser (e.g., web-based email).

Benefits of the SaaS model include

- SaaS is a software distribution model in which a third-party provider hosts application and makes them available to customers over the Internet.
- Flexible payments
- Scalable usage
- Automatic updates
- Accessibility and persistence

2.2 DEPLOYMENT MODELS

National Institute of Standards and Technology NIST defines four cloud deployment models: public clouds, private clouds, community clouds, and hybrid clouds. A cloud deployment model is defined according to where the infrastructure for the deployment resides and who has control over that infrastructure. Deciding which deployment model, you will go with is one of the most important cloud deployment decisions you will make.

Each cloud deployment model satisfies different organizational needs, so it's important that you choose a model that will satisfy the needs of your organization. Perhaps even more important is the fact that each cloud deployment model has a different value proposition and different costs associated with it. Therefore, in many cases, your choice of a cloud deployment model may simply come down to money. In any case, to be able to make an informed decision, you need to be aware of the characteristics of each environment [2].

- **Private Cloud**

The cloud is used or operated by single organization. They are more secure and able to address privacy concern than public cloud. On the other hand; they are more expensive. Such infrastructure may be managed by the organization itself to support various user

International Science and Technology Journal
Technology Journal
المجلة الدولية للعلوم والتقنية

العدد 26
Volume 26

المجلة الدولية للعلوم والتقنية
ISTJ
International Science and Technology Journal

groups, or it could be managed by a service provider that takes care of it either on-site or off-site.

- **Community Cloud**

Community Cloud supports multiple organizations sharing computing resources that are part of a community; examples include universities cooperating in certain areas of research. Members of the community are allowed to access the cloud environment. It may be managed by the organizations or a third party and may exist on premise or off premise.

- **Public Cloud**

Non-mission-critical tasks such as file-sharing, and e-mail service is the public cloud. It supports all users who want to make use of a computing resource, such as hardware (OS, CPU, memory, storage) or software (application server, database) on a subscription basis. The infrastructure is made available to the general public and is owned by an organization selling cloud services.

- **Hybrid cloud**

An interconnected of private and public cloud infrastructure produces Hybrid cloud. It is a composition of two or more clouds i.e., private, community, or public. This model is made used by many organizations when they need to scale up their IT infrastructure rapidly, such as when leveraging public clouds to supplement the capacity available within a private cloud. For example, if an online retailer needs more computing resources to run its web applications during the holiday season it may attain those resources via public clouds.

3. MOBILE CLOUD COMPUTING

The significant increase of mobile subscriptions is due to the rapid advance in mobile computing, wireless technology, and networking. Over the last few years, the Mobile Cloud Computing grows rapidly. One of the key factors contributing to this growth is the growing demand for enterprise mobility. They offer the advantages to users by allowing them to use infrastructure, platforms and software by cloud providers at low cost and elastically in an on-demand fashion [3]. Mobile Cloud Computing

International Science and
Technology Journal
المجلة الدولية للعلوم والتقنية

العدد 26
Volume 26

المجلة الدولية للعلوم والتقنية
International Science and Technology Journal
ISTJ

refers to an infrastructure where both the data storage and data processing happen outside of the mobile device. Mobile cloud applications move the computing power and data storage away from the mobile devices and into powerful and centralized computing platforms located in clouds. The access is done over the wireless connection based on a thin native client. MCC is a Mobile Computing + Cloud Computing.

3.1 MCC Architecture

The operation nature of the MCC gives its entire architecture. In performing its functions, mobile devices are connected to networks via base stations. Those stations establish and control connections and functional interfaces between the networks and mobile devices. In this architecture, information and requests are transmitted to the central processors that are connected to servers providing mobile network services. Cloud controllers process the requests to provide mobile users with the corresponding cloud services. Mobile cloud computing architecture is presented in Figure 3 below.
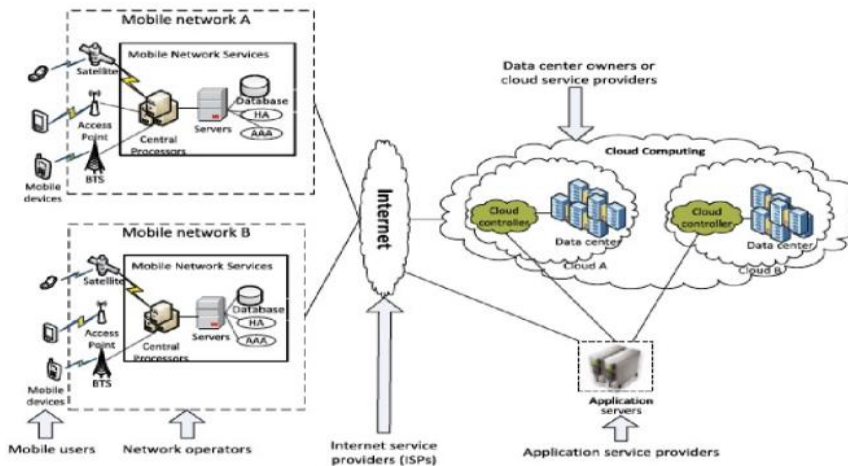
Fig. 3 Mobile Cloud Architecture

3.2 MCC Advantages

Due to its architecture, mobile cloud computing has a significance over other structures [4]. In short, MCC cause to:

International Science and Technology Journal
المجلة الدولية للعلوم والتقنية

العدد 26
Volume 26

ISTJ
المجلة الدولية للعلوم والتقنية
International Science and Technology Journal

- Extending battery lifetime.
- Improving data storage capacity and processing power.
- Improving reliability and availability.
- Dynamic provisioning.
- Scalability.
- Multi-tenancy.
- Ease of integration.

3.3 MCC Disadvantages

On the same way, and due to its nature and architecture, MCC has certain disadvantages i.e., its applications can't use specific devices software and hardware such as GPS, camera, and etc. They can only make use of browser notifications. In addition, Mobile cloud applications are totally cloud dependent and hence, they may suffer from connection problems. They have to deal with connection bandwidth drop problems, connection disconnected problems and etc. [5].

5. CONCLUSION

This paper presents an overview of cloud computing and mobile cloud computing. The delivery and deployment models for cloud computing are discussed in detail. MCC architecture, advantages and disadvantages are presented too. MCC issues including security, data offloading in static and dynamic environments can be done as a future work that must be considered when designing a mobile cloud in order to make sure that non-authorized users will not be able to access sensitive information and data on the cloud.

REFFERENCES

[1] A. Monaca, "A View Inside the Cloud," 7 June 2012. [Online]. Available: http://theinstitute.ieee.org/technology-focus/technology-topic/a-view-inside-the-cloud. [Accessed June 2013].

[2] https://www.ibm.com/cloud/learn/cloud-computing.

[3] Hoang T. Dinh, Chonho Lee, Dusit Niyato, and Ping Wang. "A survey of Mobile Cloud Computing: Architecture,

 حقوق الطبع محفوظة
للمجلة الدولية للعلوم والتقنية

International Science and
Technology Journal
المجلة الدولية للعلوم والتقنية

العدد 26
Volume 26

ISTJ

Applications, and Approaches", Wireless Communication and
Mobile Computing.

[4] M. Tantow, "Cloud Computing and Smartphones," 1 March
2011. [Online]. Available:
http://cloudtimes.org/2011/03/01/cloud-computing-and-
smartphones/. [Accessed 6 June 2013].

[5] B. Claybrook, "Best practices for developing mobile cloud
apps. revealed," October 2012. [Online]. Available:
http://searchcloudapplications.techtarget.com/tip/Best-
pracices-for-devaloping-mobile-cloud-apps-revealed.
[Accessed 10 June 2013].

Performance Study of TCP Variants in FANETs

**Mohamed Meftah Alrayes[1], Adel Dae Elgaber[2], Zayed Khlifa[3],
Abdalrahman alfagi [4]**

Faculty of information Technology[1, 3,4], University Of Zawia, faculty of
Engineering[2], University Of Sabratah
Email : m.alrayes@zu.edu.ly.

الملخص

مع التطبيق الواسع النطاق للشبكات الادهوك Ad-hoc اللاسلكية الجوية
(FANETs), أصبح هدا النوع من الشبكات تحظى باهتمام كبير في مجالي
الصناعة والبحث العلمي في السنوات الأخيرة . ومع تزايد الطلب علي شبكات اللاسلكية
الجوية بحيث يمكن ان يعتمد عليها في تأمين الاتصال و نقل البيانات بين المركبات
الجوية, فأصبحت الأبحاث العلمية في هدا المجال ضرورة ملحة من اجل الوصول الي
تصميم برتوكولات جديدة او استعمال بروتوكولات الحالية والتي يتم استخدامها في أنواع
اخري من شبكات نقل البيانات. معظم الأبحاث العلمية قامت باختبار أداء بروتوكولات
التحكم في توجيه البيانات الموجودة حاليا ولكنها لم تختبر أداء البرتوكولات الخاصة
بالتحكم في نقل البيانات في مجال الشبكات الادهوك Ad-hoc اللاسلكية الجوية.
في هدا البحث و من خلال برنامج محاكاة الشبكة NS-3 تم القيام بالعديد من التجارب
لاختبار أداء مجموعة من بروتوكولات التحكم بالنقل البيانات المعروفة وهم (-TCP
Illions, TCP-High Speed, TCP-Westwood) لمعرفة ما اد اكان يمكن
استخدام أي واحد منهم كبرتوكول التحكم في نقل البيانات ام لا. وقد تم قياس زمن
التأخير (end to end delay) ومعدل الإنتاجية (throughput) تحت تأثير كلا من
تغيرات في عدد المركبات الجوية بدون طيار وتغير في سرعة المركبات الجوية بدون
طيار وتغير في عدد البيانات المرسلة من المرسل الي المستقبل. ومن هذه الدراسة
اتضح لنا ضعف الأداء لهده البرتوكولات من ناحية زمن التأخير وكذلك معدل

الإنتاجية. وبالتالي أصبح من المهم تحسين أداء بروتوكولات نقل البيانات الموجودة حاليا والمستعملة في شبكات اخري او تصميم بروتوكول نقل جديد يلائم خصائص شبكة الادهوك Ad-hoc اللاسلكية الجوية.

Abstract

With the wide-ranging application of flying ad-hoc networks (FANETs), which have received more attention from the industry and research community in recent years. The high demand for continuous network connectivity with reliable and robust communication becomes a challenging research topic. Most researchers investigated the existing routing protocols in the network layer, but there is no attention paid to the transport layer and its associated protocols in FANETs application domain, and it is still an open research issue. In this paper, we examine through simulation scenarios the performance characteristics of three existing TCP (Transmission Control Protocol) congestion controls mechanisms, namely: Westwood, High-speed and TCP-Illinois. The focus is to investigate whether any existing mechanism could provide significant performance benefits over FANETs. To evaluate the performance of our proposed simulation, we use Network Simulator-3 (NS-3) to examine throughput and end-to-end delay metrics under a variety of density (number of UAVs), speed (mobility speed of UAVs) measurement scenarios and number of flows. The simulation results have shown that all those TCP mechanisms have a poor performance in term of throughput and end- to-end delay, hence, none of them can help to provide reliable and guaranteed end-to-end data delivery over an unreliable network.

Keywords: Flying Ad hoc Networks, Transmission Control Protocol, NS-3.

1. Introduction

The research community around the globe paid more attention to ad-hoc networks, in recent years, due to their advantages in wide range of applications such as: military Services, Security maintenance, calamity administration and Search/Rescue Operations.

International Science and
Technology Journal
المجلة الدولية للعلوم والتقنية

العدد 26
Volume 26

المجلة الدولية للعلوم والتقنية
International Science and Technology Journal
ISTJ

The ad-hoc network consists of interconnected links originating from multiple "nodes". Nodes can take the form of systems or devices (e.g. laptops, mobile phones, MP3 player and personal computers etc.). There are three main categories of Ad-hoc network, they are MANET (Mobile Ad-hoc Network), VANET (Vehicular Ad-hoc Network) and FANET (Flying Ad-hoc Network).MANET is formed by a collection of wireless mobile nodes without depending on any infrastructure. Therefore, it has featured by dynamic topology and self-configuration [1, 2].VANET has formed by a collection of moving vehicles and roadside communication infrastructure. The most know application of the VANET is intelligent transportation system where the aim is to improve driving security [3, 4].

FANET is formed in the sky among highly mobile flying nodes (i.e., drones). It has featured by self-configuration and self-organization) [5, 6]. The FANET offers infrastructure less environment with more flexible and dynamic topology. The most known example of FANETs are wireless networks have made by an incorporate a group of UAV (Unmanned Aerial Vehicle).

The UAV offer advantages of small size, low cost, fast motion and working efficiently in both individual and group manners [7]. There are some limitations of UAVs, which discussed in literature for future research work [8, 9]. This includes ensuring reliable connection between the UAVs. The most researchers have investigated the routing protocols in network layer, but there is no attention paid to the transport layer and its associated protocols in FANETs, and it is still an open research issue [10, 11]. In transport layer, there are two main protocols in transport layer, which used intensively in network communication context; they are User Datagram Protocol (UDP) and Transmission Control Protocol (TCP). TCP outperforms UDP in providing more reliable and guaranteed end-to-end data delivery over unreliable network.

Therefore, we will focus on the implementation of Transmission Control Protocols. When the traffic offered to the network exceeds the available capacity then, the congested is occur to the network. Congestion control functions have introduced by Van Jacobson [16], he has proposed three algorithms for congestion control and

avoidance: congestion avoidance (Congestion Avoidance algorithm, also known as Additive Increase/Multiplicative Decrease (AIMD) algorithm,), slow-start and fast retransmission. The improved performance of TCP has focused on the basic mechanism of AIMD with a large congestion window (*cwnd*) [17]. In this paper, we focus on the simulation on TCP protocols at the transport layer and especially on three types of TCP, they are: TCP-Westwood[12], TCP-High-Speed [13], and TCP-Illinois [14]. Up to our knowledge, there is a research gap of not examining the impact of TCP protocols on UAV networking performance within the transport layer.

In this paper, we argue that the simulation of TCP protocols need to be investigate to bridge this gap and to advance the FANETs application domain.

We implemented this simulation by using Network Simulator-3 (NS-3) [15], and we conducted a set of experiments to be further examine the impact of TCP protocols including TCP-Westwood, TCP-High-Speed, and TCP-Illinois. The rest of this paper has organized as follows: section 2, has given an overview on the protocols that have tested in this paper, Section 3 describes the experiments, including the implemented simulation and the experimental setup for the evaluation of the proposed investigating approach. Section 4 discusses the experimental simulation results, while Section 5 concludes the paper.

2. Related Work
Several studies have carried out in the area of TCP protocols and several works have been continuing further [18, 19]. TCP has many variants such as TCP WESTWOOD, TCP-Illions and TCP-highspeed. Where in the congestion control and loss recovery mechanism of TCP variant is different from each other.

2.1 High Speed TCP (HSTCP)
High speed TCP has proposed to enhance the performance of standard TCP over high-speed networks. HSTCP has presented a relation between a packet drop rate and average congestion window, HSTCP follows the basic AIMD algorithm [16], many details are available at [12].

2.2 TCP-Westwood

TCP Westwood [13] is a sender-side modification of the standard TCP; it also has known as TCPW, network with lossy links, it has handled congestion with consideration the possibility of channel losses. TCPW estimates end-to-end bandwidth to set values of cwnd and slow start threshold according to the level
of congestion

2.3 TCP Illinois

TCP Illinois is a sender-side protocol [14], proposed for high-speed networks. It has considered a hybrid congestion control algorithm. It uses both loss packets and delays as congestion signals. It has adjusted the incrementation and decrementation of delay information AIMD.

3-Simulation Setup and Parameters

In this section, we present our simulation parameters and evaluation metrics that used to set up the simulation environment for this research by using Network Simulator-3 (NS-3) [15].

3.1 Simulation Setup

All simulation parameters applied in this simulation environment have given in table1 and the simulation topology has shown in figure1.
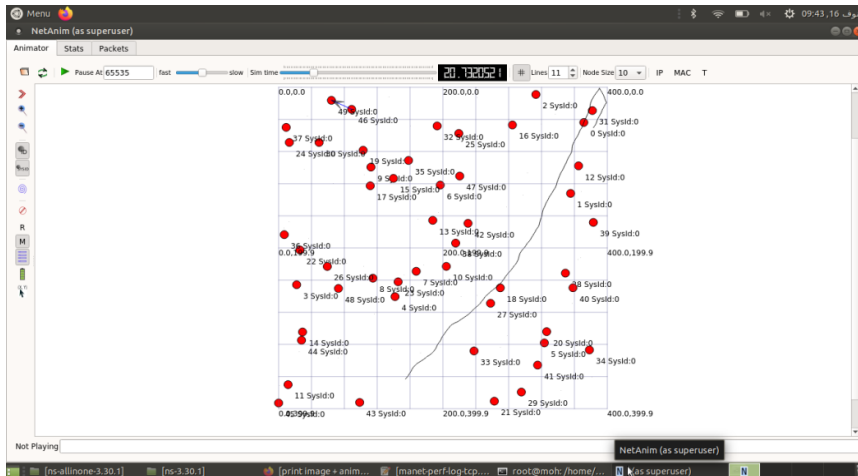
Figure1. Simulation Topology.

International Science and
Technology Journal
المجلة الدولية للعلوم والتقنية

العدد 26
Volume 26

ISTJ

Table1. Simulation Parameters.

Parameter	Value
Application Type	FTP(File transfer protocal).
Number of TCP connections.	5,10,15,20,25.
Routing Protocols.	AODV.
Simulation time.	100 seconds.
Packet Size.	1448 bytes.
Transmission Rate.	100Mbps.
Simulation area.	400m × 400m×100m.
Speed of UAVs	5,10,15,20,25 (m/s).
Number of UAVs	20,30,40,50,60.
Propagation Loss Model	Log Distance Propagation Loss Model.
Propagation Delay	Constant Speed Propagation Delay.
Physical layer	OFDM with 24MBps
Physical Rate	24Mbps.
Mobility model.	Guass Markov
MAC layer.	IEEE 802.11n with 5.
Antenna model.	Omni Antenna.
Rto (retransmission timeout)	1s

3.2 Evaluation Metrics

In this section, we introduce the metrics that used to evaluate the performance of the selected congestion controls protocols.

3.2.1 Average Throughput:-

It is the ratio of the total number of delivered successfully data packets to destinations and the time difference between received data packets and transmitted data packets.

$$\text{Average throughput(kbps)} = \frac{\text{TNSP}}{\text{TR}-\text{TS}} \qquad (1)$$

Where, TR is time of received data packet, TS is time of sent data packet and TNSP is Total number of successfully received data packets.

3.2.2 Average End to End Delay (AEED): -

It is a time difference between total time taken for sending all data packets from source to destination and total number of successfully received data packets (N).

$$\text{AEED (milliseconds)} = \text{End to End Delay} \times 1000 \qquad (2)$$

$$\text{End\_to\_End Delay} = \frac{\text{TDT}}{\text{TNSP}} \qquad (3)$$

Where TDT is the total time have taken for sending all data packets from different sources of UAVs to different UAVs destinations.

$$TDT = TDT + \sum_{i=0}^{N} delay\ [i] \tag{4}$$

$$Delay[i] = TR\ [i] - TS[i] \tag{5}$$

4- Results and Discussion

The simulation experiments have conducted for three different test scenarios as follows:

1) The impact of UAVs density.
2) The impact of UAVs' speeds.
3) The impact of flows' number.

4.1 The impact of UAVs density

To investigate the impact of network density, the number of UAVs have varied from 20 to 60. The maximum speed of mobility of UAVs have fixed to 5 m/s and the number of flows has fixed to 10. The results of this scenario have shown in figures 2 and 3.
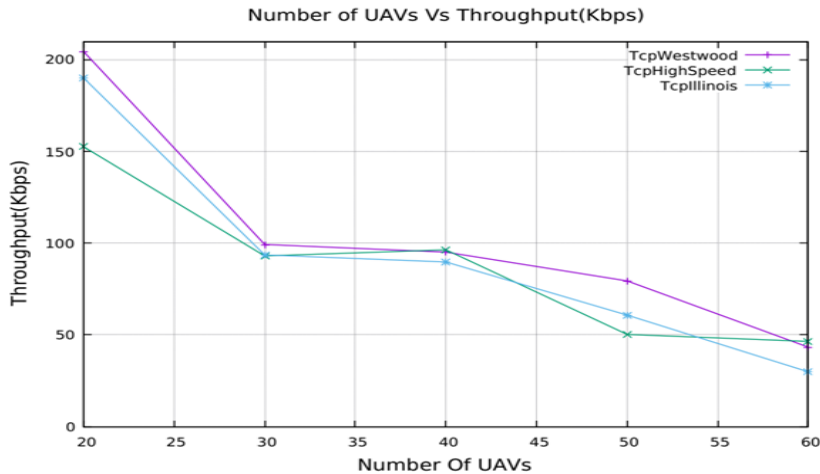
Figure2. Throughput. Vs. Density of UAVs.
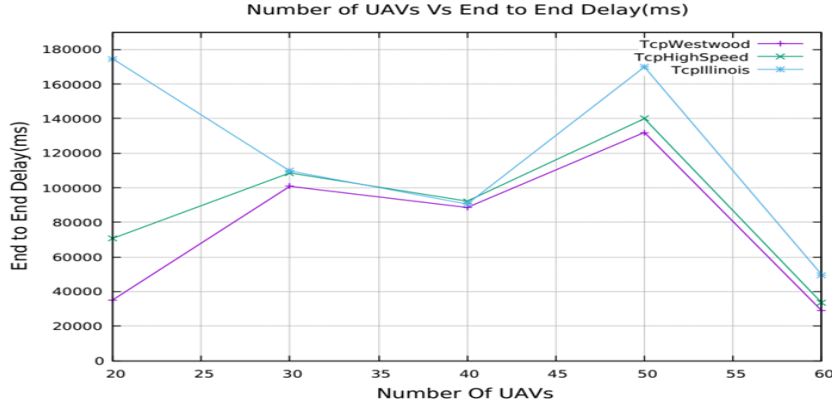
Figure3. End- to-End Delay. Vs. Density of UAVs.

As shown in figure 2, all of them have low throughput, such that, as number of UAVs increase, the throughput decreases in all those protocols, where in the intra-flow TCP or inter-flow can cause in drop data packets and drop in ACK packets. Even then, TCP Westwood achieves a better throughput in compare with TCP High-Speed and TCP Illinois.

It can been seen from figure 3, there are variations in the graph, such that, all those three congestion protocols have high end- to-end delay. During flow packets between end-to-end UAVs, there is a temporal disconnections and reconnections between them, actually short disconnection event can actually stall the TCP transmission for long period, so the data packets will takes long time to reach its destinations.

4.2 The impact of varying speed of UAVs
In this scenario, the effect of the speed of mesh clients has been observed by varying the maximum speed from 5 m/s to 25 m/s with increments of 5 m/s. The number of the flow connections between source and destination has fixed to 10, and number of UAVs is fixed to 40. The results of this scenario have shown in figures 4 and 5. Figure 4, shows that throughput degrade with the increase in speed of mesh clients. The reason for this is that movement of UAVs results in route breaks and make network partitions, and it is clear those protocols did not handle these issues properly.
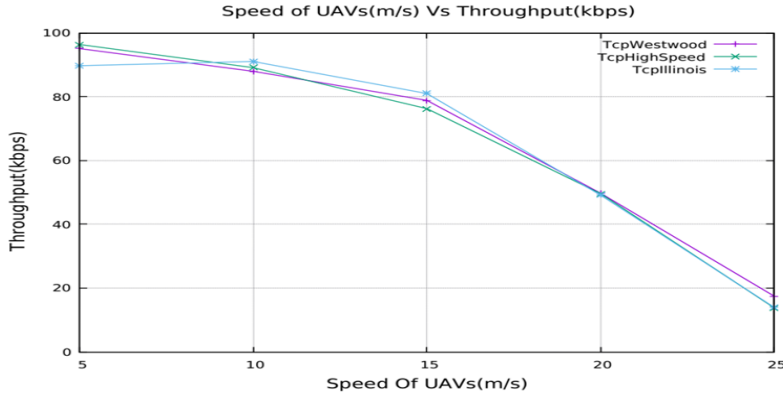
Figure 4. Throughput. Vs. Speed of UAVs.

It is clear from figure 5 that with the increase in speed of UAVs, the average end-to-end delay time also increases. This is because mobility of UAVs causes break in a link along active route between source and destination. Further, it may the repairing process of an active link or discovery of a new route takes long time, so TCP sender's retransmission timeout timer might expire before the route recovers by routing protocol. Here, TCP sender may stay in the "back off" state, and will not know about a recovered route towards the destination.
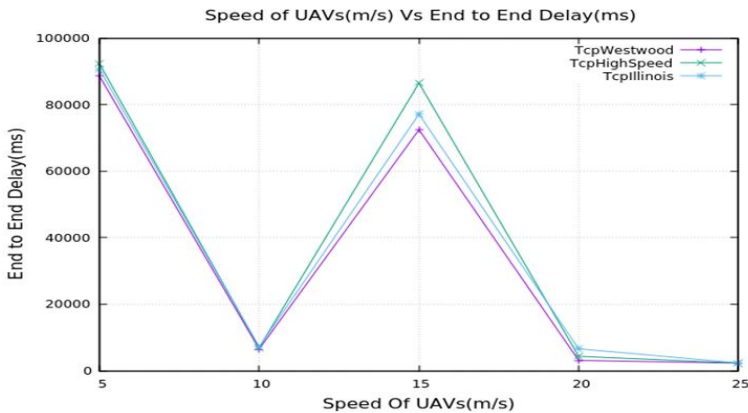
Figure5. End- to-End Delay. Vs. Speed of UAVs.

4.3 The impact of varying number of Flows

Here, we are evaluating the performance metric with number of flows, varying from 5 to 25. The number of mesh nodes has fixed to 40 and the maximum speed of mobility of UAVs has fixed to 5 m/s. figure 6 and figure7 show the results, as number of flows increase, the number of packets try to access the shared channel possibly increase, which cause an excessive contention at MAC layer.
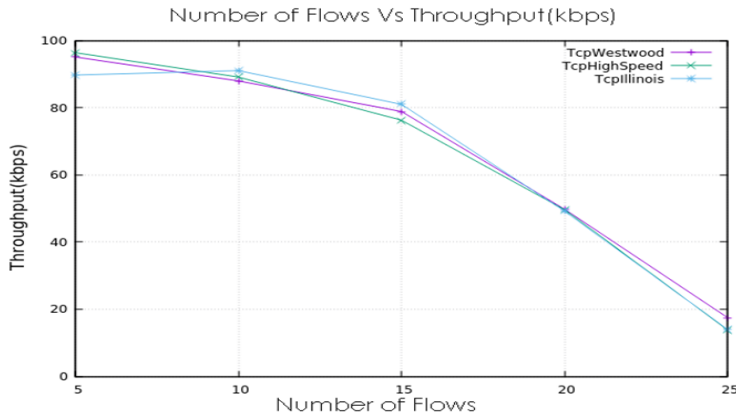
Figure 6. Throughput .Vs. Number of Flows.
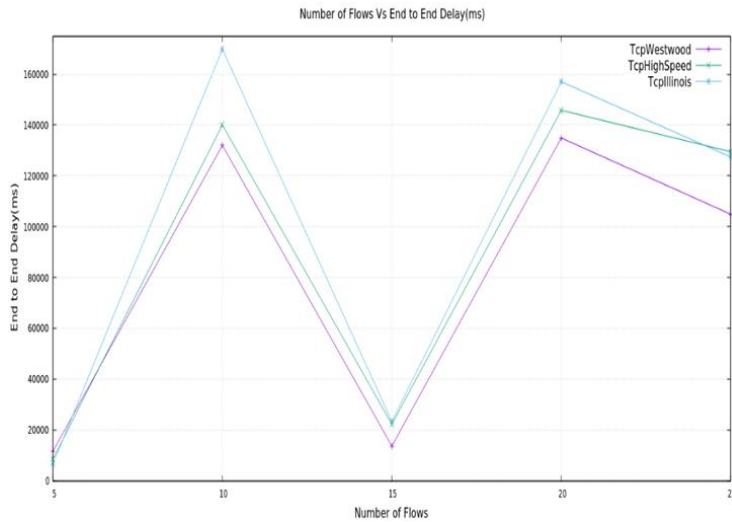
Figure7.End- to-End Delay Vs Number of flows.

In IEEE802.11 there are 3 problems which have been widely studied [20], hidden problem, exposed problem, channel captured, those factors exacerbate the unfairness of competing TCP flow. Therefore, deterioration in performance of TCP protocols will observe.

As evident from figure 6, the throughput has inverse relationship with number of flow, All of protocols have a poor throughput, as the traffic load increase, the intra flow TCP and inter flow TCP might be caused raise in lost packet rate.

Figure7 shows the End- to-End Delay versus the number of flow for TCP Westwood, high-speed and Illinois. All protocols have high end-to-end delay; where in delay is effected by contention time and retransmission time which is increased by grow in traffic load.

Conclusion

FANETs have become an emerging research field. In this paper, three different TCP protocols namely TCP-WESTWOOD, TCP-Illinois and TCP-High speed have examined and explored against the throughput and End-to-End delay measures. We have used NS-3 to demonstrate the performance characteristics of these protocols. The simulation results indicate that, these TCP protocols poorly performs in terms of throughput and End-to-End delay measures. This because of the 3D-space movement of the UAVs in which cause a frequent topology change, make high bit error rate and unstable channel characteristics.We can argue that existing TCP protocols are not performed well in FANETs, Hence, It is imperative to modify or design new protocols for providing connection-oriented and reliable transport layer services.

Reference

[1] M. Elhoseny and K. Shankar, Reliable Data Transmission Model for Mobile Ad HocNetwork Using Signcryption Technique. In: IEEE Transactions on Reliability, Sept. 2020, vol.69, no. 3, pp. 1077-1086.

[2] X. Fan, W. Cai and J. Lin, A survey of routing protocols for highly dynamic mo-bile ad hoc networks. In: IEEE 17th

International Conference on Communication Technology (ICCT), Chengdu,2017, pp. 1412-1417.

[3] H. Bagherlou, A. Gha_ari, A routing protocol for vehicular ad hoc networks using simulated annealing algorithm and neural networks. In: Journal of Super computing, 2018, vol. 74, pp. 2528-2552.

[4] A. Rasheed, S. Gillani, S. Ajmal, A. Qayyum, Vehicular Ad Hoc Network(VANET): A Survey, Challenges, and Applications. In:Advances in Intelligent Sys-tems and Computing,2017, vol 548. Springer, Singapore.

[5] D. Lakew, U. Sa'ad, N. Dao, W. Na and S. Cho, Routing in Flying Ad Hoc Net-works: A Comprehensive Survey, In: IEEE Communications Surveys &Tutorials,2020,vol. 22, no. 2, pp. 1071-1120.

[6] O. S. Oubbati, M. Atiquzzaman, P. Lorenz, M. H. Tareque and M. S. Hossain, Routing in Flying Ad Hoc Networks: Survey, Constraints, and Future Challenge Perspectives. In: IEEE Access, vol. 7, pp. 81057-81105, 2019.

[7] A. Chriki, H. Touati, H. Snoussi, F. Kamoun, FANET: Communication, mobility models and security issues. In: Computer Networks, 2019, Vol. 163.

[8] H. Nawaz, H. M. Ali and A. A. Laghari, UAV Communication Networks Issues: A Review. In: Archives of Computational Methods in Engineering, 2020.

[9] Q. Sang, H. Wu, L. Xing, P. Xie, Review and Comparison of Emerging Routing Protocols in Flying Ad Hoc Networks. In: Symmetry, 2020.

[10] G. Gankhuyag, A. P. Shrestha and S. Yoo, Robust and Reliable Predictive Routing Strategy for Flying Ad-Hoc Networks. In: IEEE Access,2017 ,vol. 5, pp. 643-654.

[11] Z. Zheng, A. K. Sangaiah and T. Wang, Adaptive Communication Protocols in Flying Ad Hoc Network. In: IEEE Communications Magazine,2018, vol. 56, no. 1, pp.136-142.

[12] S.Floyd,"Highspeed TCP for Large Congestion Windows," Request for Comments 3649, Experimental, 2003.

[13] S. Mascolo, C. Casetti, M. Gerla, M. Sanadidi, and R. Wang, "TCP Westwood: End-to-end Bandwidth Estimation of Efficient Transport over Wired and Wireless Networks", in *Proc. of ACM Mobicom*, July, 2001, Rome, Italy.

[14] Liu, S., Baˏsar, T., Srikant, R.: TCP-Illinois: a loss and delay-based congestion control algorithm for high-speed networks. In: Proceedings of the 1st International Conference on Performance Evaluation Methodologies and Tools (Value tools '06),2006, p. 55. ACM.

[15] https://www.nsnam.org.

[16] V. Jacobson, "Congestion avoidance and control," Proceedings of SIGCOMM ' 88, ACM, Stanford, CA, Aug. 1988.

[17] L. Brakmo and L. Peterson, "TCP Vegas: end-to-end congestion avoidance on a global internet," IEEE Journal on Selected Areas in Communication, vol. 13, pp. 1465-1480, Oct. 1995.

[18] K. T. J. Song, Q. Zhang, and M. Sridharan, "A compound TCP approach for high-speed and long distance networks," in Proceedings of PFLDNet, 2006.

[19] T. Kelly, "Scalable TCP: Improving Performance in High Speed Wide Area Networks" ACM SIGCOMM Computer Communication Review, 2003,vol. 33, pp. 83-91.

[20] Xu, Wei-Qiang, and Tie-Jun Wu. "TCP issues in mobile ad hoc networks: Challenges and solutions." Journal of Computer Science and Technology 21.1, 2006,pp. 72-81.

Prevalence of Multidrug Resistant Escherichia Coli in Suspected Cases of Urinary Tract Infection among Patients Attending Tobruk Medical Center, Libya

Fathia H. E. Bougafa and Rema S Tahir

Department of Zoology, Faculty of Science, Tobruk University, Tobruk, Libya
Ehrik2010@yahoo.com

الملخص:

تعد عدوى المجاري البولية من أكثر الاصابات شيوعا على مستوى المجتمع أو الوحدات العلاجية وتقاوم العديد من المضادات الحيوية. بكتيريا العصيات القولونية من أكثر الأجناس البكتريا وجودا وانتشارا في عينات الإدرار خاصة لدي مرضي التهابات المجاري البولية ونسبة لمقاومتها الشديدة للمضادات الحيوية وهذا بدوره يجعل معالجه هذا الالتهابات أكثر صعوبة. هذه الدراسة تهدف لمعرفه مدي انتشار بكتيريا العصيات القولونية لدي مرضي التهاب المسالك البولية في مركز طبرق الطبي، ليبيا ومدي مقاومتها للمضادات الحيوية. تم أخذ 3076 عينه إدرار وعوملت طبقا للطرق القياسية لعزل وتصنيف ميكروب العصيات القولونية وأجريت كذلك أجريت إختبار الحساسية للمضادات الحيوية للعينات الموجبة للعصيات القولونية باستخدام تقنية Kirby– Bauer. أكدت النتائج أن 698 من العينات موجبة للعصيات القولونية بنسبة 22.8% للبكتيريا، ومنها 581 عينة عزلت من مرضى إناث بنسبة 83.2% و117 عزلت م ذكور بنسبة 16.8% ذكور. أظهرت نتائج حساسية المضادات الحيوية بأن نسبة 56.7% من العينات مقاومة للمضادات الحيوية وأن عينات الذكور (65.0%)أكثر مقاومه للمضادات الحيوية مقارنة بعينات الإناث (56.7%). وكانت العصيات القولونية أكثر مقاومه للمضاد الحيوي الامبيسيليس بنسبة100.0% والإميكان (90.3%)وثم الاوكسالين (75.0%). وكانت أكثر حساسية للمضاد الحيوي جنتمايسين (67.9%)

International Science and Technology Journal
المجلة الدولية للعلوم والتقنية

العدد 26
Volume 26

المجلة الدولية للعلوم والتقنية
International Science and Technology Journal
ISTJ

ونتروفورانشن (59.1%). وتوصي الدراسة الأطباء بوصف المضاد الحيوى لمرضى عدوى المجاري البولية بعد إجراء اختبار الحساسية للمضادات الحيوية.

Abstract:

Urinary tract infections (UTIs) are among the commonest infections both in community and hospitals that showed emergence of multi drug resistant (MDR) *Escherichia coli* (*E. coli*) which is challenging UTI treatment. This study aimed to detect the prevalence of *E. coli* and antibioticsusceptibility patternfrom those patients suspected with urinary tract infection attending Tobruk medical center, Tobruk, Libya. A total of 3067 urine samples were collected and processed according to standard microbiological methods for the isolation and identification of *E. coli*. Antibacterial susceptibility pattern of the isolates was determined using Kirby-Bauer's disk diffusion technique. The results revealed that 698samples (22%) out of the 3067 collected samples were positive for *E. coli* with high prevalence among the female patients 581 (83.2%) compared to the male patients 117 (16.8%). The antibiotic susceptibility pattern showed that the isolated bacteria is resistant to used antibiotics by 56.7%.The *E. coli* isolates demonstrated higher resistant in male samples (65.0%) than females (55.1%). The *E. coli* isolates demonstrated higher resistance to Ampicillin (100%) followed by Amickan (90.3%) then Oxacillin (75%) while those isolates recorded the lowest resistance to Gentamicin (32.1%) and Nitrofurantoin (59.1%). The study indicated the need for physicians to prescribed antibiotics to patients following standard antibacterial susceptibility testing.

Keywords: Prevalence, *Escherichia coli*, Multi drug resistant, Urinary tract infection**,** Tobruk city.

Introduction:

Urinary tract infection (UTI) are the most common infection. Many bacteria are causing urinary infection but *Escherichia Coli* is the most common cause of (UTI)between them(Bakhtiari at el.,2020).*E. Coli* can be intrinsically resistant to some special antibiotics and have genes which responsible for resistance to

International Science and Technology Journal
المجلة الدولية للعلوم والتقنية

العدد 26
Volume 26

المجلة الدولية للعلوم والتقنية
International Science and Technology Journal
ISTJ

some special antibiotics (Raeispour and Ranjbar, 2018).Antibiotics groups, such as Amoxicillin, Ampicillinand Erythromycin are commonly used worldwide in agriculture practices(Raeispour and Ranjbar, 2018).Antibiotic resistance is a specific type of drug resistance when a microorganism has the ability of bearing the antibiotic effects (Aljebouri, 2013).This study aimed to detect the prevalence of *E. coli* amongthose patients suspected with urinary tract infection attendingTobruk medical center, Tobruk, Libya; and to investigate the antibioticsusceptibility patternof isolated *E. coli* samples.

Materials and Methods:
Source of isolates:
The study was based on information collected from Hospital (TobrukMedical Center) to determine the prevalence and antimicrobial sensitivity of *E.coli* among patients presenting with UTI visited TobrukMedical Centre during September, 2019 to January, 2021.

Isolation and identification of bacteria from urine samples
The isolated samples were investigated and identified in microbiological laboratory of Hospital.The collected samples were individually worked in microbiological laboratory for isolation and identification of any bacterial pathogens (Salem at el.,2020).The collected sample were inoculated onto (Macconkyagar, Bloodagar, Muellerhinton agar), then plates were incubated at 37˚C for 24h for growing bacteria and extended to 48h for doing susceptibility test. Samples were also identified according to the common standard procedures (Cheesbrough,2010).The isolates were further identified using standard microbiological methods for antibiotic sensitivity of UTI causes using Kirby-Bauer's disk diffusion technique (Sabir,2014).The antimicrobial tests were done to Ampicillin (Amp), Amickan (Amc), Oxacillin (Ox), Sulphamethoxazole/timethoprim (Sxt), Chloramphenicol (Ch), Nitrofurantion (Nitro) and Gentamicin (Gent), Naladixic Acid (Na), Ceftriaxone (Cr)and Ciprofloxacin (Ci).

Data Analysis:

The collected data were statistically analyzed using SPSS software version 23.Chi square test, contingency table for independence was run to verify the significant association between gender of patient and antibiotic Susceptibility pattern of*E. coli*and between different antibiotics and susceptibility of *E. coli*. The results were presented as frequency tabular manner.

Results:

The microbiology laboratoryof Tobruk Medical Center processed about 3067 urine isolates of which 698samples (22.8%) were positive for *E.coli*. Among these positive isolates, 581 (83.2 %) belonged to female patients and 117 (16.8%) belonged to males (Table 1).

Table 1. Prevalence of *E. coli* bacteria among UTI patients with relation to gender of patient

Gender	No.	%
Male	117	16.8
Female	581	83.2
Total	698	100.0

Table 2 shows the overall susceptibility activity of *E.coli* bacteria to antibiotics. The results revealed that the resistance rate is slightly higher(56.7%) than the sensitivity rate (43.3%).

Table 2. Antibiotic susceptibility patterns of *E. coli* isolated from UTI patients

Item	No.	%
Resistant	396	56.7
Sensitive	302	43.3
Total	698	100

Table 3 shows the susceptibility patterns of *E. coli*regarding to gender of patient, The results revealed the significant association (χ^2=3.87; P<0.05) between patient gender and rate of resistance; the isolated samples from male patients is higher resistance rate (65.0%) than those isolated from females(55.1%). This finding

International Science and Technology Journal
المجلة الدولية للعلوم والتقنية

العدد 26
Volume 26

المجلة الدولية للعلوم والتقنية
ISTJ

noticed that the UTI caused by *E. coli* is more complicated in male patients than females.

Table 3. Antibiotic susceptibility patterns of the isolated *E. coli* to regarding to gender of patient

Gender	Resistant		Sensitive		Total	
	No.	%	No.	%	No.	%
Male	76	65.0	41	35.0	117	100.0
Female	320	55.1	261	44.9	581	100.0
Total	**396**	**56.7**	**302**	**43.3**	**698**	**100.0**

Table 4 shows antibiotic susceptibility of isolated *E. coli*. The results of susceptibility analysis explained the highly significant association ($\chi^2=133.07$; P<0.001) between *E. coli* susceptibility and antibiotic type. The *E. coli* isolates were highly resistant to Ampicillin(100.0%), followed by Amickan (90.3%), Oxacillin (75%), Naladixic Acid (66.7%),Ciprofloxacin (62.7%)and Ceftriaxone (62.5%);while the isolates were weak (low resistant) against Gentamicin (32.1%). In contrast, the results showed that the *E. coli* isolates exhibited the highest level of sensitivity to Gentamicin (67.9%) followed by the F (59.1%) and Sulphamethoxazole/trimethoprim(49.5%), while the lowest effective antibiotics against *E. coli* were Oxacillin (25%), Amickan (9.7%) and Ampicillin (0.0%)

Table 4. Resistance and sensitivity patterns of clinical isolated *E.coli* to different antibiotics

Antibiotics	Resistant		Sensitive		Total	
	No.	%	No.	%	No.	%
Amp	8	100.0	0	0.0	8	100.0
Amc	140	90.3	15	9.7	155	100.0
Ci	32	62.7	19	37.3	51	100.0
Gent	51	32.1	108	67.9	159	100.0
Nitro	54	41.9	75	59.1	129	100.0
Sxt	50	50.5	49	49.5	109	100.0
Ch	4	50.0	4	50.0	8	100.0
Ox	3	75.0	1	25.0	4	100.0
Na	14	66.7	7	33.3	21	100.0
Cr	40	62.5	24	37.5	64	100.0
Total	**396**	**56.7**	**302**	**43.3**	**698**	**100.0**

International Science and
Technology Journal
المجلة الدولية للعلوم والتقنية

العدد 26
Volume 26

المجلة الدولية للعلوم والتقنية
International Science and Technology Journal
ISTJ

Discussion:

UTIs remain a challenge to the healthcare system because of the emergence of antimicrobial resistance. *E. coli* has been recorded as major etiological agent responsible for 70 to 80% of UTI(Anjum et al.,2014). In the present study, *E. coli* was isolated from 22.8% of the requested urine culture, this rate is greater than that reported in Nieger (13%) (Okonko et al.,2009) and nearly similarto the finding of previously study from Tripoli, Libya(Ghenghesh et al.,2003); who reported that only 24% as positive specimen of *E. coli*. However, the present rate is lower than those results were conducted from Benghaze (42%) (Al awkally et al., 2019), Masalata (55.6%) (Mohamed et al.,2016) and Misurata (50%)(Salem et al., 2017). Moreover, the present finding is lower than those showed in Sudan (48.48%), Saudi (52.17%),and Egypt (67.44%) (Azab et al.,2021). The variation of positive results of *E. coli* in urine samples among countries could be due to the large variation of *E. coli* strains, the sample size and hygiene conditions in different countries. The causes of low prevalence of *E. coli* in UTI patients in Tobruk Medical Center, could be due to that the individual with high income prefer to investigate their conditions in private clinics which they widespread in the city. In addition to the illogical use of antibiotics which are taken prior culture and antibiotics sensitivity pattern. Incomplete dose of antibiotic course could be another factor contributes to insignificant or no growth rate of the bacteria.

Regarding to the gender of patient, the results showed that 83.2% of positive samples were isolated from females and highest when compared with those samples isolated from male (16.8%). Similar findings were also reported in Pakistan (69.80%), Saudi Arabia (60.35%), Iran (86.24%) and Turkey (82.30%) (Farajnia et al.,2009; Cetin et al., 2009; Balkhi et al.,2018; Aktar et al.,2020 and Azab et al.,2021). Several factors including small urethra, deficiency of germicidal substances in prostatic fluid, hormonal imbalance is considered for the higher incidence of *E. coli* infection in females.

Observation of antimicrobial susceptibility could contribute to provide accurate antibiotic prescription and reduce the

International Science and
Technology Journal
المجلة الدولية للعلوم والتقنية

العدد 26
Volume 26

المجلة الدولية للعلوم والتقنية
International Science and Technology Journal
ISTJ

development of drug resistant regarding to antibiotic susceptibility. The overall rate of E. coli isolates resistance to antibiotics was found to be 56.7% and was slightly higher than the sensitively rate (43.3%).This finding is consistent with the findings of other studies (Kibret and Abera, 2011 and Saber et al., 2014); they attributed the increasing of resisting rate of *E. coli* isolates from UTI patients to the persistent emergence of extended spectrum beta-lactamases (ESBL).Despite the highest prevalence of *E. coli* isolates in females, interestingly the rate of antibiotic resistance is significantly highest in male patient (65.0%) when compared with female patients (55.1%). This finding is in line with the observations of previous study investigated by Drielet al., (2019), and they assumed that the highest rates of antibiotic resistance monitored in strains isolated from males, maybe it is the reason behind the difficulty of eradicating male infection and can lead to recurrent infections.

Generally; the antimicrobial resistant is very high in developing countries (Mahjan et al.,2014). The rate of resistant among uropathogen, especially *E. coli* has become increasing(Aktar et al., 2016 and Kahan et al., 2020). The results of this study also revealed increasing and variation resistance of *E. coli* isolates against investigated antibiotics. The highest resistant was found to Ampicillin (100.0%),Amickan (90.3%) and Oxacillin (75%)). In contrast the sensitivity profile was shown that to Gentamycin (67%) Nitrofurantoin (59.1%). This finding correlates with previous studies from Tripoli, Misurata, Benghaze Saudi and Nigeria (Salem et al.,2018, Salem and Ahmed,2018, Al Awkally et al.,2019, Balkhi et al., 2017 and Shitu et al.,2020). The variation in sensitivity patterns of the isolates might be due to the irrational prophylactic usage, easy availability and the over the counter sale of antimicrobials without a proper prescription and an inappropriate dosing schedule.

The finding of this study alarm that the antimicrobial resistance pattern against *E. coli* in UTI patients in Tobruk city need an argent action to control the situation as more than the half of the isolates 56.7% show resistant to almost all the antibiotic were used with range reached up to 100% for Ampicillin and 90.3% for

International Science and Technology Journal
المجلة الدولية للعلوم والتقنية

العدد 26
Volume 26

المجلة الدولية للعلوم والتقنية
International Science and Technology Journal
ISTJ

Amickan, while Gentamycin and Nitrofurantoin showed sensitive activity against *E. coli* bacteria. For these reasons clinical samples should be under go routinely microscope, culture and antimicrobial resistance test to promote responsible prescription of appropriate use of antibiotic and enhance the management of clinical infectious diseases such as UTI.

References:
Akter T, Hossain MJ, Khan MS, Sultana H, Fatema K, Sanjee SA. Isolation, identification and antimicrobial susceptibility pattern analysis of *Escherichia coli* isolated from clinical samples of Bangladesh. (2016). Asian J. Biomed & Pharm Sci; 6(54): 13-16.

Aljebouri, M. (2013). Antibiotic Resistance pattern of bacteria isolated from patients of urinary tract infections in Iraq.Open journal of urology (2013):124-131.

Azab, K. (2021). Prevalence and relation of urinary tract I bacterial pathogens to sex and ages among patients in three Arab countries. *Al-Azhar Journal of Pharmaceutical Sciences*, *63*(1), 194-206.

Balkhi, B., Mansy, W., Alghadeer, S., Alnuaim, A., Alshehri, A., &Somily, A. (2018).Antimicrobial susceptibility of microorganisms causing urinary tract infections in Saudi Arabia. *The Journal of Infection in Developing Countries*, *12*(04), 220-227.

Cetin M, Ucar E, Guven O. (2009). Community acquired urinary tract infections in Southern Turkey: Etiology and antimicrobial resistance,ClinNephrol; 71(1): 30-35.

Cheesbrouh, M. (2010). District laboratory practice in tropical countries, Cambridge University, part 2:136.

Deepak,S., Sara,E.P.,andRobert,H.(2019).Emerging Antibiotic Resistance to Bacterial Isolates from Human Urinary Tract infection in Grenada.

Farajnia, S., Alikhani, M. Y., Ghotaslou, R., Naghili, B.,Nakhlb,A. (2009). Causative agents and antimicrobial susceptibilities of urinary tract infections in the northwest of Iran.Int J Infect Dis; 13(2): 140-144.

International Science and
Technology Journal
المجلة الدولية للعلوم والتقنية

العدد 26
Volume 26

المجلة الدولية للعلوم والتقنية
International Science and Technology Journal
ISTJ

Khan, M., Alam, S., Afrin, S., & Hossain, M. J. (2020).Spectrum of Antimicrobial Susceptibility of *Escherichia coli* Isolated from Urine Samples of a Tertiary Care Hospital of Bangladesh. *Spectrum*, *24*(03).

Mahajan, R., Gupta S., Mahajan, B. (2014). Antibiotic susceptibility pattern of isolates in urinary tract infection in a tertiary care hospital.J. Rational PharmacotherRes.; 2(2): 44-49.

Maryam,,R. andReza,,R.,(2018).Antibiotic resistance virulence factors and genotyping of uropathogenic*Escherichia Coli* strains, Antimicrobial Resistance of infection control.118.

Mohammed, M. A., Alnour, T. M., Shakurfo, O. M., &Aburass, M. M. (2016). Prevalence and antimicrobial resistance pattern of bacterial strains isolated from patients with urinary tract infection in Messalata Central Hospital, Libya. *Asian Pacific journal of tropical medicine*, *9*(8), 771-776.

Muhammad,L. K.,Surui,X.,M.A.,Rizwan,A.,Ahsan,K.,Naeem, Muhammad,B. and HuFenfen, Y. (2020).Assessment of multi drug resistance in bacterial isolates from urinary tract-infected patients. Journal of Radiation Research and Applied sciences 267-275

Noor-alhooda, M., Nag, M. S., Al-awkally, R. M., Ali, M. D., Al-awkally, N. M., & Al-awkally, A. M. Antibiotic sensitivity of Escherichia coli isolated from different clinical specimens of patient human in Al-jala hospital-Benghazi Libya.(2019). Current Science International; 8(3):509-5017.

Okonko, I. O., Soleye, F. A., Amusan, T. A., Ogun, A. A., Ogunnusi, T. A., Ejembi, J.,Onajobi, B. I. (2009). Incidence of multi-drug resistance (MDR) organisms in Abeokuta, Southwestern Nigeria. *Global journal of pharmacology*, *3*(2), 69-80.

PaitanY. (2018). Current Trends in Antimicrobial Resistance of Escherichia coli.Current microbiology and Immunology:181-211

International Science and
Technology Journal
المجلة الدولية للعلوم والتقنية

العدد 26
Volume 26

المجلة الدولية للعلوم والتقنية
International Science and Technology Journal

ISTJ

Sabir, S., Anjum, A. A., Ijaz, T., Ali, M. A., Khan, M. R., Nawaz M. (2014). Isolation and antibiotic susceptibility of *E. coli* from urinary tract infection in a tertiary care hospital. Pak J Med Sci; 30(2): 389-392.

Salim, F. A., Murad, S. K., &Elbareg, A. M. (2017).Isolation of bacterial pathogens causing urinary tract infections and their antimicrobial susceptibility pattern among patients at Misurata teaching hsospital, Libya. *International Journal of Microbiology & Infectious Diseases*, *1*(2), 1-5.

Somayeh, B.,Hassan,M. and Maryam.(2020). Antibiotic resistance pattern and phylogenetic groups of the uropathogenic Escherichia coli isolates from urinary tract infections in Hamedan,West of Iran.Iranian journal of Microbiology 12(5)388-394.

Sumera,S.Aftab,A.A.,Tayyaba,L.,Muhammed,A.A.,Muti,U.,Rehman,K.,Muhammad,N.(2014).Isolation and antibiotic susceptibility of *E.coli* from Urinary tract infections in a tertiary care hospital;Pak Med Sci;30(2):389-392

VanDriel, A. A., Notermans, D. W., Meima, A., Mulder, M., Donker, G. A., Stobberingh, E. E., &Verbon, A. (2019). Antibiotic resistance of Escherichia coli isolated from uncomplicated UTI in general practice patients over a 10-year period. *European Journal of Clinical Microbiology & Infectious Diseases*, *38*(11), 2151-2158.

Study of Physical and Chemical Properties of Drinking Water for Libyan Standard Specifications at Masallata – Libya

Abdulrhman Mohammed Iqneebir

Art and Science College Masallata, Almergab University
E-mail: Abdooo198642@gmail.com

Abstract:
This study aimed to estimate drinking water contamination by comparing with Libyan standard Specifications For Drinking in water wells in some area of Masllata City as, Bn Moslem, Bn Lite, Algragsha, Almtbia, Algieel, Alakreet, Alshbahna, Alshaafieen, Bn Naaser. The result of the analysis was investigated in the chemical laboratory. And showed that the water samples from all walls under study area were accepted of Libyan standard Specifications of Drinking water. The results also showed that the Libyan standard 1000 ppm this means TDS is acceptable for drinking purposes. For Chloride ion in range is 17.1-18.5 ppm, the average is 17.5 ppm, which compared to Libyan standard for drinking 200-250 ppm, it is suitable for drinking. For Sulphate average is 83.1 ppm Such values are accepted value for drinking. For Bicarbonate average is 166 ppm, which is accepted by to drinking. while the value for such value is accepted for drinking purposes. Also Ca^{2+}, Mg^{2+}, are lowing for drinking. which is below the drinking Libyan standards. Therefore, the oxidation of ferromagnesian minerals was a possible source for Mg. Remarkable spatial variation in wells water composition was attributed to variable recharge of the house wells and different wells. The study has recommended for drilling of house wells to be conducted in parts of the area.
Key words : Physical & Chemical Properties , Drinking Water , Libyan Standard Specifications , House Wells.

ملخص البحث :

استهدفت هده الدراسة تقدير تلوت مياه الشرب بالمقارنة مع الموصفات القياسية الليبية لمياه الشرب في بعض الابار بمناطق من مدينة مسلاته احد المدن الليبية الواقعة شرق مدينة طرابلس حيت ثم جمع 10 عينات من عشر ابار في كل منطقة وهي مسلاته و بني ليث وبني مسلم والقراقشة والمطابية والقليل وقرية العكاريت والشباعنة والشعافيين وبن ناصر وقد أوضحت نتائج التحاليل بمعمل قسم الكيمياء بان المياه قيد الدراسة مقبولة للشرب وقد بينت النتائج ايضا من المواصفات الليبية 1000 جزء في المليون لمجموع الاملاح الكلية الذائبة ، وهذا يعني أن المواد الصلبة الذائبة مناسبة للشرب. اما بالنسبة لأيون الكلوريد يتراوح بين 7.1–8.5 مجم / لتر في العينات، و المعدل 7.5 مجم / لتر وبالمقارنة بالمواصفات القياسية الليبية للشرب التي كانت من 200–250 مجم / لتر ، فهو مناسب للشرب ايضا وبينما يبلغ معدل الكبريتات 83.1 مجم / لتر الدي يتراوح مابين 62–174 مجم / لتر جزء في المليون. هذه القيمة مقبولة عند ملاحظة القيمة المناسبة للشرب من 200–400 مجم / لتر. وبالنسبة لمعدل البيكربونات كان 166 مجم / لتر ، وهو مقبول ايضا عند مقارنته بالمواصفات القياسية للشرب. ولكن نلاحظ ان قيم Ca^{2+}, Mg^{2+} منخفضة قليلا عند مقارنتها بالمواصفات القياسية الليبية للشرب لان تأكسد المعادن الحديدية المغناطيسية رجح ان يكون مصدرا محتملا لايونات الماغنيسيوم ويرجع الاختلاف المكاني الكبير للتركيب الكيميائي لمياه لأبار بالمنازل الي تباين معدل التغذية لأبار المنازل وكذلك لاختلاف الابار من مكان الي اخر. وأوصت الدراسة بان تحفر ابار منزلية اكتر في المنطقة.

Introduction:

Limited surface water which is harvested during rainy season, by means of earth dams is another source, but it is only available for few months during the year. In the last decades there is a tremendous increase in number of residents because the area has an advantage of temperate weather compared to its surrounding, and being a center for cultural activities and tourism. In addition, a noticeable increase of population has occurred during this period

of time and new extensions have developed.[1] Rainwater harvesting is a technology used to collect, convey and store rain water for later use from relatively clean surfaces such as a roof, land surface or rock catchment.[2,3] The random behavior of rainfall patterns in arid or semiarid regions such as Libya makes their prediction rather difficult. However, probability and statistical methodologies provide the necessary ways for such a goal. Therefore, a prerequisite to derive empirically the frequency distributions of rainfall records at each available meteorological station.[4,5-8] In Libya, the climate is Mediterranean in the thin coastal strip and desert in the interior. Actually, although the temperatures on the coast are typical of the Mediterranean climate, the rainfall level is very low, semi-desert in Tripolitania and Cirenaica, and even desert in the Gulf of Sidra (or Sirte). Only in the hills near the coast of Cyrenaica (called Jebel Akhdar), precipitation is between 400 and 700 millimeters (16 and 27.5 inches) per year, so much so that they are covered by a Maquis shrub land. [9].

 Along the coast, which is the only plain area that receives non-sporadic rains, most of the rainfall occurs from October to early April, with a peak in December and January. The amount is usually low, between 200 and 350 mm (8 and 14 in) per year in Tripolitania and Cyrenaica, and between 100 and 200 mm (4 and 8 in) in the Gulf of Sirte (which is definitely desert in the southernmost part), while to the east of Cyrenaica, in the easternmost part of the coast, on the border with Egypt (Tobruk), it drops again to around 100 mm (4 in). The rains on the coast are due to depressions coming from the Atlantic Ocean or the Mediterranean Sea, and between one depression and the other, there are long periods of good weather even in winter; since the period when the rain can fall is limited, during some years, a decrease in the winter rainfall may cause droughts, whose effects are felt until the following autumn. [10,11]

In summer, the sun shines and it almost never rains throughout Libya, although in the southern part, in full desert, some showers may occur because of the African monsoon, which affects the Sahel region in the warmest months, and whose extreme offshoots

can sometimes arrive here. Along the coast, air humidity is high, though sea breezes blow in the afternoon, relieving the heat. Actually, in summer, the northern winds blow even at high altitude, since they are due to the baric configuration of the region, with a high pressure system over the western part of the Mediterranean and a low pressure system on the eastern side, and that's why the Libyan desert is not as hot as the Algerian desert. The average maximum temperature in summer ranges from 30 °C (86 °F) along the coast, to 35/37 °C (95/99 °F) in the north-central inland area, to 40/41 °C (104/406 °F) in the south. Throughout the year, but more often in spring and autumn, Libya can be affected by the Ghibli, a hot and dry wind, which is able to raise dust and cause sudden increases in temperature; this phenomenon is even more evident along the coast, where it also produces a sudden drop in relative humidity, which here is generally high because of the influence of the sea. In these cases, the temperature can exceed 40 °C (104 °F) from April to October even on the coast, while in winter it can reach 30 °C (86 °F). [12,13] The main Libyan cities located on the coast (Tripoli, Benghazi, Misrata) have a Mediterranean climate, with mild, quite rainy winters and hot, sunny summers, with highs in July and August around 32 °C (90 °F) in the western part (Tripoli, Al Khums) and 30 °C (86 °F) in the central and eastern parts, which are more affected by the northern winds that blow in summer in the eastern Mediterranean. [13-16]. The purpose of this study is aimed to estimate of drinking water contamination by comparing with Libyan standard Specifications For Drinking purposes at wells in some area of Masllata City Libya as, Bn Moslem, Bn Lite, Algragsha, Almtbia, Algieel, Alakreet, Alshbahna, Alshaafieen, Bn Naaser. The result of the analysis was investigated in the chemical laboratory.

Materials and Methods :
Area of study :
This work was carried out at Ashiafiyin Masallata-Libya district which has 20 km coastal stretch on the south shoreline of the Mediterranean sea, It is bounded by Gasreyar from the northwest, and Masallata from southeast.

International Science and Technology Journal
المجلة الدولية للعلوم والتقنية

العدد 26
Volume 26

المجلة الدولية للعلوم والتقنية
International Science and Technology Journal
ISTJ

Sample collection :

Ten groundwater samples were collected from 10 wells mentioned in Table (1), water was sampled during April & May Month of 2021. The Ten samples were taken from different sits from Ashiafiyin area, and conserved directly in a portable refrigerator The water samples were collected in previously cleaned polyethylene bottles of one Liter.

Table (1) : The Equipment and Measurements

TEST	Equipment	Maximum of Libyan standard Specifications For Drinking water
TDS	Water proof family (TDS)	500ppm
Cl^-	Titrate with 0.1 silver Nitrate	200ppm
SO_4^{2-}	DR6000	200ppm
HCO_3^-	Titrate with 0.1 Hydrochloride acid	250ppm
Mg^{2+}	Titrate with 0.1 EDTA Solution	30ppm
Ca^{2+}	Titrate with 0.1 EDTA Solution	75ppm
PH	PH Measurements	6.5
E.C	Water proof family (EC)	150 µS/CM
NO_3-	DR6000	10ppm

Chemicals and Reagents:

The chemical used for analysis were NaCl, HCl, NaOH, $AgNO_3$, EDTA, Ethylene Diamine Tetra Acetic Acid, Methyl-Orange , Phenol Phthalein and Methyl Red of Reidel De Haen and $BaCl_2$ From BDH. All chemicals are of analytical grand.

Experimental work:

Ten drinking water samples were collected from 10 wells, water was sampled on a monthly basis, during months may from 2021. The Ten samples were taken from Ashiafiyin **-**Masallata city from different sits [13]

Table (2) : The Data Sample Collections

Sample No.	Sample Name	Sample Type	Sample Code	Sample Volume
1	Masllata,	Well Water	A1	1 Litre
2	Bn Moslem	Well Water	A2	1 Litre
3	Bn Lite	Well Water	A3	1 Litre
4	Algragsha	Well Water	A4	1 Litre
5	Almtbia	Well Water	A5	1 Litre
6	Algieel	Well Water	A6	1 Litre
7	Alakreet,	Well Water	A7	1 Litre
8	Alshbahna,	Well Water	A8	1 Litre
9	Alshaafieen	Well Water	A9	1 Litre
10	Bn Naaser.	Well Water	A10	1 Litre

Results and Discussion:

The physical and chemical parameters of House water samples pH, EC, TDS, TH, Cl^-, Mg^+, Ca^+, CO_3^{2-}, HCO_3^-, Salinity, were analyzed and result as given in Table 3. The arithmetic average, the lowest and highest value on raining walls for the elements in the wells house samples, they were listed in Table (3)

Table (3): Analysis result of physical and chemical properties for samples of House walls:

Test	Unit	average	Std. Deviation ±	Minimum	Maximum	Libyan standard Specifications For Drinking water[15]
TDS	ppm	345.8	27.09	320	378	500-1000
Cl^-	ppm	17.8	1.98	17.1	18.4	250-200
SO_4^{2-}	ppm	83	146	62	174	400-200
HCO_3^-	ppm	146.6	20.48	122	178	400-250
Mg^{2+}	ppm	12.3	9.89	5	19	150-30
Ca^{2+}	ppm	110.5	3.107	15	23	200-75
PH	-	7.4	0.083	7.31	7.53	8.5-6.5
E.C	μS/CM	5.08	2.14	1.02	2.76	800
NO_3-	ppm	15.70	1.26	14	17	50-10

Total Dissolved Solids :

The figure 1 shows that average TDS concentration is (345.875)ppm this is low for Libyan specification because TDS

1000ppm,which is acceptable for drinking according to Libyan specification and the lowest value and good drinking and, it is suitable for drinking . The samples have TDS concentrations exceeds the acceptable range for drinking water specification.
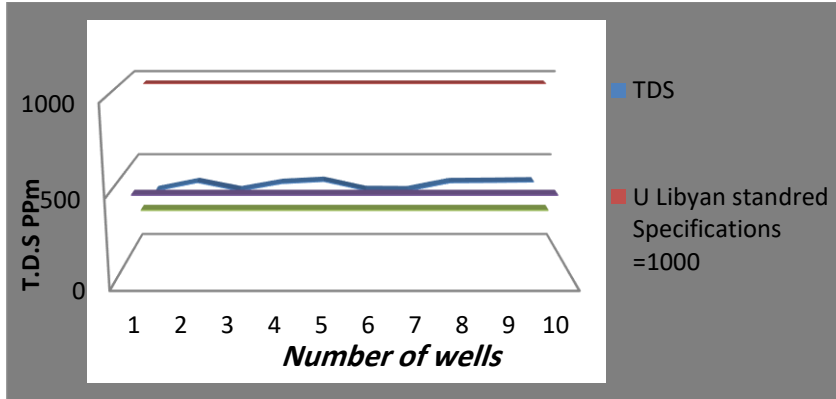
Fig (1): T.D.S values for all water samples

Electrical Conductivity

Figure (2) shows that the average E.C concentrations is (15.709) µs/cm, which is didn't acceptable for drinking according to Libyan specification. Samples have E.C low values the acceptable range for drinking water specification.
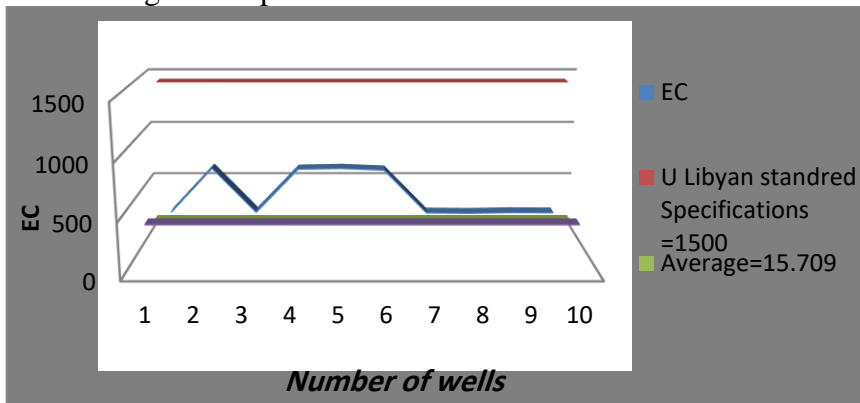
Fig (2): EC values for all water samples

International Science and
Technology Journal
المجلة الدولية للعلوم والتقنية

العدد 26
Volume 26

المجلة الدولية للعلوم والتقنية
International Science and Technology Journal
ISTJ

Acidity and basity of samples (pH-Value)

Figure (3) shows the pH value which extended between 7.1 and 8.4, these results are in agreement with international standard and Libyan specification. The results also show that pH values did not exceed pH value 8.5 mean that carbonate ions are absent.
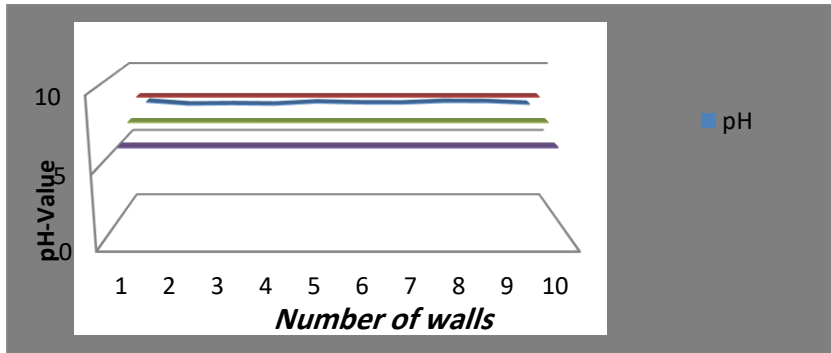
Fig (3): pH values for all water samples

Calcium Ion

Figure (4) Calcium ion concentration for water sample is show in figure 4 with an average amount of 110.5 ppm. the results shows that all samples did not exceed the permissible limit recommended by all specified standards Libyan and international.

Fig (4): Calcium ion concentration for all water samples

International Science and
Technology Journal
المجلة الدولية للعلوم والتقنية

العدد 26
Volume 26

المجلة الدولية للعلوم والتقنية
International Science and Technology Journal
ISTJ
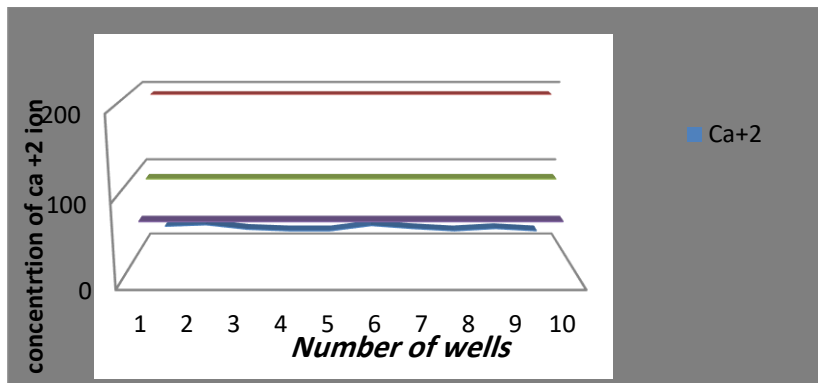
Magnesium Ion

Magnesium ion concentration for water samples is shown in figure 5 with an average amount of 12.3 ppm. the results shows that samples exceed the permissible limit recommended by all specified standards Libyan and international
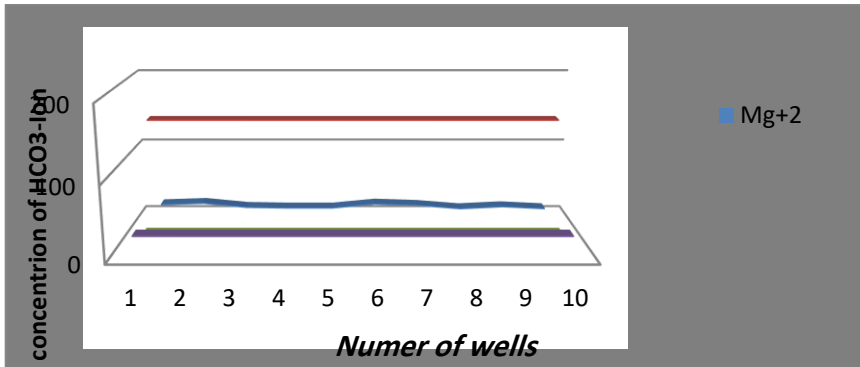
Fig (5): Concentration of Mg^{+2} ion for all water samples

Bicarbonate Ion

The studied water wells show low contents of bicarbonate and lack carbonate ion. Bicarbonate concentration ranges between (178-122)ppm at the of the study area and average (146.6) ppm at Fig 6). The low value of bicarbonate content at of the study area may be attributed to local calcareous water bearing sediments.
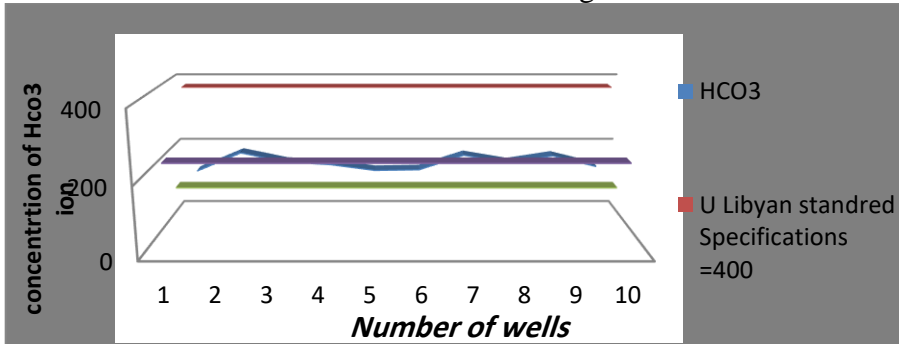
Fig (6): Bicarbonate ion concentration for all water samples

Chloride Ion

The figure (7) shows that the average chloride ions concentration is (17.743)ppm, which is didn't acceptable for drinking according to Libyan specification and also the international specifications. the figure also shows that of all well water. Samples have chloride ion concentrations didn't exceeds the acceptable range for drinking water specification.
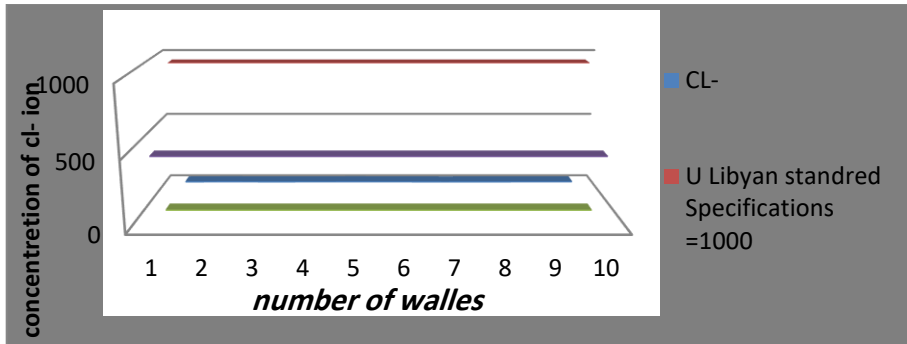
Fig (7): Chloride ion concentration for all water samples

Sulphate Ion

The results sulphate as shown in figure (8) has an average of 83.8 ppm, concentration. The Libyan standards specification recommended that the lowest concentration of sulphate expected one sample.
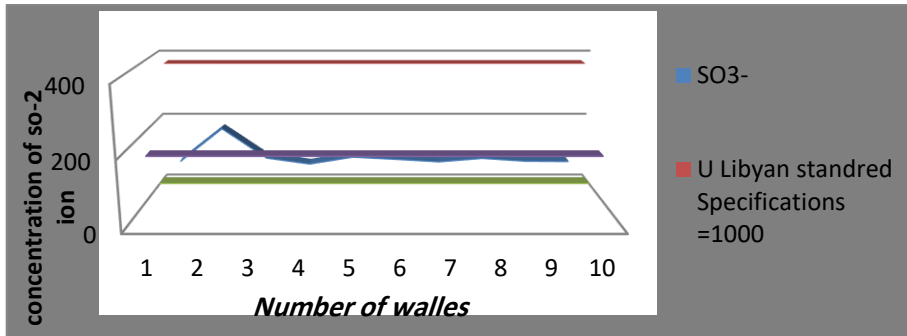
Fig (8): Sulphate ion Concentration for all water samples

International Science and
Technology Journal
المجلة الدولية للعلوم والتقنية

العدد 26
Volume 26

ISTJ

Nitrate Ion

Nitrate concentration for water samples is shown in figure (9) with an average amount of 15 ppm the results shows that all samples exceed the permissible limit recommended by all specified standards Libyan and international
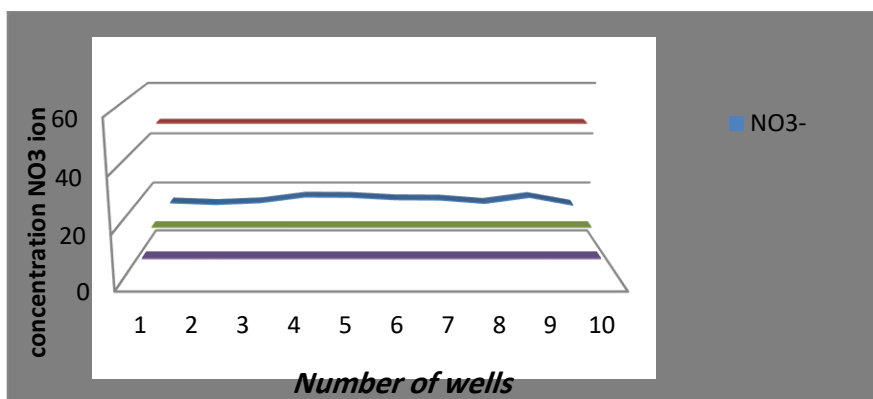
Fig (9): nitret ion Concentration for all water samples

Conclusion :

In summary, the house water of the study area is soft to neutral to slightly alkaline and can be classified according to the salinity into Fresh and brackish-water. The fresh-water is located at the all house walls of the study area with an E.C valus and TDS values. While the brackish water situated at the variable house water salinity and chemical composition were mainly attributed to variable annual recharge and variation in house wall. Hose walls water of the study area could be classified into is suitable for drinking and domestic use because most of the parameters fall within the permissible limits stated by WHO. The study recommends for drilling of water wells to be conducted in the central part of the over by house wells.

References :

[1] W. Geirnaert, M. P, Laeven (1992). Composition and history of groundwater in the western Nile Delta, J. Hydrol., 138: 169-189.

[2] J. Greenleaf, M. H, Harrison (1986). Water and electrolytes. In: Layman DK, editor. Nutrition and Aerobic Exercise, Washington, DC: American Chemical Society, 107-124.

[3] J.Greenleaf, M.H, Harrison (1986). Water and electrolytes. In: Layman DK, editor. Nutrition and Aerobic Exercise, Washington, DC: American Chemical Society, 107-124.

[4] E. Adolph . Heat Exchanges,(1947). Sweat Formation, and Water Turnover. In: Adolph EF, editor. Physiology of Man in the Desert, New York: Inter science Publishers, 33-43.

[5] C. Stewart. The Spectrum of Heat Illness. In: Stewart C, editor. EnvironmentalEmergencies. Baltimore: Williams & Wilkins, (1990):1-27.

[6] M. Elmoujabber, T, Atallah, T, Darwish, and B, Bou Samra, (2004). Monitoring of groundwater salination by seawater. intrusion on the Lebanese Coast ,Lebanese Scienece Journal 5 (2), 21-36.

[7] H.A, Minas. A, Abdel-Latif, H.H, Abuarabia. (2005). The analysis of sea water invasion, northwest Libya. GRMENA. 1: 267-279.

[8] M. Bakker (2000). The size of the fresh water zone below an elongated island with infiltration . water Resour.Res.36 (1), 109-117.

[9] D. Bradwwell.(1952) ,. Detection of seawater infiltration. The Analyst, 77, 381-19.

[10] M. Person, J.Z, Taylor and S.L, Dingman,(1998). Sharp interface models of salt water intrusion and wellhead delineation on Nantucket Island Massachusetts, Ground Water 36 (5), 731-742.

[11] C.W. Fetter (1972). Position of the saline water interface beneath oceanic islands, Water Resources Research. 8: 1307-1315.

[12] D.Todd. (1974). Salt-water intrusion and its control. Journal of American Water Works Association 66: 180-187 .

[13] G. Kallergis. (1986). Applied Hydrogeology in Greece, Publication of the Technical Chamber of Greece, 9: 1-22.

[14] J. Jiao, X. S, Wang. S.Nandy. (2006). Preliminary assessment of the impacts of deep foundations and land

reclamation on groundwater flow in a coastal area in Hong Kong, China. Hydrogeol. J. 14 (2): 100 – 114.

[15]   Libyan specification for drinking water No. 82 (2003).

[16]   A. E. Elsheikh. (2002). Water resources development and management-Red Sea State, Sudan. PhD Thesis, Al-Neelain University, Khartoum, Sudan.

The Kinetics of Organic Matter Removal in Domestic Wastewater Treatment Using Non-coated Cosmo Ball Biomedia and Activated Carbon-Coated Cosmo Ball Biomedia

Khaled Shahot [1] [*], Azni Idris[2] Hasfalina bt. Che Man[3]

[a] Department of Civil Engineering, Faculty of Engineering, University of Elmergib, Al khums, Libya.
[b] Department of Chemical and Environmental Engineering, Faculty of Engineering, University Putra Malaysia, Selangor, Malaysia
[c] Department of Biological and Agricultural Engineering, Faculty of Engineering, University Putra Malaysia, Selangor, Malaysia.

kmshahot@elmergib.edu.ly

Abstract

This paper investigates the kinetics of organic removal by non-coated Cosmo ball biomedia and activated carbon-coated Cosmo ball biomedia in the bioreactors for domestic wastewater treatment. The Modified Stover Kincannon Model and Grau Model were employed for the kinetic evaluation of the reactor performance during the operational period. The Stover Kincannon Model gives a coefficient of determination (R^2) for the straight lines of effluent concentration from the experimental data. The Stover Kincannon gives a predicted BOD_5 of 0.98 and 0.99 for the coated and non-coated media, while the values given by the Grau Model are 0.98 and 0.99. The predicted COD for the coated and non-coated media for the Stover Kincannon Model are 0.98 and 0.99 and 0.99 and 0.99 for the Grau Model. The predicted BOD_5 for the modified Stover-Kincannon Model are K_B= 0.68 g/L.d and $U_{max=}$ 0.55 g/L.d, while the corresponding values for COD are $K_B = 4.61$ g/L.d and U_{max}= 3.42 g/L.d for the non-coated Cosmo balls. The BOD_5 for the coated Cosmo ball are K_B= 2.46 g/L.d and U_{max}= 2.33 $\frac{g}{L}$. d, and the COD are K_B =5.74 g/L.d and U_{max} =4.9 g/L.d.

For Grau model the (K_s) for the BOD and COD of the non-coated Cosmo balls are 0.062 d^{-1} and 0.40 d^{-1}, and the BOD$_5$ and COD of the coated Cosmo balls are 0.289 d^{-1} and 0.836 d^{-1}. The results showed that the Stover-Kincannon model is the best kinetic model.

Keywords: Domestic wastewater, Kinetic modelling, Removal efficiency, Modified-Stover Kincannon Model, Grau Mode.

Introduction

The environmental pollution caused by the population boom, industrialization, and urbanization is a serious concern (lyas et al., 2019). The discharge of toxic compounds from industrial activities into the environment has harmful impacts on public health and the environment. Water quality is dependent on several factors. Phosphorus and nitrogen are the primary nutrients polluting the water bodies (Leyva-Díaz et al., 2013). The release of wastewater with high amounts of organic matter, phosphorus, and nitrogen into the environment is the primary cause of some problems, such as oxygen consumption, eutrophication, and toxicity (Abdelfattah et al., 2020). The removal of these contaminants from wastewater is critical to reduce environmental damage and improve the operation of existing municipal wastewater treatment plants. There is a need to develop better technologies that facilitate compliance with the current and future effluent limits and water quality guidelines (Salgot and Folch, 2018).

All sewage treatment facilities must comply with water quality standards such as BOD$_5$ levels, suspended solids concentration, and other waste substances. Most researchers considered wastewater treatment systems that use activated sludge system, oxidation ponds, trickling filtration, and aerated lagoon as inefficient (Shahot and Khmaj, 2012). In the biofilm or fixed film (attached growth) process, the microbes grow on the stone surface or plastic media. The high surface area of biofilm facilitates the adsorption of a higher amount of substrate from the influent as the wastewater passes over the media. The build-up of biofilm

provides a diverse habitat for the mineralization and transformation of wastewater constituents such as the carbon and nitrogen components, which increases the efficiency of organic substance removal from the wastewater influent. Aerobic, anoxic and anaerobic activities occur in each biofilm, and the biofilm alters the limiting substrate. These processes show the complexity of modelling fixed-film processes (APHA, 2005; Shahot, 2014). The benefits of using a fixed-film system are low operation cost, low energy demand, low reactor capacity, less requirement for settling volume, and less sludge formation (Chan et al., 2009).

The use of biofilm reactors for wastewater treatment has been increasing in recent years. Cosmo ball biofilm reactor processes have been proven reliable for the simultaneous removal of organic matter and ammonia because of the high volumetric loading rate and the low solids buildup in the reactors (Shahot, 2014). The use of activated carbon as a Cosmo balls biofilm media coating offers an alternative design for compact treatment plants that are more effective than conventional wastewater treatment systems (Shahot et al., 2019; Shahot et al., 2015). Cosmo ball is a light-weight commercial media that floats in water and can be removed and cleaned as needed. The Cosmo balls have been proven successful in eliminating acceptable levels of organic matter and nutrient.

Mathematical models are used in fundamental biological process research to evaluate the hypotheses, determine the significance of the relationships between variables, guide the experimental design, and analyse the experimental results. The Modified Stover-Kincannon model and the Grau model are among the models used to test the kinetics of organic matter removal in biofilm reactors.

This study used the Modified-Stover Kincannon Model and Grau Model to investigate the kinetics of organic matter removal using non-coated Cosmo ball biomedia and activated carbon-coated Cosmo balls media to determine the kinetic constants in the

International Science and Technology Journal
المجلة الدولية للعلوم والتقنية

العدد 26
Volume 26

المجلة الدولية للعلوم والتقنية
International Science and Technology Journal
ISTJ

treatment process. The final phase of this study compares the bio-kinetic coefficients with those obtained by previous studies.

2. Materials and Methods
2.1 Experimental set-up
Figure 1 shows the schematic of the experimental system. The lab-scale biofilm Cosmo ball reactor was installed in an actual WWTP at the Engineering Faculty hostel of Universiti Putra Malaysia. The wastewater treatment system comprises a feeding tank, peristaltic pump, anoxic tank, aeration tank, and settling tank. The feeding tank was a circular high-density polyethylene (HDPE) plastic tank that has a 700-litre capacity. The wastewater from the raw point of the wastewater treatment flowed into the feeding tank, where a mechanical stirrer mixed the sewage to obtain homogenous sewage. The system has a peristaltic pump (Heidolph Pumpdrive 5206) that pumped the influent from the feeding tank to the reactor through an inlet in the anoxic zone. The peristaltic pump has a flow rate of 5 L/h, and a 4-mm diameter plastic tube supplied the influent. The same type of peristaltic pump recycled the flow from the top of the settling tank to the anoxic zone. The peristaltic pump for the anoxic-aerobic reactor has a flow rate of 10 L/h. The reactor was covered with aluminium foil to prevent algae growth. The reactor filtering system has an up-flow system that pumped the influent from the bottom to the top of the Cosmo ball reactor (Figure 1). The aeration tank was fabricated using a 70×50×26 cm acrylic sheet and had a 90-litre working volume. The reactor was filled with a 65% standard filling ratio of non-coated and coated Cosmo ball media. There are five air diffusers at the bottom of the aeration tank to provide oxygen for the microorganism that grew and attached to the Cosmo balls. The dissolved oxygen (DO) concentration was maintained at above 2 mg/L in the aeration tank to preserve the biofilm under optimal conditions. The recycled effluent was taken from the settling tank to keep the oxygen level at zero and prevent oxygen transfer into the anoxic zone content. The settling tank is a plastic tank for collecting the treated sewage. The dimension of the tank varies with the flow and has a 1.5-hour

hydraulic retention time. Table 1 shows the operational parameters of the reactor.
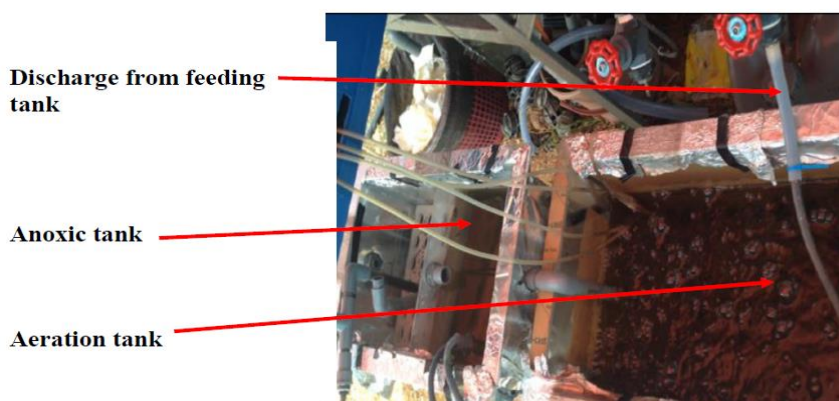
Figure 1. The Reactor was Covered with Aluminium Foil to Protect It from Direct Sunlight and was Placed at the STP

Table 1. Operation Parameters of Coated and Non-Coated Media

Parameters	Non-coated	Coated	HRT (h)	T (C°)	pH	DO
Effluent BOD (mg/L)	9.9±2	3±2	6	29±4	7.2±0.2	≥2(mg/L)
BOD removal %	91.0±2%	97.5±1%	6	29±4	7.2±0.2	≥2(mg/L)
Effluent COD (mg/L)	31.8±3	23.5±3	6	29±4	7.2±0.2	≥2(mg/L)
COD removal %	87.8±2%	92.1±2%	6	29±4	7.2±0.2	≥2(mg/L)
Effluent TSS (mg/L)	8±2	2.83±2	6	29±4	7.2±0.2	≥2(mg/L)
TSS removal %	92.4±3%	98.3±1%	6	29±4	7.2±0.2	≥2(mg/L)
Effluent VSS (mg/L)	5.7±1	2.44±1	6	29±4	7.2±0.2	≥2(mg/L)
VSS removal %	94.1±2%	97.6±1%	6	29±4	7.2±0.2	≥2(mg/L)

2.2. Biofilm media

Cosmo ball media is employed in wastewater processes. In the Cosmo ball process, the light floating carrier elements in a totally mixed reactor provides a surface for microorganisms to grow. The Cosmo ball is suitable for both aerobic and anaerobic conditions in wastewater applications. Universiti Putra Malaysia (Serdang, Malaysia) provided the suspended biofilm carriers with a filling ratio (volumetric filling in an empty reactor) of 65% and a surface area of 160 m^2/m^3. The Cosmo ball elements were fabricated from

International Science and
Technology Journal
المجلة الدولية للعلوم والتقنية

العدد 26
Volume 26

المجلة الدولية للعلوم والتقنية
ISTJ
International Science and Technology Journal

strong HDPE polyethylene plastic and have a density that is 75 kg/m^3 lower than water density. The Cosmo balls are 85 mm in diameter, and the inside and outside of the Cosmo balls have cross fins and longitudinal fins.
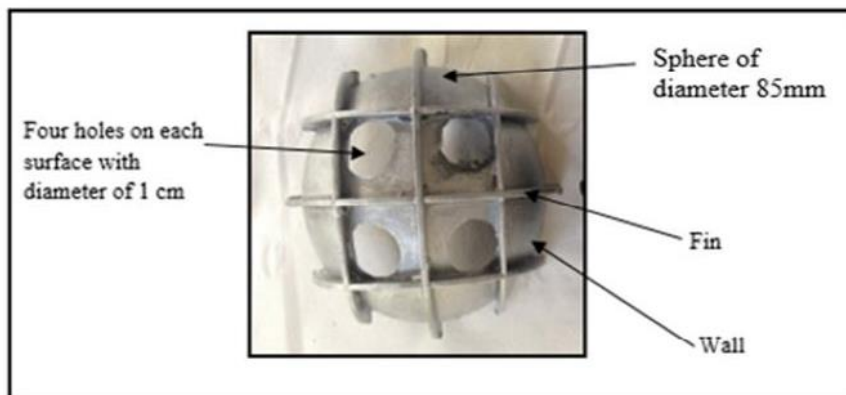
Figure 2 shows the elements of a Cosmo ball biofilm carrier.

2.3 Raw wastewater

The seeding material for the reactor is the wastewater from the hostel at the Faculty of Engineering, University Putra Malaysia. This hostel provides accommodation for 340 students and has one central kitchen. Table 2 shows the primary characteristics of raw sewage

Table 2. Characteristics of raw sewage (average ± standard deviation) Operating conditions

Parameter	Unit	Value
Biochemical Oxygen Demand (BOD)	mg/L	150 ± 20
Chemical Oxygen Demand (COD)	mg/L	290 ± 40
Total Suspended Solid (TSS)	mg/L	120 ± 30
Volatile Suspended Solid (VSS)	mg/L	84 ± 20
Turbidity	NUT	120 ± 40
Ammonium (NH$_3$-N)	mg/L	20 ± 3
Total phosphate	mg/L	6 ± 1.5
Temperature	C^o	29 ± 3
pH		7 ± 0.2
Nitrite (NO$_2$)	mg/L	0
Nitrate (NO$_3$)	mg/L	0.4-0.9

Once the plant has stabilized, two or three experiments were carried out each week. Suja and Donnelly (2008) collected data after 2 weeks started from flow has been changed to ensure stabilization and acclimation of biofilm to the new condition. Pedros et al. (2007) waited three weeks for the same reason. Both groups of researchers used constant characteristics wastewater. Yasir et al. (2018) used fluctuating municipal wastewater and waited ten days to allow for any possible change in biofilm behaviour. This study used fluctuating municipal wastewater maintaining of fixed organic load was not feasible, because of that the steady state of biofilm after each variation of flow was not anticipated this is similar to the study curried out by Yasir et al., (2018), in spite of that, almost one week waiting period was spent.

2.4 Analytical methods

The samples were taken to the laboratory in two-litre plastic bottles and immediately analysed for BOD, COD, MLSS, VSS, pH, and temperature following the American Public Health Association Standard Method. Method (5210) was for determining BOD_5, (5220 C) for COD, (2540 D) for MLVSS, (2540 B), and (4500-NH-3 C) for VSS. The DO concentration and pH were determined using an O_2 electrode and a pH electrode. This experiment maintained a dissolved oxygen (DO) level of above 2 mg/L by continuously supplying air to the aeration tank as recommended by other researchers (Cao et al., 2017; Qasim, 1999). The wastewater pH before the treatment remained at approximately 7.2±0.2. The experiments determined the effects of three hydraulic retention times (HRT) on the organic matter and nutrient removal performance of the non-coated and coated media. The recommended HRT for this set up is six hours, and the recommended filling ratio is 65%.

2.5 Mathematical and Kinetic Modeling
2.6.1. Modified-Stover Kincannon Model.

Mathematical and kinetic model are used in biological wastewater treatment to predict the performance of biological plants, and to determine important variables and critical kinetic parameters. Two

mathematical models commonly used to predict substrate removal rate are the Modified Stover-Kincannon model and the Grau model.

The Modified Stover Kincannon model has been proven to be suitable for biofilm systems. This model was used for various biofilm reactors, such as static granular bed reactor (Debik and Coskun, 2009), up-flow aerobic immobilized biomass reactor (Borghei et al., 2008), up-flow anaerobic fixed-film biomass reactor (Priya et al., 2009), and MBBR (Hassani et al., 2014).

In this model, substrate utilization rate (dS/dt) is presented as a function of organic loading rate (OLR). The generated modified Stover-Kincannon kinetic model can be expressed using equation (1) (Stover and Kincannon, 1982).

$$\frac{ds}{dt} = \frac{Q(S_0 - S)}{V} = \frac{U_{max}\left(\frac{QS_0}{V}\right)}{K_B + \left(\frac{QS_0}{V}\right)} \tag{1}$$

Where:

    ds/dt = substrate removal rate (g/L.d)

    U_{max} = maximum utilization rate constant (g/L.d)

    K_B = saturation value constant (g/L.d)

    V = reactor volume (L)

    Q = influent flow rate (L/d)

    S_0 = influent substrate concentration (mg/L)

    S = effluent substrate concentration (mg/L)

Equation (2) is obtained by inverting equation (1) as follows:

$$\left(\frac{ds}{dt}\right)^{-1} = \frac{V}{Q(S_0 - S)} = \frac{K_B}{U_{max}}\left(\frac{V}{QS_0}\right) + \frac{1}{U_{max}} \tag{2}$$

The values of (U_{max}) and (K_B) can be determined through linear regression of $\frac{V}{Q(S_0 - S)}$ versus $\frac{V}{QS_0}$ in which $\frac{1}{U_{max}}$ and $\frac{K_B}{U_{max}}$ are the intercept and slope of a linear graph, respectively.

2.6.2. Grau Model

Grau model was also used to evaluate the rate of the biodegradation process occurred in the bioreactor. The general

International Science and
Technology Journal
المجلة الدولية للعلوم والتقنية

العدد 26
Volume 26

المجلة الدولية للعلوم والتقنية
ISTJ

equation of a second order substrate removal, which was proposed by Grau (1975), is expressed by equation (3)

$$\frac{-ds}{dt} = K_s.X.\left(\frac{Se}{Si}\right)^2 \tag{3}$$

Integrating and linearizing equation (3) resulted the following equation:

$$\frac{S_i.HRT}{S_i - S_e} = HRT + \frac{S_i}{K_s.X} \tag{4}$$

The second term on the right part of this equation is assumed to be a constant, therefore:

$$\frac{S_i.HRT}{S_i - S_e} = n.HRT + m \tag{5}$$

$\frac{S_i}{S_i - S_e}$ is substrate removal efficiency and is represented by $1/E$.
Therefore, equation (5) can be rewritten as:

$$\frac{HRT}{E} = n.HRT + m \tag{6}$$

The value of m and n can be calculated respectively from the intercept and the slope of a straight line obtained by plotting HRT versus $\frac{S_i.HRT}{S_i - S_e}$. Finally, the value of K_s can be determined by using equation (7) (Borghei et al., 2008):

$$m = \frac{S_i}{K_s.X} \tag{7}$$

Where K_s is substrate removal rate constant (^{-1}d) and X is average biomass concentration in the reactor (mg/L).

3. Results and Discussions
3.1 Evaluation of Kinetic Modelling
3.1.1. Modified Stover-Kincannon Model
Several methods have been used to describe the overall kinetics of biological and biofilm reactor. To carry out this analysis, different

International Science and
Technology Journal
المجلة الدولية للعلوم والتقنية

العدد 26
Volume 26

المجلة الدولية للعلوم والتقنية
ISTJ

global parameters, such as BOD_5, COD, NH_4, PO_4, etc., are usually used as input substrate (Hassani et al., 2014). In this study, the Stover-Kincannon and Grua second order models were chosen to determine BOD and COD removal in Cosmo ball biofilm reactor.

Figures 3(a) and (b) showed the effect of total biomass concentration on the kinetic coefficients of the modified Stover-Kincannon model for both coated and non-coated media. The generated modified Stover-Kincannon kinetic model can be expressed as mentioned early in section 2.6.1 using equation (1) (Stover and Kincannon, 1982).

The value of saturation constant (K_B) and the maximum total substrate utilization rate (U_{max}) were obtained from the slope of the line by plotting $\frac{V}{Q(S_0-S)}$ versus $\frac{V}{QS_0}$ from equation 1 and can be calculated as follows:

From Figure 3(a) the equation that found it is:

$$Y = 1.2418x + 1.8072$$

Therefore, $\frac{1}{U_{max}} = 1.8070 \Rightarrow U_{max} = 0.55$ g/L.d

$$\frac{K_B}{U_{max}} = 1.2418 \Rightarrow K_B = 0.68 \text{ g/L.d}$$

Therefore, the value of U_{max} and K_B are 0.68 and 0.55 g/L.d, respectively for BOD_5, with a correlation coefficient of 0.99, while the corresponding values for COD are 4.61 and 3.42 g/L.d, with a correlation coefficient of 0.99 when non-coated Cosmo ball was used. Using coated Cosmo ball resulted in (K_B) and (U_{max}) of 2.46 and 2.38 g/L.d, respectively for BOD_5, with a correlation coefficient of 0.98, while the corresponding values for COD are 5.74 and 4.9 g/L.d, with a correlation coefficient of 0.99. Table 3. presented the constants determined in this study by using Stover-Kincannon model.

In this study the values for saturation constant K_B and maximum utilization U_{max} are larger for coated media than for non-coated media, which is similar to the results obtained by (Noroozi, 2016). K_B and U_{max} increase due to the increase in the population of microorganism in the biological system. This is because organic matters were being consumed at a faster rate by microorganism. According to the Stover-Kincannon kinetic model, the value for saturation constant K_B and U_{max} obtained in this study are within the determined range reported in other studies. The constants determined by previous studies from using these models are listed in Table 5 and compared with the coefficients obtained in this study.
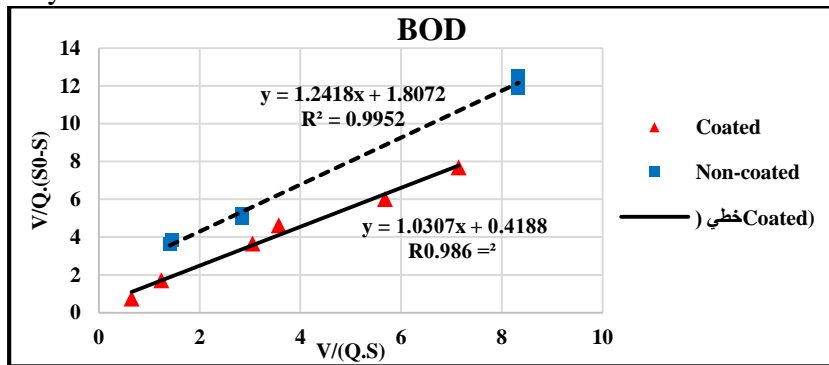
(a)
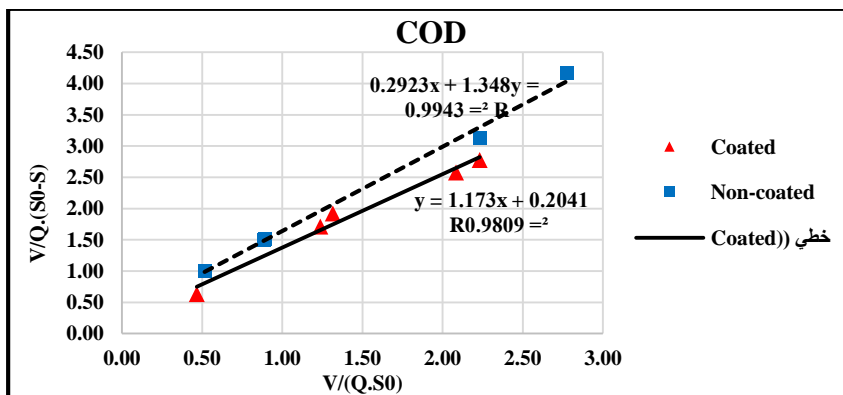
(b)

Figure 3. Modified Stover-Kincannon Model for Removal of (a) BOD and (b) COD by Coated and Non-coated Cosmo Balls/

Table 3. Kinetic Constants Using Modified Stover-Kincannon

Substrate	Modified Stover-kincannon		
	$U_{max}\ (g/L.d)$	$K_B(g/L.d)$	R^2
BOD(non-coated)	0.55	0.68	0.99
BOD (coated)	2.38	2.46	0.98
COD (non-coated)	3.42	4.61	0.99
COD (coated)	4.9	5.74	0.98

3.1.2. Grau Model

Figures 4(a) and (b) depicted the effect of total biomass concentration on the kinetic coefficients of the Grau model for both coated and non-coated media. Equation 6 was plotted (Figure 4) to determine the kinetic coefficients (m, n and K_s), and the constants determined are shown in Table 4.

For instance, in Figure 4(a) the kinetic parameters m, n and K_s were determined as follows:

$$Y= 1.085x+0.0934$$

Therefore, $m = 0.0934$ and $n = 1.085$

Then, from equation (7) the K_s and the biomass concentrations (X) in coated and non-coated media in aeration tank were determined as follows:

Total VSS = (VSS settled in the bottom of aeration tank + VSS attached to the media + VSS during the aeration process)

For coated   = 4800 + 2231 +77 = 7108 mg/L
For non-coated = 5500 + 1104 + 44 = 6648 mg/L
Therefore, X = 6.648 g/L

S_i = the average concentration of the BOD or COD in the aeration tank at different HRT

Therefore, S_i= 0.039 g/L

$$\therefore K_s = \frac{0.039}{0.0934.6.648} = 0.062\ ^{-1}\text{day}$$

Therefore, and as mentioned above the values of m and n are 0.0934 and 1.085, respectively for BOD$_5$ substrate, while the values for COD substrate are 0.045 and 1.2785, with correlation

International Science and
Technology Journal
المجلة الدولية للعلوم والتقنية

العدد 26
Volume 26

المجلة الدولية للعلوم والتقنية
International Science and Technology Journal
ISTJ

coefficients (R^2) of 0.99 for both substrates when non-coated balls were used.

When coated media were used, the values of m and n are 0.0243 and 0.983, respectively for BOD substrate, with a correlation coefficient (R^2) of 0.98; this is slightly lower than the value for non-coated media. For COD substrate, the values for m and n are 0.0195 and 1.1775, respectively with a correlation coefficient (R^2) of 0.99.

The substrate removal rate constant (K_s) was calculated as mentioned above and are found to be 0.062 d^{-1}and 0.40 d^{-1} for BOD and COD, respectively for suspended biomass, and the attached biomass concentration for non-coated Cosmo ball was 6.648 g/L. The values of (K_s) for coated Cosmo balls were 0.289 d^{-1} and 0.836 d^{-1} for BOD and COD, respectively for suspended biomass, and attached biomass concentration of 7.108 g/L.

These results indicated that K_s increased with increasing biomass concentration. In this case, the increased efficiency was due to the increased population of microorganisms in the biological systems. Organic matters are being consumed by microorganism at a faster rate, thus improving the substrate removal rate constant (K_s).

Table 5. illustrated the constants determined in this study and compared with the coefficients obtained by other researches. In this table and when Grua model was used, the (K_s) obtained by Esmaeilirad, (2015) was 13.3^{-1}d and obtained by Grua et al., (1975) recorded 0.127 $^{-1}$d, and the (K_s) obtained by our study was 0.836 $^{-1}$d. Therefore, there is a big variation between our study and the study conducted by other researches which makes it very difficult to make a comparison study and this happened to the Stover-Kincannon model as well. However, in Stover-Kincannon model very easy to figure out the parameters from the figures rather than make a complicated calculation when Grua model was used. So, Stover-Kincannon model can be recommended to be the best kinetic to use.

International Science and
Technology Journal
المجلة الدولية للعلوم والتقنية

العدد 26
Volume 26

المجلة الدولية للعلوم والتقنية
International Science Technology Journal
ISTJ

(a)

(b)
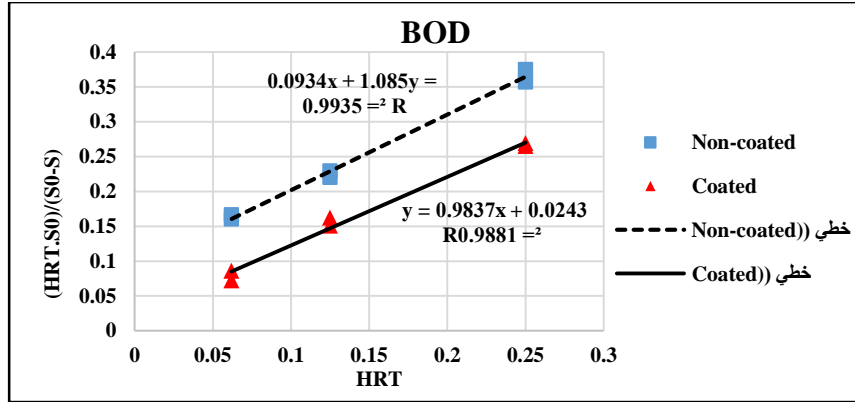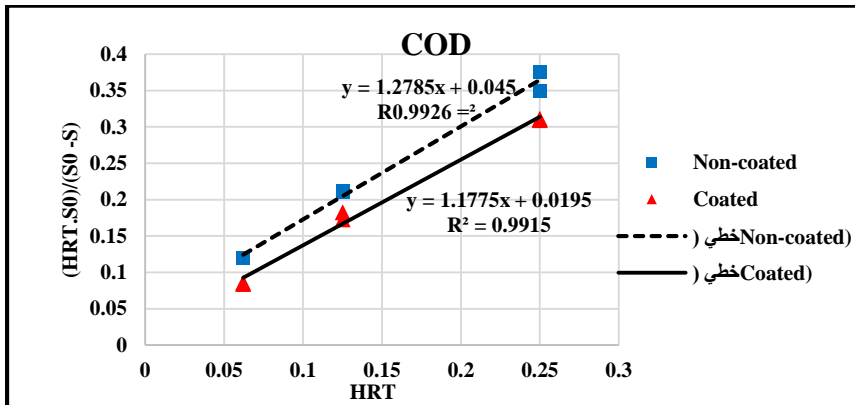
Figure 4. Grau (second order) Model for Removal of (a) BOD and (b) COD by Coated and Non-coated Cosmo Balls

Table 4. Kinetic Constants Using Grau Model

Substrate	Grau Model			
	m	n	$K_s (\frac{1}{d})$	R^2
BOD(non-coated)	0.0934	1.085	0.062	0.99
BOD (coated)	0.0243	0.9837	0.289	0.98
COD (non-coated)	0.045	1.2785	0.40	0.99
COD (coated)	0.0195	1.1775	0.836	0.99

International Science and Technology Journal
المجلة الدولية للعلوم والتقنية

العدد 26
Volume 26

المجلة الدولية للعلوم والتقنية
ISTJ
International Science and Technology Journal

Table 5. Comparison of Kinetic Constants Using Modified Stover-Kincannon and Grau Models Obtained in the Study with Previous Study

Substrate	Stover-Kincannon			Grau Second order				Reference
	U_{max} $(g/L.d)$	K_B $(g/L.d)$	R^2	m	n	K_s $(\frac{1}{d})$	R^2	
BOD (Non-coated)	0.55	0.68	0.99	0.0934	1.085	0.062	0.99	This study
BOD (Coated)	2.38	2.46	0.98	0.0243	0.9837	0.289	0.98	
COD(Non-coated)	3.42	4.61	0.99	0.045	1.2785	0.40	0.99	
COD (Coated)	4.9	5.74	0.98	0.0195	1.1775	0.836	0.99	
COD	11.74	12.32	0.99	0.1084	0.9547	13.3	0.99	Esmaeilirad, (2015)
COD	101	106.8	-	0.047	1.007	3.582	-	Borghei et al., (2008)
COD	1	2.13	0.99	1.839	2.84	-	0.96	Sahariah & Chakraborty, (2013)
COD	-	-	-	0.002	1.346	0.217		Grau et al., (1975)

4. Conclusion

This study evaluated the kinetic parameters for BOD_5 and COD substrate using the Modified Stover-Kincannon and Grua models. The BOD_5 values for the Modified Stover-Kincannon model are K_B= 0.68 g/L.d and $U_{max=}$ 0.55 g/L.d, and the corresponding values for COD are K_B = 4.61 g/L.d and U_{max}= 3.42 g/L.d when using the non-coated Cosmo balls. The values for coated Cosmo balls are K_B= 2.46 g/L.d and U_{max}= 2.33 g/L.d for BOD_5, and the corresponding values for COD are K_B =5.74 g/L.d and U_{max} =4.9 g/L.d. The experimental values are similar to those from the Modified Stover-Kincannon model; the correlation coefficient (R^2) is 0.99 for both the coated and non-coated media. The BOD_5 values for the Grua model are $m = 0.0934$ and $n = 1.085$, and the corresponding values for COD are $m = 0.045$ and n =1.2785 when using non-coated Cosmo balls. For the coated media, $m = 0.0243$ and $n = 0.983$ for the BOD_5 substrate, and $m = 0.0195$ and $n = 1.1775$ for COD. The (K_s) values for the BOD and COD of the non-coated media are 0.062 d^{-1} and 0.40 d^{-1}. The values for the BOD_5 and COD of the coated Cosmo balls are 0.289 d^{-1} and 0.836 d^{-1}. The experimental values are similar to those from the Grua model; the correlation coefficient (R^2) is 0.98 and 0.99 for the coated media and non-coated media. In the

International Science and
Technology Journal
المجلة الدولية للعلوم والتقنية

العدد 26
Volume 26

المجلة الدولية للعلوم والتقنية
International Science and Technology Journal
ISTJ

Stover-Kincannon model, the parameters can be easily determined from the figure, while the Grua model requires complex calculations to determine the parameters. Therefore, the Stover-Kincannon model is suitable for evaluating the kinetic removal of BOD_5 and COD from domestic wastewater treated in a biofilm reactor.

Acknowledgement

References:
[1] Abdelfattah, A., Hossain, M. I., Cheng, L. 2020. High-strength wastewater treatment using microbial biofilm reactor: a critical review. World Journal of Microbiology and Biotechnology, 36, 1-10.

[2] American Public Health Association (APHA), American Water Works Association (AWWA) and Water Environment Federation (WEF). 2005. Standards Methods for Examination of Water and Wastewater 19th edition. Washington, DC.

[3] Borghei, S. M., Sharbatmaleki, M., Pourrezaie, P., & Borghei, G. 2008. Kinetics of organic removal in fixed-bed aerobic biological reactor. Bioresource technology, 99(5), 1118-1124.

[4] Cao, Y., Zhang, C., Rong, H., Zheng, G., Zhao, L. 2017. The effect of dissolved oxygen concentration (DO) on oxygen diffusion and bacterial community structure in moving bed sequencing batch reactor (MBSBR). Water Research, 108, 86-94.

[5] Chan, Y. J., Chong, M. F., Law, C. L., Hassell, D. G. 2009. A review on anaerobic–aerobic treatment of industrial and municipal wastewater. Chemical Engineering Journal:155(1), 1-18.

[6] Debik, E., Coskun, T. 2009. Use of the Static Granular Bed Reactor (SGBR) with anaerobic sludge to treat poultry slaughterhouse wastewater and kinetic modeling. Bioresource Technology, 100(11), 2777-2782.

[7] Esmaeilirad, N., Borghei, S. M., Vosoughi, M. 2015. Kinetics of Ethylene Glycol Biodegradation in a Sequencing Moving Bed Biofilm Reactor. Journal of Civil Engineering and Environmental Sciences, 1(1), 02-07.

[8] Grau, P., Dohanyos, M., Chudoba, J. 1975. Kinetics of multicomponent substrate removal by activated sludge. Water Research, 9(7), 637-642.

[9] Hameed, Y. T., Idris, A., Hussain, S. A., Abdullah, N., Man, H. C., Suja, F. 2018. A tannin–based agent for coagulation and flocculation of municipal wastewater as a pretreatment for biofilm process. Journal of cleaner production, 182, 198-205.

[10] Hassani, A. H., Borghei, S. M., Samadyar, H., & Ghanbari, B. 2014. Utilization of moving bed biofilm reactor for industrial wastewater treatment containing ethylene glycol: kinetic and performance study. Environmental technology, 35(4), 499-507.

[11] Ilyas, M., Ahmad, W., Khan, H., Yousaf, S., Yasir, M., Khan, A. 2019. Environmental and health impacts of industrial wastewater effluents in Pakistan: a review. Reviews on environmental health, 34(2), 171-186.

[12] Leyva-Díaz, J. C., Calderón, K., Rodríguez, F. A., González-López, J., Hontoria, E., & Poyatos, J. M. 2013. Comparative kinetic study between moving bed biofilm reactor-membrane bioreactor and membrane bioreactor systems and their influence on organic matter and nutrients removal. Biochemical Engineering Journal, 77, 28-40.

[13] Noroozi, A., Farhadian, M., Solaimanynazar, A. 2016. Kinetic coefficients for the domestic wastewater treatment using hybrid activated sludge process. Desalination and Water Treatment, 57(10), 4439-4446.

[14] Pedros, P. B., Wang, J. Y., Metghalchi, H. 2007. Single-submerged attached growth bioreactor for simultaneous removal of organics and nitrogen. Journal of Environmental Engineering, 133(2), 191-197.

International Science and Technology Journal
المجلة الدولية للعلوم والتقنية

العدد 26
Volume 26

المجلة الدولية للعلوم والتقنية
International Science and Technology Journal
ISTJ

[15]   Priya, K. R., Sandhya, S., Swaminathan, K. 2009. Kinetic analysis of treatment of formaldehyde containing wastewater in UAFB reactor. Chemical Engineering Journal, 148(2), 212-216.

[16]   Qasim, S. R. 1999. Wastewater treatment plants: planning, design and operation. CRC Press. 2nd edition. Pennsylvania.

[17]   Sahariah, B. P., Chakraborty, S. 2013. Performance of anaerobic–anoxic–aerobic batch fed moving-bed reactor at varying phenol feed concentrations and hydraulic retention time. Clean Technologies and Environmental Policy, 15(2), 225-233

[18]   Salgot, M., Folch, M. 2018. Wastewater treatment and water reuse. Current Opinion in Environmental Science & Health, 2, 64-74.

[19]   Shahot, K., Ekhmaj, A. 2012. Evaluation Biofilm Sewage Treatment Plant. In Proceedings of World Academy of Science, Engineering and Technology. World Academy of Science, Engineering and Technology, 6(2), 62-65.

[20]   Shahot, K., Habib, I., & Ekhmaj, A. 2015. Performance of a Full-Scale Activated Sludge Process for Sakket (Musrata–Libya) Municipal Wastewater Treatment Plant. New York Science Journal, 8(10), 34-37.

[21]   Shahot, K., Idris, A., Omar, R., Che, H., Suja, F. 2019. Investigation of Activated Carbon Coating in the Adsorption Process of Methylene Blue from Aqueous Solution. Advanced Science, Engineering and Medicine, 11(9), 879-887.

[22]   Stover, E.L., Kincannon, D.F., 1982. Rotating biological contactor scale-up and design. In: Proceedings of the 1st International Conference on Fixed Film Biological Processes. Kings Island, Ohio, USA. 1–21.

[23]   Suja, F., Donnelly, T. 2008. Effect of full and partial-bed configuration on carbon removal performance of biological aerated filters. Water Science and Technology, 58(5), 977-983.

The possibility of using iron made in the Libyan Iron and Steel Company in the manufacture of cooking gas cylinders locally (LPG)

إمكانية استخدام الحديد المصنوع في الشركة الليبية للحديد والصلب في صناعة اسطوانات غاز الطبخ محلياً

Abdulaithem M.Abdallah

عبد العظيم محمد عبد الله

College of Oil and Gas Engineering, Zawia University
Zawia Libya

a.hadi@zu.edu.ly

الملخص

غاز الطهي أو ما يسمى بالغاز الطبيعي ، مادة هامة جدا لكل المجتمعات ، وعملية نقله وتوزيعه علي البيوت من اكثر الاشياء التي تشغل الادارة المحلية في كل الدول، ولقد تعددت في هذا الزمان طرق ووسائل نقل وتوزيع الغاز الطبيعي، فبعض الدول تستخدم شبكة التوزيع والبعض الاخر يستخدم الخزنات المنزلية والبعض يستخدم الأسطوانات وفي الكثير من الاحيان يتم استخدام اكثر من طريقة لنقل وتوزيع الغاز للمنزل حسب الظروف المكانية، و لكن في بلادنا اختصر الامر علي استخدام أسطوانات الغاز المنزلي (LPG) في نقل وتوزيع الغاز علي البيوت، مما زاد حاجة الاسواق المحلية علي طلب أسطوانات الغاز مع تزايد عدد السكان وزيادة الطلب علي مادة الغاز، الامر الذى أدى الي زيادة استراد أسطوانات الغاز من الخارج بالعملة الصعبة ($)، مع ان الدولة الليبية تمتلك مصنعين للأسطوانات في المنطقة الغربية واحد في منطقة الرابطة والاخر في منطقة الاسطى ميلاد يمكن الاستفادة منهما في تصنيع أسطوانات الغاز لتغطية الطلب في الاسواق المحلية وتقليل الاستيراد من الخارج وفي نقس الوقت يمكن الاستفادة من مادة الحديد المنتج في مصنع شركة الحديد والصلب بمصراته وهذا موضوع.

في هذه الورقة تم دراسة امكانية الاستفادة من مادة الحديد لشركة الليبية للحديد والصلب في تصنيع اسطوانات الغاز المحلية، وقد اثبتت كل الاختبارات والاشتراطات للموصفات الدولية (ISO4706 – ISO 6892–ISO22991 and BSI5045) التي تم اجراؤها انه يمكن تصنيع أسطوانات الغاز (LPG) بكل نجاح في داخل البلاد وتوفير مبلغ كبيرة من النقد الاجنبي التي تصرف علي استيراد الأسطوانات

Abstract

Cooking gas, or the so-called natural gas, is a very important substance for all societies, and the process of transporting it and distributing it to homes is one of the things that occupy the local administration most in all countries, At this time, there have been many methods and means of transporting and distributing natural gas, some countries use the distribution network, others use home tanks, and some use cylinders and in many cases more than one method is used to transport and distribute gas to the home according to spatial conditions. But in our country, the matter was reduced to the use of domestic gas cylinders (LPG) in transporting and distributing gas to homes, which increased the local market's need to demand gas cylinders with the increase in the population and the increasing demand for gas. This led to an increase in the import of gas cylinders from abroad in hard currency ($), even though the Libyan state has two cylinders factories in the western region, one in the League and the other in the Usti Milad region, which can be used in the manufacture of gas cylinders to cover the demand in the local markets and reduce the import from At the same time, it is possible to make use of the iron produced in the Iron and Steel Company factory in Misurata, and this is a matter. This is a topic.

In this paper, the possibility of using iron material for the Misurata Iron and Steel Company was studied in the manufacture of local gas cylinders, and all the tests and requirements of international specifications (ISO4706 - ISO 6892-ISO22991 and BSI5045) that have been conducted have proven that gas cylinders (LPG) can be manufactured with success. Inside the country and the saving of a large sum of foreign exchange that is spent on importing cylinders

1-Introduction

Given the importance of domestic gas in our daily life, and the lack of any means in our country to distribute household gas other than cylinders (LPG), therefore it was necessary to research and study the possibility of developing and improving specifications for these cylinders. One of the important points in the topic is the manufacture of these local cylinders to reduce the import of household cylinders in order to cover the local demand of cylinders and reduce the cost of importing cylinders to facilitate transportation and handling and reduce the cost of production. To achieve these goals, the type of cylinder under study was determined (LPG 26L). The manufacture of the cylinder is through iron metal (iron type) produced from the Iron and Steel Factory Misurata, which was used in the manufacture of the cylinder body and that is within the framework permitted in the international standards used in the manufacture of cylinders (ISO4706 –ISO 6892-ISO22991 and BSI5045).

For the success of the study, a group of fourteen cylinders were manufactured, with a capacity of 26L, and a thickness of 3mm millimeter. The metal was used according to the approved specifications locally produced "in the Misurata Iron and Steel Company. Due to the necessity of adopting the results, all cylinders were subjected to a process of manufacturing tests and experimental tests, which included a visual detection test, a static pressure test, an underwater air pressure test, and an X-ray detection test. And the blasting test on samples and all these tests and measurements were 99% in accordance with international specifications. The average weight of 14 cylinders produced in the Al Rabita factory, which was once all tested, was (16.8 kg).

All the tests have proven that these results obtained are a good indication of the use of locally produced iron in Misurata Iron and Steel Company in the manufacture of cylinders locally.

2-Types of Cylinders

Here are two types of LPG Gas cylinders:

(1) Standard-type cylinder; A pressure relief valve is installed on the top of the standard LP Gas cylinder.

(2) Universal-type cylinder; the universal type cylinder may be used either in an upright or a horizontal position. A special pressure relief valve is installed on the universal type cylinder [1]

3- Sizes of Cylinders

Then are different Sizes of Cylinders used for gas Storage shown in figure (2.13) such as the following Sizes may be use [1]

- Butane cylinders
    - Usually 7 or 11Kg, self-closing valve
- Propane cylinders
    - Manual-shutoff, hand wheel valve
    - 11 Kg, 34Kg, 47Kg approximate sizes
- Forklift cylinders
    - 15 to 20 Kg, self-closing valve

4-Design of the cylinders

The design of a 'cylinders gas LPG' of those used in homes and Industries to store gases as fuel, There are several designs of cylinder, each tailored for A specific application and each tailored for a specific standards This specification was Formulated to provide for the availability of safe, This specification is limited to Mechanical connections, Technical content provides requirements for performance, Design, materials, tests and inspection, marking, handling, storing and shipping. this standard complements recommendations given provides a basis for design with Reference to strain limits and flexibility analysis analogous to those applied for design Of ferrous cylinders ,systems in accordance standards are documents describing how materials and products should be Manufactured, defined, measured, or tested[2]

4.1 Description of the cylinder design

The body of the cylinder is made of two drawn ends (two-part cylinders) or of two drawn ends and a longitudinally welded cylindrical shell (three-part cylinders). A neck is welded into the hole of the upper end for fitting the valve. A base is welded onto the lower end to ensure the stability of the cylinder. The base is equipped with holes in its lower part in order to prevent the accumulation of moisture. A collar is welded onto the upper end

International Science and Technology Journal
المجلة الدولية للعلوم والتقنية

العدد 26
Volume 26

المجلة الدولية للعلوم والتقنية
ISTJ
International Science and Technology Journal

for the protection of the valve and for carrying the cylinder. One or two handles (according to the size of the cylinder) can be welded instead of the collar. In the case of handles either a plastic cap secured with a steel cotter pin onto the neck or a zinc-coated steel cap screwed onto the external thread of the neck W80x1/11" can be used for the protection of the valve. Both plastic and steel protective caps conform to the requirements of EN 962[3]. If any of the big three-part cylinders are not equipped with a collar or handles, there is a steel plate with technical data welded onto the upper end.[4]

5-Materials of cylinders

Then are different materials used for gas cylinders such as the following materials may be used carbon steel ,alloy steel, copper Aluminium alloy ,Composite material ,Synthetic materials, Glass[4].

In this experiment, the iron material produced in the Libyan Iron and Steel Company's plant in Misurata is used, and this is a topic the paper

5.1- Material characteristics to be considered are, when applicable:

- ❖ yield stress;

- ❖ tensile strength;

- ❖ time-dependent strength;

- ❖ fatigue data;

- ❖ Young's modulus (modulus of elasticity);

- ❖ appropriate amount of plastic strain;

- ❖ impact strength;

- ❖ fracture resistance[5]

5.2 Steel sheets, plates and strip for gas cylinders

This Industrial Standard specifies the hot-rolled steel plates, sheets and strip (hereafter referred to as steel plates, sheets and strip) to

be used for welded gas cylinders with a capacity of 500 liters or under which contain such high-pressure gases as LP gas, acetylene and various kinds of propane gas.

6- Welded low carbon steel cylinders low pressure

The majority of gas cylinders in the world are of welded design, notably cylinders for LPG (liquefied petroleum gases) and acetylene .The cylinder shall be of welded construction having a cold or how drawn cylindrical portion with hemispherical, ellipsoidal or tori-spherical ends welded to it, or two halves of cold or hot drawn and circumferentially welded together, or any other construction approved by the statutory authority. The calculation of the thickness of pressure parts of the gas cylinder is related[6] to the minimum value of yield strength guaranteed by the cylinder manufacturer for the finished cylinder and the test pressure.

Calculation of the minimum wall thickness LPG

For the design of the cylinders, the most significant step in the design of the cylinder is the calculation of the minimum wall thickness of the cylindrical part of the cylinder. For both the ISO 4706 standard and the ISO 22991 draft standard, the wall thickness of the cylindrical shell is calculated based on the guaranteed minimum yield' strength of the material and the test pressure of the cylinder. Both the ISO 4706 standard and the ISO 22991[7] draft standard use the same basic formula to calculate the minimum wall thickness of the cylindrical shell.

The ISO 4706[8] standard requires that the minimum wall thickness of the cylindrical shell be calculated by the following equation:

$$\text{Minimum wall thickness } a = \frac{\frac{Ph \times D}{20 \times Re \times J}}{1.33} + Ph \ \dots (1)$$

Where:

a   Calculated minimum thickness, in millimeters, of the cylindrical shell

International Science and Technology Journal
Technology Journal
المجلة الدولية للعلوم والتقنية

العدد 26
Volume 26

المجلة الدولية للعلوم والتقنية
International Science and Technology Journal
ISTJ

Ph Test pressure, in bar, above atmospheric pressure

D Outside diameter, in millimeters, of the cylinder

Re Minimum value of yield stress, in new tons per square millimeters guaranteed by the cylinder manufacturer for the finished cylinder

J . Stress reduction factor (also known as the weld joint efficiency factor)

❖ Calculated Wall Thickness in the BSI 5045 [7] draft standard use the basic formula to calculate the wall thickness of the cylindrical shell by equations:

$$t = \frac{0.3 \times P1 \times Di}{7 \times fe - P1} \text{ --------- (2)}$$

and the minimum wall thickness of the cylindrical shell be calculated by the following equation

$$t = 2.48\sqrt{\frac{Di}{\tau}} \text{ ----------(3)}$$

Where:

τ . Tensile strength **(N/mm^2)**

t . Calculated minimum thickness, in millimeters, of the cylindrical shell

Di . Outside diameter, in millimeters, of the cylinder

fe . Is the maximum permissible equivalent stress (N/mm^2) at test pressure

P$_1$. Minimum test pressure (bar)

Example: of calculation of the wall thickness of the gas cylinders by the(**BSI 5045**) standard. In this study see the data obtain from the table (1), equation 2 and 3

$$t = \frac{0.3 \times 23.86 \times 311.2}{7 \times 172.7 - 23.8} = 1.88mm \text{ -----------(2)}$$

$$t = 2.48\sqrt{311.2 / 396.1} = 2.198 \equiv 2.2mm \text{ -----------(3)}$$

International Science and Technology Journal
المجلة الدولية للعلوم والتقنية

العدد 26
Volume 26

ISTJ
المجلة الدولية للعلوم والتقنية
International Science and Technology Journal

Table (1): Comparison of Calculated Wall Thickness [9]

	OUTSIDE DIAMETER			STANDARDS					
				ISO 4706		ISO 22991		DOT 4 BW	
Ph	D	J	Re	a	Min. a	a	Min. a	a	Min. a
bar)	(mm)		(N/mm^2)	(mm)	(mm)	(mm)	(mm)	(mm)	(mm)
30	100	0.9	400	0.733	1.500	0.648	1.100	0.709	-
30	100	0.9	490	0.600	1.500	0.529	1.100	0.607	-
30	100	0.9	600	0.433	1.500	0.433	1.100	0.607	1.980
30	250	0.9	400	1.834	1.800	1.619	1.700	1.772	1.980
30	250	0.9	490	1.499	1.800	1.082	1.700	1.518	1.980

8-- Manufacturing of LPG cylinders

Samples, produced at Arrabta, Factory LPG cylinders can be manufactured basically by the processes which are illustrated (1). The LPG cylinder were made for carbon steel with these were product at Libyan steel company ,the chemical composition shown in the table (2) .

Table (2) Chemical composition of samples

Heat No.	Coil No.	Dimensions (mm)	Chemical Composition (Wt %)					
			C	Si	Mn	P	S	Al
65136	616945	3.40* 600	0.09	0.01	0.30	0.016	0.003	0.042
65136	616946	3.40*600	0.09	0.01	0.30	0.016	0.003	0.042
65135	617119	3.40*600	0.09	0.03	0.41	0.018	0.004	0.039
65135	617121	3.40*600	0.09	0.03	0.41	0.018	0.004	0.039

8.1 -Manufacturing Stages in LPG cylinders

Cylinders these stages are divided into four essential processes as follows [10]

8.2-Cutting and forming operations.

This stage involves different steps starting from cutting the raw material into the metal passes through the following machines,40 of samples with a diameter of (54mm) and (50)

International Science and Technology Journal
المجلة الدولية للعلوم والتقنية

العدد 26
Volume 26

المجلة الدولية للعلوم والتقنية
ISTJ
International Science and Technology Journal

Deep drawing was carried for all parts (90 piece)to produce the upper and lower part of the LPG cylinder, to facilitate the engagement between the two parts of the cylinder as illustrated in specified machine is used to trim the metal burrs from the upper shell and then it bends the circular edge of the lower shell.

The two trimming and bent parts of cylinder are cleaned to remove impurities and oil drops . Degreasing and drying is only needed for samples

8.3. Welding process :-

In LPG cylinder two essential technique are used , Inert gas electrical arc welding and Submerged arc welding .

8.3.1- Inert Gas Electrical Arc welding .

The Inert gas electrical arc welding operation is used in LPG cylinders to weld the base

8.3.2 Submerged Arc Welding

In this process, the upper and lower sections of cylinders were welded together by   Automatic submerged arc welding , for circumferential   the joint of upper and lower sections of the cylinders.

8.3.3 -weld of bung

The valve base (bung) welded by   Automatic submerged arc welding on the upper section of the cylinders

Table (2) Mechanical properties of weld

welded Raw material		Yield strength (σs)	Tensile strength (σp)MPa	Elongation ($\delta 5$) %
Welding Electrode	E5015	≤ 410	≤ 490	≤ 22

9. Test and Results

9.1 Tensile tests

Tensile specimens per perpendicular to the weld were machined according to ISO 6890 standard, table (3) also figure (1).

Ammonium two specimens were testing for each gas cylinders the testes were carried out using a Machine-Type WE -600 B- Grade of Max testing force 600KN the ultimate tensile strength elongation at average were determined for each cylinder.

Table (3) Dimensions of tensile in metal piece

Samples	Dimensions of the test piece					Standards
X grope	Readies R(m.m)	Thickness ± 0.1mm	Width of test piece		Total length.(mm)	ISO 6892
			min±	max		
	31.5	3	201	30	214	
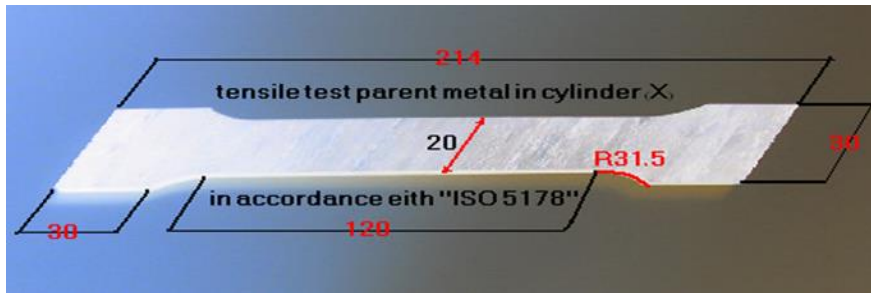
Figure (1) Dimensions of tensile sample

9.2.Thickness Uniformity Test

Ultrasound device (DM3) is used to measure the thickness of the cylinder. Thickness measurements were made at different locations on the cylinder's body and new values of the thickness were obtained as illustrated in the table (4). also figure (2)

Table(4) new thickness *(All measuring are in millimeter)*

Nominal thickness of material mm	Min wall thickness mm	Thickness at carve mm	Thickness at joint of weld mm	Thickness of shroud mm (base)	Thickness of footing mm (base)
3±0.1	2.9±0.2	2.9±0.2	3.4±0.2	2.5±0.1	2.5±0.1
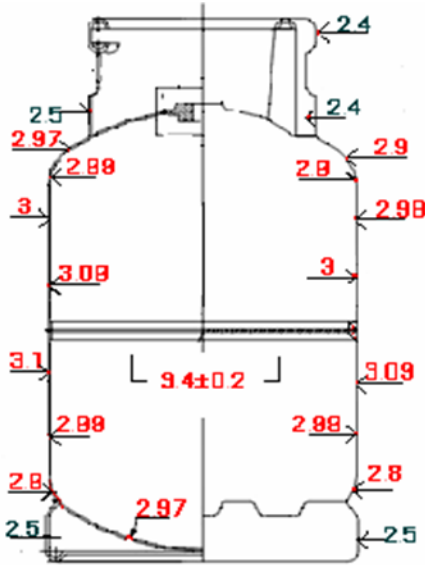
Figure (2) New design of the cylinder

Mechanical properties tests of parent metal

9.3 Tensile Test on Parent Metal

Tensile test for the parent metal of the cylindrical part was achieved in the longitudinal direction by a Testing Machine-Type WE -600 B- Grade of Max testing force 600KN and the results were obtained as shown in the table (5),(6),(7) .

9.4 yield stress test

Tensile test results for stresses at yield were compared with international standards as in the table (8).as can be seen in the table that the values of yield stress is in rang between 216-316 MPa. All the results are within the rang the standards international in table (5) Accepted two gas cylinders which are X3andX5

International Science and Technology Journal
المجلة الدولية للعلوم والتقنية

العدد 26
Volume 26

ISTJ
المجلة الدولية للعلوم والتقنية
International Science and Technology Journal

Table(5) Comparison Of The Stresses At Yield

Produced in Arrabta Factory			International standard		
Samples	cylinder serial no	Stress at yield MPa	ISO-6892 min 240 MPa	BSI-BS 5045 min 215MPa	ISO 22991: 2004(E) min 240 MPa
X2	2069	250	Accepted	Accepted	Accepted
X3	2250	233	Non accepted	Accepted	Non accepted
X4	1725	300	Accepted	Accepted	Accepted
X6	1962	320	Accepted	Accepted	Accepted
Average		271MPa	75%	100%	75%

9.5 .Tensile Strength Of Parent Metal

Tensile strength test for the parent metal of the cylindrical part was achieved in the longitudinal direction and the results of this test were put in a comparison with the international standard as in the Table (6). The results are in the range of 336-455 MPa however the average of tensile strength is 396.1 MPa . Although , two gas cylinders are out of standard .

Table (6) Comparison between tensile strength and international standards

Produced in Arrabta Factory			International standard		
Symbol	cylinder serial no	tensile strength (MPa)	ISO-6892 min 350-440 (MPa)	BSI-BS 5045 min 340-430 (MPa)	ISO 22991: 2004(E) min 350-440 (MPa)
X2	2069	366	Accepted	Accepted	Accepted
X3	2250	.336	Non accepted	Non accepted	Non accepted
X4	1725	416	Accepted	Accepted	Accepted
X6	1962	443.3	Accepted	Accepted	Accepted
Average		396.1	Accepted 75%	Accepted 75%	Accepted 75%

9.10 Engineering Strain test on the parent metal

The results of the strain test was obtained by the tensile machine and compared with the international standards . The table (7)

International Science and Technology Journal
المجلة الدولية للعلوم والتقنية

العدد 26
Volume 26

المجلة الدولية للعلوم والتقنية

ISTJ

shows that all the gas cylinders have % engineering Strain around 28 % . A maximum engineering Strain of 36% was obtained whilst a minimum engineering Strain of 27% obtained for X3 gas cylinders and its results is out of range of BS5045 standards which indicate to a minimum engineering Strain around 28 % .

Table (7) Comparison between the strain test results and the international standards

Produced in Arrabta Factory			International standard		
Samples	cylinder serial no	Engineering Strain %	ISO-6892 min (22%)	BSI-BS 5045 min (28%)	ISO 22991: 2004(E) Min (22%)
X2	2069	29.2	Accepted	Accepted	Accepted
X3	2250	27.5	accepted	Non accepted	accepted
X4	1725	29.1	Accepted	Accepted	Accepted
X6	1962	27.5	Accepted	Non Accepted	Accepted
Average		29.4625%	100%	75%	100%

9.11 Tensile test on welds

This test was achieved perpendicular to the weld of test specimen having a thickness of 3 mm, 25mm width and a length extending up to 15 mm beyond the edges. The results of such a test were obtained by the same tensile machine and compared with international standards as shown in the table (8),(9),(10).

9.12 Yield Stress

the yield stress is higher them 233MPa in all cases , all gas cylinders for group X are within the range of BS5045 standard however ,the yield stress of the X3gas cylinder is out of range of ISO 6892 and ISO 22991 as in the table (8).

International Science and
Technology Journal
المجلة الدولية للعلوم والتقنية

العدد 26
Volume 26

المجلة الدولية للعلوم والتقنية
International Science and Technology Journal
ISTJ

Table (8) Comparison between the test results of the tensile strength at yield and the international standards

Produced in Arrabta Factory			International standard		
Samples	cylinder serial no	Stress at yield MPa	ISO-6892 min 240 MPa	BSI-BS 5045 min 215MPa	ISO 22991: 2004(E) min 240 MPa
X2	2069	240	Accepted	Accepted	Accepted
X3	2250	233.3	Non accepted	Accepted	Non accepted
X4	1725	322.2	accepted	Accepted	Accepted
X6	1962	346.6	Accepted	Accepted	Accepted
Average		308.9125	77.7%	100%	77.7%

10.1 Results Of Tensile Stress At Fracture

Tensile strength test for the weld of the cylindrical part was achieved in the perpendicular direction to the weld and then the results of this test was put in a comparison with the international standard as in the Table (9).The tensile strength are within the range of [ISO6892 and BS5045 standard] .

Table (9) Comparison between the test results of the tensile stress at fracture and the international standards

Produced in Arrabta Factory			International standard	
Samples	cylinder serial no	tensile strength Rm(MPa)	ISO-6892 min 350-440 Rm(MPa)	BSI-BS 5045 min 340-430 Rm(MPa)
X2	2069	361	*Accepted*	Accepted
X3	2250	355.5	*accepted*	accepted
X4	1725	460	*Accepted*	Accepted
X6	1962	498.6	Accepted	Accepted
AVERAGE		424.25	100%	100%

10.2 Engineering Strain test on the weld

The results of the strain test was obtained by the tensile machine and compared with the international standards as shown in the table (10). A maximum engineering strain of 40% occurred for are gas cylinder whilst a minimum engineering strain of 25% a

International Science and Technology Journal
المجلة الدولية للعلوم والتقنية

العدد 26
Volume 26

المجلة الدولية للعلوم والتقنية
ISTJ

occurred for X7 cylinder . The engineering strain is accepted in all cases based on the international standards.

Table (10) Comparison between the strain test results and the international standards.

Produced in Arrabta Factory			International standard		
Samples	cylinder serial no	elongation %	ISO-6892 min (22%)	BSI-BS 5045 min (28%)	ISO 22991: 2004(E) Min (22%)
X2	2069	35	Accepted	Accepted	Accepted
X3	2250	35	accepted	accepted	accepted
X4	1725	37.5	Accepted	Accepted	Accepted
X6	1962	28.5	Accepted	Accepted	Accepted
Average		32.9375	100%	100%	100%
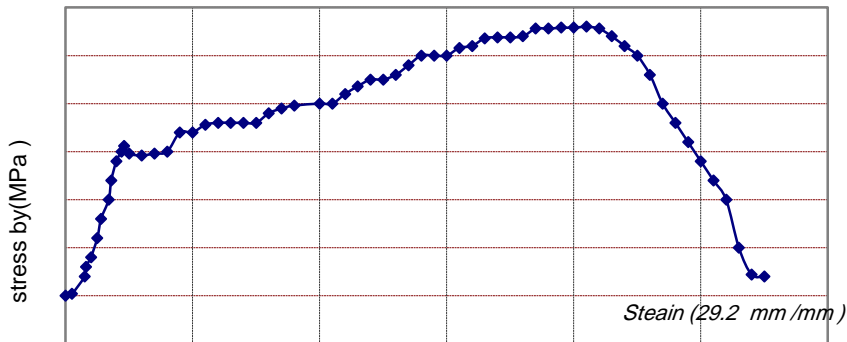
Figure (3) THE STRESS-STEAIN CURVE FOR "X2" Samples

10.3 Bend Test

This test was achieved perpendicular to the weld has it has been bent through angle180. The results of such a test were obtained by the same tensile machine and compared with international standards. This test was made to the welding joint of the two halves of the cylinder. machine with special specifications was prepared to test these welding joints and then capturing for them .Results showed that there were no cracks, existed i.e., there

International Science and
Technology Journal
المجلة الدولية للعلوم والتقنية

العدد 26
Volume 26

المجلة الدولية للعلوم والتقنية
ISTJ

are no defects in the welding joints for the (X) samples and (k) samples, as shown in figures (4)

Figure (4) Bend Test for the samples (X1 to X3,) Cylinders

10.5 Results Of Burst Pressure Test .

The test results of burst pressure were obtained by burst pressure device and then compared with the minimum values of the burst pressure according to the International Standards the minimum requirements of the international Standards used in than work [ISO 6892 ,BSI5054 and ISO 22991] are 81,60 and 50 bar . The results of 12 gas cylinders table (11) shows that in all case the pressure test is higher than the minimum requirements.

Table (11) Burst Pressure Test compared with international Standards

Samples	cylinder serial no	Presser at yield	Presser at burst	ISO-6892 Min -81 BAR	BSI-BS 5045 Min -60 BAR	ISO 22991: 2004(E) Min-50 BAR
X2	0005	68	121	Accepted	Accepted	Accepted
X3	1744	69	110	accepted	accepted	accepted
X4	2245	65	100	Accepted	Accepted	Accepted
X6	1957	65	111	Accepted	Accepted	Accepted
AVERAGE		67.08	110.33	100%	100%	100%

Figure(5) demonstrates the relationship between the values of burst pressure and the yield point of the cylinder. Based on this figure ,It is clear that the burst pressure values increase relatively with the yield point.

Some of the samples which have been selected and subjected to the burst pressure were sheared perpendicular to the weld while others were sheared only in the weld zone as shown in the figure (5) Accordingly, this does not make any difference to the quality of the cylinder and then all the samples are accepted according to the International Standards.

Figure (5) Burst shape of the (X) samples which have been selected and subjected to the burst pressure

11. Conclusion

Supporting industry and domestic production must first begin with self-sufficiency, to increase production and raise the level of the economy in the Libyan state. The production of gas cylinders in the local markets, and this competition has started in this Libyan article for talk and steel in the city of Misurata, and this harms to reduce production costs, making it the engine of cylinders in the local markets and reducing the burden on the shoulders of the citizen.

12. Recommendations

1- We recommend using the iron metal produced in the Libyan Iron and Steel Company in the manufacture of cooking gas cylinders locally.

2- We recommend making use of the Rabbah plant as well as the Bir al-Sasta Milad plant in the manufacture of gas cylinders with the use of the Libyan company's crude plant

3- We recommend the Brega Oil and Gas Marketing Company, as it is the responsible and monopolist in the cooking gas cylinders market, to support local production and internal investment in the context of raising the level of the Libyan state's economy.

4- We recommend an increase in research and development in this field, especially with the provision of the appropriate environment and ground to achieve the manufacture of cooking gas cylinders locally

13. Acknowledgements

References

[1] Cylinder tapes **and sizes** .

[2] http://yangfan-group.en.alibaba.com/.

[3] Cylinder (geometry). (2006, December 13). In Wikipedia, The Free Encyclopedia.

[4] http://yangfan-group.en.alibaba.com/.

[5] International Organization for Standardization (ISO 22991:

[6] Head of LBG gas cylinders.

[7] International Organization for Standardization (ISO 4136 Tensile Test On Welds) .

[8] Technical Specification design And Construction Of Refillable Welded Steel Gas cylinders For LPG.

[9] Retrieved from "http://en.wikipedia.org/wiki/Hydrostatic_test

[10]   Technical Specification design And Construction Of Refillable Welded Steel Gas cylinders For LPG.

Thermal conduction equation with maple

Raja Mohammad Elborio
Higher Institute of Engineering Technology Benghazi
raja.albarjo@limu.edu.ly

Abstract

In this paper, we use Maple to investigate different solutions of the heat equation, starting with initial heat profile in one dimensional media under suitable assumptions. We used two different

methodologies to solve the equation and to compare the results with numerical solutions. Moreover, the well-known Cauchy problem of heat equation was explored in details to verify consistency in the solutions.

Keywords: heat equation, Fourier transform, Cauchy problem, maple.

الملخص

في هذا البحث ، استخدمنا البرنامج Maple لاستكشاف الحلول المختلفة لمعادلة الحرارة ، بدءًا من توزع الحرارة الأولي في وسط أحادي البعد وفقًا لافتراضات مناسبة. استخدمنا نوعين مختلفين من المنهجيات لحل المعادلة ومقارنة النتائج بالحلول العددية. علاوةً على ذلك ، تم استكشاف إمكانية حل مشكلة كوشي المعروفة لمعادلة الحرارة بالتفصيل للتحقق منها الاتساق في الحلول التي تم الحصول عليها.

1. **Introduction**

Partial differential equations (PDEs) are important in many fields of science, because they can be formulated whenever a change in a system is happened. Since the time of Newton, differential equations were increasingly used to help understanding the physical, chemical and biological phenomena. In recent years, their uses extended in the industrial, engineering, economic and social sciences. In fact, most of the natural laws in physics such as Maxwell's equations, Newton's laws of cooling and motion, Navier-Stokes's equations and Schrödinger equation in quantum mechanics can be written in terms of partial differential equations. In other words, these laws describe physical phenomena by

International Science and Technology Journal
المجلة الدولية للعلوم والتقنية

العدد 26
Volume 26

المجلة الدولية للعلوم والتقنية
International Science and Technology Journal
ISTJ

finding relationships between space and partial derivatives with respect of time. The partial appears in these equations because they represent natural things (such as velocity, acceleration, force, friction, flux and current), and accordingly we get equations that link partial derivatives of unknown quantities that we want to know.

Several methods have been employed in order to solve PDFs. The common method is the reduction of PDFs into an ordinary differential equation (ODFs), which can be viewed as a special case of a symmetry reduction [1, 2]. Fourier transform and Fourier series are also widely used in this field. [3]. Recently, the numerical methods were extensively used to approximate the solutions of PDEs. This includes the finite element method (FEM), finite volume methods (FVM) and finite difference methods (FDM)[4, 5]. Most of these methods are adopted in educational different software and can easily be employed in personal computers.

Recently, remarkable progress has been achieved in computer algebra software and graphical drawing utilities. Mathematical, maple and Matlab are the mostly used software in this field. While Matlab is appropriate for large-scale numerical calculations, Maple was demonstrated to be the best for mathematical science education. This is probably due to simplicity in manipulating the mathematical formulas. The use of such advanced computer software can improve forms and methods of educational and learning activities through efficient combination of traditional methods of teaching higher mathematics and modern achievements computer mathematics.

The heat equation is an essential partial differential equation in physics, which describes the distribution of heat (or variation in temperature) in a given region over time. Engineers are always encountered with heat equation when designing heat exchanger, heat sinks and cooling systems. Moreover, heat equation is widely used to determine the temperature in inaccessible areas, such as surface of fuel rod in nuclear reactor or core of the sun.

In this paper, we will study the heat flow where the conduction of thermal energy is much more important than convection (That

is primarily the heat flow though solids) [6, 7]. We shall simulate the heat equation for one dimensional media. Two different methods will be employed as implemented in the computer program Maple. Results from simulation will be compared and evaluated against the known solutions.

2. Project design

As we mentioned above, the heat equation is a PDE describing the distribution of temperature (denoted as *u(x,t)*) over time. In one spatial dimension the temperature obeys the relation:

$$\frac{\partial u}{\partial t} = c^2 \frac{\partial^2 u}{\partial^2 x} \qquad (4)$$

Where c^2 is called the speed of the wave ($c^2 = {K}/{\sigma.\rho}$: thermal conductivity / (specific heat × density)) and it depends solely on the medium. Typically, projects related to partial differential equations are supplemented with initial and boundary conditions.

Since the equation (1) contains the first derivative in time, the initial value problem consists of solving the differential equation with one prerequisite. In other words, the initial temperature (usually at *t*= 0) should be given as initial condition. It is possible that the initial temperature is not constant, but depends on the spatial variable (x). Hence, the temperature distribution should be known:

$$u(x, 0) = \Phi(x) \qquad (2)$$

Various types of boundary conditions can be considered depending on the situation we are dealing with. For instance, when the end of the rod is in contact with a heat bath (heat reservoir), the temperature at this end can be approximated by the following specified temperature:

$$u(0, t) = u_B(t) \qquad (3)$$

International Science and
Technology Journal
المجلة الدولية للعلوم والتقنية

العدد 26
Volume 26

المجلة الدولية للعلوم والتقنية
International Science and Technology Journal
ISTJ

Where the $u_B(t)$ is the heat of the path. Other boundary condition when the end of the rod is completely isolated can be written as:

$$u(L, t) = 0 \tag{4}$$

Where L is the length of the rod

One should mention that when analytical solution of heat equation cannot be obtained, numerical methods can be useful in such cases.

3. Examples and discussions

In order to illustrate the efficiency of the previous methods, solutions of heat equation for some represented examples will be shown in this section. We will consider the heat equation in 1D finite bar with length of l with initial condition of (free heat transfer at the end):

$$u(x, 0) = \Phi(x) = x(l - x), \quad u(0, t) = 0, \\ u(l, t) = 0 \tag{5}$$

3.1 The fundamental solutions

The fundamental solution of the heat equation (1) with set of boundary condition given by (5) can be written as: (see appendix A for maple program).

$$u(x, t) = A_n \sin(\frac{n\pi x}{L}) e^{-\lambda_n^2} \tag{6}$$

Where
$$\lambda = \frac{cn\pi}{L} \tag{7}$$

Starting with n=1, $l = 2\pi$ and c=2, the fundamental model has the formula (see figure 1):
$$u(x, t) = \sin(\frac{x}{2}) e^{-t} \tag{8}$$

International Science and
Technology Journal
المجلة الدولية للعلوم والتقنية

العدد 26
Volume 26

المجلة الدولية للعلوم والتقنية
International Science and Technology Journal
ISTJ
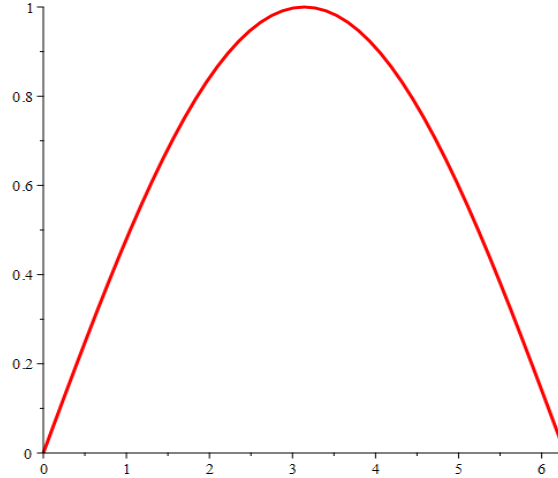
Figure 1. The fundamental solution of heat equation. It can be easily verified that this mode in (8) is indeed a solution of the heat equation.

3.2 Solution Using Fourier Transforms

In order to solve the heat equation using Fourier Transforms, we follow the four following steps: (see appendix B for maple program)
(1) Transform the equation into Fourier space.
(2) Solving the resulting ordinary differential equation. (That is finding Eigenvalues and eigenfunctions).
(3) Transform the results back into real space.
(4) Evaluate the solution (That is inverse Fourier integral).

Applying the previous steps using maple, the final solution for the heat equation using the same boundary conditions in (5) can be written as:

$$solution = \sum_{m=0}^{\infty} \frac{8l^2 e^{-\frac{\pi^2 c^2 (2m+1)^2 t^2}{l^2}} sin\left(\frac{(2m+1)\pi x}{l}\right)}{(2m+1)^3 \, \pi^3} \qquad (9)$$

Using the same values for the constant as above ($l = 2\pi$ and $c=2$), we obtain the fundamental mode by substituting m with 0:

International Science and Technology Journal
المجلة الدولية للعلوم والتقنية

العدد 26
Volume 26

المجلة الدولية للعلوم والتقنية
International Science and Technology Journal
ISTJ

$$S_0 = \sin(\frac{x}{2})e^{-t} \tag{10}$$

This is equal to that obtained in the previous method.

3.3 Solving Cauchy problems for heat equations

The Cauchy problem for the heat equation is the pure initial value problem. It is s quite known to be ill-posed. In other word, errors measurement can be significantly enlarged and ruin the solution. Hence, the solution is no longer continues [8, 9]. The problem arises when scientists attempt to finds the temperature at the surface of a body using inner measurement. Several methods haven been employed in order to tackle the Cauchy problem for heat equation. Nanfuka *et al.* approximate the time derivative by using a cubic smoothing spline. Their method gives goo results at the ends of the measurement interval [10]. Elden studies a modification of the heat equation, where a fourth-order mixed derivative term is added. The error estimation for the modified equation shows that the solution approximate of the solution of the Cauchy problem [11, 12].

Mathematically the problem can be expressed as: (see appendix B for maple program)

$$\begin{cases} u_t - \Delta u = 0 \qquad t \geq 0, \\ u(x, 0) = \Phi(x) \end{cases} \tag{11}$$

Assume the same formula for $\Phi(x)$ as in the previous sections and considering passion's formula:

$$\frac{\int_{-\infty}^{\infty} \xi(1 - \xi)e^{-\frac{(x-\xi)^2}{4t}} d\xi}{2\sqrt{2\pi t}} \tag{12}$$

We obtained the solution:

$$\frac{\int_{-\infty}^{\infty}(\xi\, e^{\frac{x^2}{4t}} e^{\frac{x\xi}{2t}} e^{-\frac{\xi^2}{4t}} l - \xi^2 e^{\frac{x^2}{4t}} e^{\frac{x\xi}{2t}} e^{-\frac{\xi^2}{4t}})d\xi}{2\sqrt{\pi t}} \tag{13}$$

This can be simplified to be written as:
$$sol = xl - x^2 - 2t \tag{14}$$

It is clear that at the solution is continues and satisfy the boundary condition at:

$$u(0,t) = 0, \qquad u(l,t) = 0$$

4. Conclusion

As demonstrated in the results, heat equation was solved very efficiently by two different methods using Maple software. The solution for the studied case were identical to those expected. Moreover, Maple was able to handle the Cauchy problem for heat equation very effectively without any modifications or approximations.

References

[1] G. Bluman, "Review: Peter J. Olver, Applications of Lie groups to differential equations," *Bulletin (New Series) of the American Mathematical Society*, vol. 18, 1988.

[2] G. Bluman and K. Sk, "Symmetries and Differential Equations", Springer-Verlag, 1989.

[3] L. Kohaupt, "Introduction to the discrete Fourier series considering both mathematical and engineering aspects - A linear-algebra approach", *Cogent Education*, vol. 2, Issue. 1, (1064560), 2015.

[4] S. Mazumder, " *Numerical Methods for Partial Differential Equations* ", Academic Press, 2016.

[5] [H. Niroumand, " *Irregular Shape Anchor in Cohesionless Soils*", Butterworth-Heinemann, 2017.

[6] H. S. Carslaw. and J. C. Jaeger, "Conduction of Heat in Solids", Springer Cham, 1947.

[7] L. S. Goddard, "Mathematics and the Conduction of Heat in Solids," *Nature*, vol. 186, Issue. 4723, (421-422), 1960.

[8] S.-Y. Chung, "Uniqueness in the Cauchy problem for the heat equation," *Proceedings of the Edinburgh Mathematical Society*, vol. 42, Issue. 3, (455-468), 2009.

[9] F. F. Dou and Y. C. Hon, "Kernel-based approximation for Cauchy problem of the time-fractional diffusion equation," *Engineering Analysis with Boundary Elements*, vol. 36, Issue. 9, (1344-1352), 2012.

[10] M. Nanfuka, F. Berntsson and G. Kakuba, "Solving a Cauchy problem for the heat equation using cubic smoothing splines," *Applicable Analysis*, (1-16), 2021.

[11] L. Elden, "Approximations for a Cauchy problem for the heat equation," *Inverse Problems*, vol. 3, Issue. 2, (263-273), 1987.

[12] L. Elden, "Hyperbolic approximations for a Cauchy problem for the heat equation," *Inverse Problems*, vol. 4, Issue. 1, (59-70), 1988.

Appendix A

```
>      restart;assume(n,integer):with(plots):
```

- The fundamental solutions

```
>      Su:=u=(A[n]*sin(n*Pi*x/l))*exp(-lambda[n]^2*t);
>      Slambda:=lambda[n]=c*n*Pi/l;
```

- verify the solution of the equation:

```
>      Diff(u,t) -
c^2*Diff(u,`$`(x,2))=eval(subs(Su,diff(u,`$`(t,2)) -
c^2*diff(u,`$`(x,2)))));

>      M1:=subs(n=1,l=2*Pi,c=2,subs(Su,Slambda,A[n]=1,u));

>      Plot( M1,x=0..2*Pi, color=red,thickness=3);
```

International Science and
Technology Journal
المجلة الدولية للعلوم والتقنية

العدد 26
Volume 26

المجلة الدولية للعلوم والتقنية
International Science and Technology Journal
ISTJ

Appendix B

• Set the equation and the BCs

```
>       restart;with(linalg):

>       eq:=diff(u(x,t),t)-c^2*diff(u(x,t),x,x)=0;0<x,x<l,t>0;

>       init_c:=u(x,0)=phi(x);

>       bound_c:=u(0,t)=0,u(l,t)=0;

>       phi:=x->x*(l-x);

>       l>0;
```


•   Eigenvalues and eigenfunctions

```
>       L:=-diff(y(x),x,x)=lambda*y(x);

>       s1:=y(0)=0; s2:=y(l)=0;

>       assume(lambda>0,l>0,c>0);

>       dsolve(L,y(x));

>       y :=unapply( rhs(%),x);

>       sist:={s1,s2};

>       genmatrix(sist,{_C1,_C2});

>       chl:=det(%);

>       _EnvAllSolutions := true:

>       solve(chl,lambda);

>       indets(%) minus [1];

>       subs(%[1]='k',%%):

>       ev:=unapply(%,k);

>       y:='y':assume(k,posint);
```

> subs(lambda=ev(k),L);

> dsolve({%,s1,s2},y(x));

> rhs(%)/sqrt(int(rhs(%)^2,x=0..l));

> simplify(%,radical,symbolic):

> ef:=unapply(%,(k,x)):

> ev(k);ef(k,x);

• Solution we find in form:

> spr:=Sum(T[k](t)*ef(k,x),k=1..infinity);

• Solving the ODE:

> ode:={diff(u(t),t)+c^2*ev(k)*u(t)=0,

> u(0)=int((phi(x))*ef(k,x),x=0..l)};

> dsolve(ode,u(t));

• Solution

> sol:=subs(T[k](t)=rhs(%),spr);

We convert this solution to other form. Index   change to   :

> subs(k=2*m+1,op(1,%));assume(m,integer):

> simplify(%):factor(%);

> Sum(%,m=0..infinity):

> solution:=subs(c='c',k='k',l='l',m='m',%);

International Science and
Technology Journal
المجلة الدولية للعلوم والتقنية

العدد 26
Volume 26

المجلة الدولية للعلوم والتقنية
International Science and Technology Journal
ISTJ

Appendix C

- Solving Cauchy problems for heat equations

```
>       restart;
>       eq:=diff(u(x,t),t)-diff(u(x,t),x,x)=0;
>       ic:=u(x,0)=x*(l-x);c:=sqrt(-coeff(lhs(eq),diff(u(x,t),x,x)));
>       phi:=unapply(rhs(ic),x);
```

- Solving the equation By Poisson formula:

```
>       1/sqrt(4*c^2*Pi*t)*Int(phi(xi)*exp(-(x-
xi)^2/(4*c^2*t)),xi=-infinity..infinity);
>       assume(t>0);
>       convert(%,exp);
>       expand(%);
>       value(%);
>       evalc(%);
•       The Solution
>       sol:=simplify(%);
•       Verfiy the solution
>       u:=unapply(sol,(x,t)):
>       simplify(lhs(eq)-rhs(eq));
>       simplify(lhs(ic)-rhs(ic));
>       u:='u':
```

To Analyze and Compare BS and ACI Code Identifying Minimum Cost for Building Materials Used In Building Construction.

Abdurauf Jumma s. Alnaif [1] .
[1]leacture At Alkoms High Institute.

rawoff@yahoo.com

Abstract

All the building structures have to design based on the relevant code of practice of standard. The choice of the standard code to be applied is vary and sometimes depending on the requirement of the local authority or familiarity of the designers. Standard code is essential in the reinforced concrete structures design to provide a safety and economic design. Currently, BS 8110 and ACI-318 are the most widely use standards in designing reinforced concrete structures based on limit state principle. However, some of the design requirements such as partial safety factors, material properties, load combinations, etc. are difference between BS 8110 and ACI-318. This may affect the cost of building structures that were designed using these two standards. The aim of this study is to compare the cost of the reinforced concrete structures for a four storey shop office building which will be designed using BS 8110 and ACI-318. The material properties such as characteristics strength of reinforcements and concrete, and dimensions of the structure elements are fixed. ESTEEM 7 as the reinforced concrete structure design package will be used to design and produce the structural detailing for the building based on BS 8110 and ACI-318. The output of the structural detailing will be analysed to compare the cost of structure elements. The optimum reinforced concrete structure design standard will be identified. As a final result for both ACI & BS CODES, it's clear that every method has

International Science and
Technology Journal
المجلة الدولية للعلوم والتقنية

العدد 26
Volume 26

المجلة الدولية للعلوم والتقنية
International Science and Technology Journal
ISTJ

its main strength and weakness in each individual part of the design.

Keywords: Reinforced concrete structures, cost, and design code.

الخلاصة :

تصمم عادة المنشأة بناء على مواصفات وشروط محددة ، تضمن معياريين التصميم المشهورين الأمان والإقتصادية، هذه المواصفات والتي تحدد أبعاد العناصر الإنشائية وكميات التسليح في النهاية، بناء على أوزان المنشأ وأحمال قد يتعرض لها، تختلف من بلد إلى أخرى، على العموم المواصفات الأمريكية والمواصفات الإنجليزية، الخاصة بتصميم المنشأة الخرسانية ،تضمن معياري التصميم المهمين، الأمان والإقتصادية، إلا أنه تم الكثير من الفوارق بينهما فعلى سبيل المثال الأحمال المستخدمة في التصميم وطريقة تضخيمها ، وعوامل الأمان وغيرها. الأمر الذي دعانا إلى مقارنة المواصفات الامريكية والمواصفات البريطانية، وبالتحديد دراسة أكثرهم إقتصادية، مبنى خرساني صمم بالطريقتين بإستخدام برنامج (اس تيم) والنتائج تم تحليلها. وفي النهاية بالنسبة للمواصفات الامريكية أو الانجليزية يتضح أن لكل طريقة نقاط قوة وضعف لكل قطاع أو عنصر .

1.0 Introduction.

Structural design is a process of selecting the material type and conducting in-depth calculation of a structure to fulfill its construction requirements. The main purpose of structural design is to produce a safe, economic and functional building. Structural design should also be an integration of art and science. It is a process of converting an architectural perspective into a practical and reasonable entity at construction site. (Chan Chee, 2007). One of the important things to be considered in any construction is the cost effectiveness (i.e. how economical the construction will be at the end of construction). Often a times, constructions become uneconomical (too expensive) when too much emphasis is laid on the quality alone. Therefore there should be a balance between quality control and cost effectiveness. The codes and standards that

International Science and
Technology Journal
المجلة الدولية للعلوم والتقنية

العدد 26
Volume 26

المجلة الدولية للعلوم والتقنية
ISTJ
International Science and Technology Journal

impact modern building construction are constantly in flux and changing, and it is difficult to keep up with copious changes and how they will impact building design. In the structural design of concrete structures, Refereeing to standard code is essential. A standard code serves as a reference document with important guidance. The contents of the standard code generally cover comprehensive details of a design. These details include the basis and concept of design, specification to be followed, design methods, safety factors, loading values and etc. These codes and standards define the parameters in the reinforced concrete design process that affect the cost of materials. This would include the dimensions(X, Y, Z) of the different reinforced concrete elements, the area of reinforcements and ratio of reinforcement limit values.

For the purpose of this research, two standard codes namely "British Standard and American Standard Codes" are selected for comparison in terms of their design outcomes and at the end to evaluate and compare the costs from the two systems of codes used in the design. The aim of this study is to make a comparison between ACI and BS code to obtain minimum cost designs of reinforced concrete structure and the objective function is the total cost of the building including the cost of the concrete, reinforcing steel and labor for concrete and reinforcing steel.

1.1 Problem Statement.

Cost indicators are important during the design phase to minimize the construction cost. Excellent designers must have the ability to organize and manage the process of design so with special consideration to cost effectiveness during the design process. In today's construction industry, the commonest codes of practice used are the ACI and BS codes. However the problem of cost ineffectiveness is becoming so rampant. Although lack of experience from the engineers also affects the design which eventually affect the cost. For this reseason this research is

International Science and Technology Journal
Technology Journal
المجلة الدولية للعلوم والتقنية

العدد 26
Volume 26

المجلة الدولية للعلوم والتقنية
International Science and Technology Journal
ISTJ

dedicated to find out the cause through comparing the effectiveness of the two aforementioned codes.

1.2 Objectives.

The main objectives of this study are:

1- To make comparison of related parameters between ACI and BS codes in order to obtain the most economical alternative solution.

2- To ascertain the accuracy of the analysis and the design using software (ESTEEM).

3- To achieve an ultimate design in terms of quality at minimal cost.

1.3 Scope Of Study.

The project focuses mainly on cost of concrete and reinforcement, the structure is a four storey building. This structure is intended to serve as an office building. The codes used are the ACI 318-02 and BS PART 1:1997. And the selected software to used is ESTEEM.

2.0 Literature Review.

2.1 Building Codes and Standards.

The codes and standards that impact modern building construction are constantly in flux, and it is difficult at best to keep up with copious changes and how they will impact building design. For engineers and architects who is working with structural design.

2.1.1 BS 8110 Building Code: Part 1:1997.

BS 8110 part 1 gives recommendations for the structural use of concrete building and structures, excluding bridges and structural concrete made with high alumina cement. The aim of design is the achievements of an acceptable probability that structures being design will perform satisfactory during their intended life. With an appropriate degree of safety, they should sustain all the loads and deformation of normal construction and use and have adequate durability and resistance to the effects of misuse and fire. The

International Science and
Technology Journal
المجلة الدولية للعلوم والتقنية

العدد 26
Volume 26

المجلة الدولية للعلوم والتقنية
International Science and Technology Journal
ISTJ

structure should be so designed that adequate means exist to transmit the design ultimate dead, wind and imposed loads safely from the highest supported level to the foundations (British code, 1997). The design strengths of materials and design loads should be based on the loads and material properties as in the BS 8110 and as appropriate for the serviceability limit state (SLS). The design should satisfy the requirement that no SLS is reached by rupture of any section, by overturning or by buckling under the worst combination of ultimate loads.

2.1.2 ACI 318 Building Code (ACI 318-02).

The American concrete institute standard 318, building code requirements for reinforced concrete, has permitted the design of reinforced concrete structure in accordance with limit state principles using load and resistance factors since1963. A probabilistic assessment of these factors and implied safety levels is made, along with consideration of alternate factors values and formats. (A discussion of issues related to construction safety of existing structure is included). Working stress principles and linear elastic theory formed the basis for reinforced concrete design prior to 1983, when the concept of ultimate strength design was incorporated in the ACI building code (ACI318-02), (Edward cohen, 1971). Because of the highly nonlinear nature of reinforced concrete behavior, the linear approach was unable to provide a realistic assessment of true safety levels (Andrew Scanlon, 1992).

The developers of ACI 318-02, who introduced the idea of load and resistance factors to account for uncertainties in both load and resistance .Probabilistic methods were developed and refined during the late 1960s in response to the need to consider variability and uncertainty, explicitly and rationally. Proposed formulations include code incorporation of explicit second moment probabilistic procedures. In such an approach, the designer would select a desired safety index "B" and carry out the design utilizing the

International Science and Technology Journal
المجلة الدولية للعلوم والتقنية

العدد 26
Volume 26

المجلة الدولية للعلوم والتقنية
International Science and Technology Journal
ISTJ

means standard deviations of the load and resistance variables. The safety index positions the mean load effect to ensure attainment of the target reliability (American code). The explicit second moment approach was not considered by ACI38 or other major code writing organizations. (Edward Cohen, 1971).

2.2 Optimum Cost Of Reinforced Concrete Building.

The meaning of the optimum cost of reinforced concrete building with some studies, which it is minimum quantity of concrete and steel in any construction or it is the minimum cost of the construction but the most studies explains the optimum cost by minimum quantity of concrete and steel in any construction. The primary objective of economic analysis is to secure cost-effectiveness for the client. In order to achieve this, it is necessary to identify and to evaluate the probable economic outcome of a proposed construction project. An analysis is required from the viewpoint of the owner of the project when doing the proposal, the analysis can be evaluated the followings (Ashworth A., 1994) to achieve maximum profitability from the project concerned, to minimize construction costs within the criteria set for design, quality and space, to maximize any social benefits, to minimize risk and uncertainty and to maximize safety, quality and public image. Cost is one of the important factors that will affect method of construction, quality of work, period of the construction and most of all, the success of a project. Cost studies of building are part of the economic studies. It seeks to ensure the efficient use of all available sources to construction. Client's requirements, possible effect on the surrounding areas, relationship of space and shape, assessment of the initial cost, the reason for, and method of, controlling costs, the estimation of the life of buildings and material need to be studied so as to improve the efficiency of cost control in construction (Flanagan R. and Tate B., 1997).

International Science and Technology Journal
المجلة الدولية للعلوم والتقنية

العدد 26
Volume 26

المجلة الدولية للعلوم والتقنية
International Science and Technology Journal
ISTJ

2.3 Factors Contributing To The Cost Of Building Construction.

Implementation of a construction projects is a complicated and complex process (Neap H.S and Celik T., 2001). Costs of construction are divided into categories such as material, labor, plant, and overhead costs according to cost break down structure (Rasdorf and Abudayyeh, 1991; Wanh and Huan, 2000). Cost variance report shows the actual costs, work hours, and earning of construction; comparing the cost of construction to the budget and calculating the variance which can highlight problem areas; calculate the forecast final cost of construction and to compare this to the final earnings and budget (Teicholz, 1974). All disturbances regarding the cost must be detected periodically (Popescu, 1977). The collection, analysis, publication and retrieval of cost and price information are very important to the construction industry. Contractors and surveyors will tend, wherever possible, to use their own generated data in preference to commercially published data, since the former incorporate those factors which are relevant to them. Published data will therefore be used for backup purpose. The existence of a wide variety of published data leads one to suppose, that it is much more greatly relied on than is sometimes admitted (Ashworth A., 1994)

2.4 Construction Cost.

Building costs are a subject that has been studied thoroughly over the years. Several factors influence the total expenditure; material choices, labor costs and the working hours of those involved in executing the work, and cost for machinery used in executing the work. Furthermore the cost capital (financing) for the investor as well as the contractor has to be considered. A comparative breakdown of the construction costs of a concrete building (office or residential) reveals that the superstructure represents approximately 10 to 15 percent of the total cost, a figure which has

International Science and Technology Journal
المجلة الدولية للعلوم والتقنية

العدد 26
Volume 26

المجلة الدولية للعلوم والتقنية
International Science and Technology Journal
ISTJ

decreased during the years. The main difference today is that the costs for cladding, finish and especially service installations have increased during the years. Owners and occupiers today have greater demands and different needs. And they expect higher standards. Valence emphasis's the fact that the cost of construction is only a small part of the total costs of a building during its life cycle (Best & Valence 1999).

2.5 Basic Principles Of Cost.

Most decision makers recognize that there are only a few variables that have a large influence on a building's costs. Brandon has classified these variables into two categories decisions concerning the size of the buildings and decisions concerning material specifications and building configuration (Figure 1). This section will review these major factors that contribute to the cost of the building.

Figure 1 Design / Costs relationships.

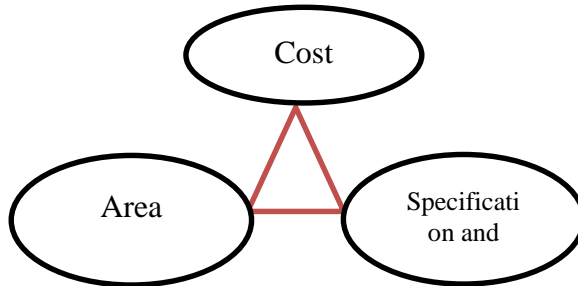## 3.0 Research Methodology.

The proposed methodology is based on designing the building by software program (ESTEEM) with two codes, each code has different properties of concrete and steel ,such as the concrete compressive strength (fc), the yield strength of steel (fy) ,the various combinations of the load, the allowable ratio for minimum and maximum reinforcement and other properties , in

practice ,designed of the elements are governed by various architectural requirements. If the height and width of the beam are located ,the designs allocatr the right amount of steel but, in this study ,we assumed that the dimension of the beams and columns are not given .hence ,during the design by ESTEEM software, we will start with small dimensions ,in this case the program will check if the dimensions were acceptable or not ,here if the dimensions are small this message from program report will come out "please note: max/min reinforcement sizes do not permit acceptable bar spacing ,increase member size" .so, we will increase the member size till we get the first acceptable dimensions that have the first acceptable amount of steel. After designed the model according to BS and ACI code, the minimum cost will be the one which has the minimum total cost of concrete and steel.

3.1 Model Of Design.

The model that will be designed is a multi-stories reinforced concrete commercial building which has length of 20.00 m x 15.00 m width and the building consists of four stories, three stories upon the ground with height 3.5 m. Figure 2 ,3, 4 ,5 shows the plan of the building, Table 1 shows the Design detail of the building.
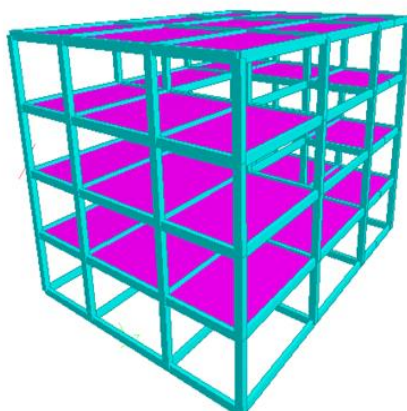
Figure 2 Isometric.
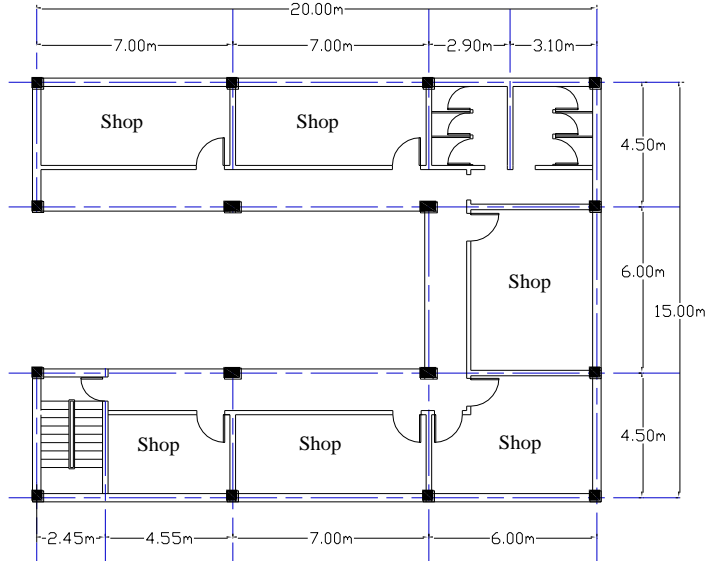
Figure 3 First & second floor Plan.
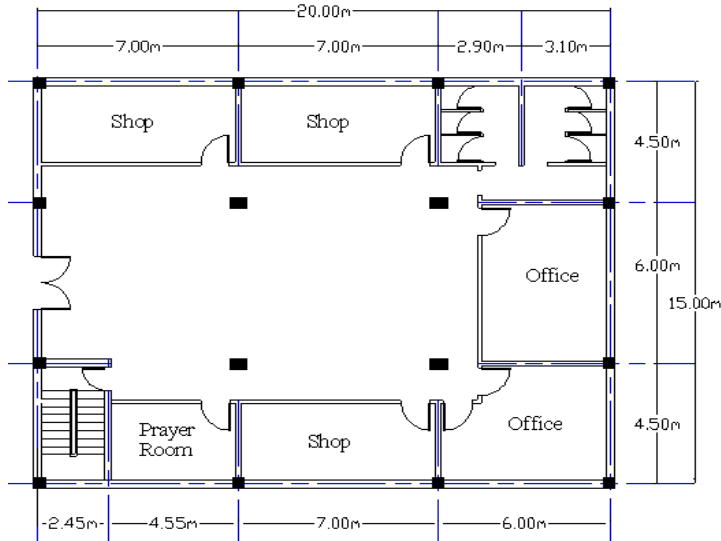
Figure 4. Ground floor Plan.

حقوق الطبع محفوظة
للمجلة الدولية للعلوم والتقنية

International Science and
Technology Journal
المجلة الدولية للعلوم والتقنية

العدد 26
Volume 26

المجلة الدولية للعلوم والتقنية
International Science and Technology Journal
ISTJ
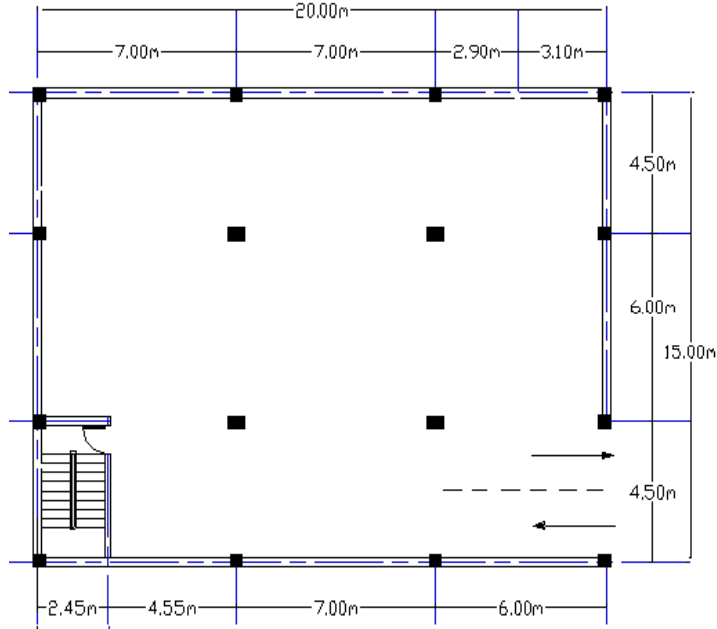
Figure 5. Basement floor Plan.

Table 1 Design detail of the building.

Building usage	offices	
Story height	Basement	3.50 m
	Ground floor	3.50 m
	1th & 2th	3.50 m
Length of building		20.0 m
Width of building		15.0 m
Height of building		14.0 m

3.2 DESIGN SPECIFICATIONS AND PROPERTIES OF THE STRUCTURE.

The initial sizing of members and specifications of the frame building are shown in Table 2&3. The initial sizes of member were checked against the conditions according to serviceability limit state and ultimate limit state. The sizes were adjusted until the

conditions of serviceability limit state and ultimate limit state stated in BS 8110 and ACI318-02 were satisfied.

Table 2 Initial sizes and specification of the building according to BS8110 code

Structural Elements		Dimensional
Columns	Basement	400x350 mm
	Ground floor	400x350 mm
	1th to 2th	400x350 mm
Beams		400x200 mm
Slab		225 mm THK.
No. of stories		4 stories
Beam to column connection = fixed		
Column to base connection = fixed		

Table 3 Initial sizes and specification of the building according to ACI318 code.

Structural Elements		Dimensional
Columns	Basement	400x300 mm
	Ground floor	400x300 mm
	1th to 2th	400x300 mm
Beams		400x200 mm
Slab		175 mm THK.
No. of stories		4 stories
Beam to column connection = fixed		
Column to base connection = fixed		

3.3 Modeling and Simulation Of The Building.
3.3.1 Methodology.

The proposed methodology is based on designing the building by software program (ESTEEM) with two codes, BS8110 :Patr 1: 1997 & ACI 318-02.In this study, will be use four load cases as following:-

Table 4 cases of design

NO. OF CASE	CODE USED	LOAD CASE USED
1	BS 8110-1997	BS 8110-1997
2	ACI 310-02	ACI 318-02
3	BS 8110-1997	ACI 318-02
4	ACI 318-02	BS 8110-1997

3.4 Research procedure.

Throughout the study, all properties of element and concrete elements diminution will be predetermined and fixed for all analysis and design for each code The plan of the model will be first drafted using the AutoCAD. The plan will then be imported to (ESTEEM).elements will be assign based on the plan and a 3D model will be generated. The properties of each element will then be assign. The model will then be analysis and design by (ESTEEM) software through the 'external tools' for analysis.

3.4.1 Material Properties.

Every material has different properties that are simply of their own. Similarly, the material used in the design of the structure in this research also has different properties and strength. Table 5&6 lists the material properties applied in the preliminary analysis of the design of the structural members (beams, slabs and columns, etc.) The values of compressive strength of concrete, yield stress of reinforcement, concrete density and modulus of elasticity conforms to BS 8110: Part 1: 1997 and BS 8110: Part 2: 1985 & ACI 318.

Table 5 Material Properties conform to BS8110 code

Structure Elements	Parameters
Compressive strength; $f$cu. Beams, Slabs, Columns	30 N/mm^2
Density of concrete	24 kN/m^3
Modulus of elasticity; E	21.718 KN/mm^2
Yield stress fy	460 N/mm^2

International Science and Technology Journal
المجلة الدولية للعلوم والتقنية

العدد 26
Volume 26

المجلة الدولية للعلوم والتقنية
ISTJ

Table 6 Material Properties conform to ACI318 code

Structure Elements	Parameters
Compressive strength; fcu. Beams, Slabs, Columns	$28\ \text{N/mm}^2$
Density of concrete	$24\ \text{kN/m}^3$
Modulus of elasticity; E	$21.718\ \text{KN/mm}^2$
Yield stress fy	$416\ \text{N/mm}^2$

3.4.2 Procedures Of Determination Of Loading.

The simulation of load determination on members of the structure on three dimensional structural frames was used; the procedure utilizes load analysis to find the dimension of members to be used later on finding the optimal economic code. Dead load and live load were applied to the structure.

3.4.2.1 Determination Dead Load.

All of the dead loads are according to the (ACI318 &BS8110) Codes. It is defined as the sum of all constant and continuous loads occurred on the building

Which represents:

- Own weight of structure
- Floor covering
- Wall loads

➢ **Own weight of structure**

Own weight of structure represents the weight of the main elements of the building, such as slabs, beams and columns. Table 7&8 shows the details of slabs weight according to BS8110 and ACI318-02 codes.

Table 7 Details of slab self-weight according to BS8110 Code

DEAD LOAD			
FROM	TYPE	MAGNITUDE	UNIT
Slab self-weight of 225mm thickness (without finishes)	Area pressure	5.4	KN/m^2

International Science and Technology Journal
المجلة الدولية للعلوم والتقنية

العدد 26
Volume 26

المجلة الدولية للعلوم والتقنية
ISTJ
International Science and Technology Journal

Table 8 Details of slab self weight according to ACI318 Code

DEAD LOAD			
FROM	TYPE	MAGNITUDE	UNIT
Slab self-weight of 175 mm thickness (without finishes)	Area pressure	4.2	KN/m^2

> **Flooring Cover.**

Flooring cover represents the weight of finishing materials on floor, such as sand, bitumen, mortar and marble. Table 9 shows the details of dead load on floor and surface slabs.

Table 9 Details of dead load on surfaces as component of concrete slab

DEAD LOAD (FLOORING COVERING)			
FROM	TYPE	MAGNITUDE	UNIT
floor slab	Area pressure	1.00	KN/m^2
Surface slab	Area pressure	2	KN/m^2

> **Wall loads.**

The wall in the building is from concrete blocks, the thickness of wall is 0.25m for exterior wall and 0.2m for interior wall, therefore, the load of wall on beam will be:

> For exterior walls:

H = 3.5m

W= 0.25 X 3.5 X18 + 0.02 X 3.5 X 24 =17.430 KN/m

> For interior walls:

H = 3.5m

W= 0.2 X 3.5 X18+ 0.02 X 3.5 X 24 = 14.380 KN/m

International Science and
Technology Journal
المجلة الدولية للعلوم والتقنية

العدد 26
Volume 26

المجلة الدولية للعلوم والتقنية
International Science and Technology Journal

ISTJ

3.4.2.2 Determination Live Load.

It is defined as the sum of all variable movable loads occurring in the building.

This represents:

Human weights, Furniture weights, Table 10&11 shows standard design of live load on the building.

➢ **According to BS standard code.**

Table 10 British standard design of live load on the building.

Type of building (office building)	LOAD (KN/m^2)
Catwalks for maintenance access	1.0
Stationary stores	4 for each meter of storage height
Boiler rooms ,motor rooms ,fan rooms and the like, including the weight of machinery	7.5
Corridors, hallways, etc. subject to loads greater than from crowds , such as wheeled vehicles, trolleys and the like	5.0
File rooms ,filing and storage space	5.0
Corridors ,hall ways, stairs, landings, footbridges,etc	4.0
Offices with fixed computers or similar equipment	3.5
Laboratories (including equipment), kitchens, laundries	3.0
Banking halls	3.0
Offices for general use	2.5
Toilet rooms	2.5
Balconies	Same as rooms to which they give access but with a minimum of 4.0

Note: refer to: BS6399 part 1:1984, Section 4, table 8, Code of practice for imposed load (formerly cp3: chapter v: part 1).

➢ **According to BS standard code.**

Table 11 American standard Design Minimum Loads for Building.

Type of building (office building)		LOAD (KN/m^2)
Catwalks for maintenance access		1.92
Access floor system	Office use	2.4
	Computer use	4.79
File and computer rooms shall be designed for heavier loads based on anticipated occupancy Lobbies and first-floor corridors		4.79
Offices		2.40
corridors above first floor		3.83
Balconies (exterior)		4.79
Catwalks for maintenance access		1.92
Private rooms and corridors serving them		1.92
Public rooms and corridors serving them		4.79

Note: Refer to **ASCE 7-05 Section 4.9** (pg 12), Table 4.1.

3.4.2.3 Design Load Combinations:-
  ➢ **Load Factors According To ACI Code.**
The design load combinations are the various combination of the load cases for which the structure needs to be designed. For ACI 318-08 if a structure is subjected to dead load (D), live load (L), the required strength U to resist dead load D and live load L shall not be less than Combination factors (LRFD):

- U = 1.4D
- U = 1.2D + 1.6L

Where:
- o D = dead load;
- o L = live load.
  ➢ **Load Factors According To BS Code.**
The design load combinations are the various combination of the load cases for which the structure needs to be designed. The design load combinations are obtained by multiplying the characteristic

loads by appropriate partial factors of safety, γf (BS2.4.1.3). For BS8110 -1997, if a structure is subjected to dead load and live load, the basic combination without lateral load is

- U= 1.4DL+1.6LL

Where:

o In which d D and L are dead and live load, respectively. The higher load factor for live load reflects its higher variability.

4.0 .Result.

Figure 6 shows the output result of the designing program (ESTEEM7) Showing the quantity of steel & concrete for BS and ACI Codes.
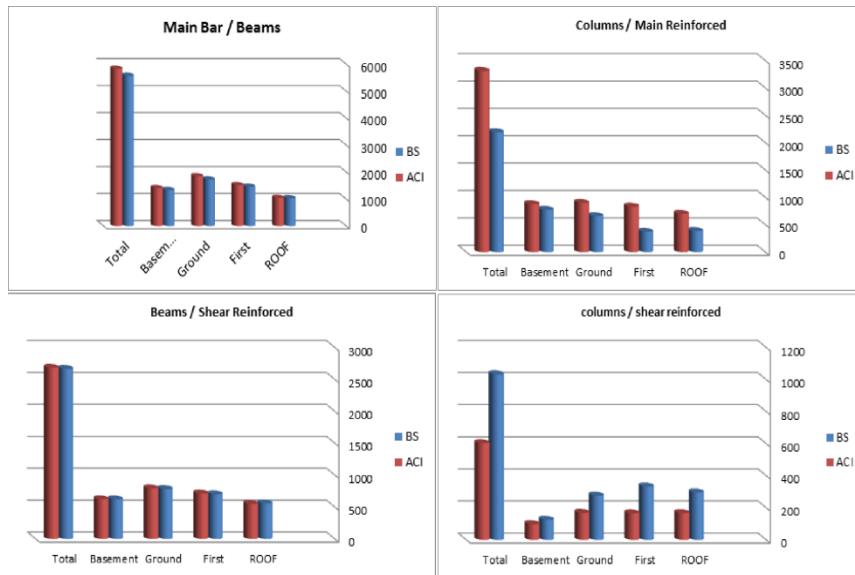

Figure 6 Main& shear bars quantity of the elements.

International Science and Technology Journal
المجلة الدولية للعلوم والتقنية

العدد 26
Volume 26

المجلة الدولية للعلوم والتقنية
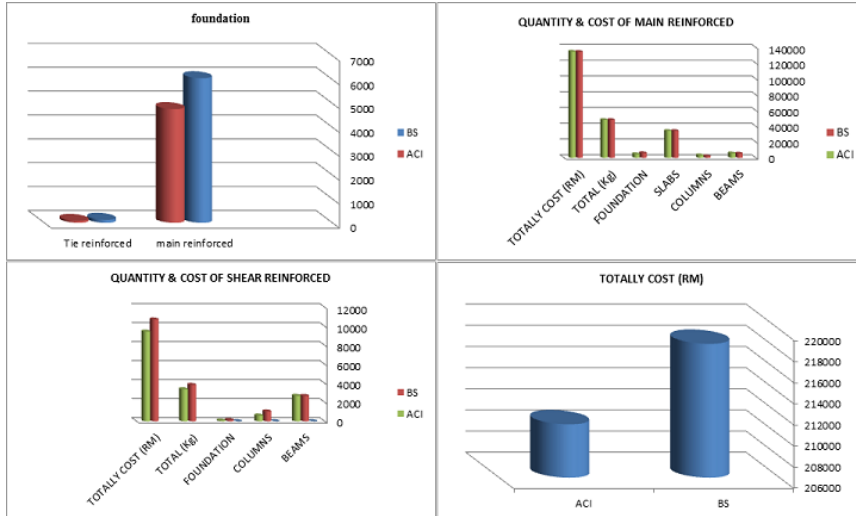International Science and Technology Journal
ISTJ

Figure 7   Cost of The Building.

As a final result for both ACI & BS CODES ,it's clear that every method has its main strength and weakness in each individual part of the design. In general the financial part can be considered as one of the important factors that affect the reinforced concrete buildings. figure 7 shows that, the total cost of BS8110 code is more than ACI code by 3.6%, calculation as show, by which this answers the second objective of the research, which an ultimate design in terms of quality at minimal cost.

4.0 REFERENCES.

[1] ACI, 2008. Building Code Requirements for Structural Concrete (Aci318-08) and Commentary (ACI318R-08), American Concrete Institute.

[2] Ashworth, 1994. Cost Studies of Buildings .Harlow: Longman Group Limited.

[3] BS 8110. 1997. Structural use of concrete, code of practice for design and construction. London: British Standards Institution.

[4] Best and Valence. 1999. Getting it right at the start In Building in value, Arnold, London, pp. 1-9.

[5] Edward Cohen, 1971.Commentary on Building Code Requirements for Reinforced Concrete (ACI 318-71). American Concrete Institute, Redford Station Detroit, Michigan.

[6] Edward Cohen, 1971.Commentary on Building Code Requirements for Reinforced Concrete (ACI 318-71). American Concrete Institute, Redford Station Detroit, Michigan.

[7] Flanagan, R.And Tate, B (1997) Cost Control in Building Design: An Interactive Learning Tool (Blackwell Science).

[8] Neap H. S. And Celik T. 2001. Knowledge-Based System for Determination of Marginal Value of Building Projects Journal of Expert System with Application, Vol.21, Pp.119-129.

[9] Popescu C. 1977. CPM-Cost Control bu Computer Journal of the Construction Division, Vol. 103 (C04), pp .593-609.

[10]   Rasdorf, w.j.and abudayyeh, o. y. 1991. Cost-and schedule- control integration issues and needs. Journal of contraction engineering and mangament, 117(3), 486-502.

[11]   Teicholz, P. 1974. Requirements of Construction Company Cost System. Journal Of The Construction Division, 100(Co3), 255-263.

[12]   Wang. H. And Huang, Y. C. 2000. A New Approach to Calculating Project Cost Variance. International Journal of Project Management, 18,263-138.

TRANSFORMED METHOD FOR SOLVING BLACK-SCHOLES PDE OF THE ASIAN OPTION

ZIENEB ALI ELSHEGMANI[1]

MANAL ALTAHER ELZEDANI[2]

[1,2]Faculty of Education, Misurata University, Libya
Email: [1]z.elshegmani@edu.misuratau.edu.ly
[2]m.elzidani@edu.misuratau.edu.ly

Abstract

Analytical solution of the arithmetic Asian options of the Black-Scholes partial differential equation (PDE) is not known in a closed-form solution, this is due to the difficulty of transforming this PDE to a simpler equation, which could be easier to solve. In this paper, we derive a closed form solution for a continuous arithmetic Asian option by means of partial differential equations. and provide a new transformed method for solving arithmetic Asian options PDEs using general transformation techniques, this transformation reduces the two dimensions PDE of the arithmetic Asian options to the classical Black-Scholes PDE with one dimension. In addition, we use Mellin transform to obtain the final solution to the arithmetic Asian option partial differential equation.
Keywords: Black-Scholes PDE, arithmetic Asian option, Mellin transform.

الملخص

الحل التحليلي لمعادلة الخيار الأسيوي الحسابي التفاضلية الجزئية لبلاك سكوليز ليس معرفا بصيغة تحليلية صريحة، وذلك لصعوبة تحويل هذه المعادلة إلي معادلة تفاضلية ابسط يسهل حلها. في هذا العمل نستنتج صيغة جديدة لحل المعادلة وذلك باستخدام بعض التحويلات العامة للمعادلات التفاضلية الجزئية. حيث تم تحويل المعادلة التفاضلية للخيار الأسيوي الحسابي إلي الصيغة المبسطة لمعادلة بلاك سكوليز، والتي

International Science and
Technology Journal
المجلة الدولية للعلوم والتقنية

العدد 26
Volume 26

ISTJ

من خلالها تم تحويل معادلة الخيار الأسيوي من معادلة تفاضلية جزئية في بعدين
إلي معادلة ذات بعد واحد. و للحصول على الحل التحليلي النهائي تم استخدام تحويل
ميلان.

1. INTRODUCTION

Asian option is a kind of path-dependent option where the payoff function depends on the historical average of the underlying asset. Asian options are very useful in the financial industry. They can be used to hedge a thinly traded asset over a certain period of time. The hedge is cheaper than a portfolio of plain vanilla options. In addition to the cost-effectiveness, the Asian option has another advantage over the plain vanilla option in that it can be used to protect against price manipulation by either contract party on the maturity date. However, the pricing of Asian option remains a challenge.

There are only some simple cases where the price of path-dependent contingent claims can be obtained in closed-form [2];if the underlying asset price follows a lognormal stochastic process, then its geometric average has a lognormal probability density and in this case there is a closed-form solution [1]. However, for the arithmetic average case there is no closed-form solution to value these types of options. There are some numerical procedures for both geometric and arithmetic Asian options using Monte Carlo and finite difference methods. Using stochastic calculus, and specifically the Bessel processes, [7] used Laplace transform in time of the Asian option price. However, this transform is only applicable in some cases. [10] transformed the problem of valuing Asian options to the problem of solving a parabolic equation in two variables from a second order. However, it is difficult to solve this equation analytically or numerically. And they derived lower-bound formulas for Asian options by computing the expectation based on some zero-mean Gaussian variable. [12] presented a theory of continuously-sampled Asian option pricing; he solves the PDE with perturbation approach. And he showed that, the PDE of the arithmetic Asian option cannot be transformed to the heat equation with constant coefficients. [11] is based on Asian option as option on a traded account; he provided a one-dimension PDE

International Science and Technology Journal
Technology Journal
المجلة الدولية للعلوم والتقنية

العدد 26
Volume 26

المجلة الدولية للعلوم والتقنية
International Science and Technology Journal
ISTJ

for Asian options. [4] obtained the same solution of Geman and Yor for arithmetic Asian options using Partial differential equations, integral transforms, and Mathematica programming, instead of Bessel processes. [5] obtained an analytical formula for the Laplace transform in time of the Asian option, and they obtain asymptotic solutions for Black-Scholes PDE of Asian options for low-volatility limit which is the big problem on using Laplace transform. Using general stochastic differential equations [6] derived a modified arithmetic Asian option PDE, and they provided its analytical solution. [3] got pricing of arithmetic Asian options under stochastic volatility dynamics.

This article is provides analytical solution for the arithmetic Asian option PDE by using general transformation techniques, and Mellin transform.

Definition 1.1 [1]

Black-Scholes model is a mathematical model that is investigated to describe values of European options. The model is basically a second order partial differential equation in two variables, and the solution of this model provides the value of the European options at every single time.

There are different kinds of the options in the real financial world, but we will address the most commonly used, European options, American options, and Asian options. Option which can be exercised only at expiration date is called European options, option which can be exercised at any time up to expiration date is called American options, and option that its payoff depends on the average of stock price is called Asian options.

Definition 1.2 [10]

Option is a contract that gives the holder of the option (long position) the right but not obligation to exercise the option with a writer (short position). Exercise the option means that, buy or sell a specific amount of a given stock, commodity, currency, dept, or index at a specific price called the strike price or exercise price, during a specific period of time called life of the option or at the expiration date. The writer is obligated to exercise if the holder do

so. The value of the option at its expiration date is called the payoff function.

2. Transformation Method

The value of the arithmetic Asian option is characterized by a function in two variables $V(t, S, A)$, which is a solution of the following PDE.

$$\frac{\partial V}{\partial t} + \frac{1}{2}\sigma^2 S^2 \frac{\partial^2 V}{\partial S^2} + rS\frac{\partial V}{\partial S} + S\frac{\partial V}{\partial A} - rV = 0 \Bigg\}$$
$$V(T, S, A) = \varphi(S, A). \tag{1}$$

Where S_t is stock price at time t, r is the interest rate, σ is the asset volatility, T the expiration date, $A_t = \frac{1}{t}\int_0^t S_u du$ is the average of the stock price, and the payoff function $\varphi(S, A)$ depends on the type of the options as following:

1. Fixed strike call option
$$\varphi\left(\frac{A_T}{T}, S_T\right) = \left(\frac{A_T}{T} - k\right)^+$$

2. Fixed strike put option
$$\varphi\left(\frac{A_T}{T}, S_T\right) = \left(k - \frac{A_T}{T}\right)^+$$

3. Floating strike call option
$$\varphi\left(\frac{A_T}{T}, S_T\right) = \left(S_T - \frac{A_T}{T}\right)^+$$

4. Floating strike put option
$$\varphi\left(\frac{A_T}{T}, S_T\right) = \left(\frac{A_T}{T} - S_T\right)^+$$

Where k is the strike price.

To solve equation (1) we apply the following transformation

$$V\left(t, S, A\right) = e^{-r\tau} U\left(\tau, S, A\right), \ \tau = T - t$$

Equation (1) is reduced to

$$\left.\begin{array}{l} \dfrac{1}{2}\sigma^2 S^2 \dfrac{\partial^2 U}{\partial S^2} + rS \dfrac{\partial U}{\partial S} + S \dfrac{\partial U}{\partial A} - \dfrac{\partial U}{\partial \tau} = 0 \\[2ex] U\left(0, S, A\right) = \varphi\left(S, A\right) \end{array}\right\} \quad (2)$$

Note that, the boundary condition becomes now initial condition.
Employing the transformation below:

$$U\left(\tau, S, A\right) = A f\left(\tau, S\right), \ A = nS$$

Where n is a changed real number over the time.
Leads Eq. (2) to:

$$\frac{\partial U}{\partial S} = A \frac{\partial f}{\partial S} + nf \quad (3)$$

$$\frac{\partial^2 U}{\partial S^2} = A \frac{\partial^2 f}{\partial S^2} + n \frac{\partial f}{\partial S} + n \frac{\partial f}{\partial S} \quad (4)$$

$$\frac{\partial U}{\partial A} = f\left(\tau, S\right) \quad (5)$$

$$\frac{\partial U}{\partial \tau} = A \frac{\partial f}{\partial \tau} \quad (6)$$

Substituting Eq. (3)-(6) into Eq. (2):

$$\frac{1}{2}\sigma^2 S^2 \left(A \frac{\partial^2 f}{\partial S^2} + n \frac{\partial f}{\partial S} + n \frac{\partial f}{\partial S} \right) + rS \left(A \frac{\partial f}{\partial S} + nf \right) + Sf - A \frac{\partial f}{\partial \tau} = 0 \quad (7)$$

$$\frac{1}{2}\sigma^2 S^2 A \frac{\partial^2 f}{\partial S^2} + (\sigma^2 S^2 n + rSA) \frac{\partial f}{\partial S} + + S\left(rn+1\right) f - A \frac{\partial f}{\partial \tau} = 0 \quad (8)$$

International Science and
Technology Journal
المجلة الدولية للعلوم والتقنية

العدد 26
Volume 26

المجلة الدولية للعلوم والتقنية
International Science Technology Journal
ISTJ

But $A = nS$

So Eq. (8) becomes

$$\frac{1}{2}\sigma^2 S^2 A \frac{\partial^2 f}{\partial S^2} + (\sigma^2 SA + rSA)\frac{\partial f}{\partial S} + + \frac{A}{n}(rn+1)f - A\frac{\partial f}{\partial \tau} = 0 \qquad (9)$$

$$\left.\begin{array}{l} \frac{1}{2}\sigma^2 S^2 \frac{\partial^2 f}{\partial S^2} + S(\sigma^2 + r)\frac{\partial f}{\partial S} + \left(r+\frac{1}{n}\right)f - \frac{\partial f}{\partial \tau} = 0 \\[2mm] f(0,S) = \varphi(nS) \end{array}\right\} \qquad (10)$$

Assume that, $r + \dfrac{1}{n} = m$

Let $f(\tau, S) = e^{m\tau} g(\tau, S)$ then, Eq. (10) is reduced to:

$$\left.\begin{array}{l} \frac{1}{2}\sigma^2 S^2 \frac{\partial^2 g}{\partial S^2} + S(\sigma^2 + r)\frac{\partial g}{\partial S} - \frac{\partial g}{\partial \tau} = 0 \\[2mm] g(0,S) = \varphi(nS) \end{array}\right\} \qquad (11)$$

For the solution of Eq. (11) we shall apply Mellin transform in S , [8]. The Mellin transform of a function $g(S)$ is defined by

$$y(\tau)(z) = M\left[g(\tau)(S)\right](z) = \int_0^\infty g(S)S^{z-1}dS,$$

The inverse Mellin transform is

$$M^{-1}\left[y(z)\right](S) = \frac{1}{2\pi i}\int_{\beta-i\infty}^{\beta+i\infty} y(z)s^{-z}dz,$$

We obtained the following equation

$$\frac{1}{2}\sigma^2\left(z^2 + z\right)y - (\sigma^2 + r)zy - \frac{\partial y}{\partial \tau} = 0$$

$$\left[\frac{1}{2}\sigma^2\left(z^2 + z\right) - (\sigma^2 + r)z\right]y - \frac{dy}{d\tau} = 0 \qquad (12)$$

This is ordinary differential equation from the first order, its solution is

International Science and
Technology Journal
المجلة الدولية للعلوم والتقنية

العدد 26
Volume 26

المجلة الدولية للعلوم والتقنية
International Science and Technology Journal
ISTJ

$$y(\tau, z) = c \exp\left[\frac{1}{2}\sigma^2\left(z^2 + z\right) - (\sigma^2 + r)z\right]\tau \tag{13}$$

Where , c is a constant.

Mellin transform for the initial condition is

$$\mathrm{M}\left[g(0, S)\right] = \int_0^\infty S^{z-1}\left[\varphi(nS)\right]dS$$

$$= \int_0^\infty S^{z-1}\left[\varphi(nS)\right]dS$$

$$= n^{-z}\int_0^\infty S^{z-1}\left[\varphi(S)\right]dS$$

$$= n^{-z}\varphi(z)$$

We have $y(0, z) = n^{-z}\varphi(z)$

$$y(0, z) = n^{-z}\varphi(z) = c$$

$$y(\tau, z) = \left[n^{-z}\varphi(z)\right]\exp\left(\frac{1}{2}\sigma^2\left(z^2 + z\right) - (\sigma^2 + r)z\right)\tau \tag{14}$$

$$y(\tau, z) = \left[n^{-z}\varphi(z)\right]\exp\left(\frac{1}{2}\sigma^2\left(z^2 - z\right) - rz\right)\tau \tag{15}$$

Applying inverse Mellin transform to the above equation, the results below are achieved

$$g(\tau, S) = \frac{1}{2\pi i}\int_{\beta-i\infty}^{\beta+i\infty}\left\{\left[S^{-z}n^{-z}\varphi(z)\right]\exp\left(\frac{1}{2}\sigma^2\left(z^2 - z\right) - rz\right)\tau\right\}dz \tag{16}$$

$$f(\tau, S) = \frac{1}{2\pi i}\int_{\beta-i\infty}^{\beta+i\infty}\left\{\left(S^{-z}n^{-z}\varphi(z)\right]\exp\left(\frac{1}{2}\sigma^2\left(z^2 - z\right) - rz + m\right)\tau\right)\right\}dz \tag{17}$$

$$U(\tau, S, A) = \frac{A}{2\pi i}\int_{\beta-i\infty}^{\beta+i\infty}\left\{\left[S^{-z}n^{-z}\varphi(z)\right]\exp\left(\frac{1}{2}\sigma^2\left(z^2 - z\right) - rz + m\right)\tau\right)\right\}dz \tag{18}$$

International Science and Technology Journal
Technology Journal
المجلة الدولية للعلوم والتقنية

العدد 26
Volume 26

المجلة الدولية للعلوم والتقنية
International Science and Technology Journal
ISTJ

$$V\left(t,S,A\right)=\frac{A}{2\pi i}\int_{\beta-i\infty}^{\beta+i\infty}\{\left[S^{-z}n^{-z}\varphi\left(z\right)\right] \\ \exp\left(\frac{1}{2}\sigma^2\left(z^2-z\right)-rz+m-r\right)(T-t)\}dz \tag{19}$$

To prove that, our solution is an explicit solution for Eq. (1) differentiate Eq. (19) respect to all variable $t,S,A,$ and then substitute in Eq. (1) producing the equation below:

$$\frac{\partial V}{\partial t}+\frac{1}{2}\sigma^2S^2\frac{\partial^2V}{\partial S^2}+rS\frac{\partial V}{\partial S}+S\frac{\partial V}{\partial A}-rV=0$$

Note that, Eq. (11) is very similar to the classical Black-Schole PDE which can be easily transformed to a parabolic equation with constant coefficients, and one can easily solve it.

Let $Z=\ln S,\ S>0$

And taking into account that

$$S^2\frac{\partial^2 g}{\partial S^2}=\frac{\partial^2 g}{\partial Z^2}-\frac{\partial g}{\partial Z},\ S\frac{\partial g}{\partial S}=\frac{\partial g}{\partial Z}$$

Then Eq. (11) becomes:

$$\frac{1}{2}\sigma^2\frac{\partial^2 g}{\partial Z^2}+\left[r+\frac{1}{2}\sigma^2\right]\frac{\partial g}{\partial Z}=\frac{\partial g}{\partial \tau} \tag{20}$$

$$\frac{1}{2}\sigma^2\frac{\partial^2 g}{\partial Z^2}+\rho\frac{\partial g}{\partial Z}=\frac{\partial g}{\partial \tau} \\ g\left(0,Z\right)=\frac{1}{ne^Z}\varphi\left(ne^Z\right)=\varphi(ne^Z) \tag{21}$$

Now apply the followings change of variables

$$h\left(\tau,\xi\right)=g\left(\tau,Z=\xi+\rho\tau\right)$$

International Science and
Technology Journal
المجلة الدولية للعلوم والتقنية

العدد 26
Volume 26

المجلة الدولية للعلوم والتقنية
International Science and Technology Journal
ISTJ

$$\left.\begin{array}{l} \dfrac{\partial h}{\partial \tau} = \dfrac{\sigma^2}{2}\dfrac{\partial^2 h}{\partial \xi^2} \\[2mm] h(0,\xi) = \varphi(e^{\xi}) \end{array}\right\} \qquad (22)$$

Introducing further a new independent variable η by $\xi = \dfrac{\sigma}{\sqrt{2}}\eta$

Then Eq. (14) is transformed into a simplest parabolic equation

$$\left.\begin{array}{l} \dfrac{\partial h}{\partial \tau} = \dfrac{\partial^2 h}{\partial \eta^2} \\[2mm] h(0,\eta) = \varphi(e^{\eta}) \end{array}\right\} \qquad (23)$$

This is a simplest parabolic equation that has a known solution. For full details of the parabolic equation solution see [9].

CONCLUSION

Pricing arithmetic Asian options with continues sampling have been an outstanding issue in finance for several decades. Solving Black-Scholes PDE for Asian option is found to be difficult in Mathematics. This paper solved the problem of determining the price of continuous arithmetic Asian option using partial differential equations (PDEs). We get solution of the arithmetic Asian options PDE by considering some transformation techniques, this solution can be used for both types; call and put options.

REFERENCES

[1] J. Angus, "A note on pricing Asian Derivatives with continuous geometric averaging," *Journal of Future Markets* vol.19, pp. 845-858, 1999.

[2] E. S. Barucci, and V. Vespri, "Some results on Partial differential equations and Asian Options, *Math. Models Methods*," *Math. Models Methods Appl. Sci*., 11(3), pp. 475-497. 2001.

[3] C. Chih, G. Chung, and J. Tsung, "Pricing of arithmetic Asian options under stochastic volatility dynamics: overcoming the

risks of high-frequency trading"*Journal of Mathematics*, vol. 8 2020.

[4] D. I. Cruz-Baez, and J. M. Gonzalez-Rodriguez, "A different approach for pricing Asian options," *Journal of Applied Mathematics Letters,*vol.21, pp. 303-306.2008.

[5] J. N. Dewynne, and W. T. Shaw, "Differential equations and asymptotic solutions for arithmetic Asian options: 'Black–Scholes formulae' for Asian rate call", *Journal of applied Mathematics*. 19, 353–391.vol. 19, 2008.

[6] Z. A, Elshegmani, R. R. Ahmad and S. H. Jamaan, "On the modified arithmetic Asian option equation and its analytical solution," *Applied Mathematical Sciences,* vol. 5, pp. 1217-1227.2008.

[7] H. Geman, and M.Yor, "Bessel process, Asian options and perpetuities, "*Mathematical Finance,* 3(4), pp.349-375. 1993.

[8] L. Jódar,Sevilla-Peris, J.C. Cortés and R. Sala, "A new direct method for solving the Black–Scholes equation, "*Journal of Applied Mathematics Letters,*vol. 18, pp. 29–32. 2005.

[9] P. J. Olver, *Applications of Lie Groups to differential equations*, Graduate Texts in Mathematics.vol. 107, Springer Verlag, New York. 1993.

[10] L. C. Rogers,and Z. Shi. "The value of an Asian option."*Journal of Applied Probability,* vol. 32 pp. 1077-1088, 1995.

[11] J. Vecer, "A new PDE approach for pricing arithmetic average Asian option "*Journal of Computational Finance*, vol. 4, pp. 105-113. 2001.

[12] J. E, Zhang, "Theory of continuously-sampled Asian option pricing," working paper City University of Hong Kong. 2000.